

**Geochronology, geochemistry and isotopic compositions of the volcanic
rocks from oceanic (Hawaii) and continental (Eifel) intra-plate
environments**

**Dissertation
zur Erlangung des Grades
„Doktor der Naturwissenschaften“**

**Am Fachbereich Geowissenschaften
Der Johannes Gutenberg-Universität in Mainz**

**Zuzana Fekiacova
geb. am 19. 8. 1977 in Slowakei**

Mainz, 2004

All views and results presented in this thesis are those of the author, unless stated otherwise.

Ich versichere, dass ich die vorliegende Arbeit selbständig und nur unter Verwendung der angegebenen Quellen und Hilfsmittel verfasst habe.

Mainz, den 17. December 2004

Tag der mündlichen Prüfung: 14. 02. 2005

To my family and to Sylvain

Acknowledgments

Three years for a Ph.D. appeared to me as a long period when I was at the beginning. As the first questions started to be answered, new ones, more complicated arose and the time went faster and faster. Suddenly, I found my self at the end of these three years. I had nice and fun times in Mainz, but I didn't avoid the difficult ones, when I was full of questions and doubts. But during all the time I had people around me with whom I shared the happy moments and who supported me when the times were hard. Today, I would like to say THANK YOU to all of these people.

First of all, I would like to thank my parents and family. Although they are very far from Mainz, they always supported me and gave me the courage and strength to never give up.

I want to thank my advisors and collaborators: for the opportunity to work on the interesting projects, for the scientific background and financial support, for the enthusiasm, moral support and motivation.

I would like to thank the people in Berkeley who introduced me into the world of Ar-dating, Seb, Kim and Roland who made my journeys at Berkeley nice and interesting. I'd like to thank my colleagues who contributed to work in a nice atmosphere, thanks to Osama and Ismail who shared my office for three years.

Next, because these last three years were not only about work, it was very nice to have great friends around me. Thank you François, Christoph, Marie, Aurelie, Simone, who were always ready for celebrating whatever was the occasion. Thank you climbers: Karsten, Tim, Celine, Andy, and Antoine, it is always challenging to climb with you and it helps keeping the body and mind in a good health.

I met many nice people and I cannot put all the names in this short paragraph, but I think about everybody who influenced my stay here, in Mainz.

And the most important person, who gave me his love and understanding, who motivated me and was always close to me: Thank You Sylvain!

Contents

Acknowledgments

Abstract

Chapter 1: Introduction	1
1 – Intra-plate volcanism	1
1.1 – Continental intra-plate volcanism	3
1.1.1 – Type of intra-plate volcanism	3
1.1.2 – Passive rifting	4
1.1.3 – Active rifting	6
1.2 – Oceanic intra-plate volcanism	9
1.1.2 – Ocean Island Basalts (OIB)	9
2 – Aims of this Ph.D. thesis	16
2.1 – Geodynamic setting of the Tertiary Hocheifel volcanism	16
2.2 – Ko’olau volcano, Oahu, Hawaii	18
3 – Contribution to this thesis	21
References	22

Chapter 2 – Geodynamic setting of the Tertiary Hocheifel volcanism

(Germany), Part I: $^{40}\text{Ar}/^{39}\text{Ar}$ dating	1
Abstract	2
1 - Introduction	3
2 – Geological setting and sampling	3
3 – Sample preparation and analytical method	5
4 – Results	6
5 – Discussion	8
5.1 – Comparison with conventional K-Ar ages	8
5.2 – Hocheifel age distribution and relation to tectonics	10
5.3 – Relation to Upper Rhine Graben Taphrogenesis	11
5.4 – Relation to neighbouring Tertiary volcanism	12

6 – Conclusions	13
7 – Acknowledgments	15
References	16
Figure captions	18
Appendix: figures and tables	19

Chapter 3 – Geodynamic settings of the Tertiary Hocheifel volcanism (Germany), Part II: Geochemistry and Sr, Nd and Pb isotopic

compositions	1
Abstract	2
1 - Introduction	4
2 – Geologic setting	5
3 - Methods	7
3.1 - Samples	7
3.2 – Analytical methods	7
4 - Results	9
4.1 –Major and trace elements	9
4.2 – Sr, Nd and Pb isotopic compositions	12
5 - Discussion	14
5.1 – Major and trace elements	14
5.1.1 – Crustal contamination	14
5.1.2 – Mantle source of the Hocheifel magmas	16
5.2 – Isotopic compositions	17
5.2.1 – Source(s) of the Hocheifel magmas – deep mantle involvement?	18
5.2.2 – Mantle plume component in the Hocheifel magmas?	20
5.3 – Comparison with other CEVP occurrences	23
6 - Conclusion	26
Acknowledgments	27
References	28
Figure captions	32
Appendix: figures and tables	35

Chapter 4 – The Ko’olau Scientific Drilling Project: Lead isotope evolution of Ko’olau volcano	1
Abstract	2
1 - Introduction	3
2 - Samples and methods	5
3 - Results	6
3.1 – Pb and Sr isotope stratigraphy	6
3.2 – Isotope covariations	8
4 - Discussion	9
4.1 – Pb isotopes – implications on source(s) and evolution of Ko’olau volcano	9
4.2 – Pb isotope stratigraphy	14
4.3 – Source(s) of post-erosional Honolulu Volcanics	15
5 - Conclusions	19
References	21
Figure captions	24
Appendix: figures and table	28
Chapter 5 - Conclusions	1
1 – The Tertiary Hocheifel volcanism and the Central European Volcanic Province	1
2 – The Ko’olau volcanism	3
3 - Perspectives	5

Appendix : Curriculum vitae

Abstract

The Cenozoic Eifel volcanic fields (West Germany) are located close to the Rhine Graben rift system and are part of the Central European Volcanic Province (CEVP). Where as the Quaternary Eifel volcanism appears to be related to a mantle plume, the origin of the Tertiary Hocheifel volcanism is not clear. In order to get indications on the geotectonic setting of the Tertiary volcanism geochronological, geochemical and isotope data were measured. On the basis of $^{40}\text{Ar}/^{39}\text{Ar}$ dating, two periods of Hocheifel activity from 43.6 to 39.0 Ma and from 37.5 to 35.0 Ma, respectively, are inferred. The Hocheifel activity is interpreted to represent the propagation of the pre-rifting volcanism of the northern Upper Rhine Graben (59 to 47 Ma) to the NW because it closely follows in time northern Upper Rhine Graben volcanism, the older period of Hocheifel activity shows propagation of younger volcanism to the north and the Hocheifel tectonic pattern derived from the time - space relation of volcanism corresponds to stress field conditions identical to those of the Upper Rhine Graben at the time of Hocheifel volcanic activity. Magma generation therefore appears to be related to decompression by extension during Middle to Late Eocene. The geochemical data indicate that the Hocheifel magmas were produced by partial melting from a garnet peridotite source at ca. 75-90 km depth. Crustal contamination is minor although the magmas erupted through a relatively thick continental lithosphere. Sr, Nd and Pb isotopic compositions suggest that the source of the Hocheifel magmas represents a mixture between depleted Focal Zone (FOZO) or high- μ (HIMU)-type and enriched mantle 2 (EM2)-type material. The Tertiary Hocheifel and the Quaternary Eifel lavas appear to have a common enriched end-member. However, the other sources are likely to be distinct. In addition, the Hocheifel lavas share a depleted component with the other Tertiary CEVP lavas. Although the Tertiary Hocheifel and the Quaternary Eifel lavas appear to originate from different sources, the potential involvement of a FOZO-like component would indicate the contribution of deep mantle material. Thus, on the basis of the geochemical and isotope data, we cannot rule out the involvement of plume-type material in the Hocheifel magmas. Summarizing, for the genesis of the Tertiary Hocheifel volcanic activity we suggest, that a previously with plume-type material contaminated mantle source is tapped by the Eocene volcanism generated by lithospheric extension (passive rifting?)

The Ko'olau Scientific Drilling Project (KSDP) has been initiated in order to evaluate the long-term evolution of Ko'olau volcano and obtain information about the Hawaiian mantle plume. High precision Pb triple spike data, as well as Sr and Nd isotope

data on KSDP lavas and Honolulu Volcanics (HVS) reveal compositional source variations during Ko'olau growth. Pb isotopic compositions indicate that, at least, three Pb end-members are present in Ko'olau lavas. Changes in the contributions of each component are recorded in the Pb, Sr and Nd isotopes stratigraphy. The radiogenic component is present, at variable proportion, in all three stages of Ko'olau growth. It shows affinities with the least radiogenic "Kea-lo8" lavas present in Mauna Kea. The first unradiogenic component was present in the main-shield stage of Ko'olau growth but its contribution decreased with time. It has EM1 type characteristics and corresponds to the "Ko'olau" component of Hawaiian mantle plume. The second unradiogenic end-member, so far only sampled by Honolulu lavas, has isotopic characteristics similar to those of a depleted mantle. However, they are different from those of the recent Pacific lithosphere (EPR MORB) indicating that the HVS are not derived from MORB-related source. We suggest, instead, that the HVS result from melting of a plume material. Thus the evolution of a single Hawaiian volcano records the geochemical and isotopic changes within the Hawaiian plume.

Kurzfassung

Diese Doktorarbeit beschäftigt sich mit Vulkanen deren Aktivitäten mit Mantel-Plume verbunden sind. Zwei Beispiele werden gegeben, der Eifel Vulkanismus in Deutschland und der Hawaii Vulkanismus im Pazifik.

Der Eifel Vulkanismus gehört zu Mitteleuropäischen Vulkanischen Provinz (CEVP) und liegt im Rheinischen Massiv, in der Nähe von den Rhein und Leine Gräben. Der Quartäre Eifel Vulkanismus scheint mit einer Mantel-Plume Aktivität verbunden zu sein. Jedoch bleiben die Ursachen des Tertiären Hocheifel Vulkanismus diskutiert. Im ersten Teil dieser Arbeit präsentieren wir die Ergebnisse von datierungen, geochemischen und isotopischen Bestimmungen, um die geotectonischen Einstellungen des Tertiären Eifel Vulkanismus zu bewerten.

Auf Grund der $^{40}\text{Ar}/^{39}\text{Ar}$ -Datierung haben wir zwei Perioden in der Hocheifel Aktivität identifiziert: von 43.6 bis 39.0 Ma und von 37.5 bis 35.0 Ma. Wir zeigen auch, dass der vor-rifting Vulkanismus im nördlichsten Oberen Rheingraben (59 bis 47 Ma) kurz von der Hocheifel vulkanischen Aktivität statt findet. Außerdem, zerbreitet sich der Vulkanismus vom Süden nach Norden innerhalb der ältesten Phase der Hocheifel Aktivität fort. Zur Zeit vom Hocheifel Vulkanismus wurde die tektonische Aktivität im Hocheifel durch identische Stressfelderbedingungen, dass im Oberen Rheingraben kontrolliert.

Deshalb scheint die Magma-bildung im Hocheifel durch die Dekompression aufgrund der von Mitte bis Spät Eozän Ausdehnung verursacht zu werden.

Unsere geochemische Daten zeigen, dass die Hocheifel Magmen durch das teilweise Schmelzen eines Granats peridotites an 75-90-Km-Tiefe erzeugt wurden. Wir zeigen auch, dass Kontamination von der Kruste unbedeutend ist, obwohl die Magmen durch eine relativ dicke Kontinentallithosphäre ausbrachen. Sr, Nd und Pb Isotopenzusammensetzungen schlagen vor, dass die Quelle von Hocheifel Magmen aus einer Mischung zwischen entleertem FOZO oder HIMU Material und angereichertem EM2 Material besteht. Der Tertiäre Hocheifel und die Quartäre Eifel Laven scheinen ein allgemein angereichertes Endmitglied zu haben. Jedoch werden die anderen Quellen wahrscheinlich verschieden sein. Außerdem teilen die Hocheifel Laven einen entleerten Komponenten mit den anderen Tertiären CEVP Laven. Obwohl der Tertiäre Hocheifel und die Quartäre Eifel Laven von verschiedenen Quellen stammen scheinen, würde den eventuellen Beitrag von einem FOZO Komponenten auf einen tiefen-Mantel Material hinweisen. Auf der Grundlage von geochemischen und isotopischen Daten, können wir deshalb die Beteiligung des Plume-Typ Material in den Hocheifel Magmen nicht ausschließen.

Unsere zweites Beispiel beschäftigt sich mit dem Vulkanismus von Hawaii. Das Ziel das Ko'olau Wissenschaftliche Bohrungs-projekts (KSDP) ist die Langzeitevolution des Ko'olau Vulkans zu bewerten und Informationen über die hawaiische Mantel-Plume zu erhalten.

Hohe Präzision Pb Daten, sowie Sr und Nd Isotopen Daten auf KSDP Laven und Honolulu Vulkanische Gesteine (HVS) offenbaren Kompositionen Variationen der Quellen während der Ko'olau Entwicklung. Pb isotopische Zusammensetzungen zeigen dass, mindestens, drei Pb Komponente in Ko'olau's Laven gegenwärtig sind. Änderungen in den Beiträgen jedes Komponenten werden in Pb, Sr und Nd Isotopenstratigraphie registriert. Der radiogene Komponent gibt es in unterschiedliche Proportionen in allen drei Phasen der Entwicklung von Ko'olau Vulkan. Es zeigt Affinitäten mit der am wenigsten radiogenem "Kea-108" Lava von Mauna Kea. Der erste nichtradiogene Komponent war in der Hauptphase der Entwicklung von Ko'olau Vulkan gegenwärtig, aber sein Beitrag nahm mit der Zeit ab. Er hat EM1-Eigenschaften und entspricht dem "Ko'olau" Komponent der hawaiischen Mantel-Plume. Der zweite nichtradiogene Komponent, der bis jetzt nur in den Honolulu Laven gefunden wird, zeigt ähnlichen isotopischen Eigenschaften dass den entleerten Mantel. Die isotopischen Eigenschaften der zwei Komponente unterschieden sich aber von der jungen Lithosphäre des Pazifik (EPR MORB). Deshalb stammen HVSs nicht

von Quellen die den MORBs ähnlich sind. Wir schlagen eher vor, dass die HVSS vom schmelzen eines Plume-Materials stammen. Für diesen Grund, registriert die Entwicklung eines einzelnen Hawaiischen Vulkans die geochemische und Isotopische Änderungen innerhalb der Hawaiischen Plume.

Chapter 1

Introduction

1 - Intra-plate volcanism

About 90% of the magmatic activity on Earth (Fig. 1) is confined to plate boundary tectonic settings: constructive plate margins (mid-ocean ridges, back arc spreading centers) and destructive plate margins (island arcs, active continental margins). Nevertheless, the volume of volcanism occurring within the tectonic plates, far from the plate boundaries, is not negligible. The various types of intra-plate volcanism can be subdivided into (Wilson, 1989):

- oceanic intra-plate setting: ocean islands,
- continental intra-plate setting: continental flood basalt provinces, continental rift zones magmatism, potassic and ultra-potassic magmatism not related to rift zones.

During my thesis I had the opportunity to work on volcanic products from two different intra-plate settings. The Tertiary Hocheifel volcanism is an example of continental intra-plate volcanic activity. Recent Hawaiian volcanism represents oceanic intra-plate magmatic activity (Fig. 1). While it is generally accepted that the Hawaiian volcanism is related to the activity of the Hawaiian mantle plume, the origin of the Tertiary Hocheifel activity remains a matter of debate.

In the following chapter I will give an overview of the various types of intra-plate tectonic settings and magmatic activity related to them. Then I will describe more specifically the two areas of research I have been working on and introduce the studies I have conducted during my Dr. rer. Nat. dissertation.

Tectonism and Volcanism of the Last One Million Years

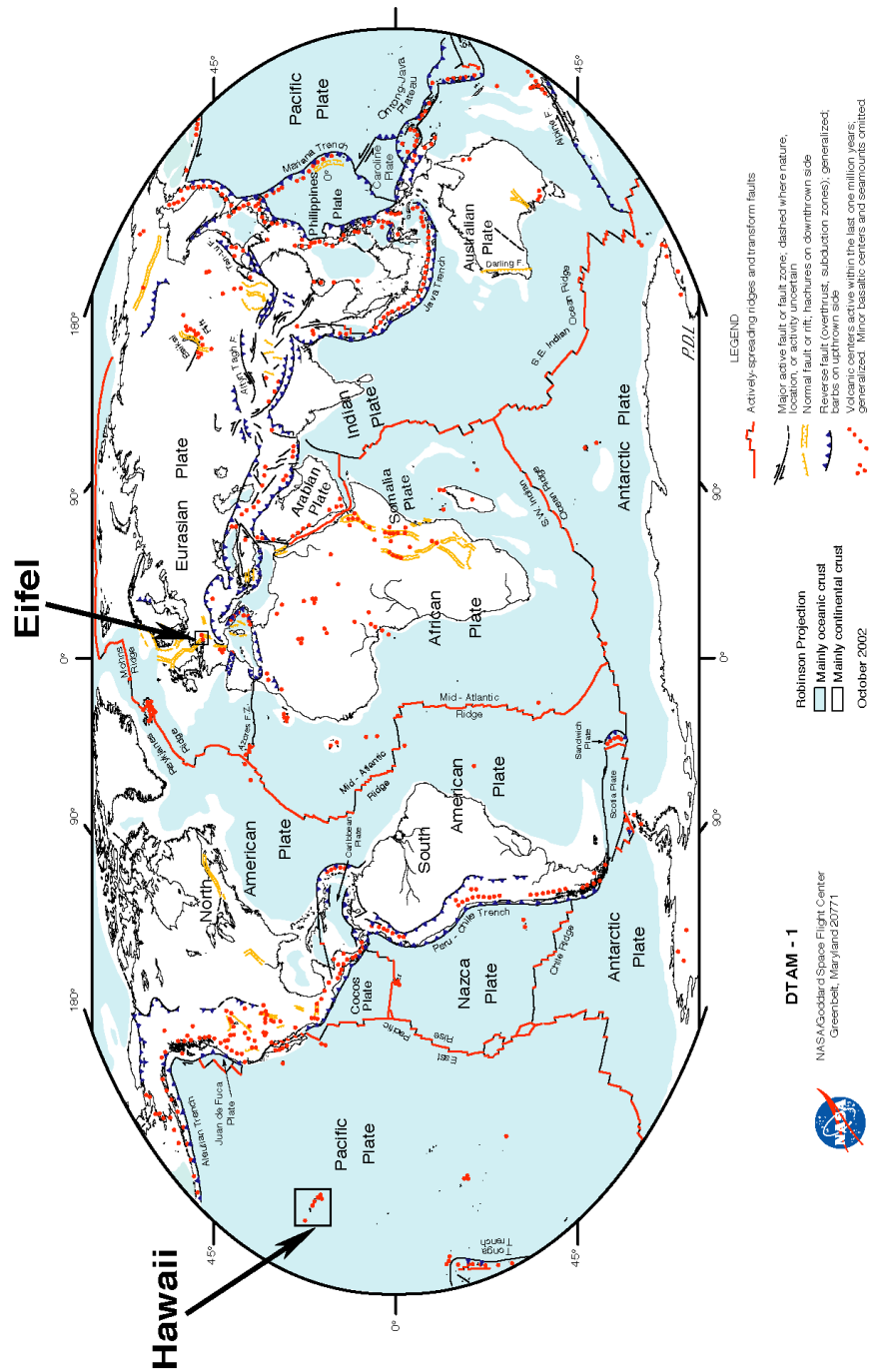


Figure 1: Distribution of the volcanic and tectonic activities on Earth (modified from <http://denali.gsfc.nasa.gov/dtam/>). The two black squares indicate the two volcanic areas studied in this project: Eifel and Hawaii.

1.1 - Continental intra-plate volcanism

1.1.1 - Types of intra-plate volcanism

The major manifestations of continental intra-plate magmatism are: the Continental Flood Basalt (CFB) provinces (e.g., Etendeka, Parana, Deccan Traps), the volcanic activity related to continental rift zones (e.g., East African Rift, Rhine Graben) and potassic and ultra-potassic magmatism which appear to be related with particular geodynamic settings (above subduction zones, during or after continental collision, extension intra-continental plate magmatic activity) (Thompson and Fowler, 1986).

One of the objectives of my dissertation was to study the Tertiary Hocheifel volcanism which appears to be related to lithospheric extension (Fekiacova et al., submit.). Therefore, I will focus the following section on magmatism related to rift zones.

(Wilson, 1989) defined continental rift zones as “areas of localized lithospheric extension characterized by a central depression, uplifted flanks and a thinning of the underlying crust”. In general, they are associated with high heat flow, regional uplift and magmatism. While small volumes of magmatism occur in “dry” rifts (e.g., Baikal Rift Zone), extensive effusive magmatism predominates in “wet” rifts (e.g., Kenya Rift). In contrast to alkaline rocks which are abundant in Western Kenya and Baikal rifts, bimodal volcanism occurs in Rio Grande and West Antarctica rifts (Ruppel, 1995). The variations in petrology and geochemistry of rift-related volcanic products appear to reflect, on one hand variations in degree of melting, on the other hand changes in depth of melting (Wendlandt and Morgan, 1982). In general, three main parameters are thought to control the evolution of a rift: 1/ thermal regime in the crust and mantle, 2/ rheology of the lithosphere and 3/ duration and rate of rifting (Ruppel, 1995). Traditionally, rifts are classified on the basis of the

relative importance of plate boundary forces (passive rifting) and sublithospheric mantle dynamics (active rifting) (e.g., Sengör and Burke, 1978; Turcotte and Emermen, 1983; Keen, 1985; Christensen, 1992). Relative timing of extension, volcanism and uplift/subsidence provides key information to determine whether the rifting is active or passive. Although relative succession of these processes brings straightforward indication to discriminate between passive and active rifting, both are related to similar geophysical and geological characteristics (e.g., magmatism, deep lithospheric melting, thermal weakening of the lithosphere, lithospheric thinning). Thus, the classification of a rift as passive or active is rarely simple, and several rifts (e.g., East Africa, Baikal, Rio Grande, Rhine Graben) have been interpreted as active (Logatchev et al., 1978; Sengör and Burke, 1978; Illies, 1981; Zorin, 1981; Parker et al., 1984) and passive (Oxburgh and Turcotte, 1974; Sengör and Burke, 1978; Eaton, 1979; Tapponnier and Molnar, 1979; Ingersoll et al., 1990; Strecker et al., 1990).

In the two following sections, I present the models of passive and active rifting, as they were discussed by Ruppel (1991).

1.1.2 - Passive rifting

During passive rifting (Fig. 2a), extension and thinning of the lithosphere are produced in response to stress generated at the boundaries of the tectonic plates. The main mechanisms that create stress at the boundaries of the tectonic plates are ridge push, slab pull (e.g., Forsyth and Uyeda, 1975) and continent-continent collision (e.g., Houseman and England, 1986b). The stress is transmitted from the plate boundary towards the interior of the plate where pre-existing zones of weaknesses determine the localization of rift (e.g., Braun and Beaumont, 1989; Dunbar and Sawyer,

1989b; Bassi et al., 1993). Volcanism related to passive rifting occurs either simultaneously with thinning of the lithosphere or later, when the extension has been completed. Uplift develops only late in the rifting process, after the lithosphere was heated significantly. Passive rifting is accompanied by passive asthenospheric upwelling, which is a key process in response to thinning of the lithosphere. The asthenospheric upwelling can induce decompressional melting (e.g., McKenzie and Bickle, 1988), crustal and lithospheric underplating (e.g., White et al., 1987b; Lister et al., 1991), large lateral gradient in lithospheric thickness between extended and unextended regions (e.g., Moretti and Froidevaux, 1986) and in several cases also the eruption of continental flood basalts (e.g., White and McKenzie, 1989; Harry and Sawyer, 1992).

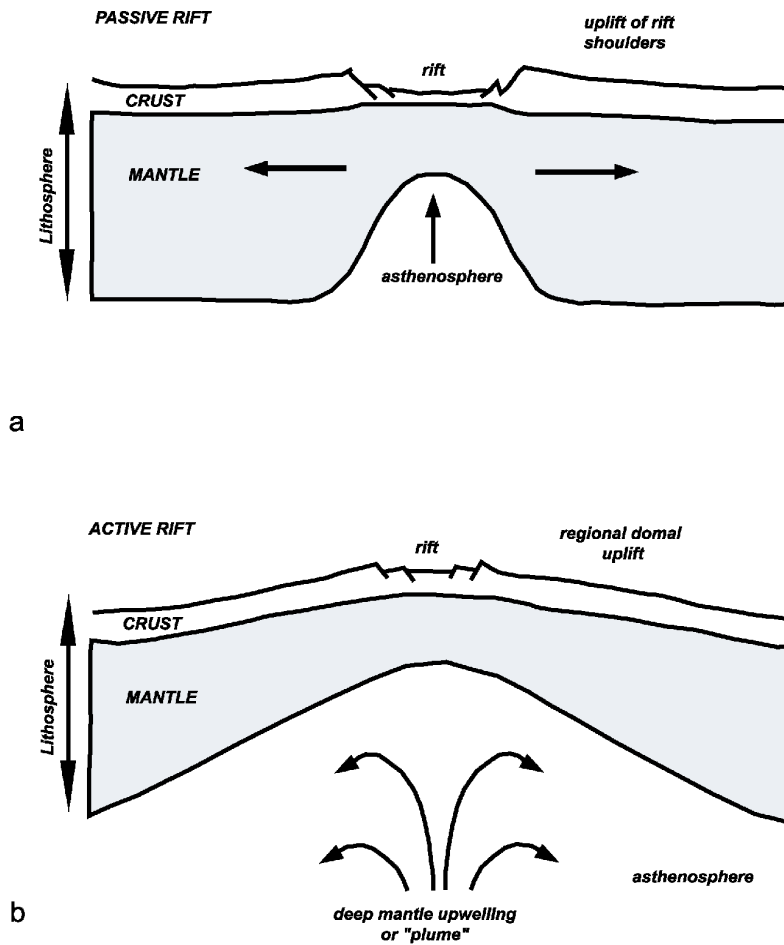


Figure 2: Models of (a) passive and (b) active rifting (Wilson, 1989)

1.1.3 - Active rifting

In several places on Earth, the geochronological, geophysical, tectonic and petrological data cannot be explained by passive rifting mechanisms alone (e.g., White, 1989; Sengör et al., 1978). For these cases a model of active rifting associated with mantle dynamics has been proposed (Fig. 2b).

The active rifting mechanism is thought to be related to mantle plumes and to result from thermal convection in the mantle. The plume material rises up due to buoyancy differences and

cause the deformation of the overlying lithosphere (Withjack, 1979; Spohn and Schubert, 1982; Olson et al., 1988; Griffiths and Campbell, 1991; Schubert, 1982). In the active rifting model, the laboratory experiments of Griffiths and Campbell (1991) show that the uplift occurs long time before the plume head reaches the base of the lithosphere, tens of millions of years before the onset of volcanism. The extension is delayed compared to the volcanism by millions of years. The problem that arises from the active rifting model is that dynamic uplift alone is not sufficient to produce extensional failure (e.g., Houseman and England, 1986a; Cloetingh and Wortel, 1988; Hill, 1991). Therefore, if an active rifting is driven by a plume, an additional factor, such as local crustal weakening must be associated with the uplift in order to induce extension (e.g., Westaway, 1993).

Because passive and active rifting can produce similar tectonic, geophysical and geochemical signatures, several cases of extension-related magmatism remain debated. The Tertiary Hocheifel volcanism is an example of such a controversial case. Tertiary and Quaternary volcanic activity occurred in the Eifel area. Seismic tomography imaging revealed the presence of a columnar low velocity anomaly below the Quaternary Eifel volcanic fields (Ritter et al., 2001). This anomaly extends to, at least, 400 km depth (Fig. 3) and is attributed to temperature excess of about 150-200K. It has been suggested that this so-called Eifel mantle plume, caused the Quaternary West and East Eifel volcanic activity (Ritter et al., 2001). This hypothesis is supported by the geochemical and isotopic characteristics of the Quaternary Eifel lavas because their trace elements and isotope compositions (Hoernle et al., 1995; Wedepohl and Baumann, 1999) are similar to those of typical Ocean Island Basalts (OIB) which are associated with mantle-plumes (Weaver, 1991; Hofmann, 1997). Neither the time-life, nor the starting point of the Eifel mantle plume are constrained: Because of a lack of studies, the origin of the Tertiary Hocheifel volcanic activity is

not clearly known. Two main hypotheses are debated: 1) since the Hocheifel lie close to a complex fractured zone which is a triple junction between the Upper Rhine, Lower Rhine and Leine grabens, the Tertiary Hocheifel volcanic occurrences could have resulted from tectonic extension or 2) the Tertiary Hocheifel volcanic activity could be related to mantle dynamics and/or be the precursor of the Eifel mantle plume. Thus, we have conducted geochronological, geochemical and isotopic investigations to try to answer the question whether the Tertiary Hocheifel lavas represent a mantle plume precursor - type activity or extension-related volcanism.

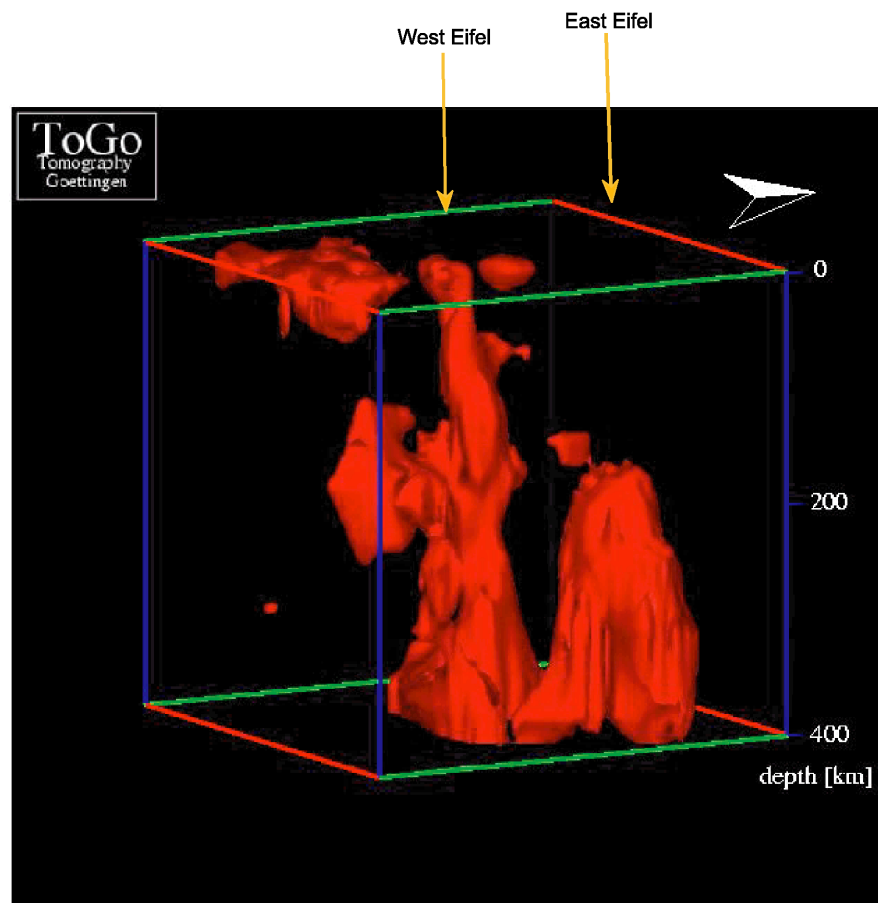


Figure 3: 3D model of the actual Eifel plume. The reddish structure represents a seismic anomaly with at least 1% reduction of the seismic wave velocity. This is equivalent to an increase of temperature of about 150-200K (from <http://www.uni-geophys.gwdg.de/~eifel/>). The locations of the West and East Eifel are from M. Jordan, Eifel Plume Team (pers. comm.)

1.2 - Oceanic intra-plate volcanism

1.2.1 - Ocean Island Basalts (OIB)

Ocean Island Basalts (OIB) are typical examples of magmatic activity in the oceanic intra-plate environment. Both OIB and Mid Ocean Ridge Basalts (MORB) have a mantle origin. However, OIB geochemical and isotopic characteristics usually differ from those of Mid Ocean Ridge Basalts (MORB), which indicates that they are derived from different mantle source regions. While the MORB are thought to sample the “depleted” upper mantle (e.g., Hofmann, 1997), the OIB appear to originate from the lower mantle (e.g., Morgan, 1972a; Morgan, 1972b) and have relatively enriched geochemical characteristics. As inferred from geochemical and isotopic studies (e.g., Zindler and Hart, 1986; Hart, 1988; Hart et al., 1992) the composition of the OIB reflects a mixture between multiple source components such as primitive mantle, recycled oceanic crust or recycled subcontinental lithosphere. Four isotopically distinct mantle components, identified by White (1985), are generally accepted to represent the source of the OIB (White, 1985). They were named by Zindler and Hart (1986) high- μ (HIMU), enriched mantle 1 and 2 (EM 1 and EM 2) and depleted MORB mantle (DMM) (Fig. 4). There are several hypotheses about the provenance of the individual mantle reservoirs. HIMU is characterized by a high time integrated $^{238}\text{U}/^{204}\text{Pb}$ ratio and the least radiogenic strontium. It is generally thought that the HIMU OIBs are formed by recycled oceanic crust (Hofmann and White, 1980; Chase, 1981; Hofmann and White, 1982) affected by the lost of alkalis and lead during alteration and subduction

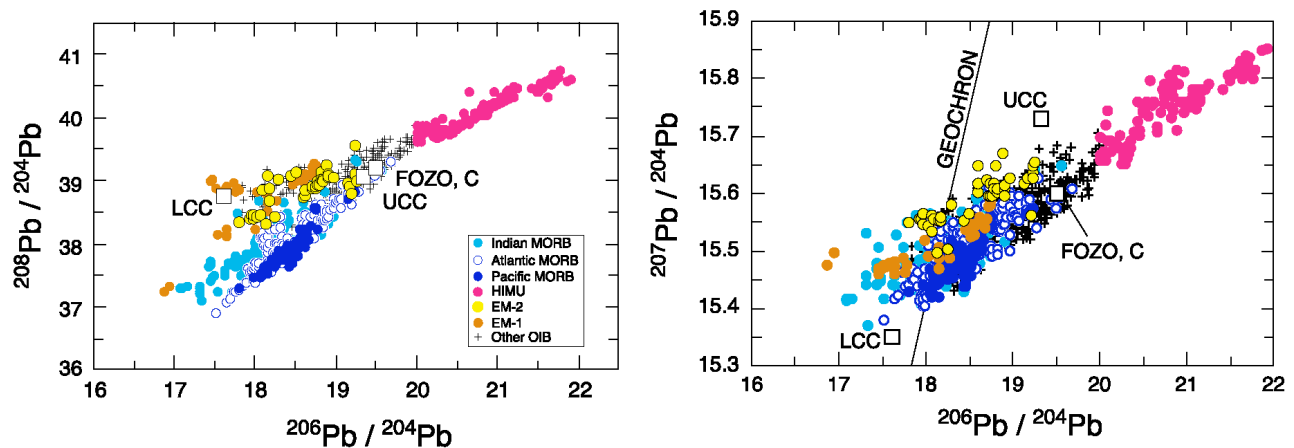


Figure 4: Mantle reservoirs distinguished on the basis of the Pb isotopic compositions plotted together with MORB data from three regions of the Earth: Indian ocean, Atlantic and Pacific. LCC: lower continental crust, UCC: upper continental crust, FOZO: focal zone, C: “common” (see text for explanations. Figure from Hofmann, 1007 (Hofmann, 1997).

(Chauvel et al., 1992). The origin of the enriched mantle end-members remains controversial. The EM 1 component exhibits very low $^{143}\text{Nd}/^{144}\text{Nd}$, relatively low $^{87}\text{Sr}/^{86}\text{Sr}$ and high $^{208}\text{Pb}^*/^{206}\text{Pb}^*$ ratios¹. The EM 1 basalts are thought to originate either from recycling of subcontinental lithosphere (e.g., McKenzie and O’Nions, 1983; Hawkesworth et al., 1986, LeRoex (1996); Mahoney et al., 1991; Milner and le Roex, 1996) or from recycling of subducted ancient pelagic sediment (e.g., Ben Othman et al., 1989; Weaver, 1991; Chauvel et al., 1992; Rehkämper and Hofmann, 1997; Plank and Langmuir, 1998; Eisele et al., 2002). The EM 2 component is characterized by high $^{87}\text{Sr}/^{86}\text{Sr}$ and high $^{207}\text{Pb}/^{204}\text{Pb}$ ratios (for a given $^{206}\text{Pb}/^{204}\text{Pb}$ ratios) which are isotopic signatures similar to those of terrigenous sediments. Therefore, the EM 2 reservoir was thought to be formed by recycled oceanic crust with an addition of small amounts of subducted

¹ The $^{208}\text{Pb}^*/^{206}\text{Pb}^*$ ratio represents the time integrated $^{238}\text{U}/^{232}\text{Th}$ ratio since the formation of the Earth and is defined as $[(^{208}\text{Pb}/^{204}\text{Pb})_{\text{sample}} - 29.475] / [(^{206}\text{Pb}/^{204}\text{Pb})_{\text{sample}} - 9.307]$ (Galer and O’Nions, 1985).

sediments (e.g., White and Hofmann 1982). However, the most recent studies suggest that the recycled sediment cannot be at the origin of the enriched EM 2 compositions. It has been suggested instead, that the metasomatism of the subducted oceanic lithosphere followed by long time storage in the deep mantle are mechanisms responsible for the EM 2 signature (Workman et al., 2004). The depleted geochemical characteristics of DMM, which is sampled by MORB, suggest that it was formed by extraction of incompatible trace elements during the formation of continental crust (Hart, 1988). Recent studies have demonstrated that there is another component in the OIB isotopic signatures. The He isotopic characteristics of this component suggest that it originates from the lower mantle (Hart et al., 1992; Hauri et al., 1994). This additional reservoir was named FOZO (for Focal Zone) by Hart et al. (1992). The FOZO Sr and Nd isotopic compositions are comparable to those of a depleted MORB mantle (DMM), in contrast, it has significantly more radiogenic $^{206}\text{Pb}/^{204}\text{Pb}$ ratios compared to DMM (Hofmann, 2003). 'C' or common mantle component is a reservoir that resembles FOZO since it has the same Pb isotope ratios. However, 'C' was envisaged as dispersed within the MORB reservoir (Hanan and Graham, 1996).

The geochemical and isotopic heterogeneity of OIB results from the mixing between different mantle reservoirs the recycling of subducted material has an important place in the OIB source (Hofmann and White, 1982). The occurrences of OIB on the surface are attributed to hot-spots or mantle plumes activity because 1) the oceanic intra-plate volcanism appears to be independent of plate tectonics (e.g., Wilson, 1989) and 2) the OIB sample deeper mantle reservoirs than MORB. Although the features such as particular geochemical and isotopic characteristics, heat flow, uplift and thermal erosion are part of a basic diagnostic, the starting point and the evolution of

mantle plumes remains a matter of intense debate (e.g., Hofmann, 1988) and various models of the Earth interior have been drawn (Fig. 5).

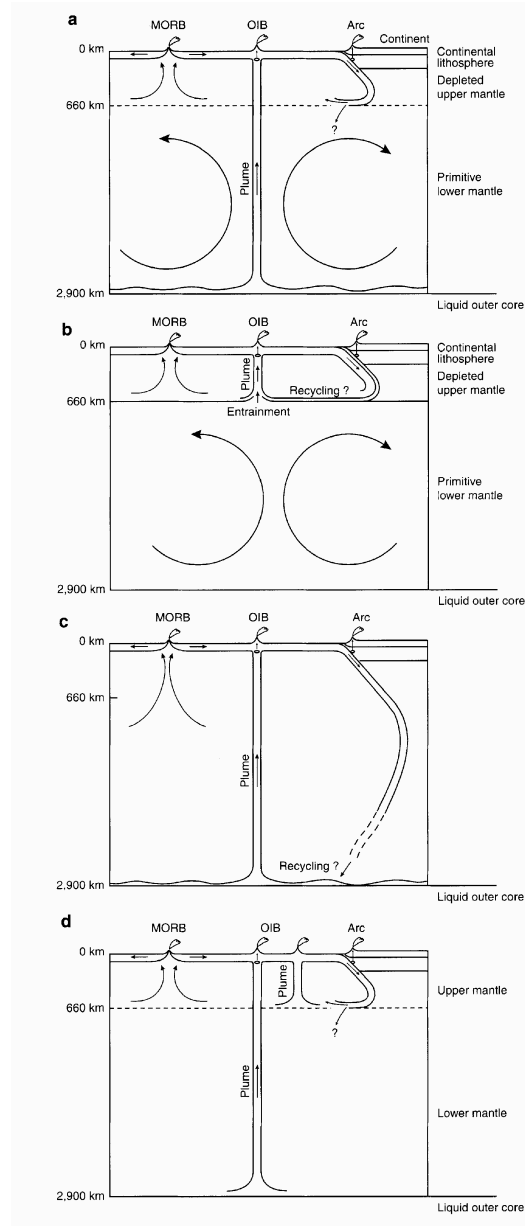


Figure 5: Models of mantle convection. (a) old "standard model" of two-layer circulation, (b) two-layer circulation with nearly complete isolation between upper and lower layers, (c) whole-mantle, single-layer circulation with plumes rising from the core-mantle boundary (d) hybrid model with limited exchange by means of occasional foundering of subducted lithosphere and rise of strong plumes from the core-mantle boundary. Figure from Hofmann (1997).

During my Dissertation, I had the opportunity to study lavas from Ko'olau volcano on the Oahu Island in Pacific Ocean (Fig. 1). The samples are coming from the KSDP (Ko'olau Scientific Drilling Project) drilling. I will present the results of my investigations in this report.

One of the most actively studied hot-spot occurrences on Earth are Hawaiian Islands in the Pacific Ocean. The islands and seamounts of the Hawaiian-Emperor chain form a 6000 km-long volcanic chain (Fig. 6). The age of the chain progress from the active volcanoes located at the southeast end to the 80-75 Ma volcanoes located at the northwest end of the Emperor seamounts chain. Wilson 1963 (Wilson, 1963) was the first to propose that the Hawaiian-Emperor chain was formed by the movement of the sea-floor over a source of lava located in the asthenosphere. Later, the islands and seamounts formed by the Hawaiian-Emperor chain were shown to reflect the activity of a mantle plume: the alignment of individual Hawaiian volcanoes reflects the movement of the Pacific plate over the Hawaiian hot-spot (Clague and Dalrymple, 1987). (Fig. 7 a, b). At present, based on dating, geophysical and geochemical data, the hot-spot appears to be centered between Mauna Loa, Kilauea and Loihi volcanoes (Gripp and Gordon, 2002) which are the currently active volcanoes.

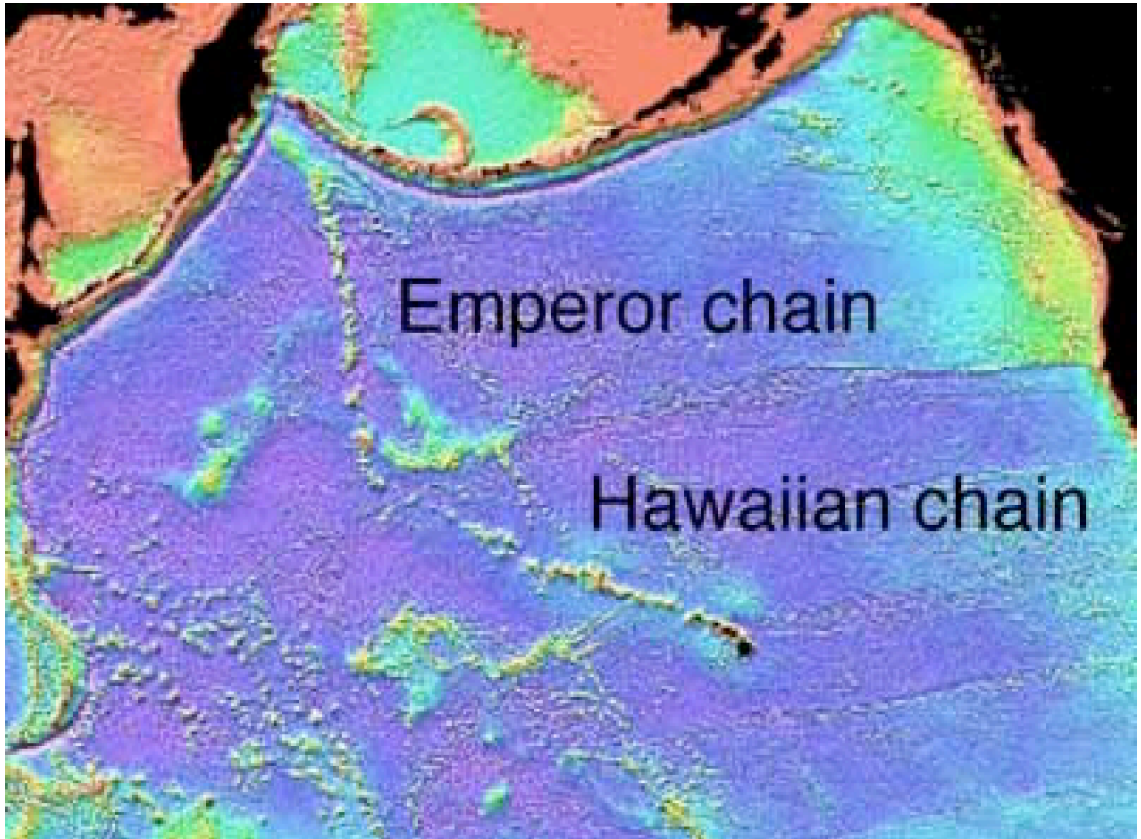


Figure 6: Hawaiian-Emperor volcanic chain in the Pacific ocean (<http://www.mantleplumes.org>)

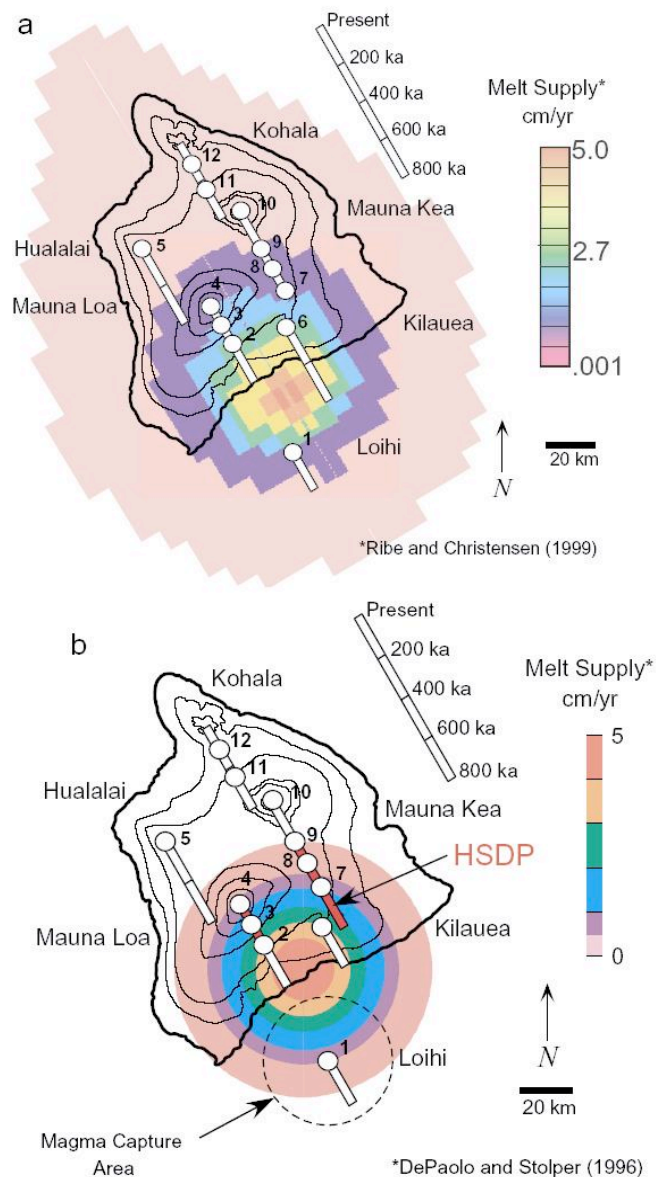


Figure 7: (a) Map of Hawaii showing the volcanoes superimposed on the map of melt supply calculated by Ribe and Christensen 1999 (Ribe and Christensen, 1999). (b) After Figure 1a using the melt supply model of DePaolo and Stolper (1996) (DePaolo and Stolper, 1996). In both figures the positions of each of the volcano summit is shown as function of time in the past, assuming a Pacific plate velocity of 9 cm/yr. The main melt supply region (bounded approximately by the 2cm/yr contour) is centered between Mauna Loa and Loihi, which provides the best fit to the modern lava accumulation rates for Mauna Loa and the historical eruption rate of Kilauea. From DePaolo et al (2001) (DePaolo et al., 2001)

2 - Aims of this dissertation

My Dissertation thesis was composed of two separate projects focused on the study of intra-plate volcanism. The aim of the first project was to study the geotectonic settings of the Tertiary Hocheifel volcanic activity, an example of continental intra-plate volcanism. The objective of the second project was to study the evolution of the Pb isotopic compositions of Ko'olau volcano, Oahu, Hawaii, an example of oceanic intra-plate volcanism.

2.1 - Geodynamic setting of the Tertiary Hocheifel volcanism

The Eifel volcanic area is located in the Hercynian Rhenish Massif in Western Germany and belongs to the extensive Central European Volcanic Province (CEVP) (Fig. 8). The Hocheifel volcanic activity occurred during the Tertiary while the West and East Eifel volcanic fields have formed during the Quaternary. Several of the major volcanic occurrences of the CEVP, e.g., Tertiary Hocheifel, Quaternary West and East Eifel, Vogelsberg and Westerwald, lie close to a complex fractured zone, which is a triple junction between the Upper Rhine, Lower Rhine and Leine grabens (Fig. 8). While geophysical studies tend to show that the Quaternary West and East Eifel volcanism is explained by the activity of a mantle plume (Fig. 3) (Ritter et al., 2001), the origin of the Tertiary Hocheifel volcanism remains a matter of debate: does the Tertiary Hocheifel volcanism represent a precursor activity of the Eifel mantle plume? Or is it an example of the extension-related magmatic activity?

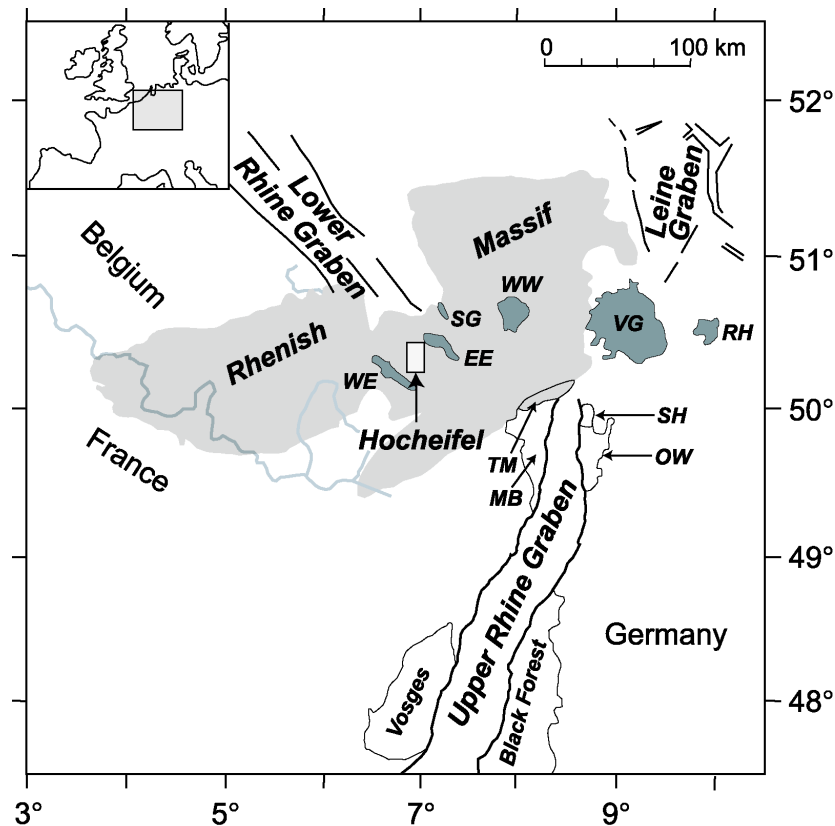


Figure 8: Volcanic occurrences of the Central European Volcanic Province (CEVP). Upper Rhine, Lower Rhine and Leine grabens represent the major tectonic features of the Central Europe. The light gray field represents the Rhenish Massif, dark gray fields corresponds to the individual volcanic fields of the CEVP: WE-West Eifel, EE--East Eifel, SG-Siebengebirge, WW-Westerwald, VG-Vogelsberg, RH-Rhön. TM-Taunus Mountains, MB-Mainzer Becken, SH-Sprendlinger Horst, OW-Odenwald.

I followed two main objectives in the study of the Tertiary Hocheifel volcanism. 1) I determined the age of the individual Tertiary Hocheifel volcanic occurrences using the $^{40}\text{Ar}/^{39}\text{Ar}$ dating technique. 2) I have analysed the major and trace elements, as well as the Sr, Nd and Pb isotopic compositions of the Hocheifel lavas. These data represent the basis for the geochemical and isotopic characterisation of the Tertiary Hocheifel magmas, for an estimation of the melt-generation conditions and for identification of the source components involved in the Hocheifel magmas. This study was extended to Tertiary volcanic rocks from the Upper Rhine Graben area in order to

determine the possible relationship between the Hocheifel and the Upper Rhine Graben volcanism which is thought to be related to lithospheric extension. By establishing a chronology of the Hocheifel volcanism and by comparing the isotopic and geochemical characteristics of the Hocheifel lavas with those of the other CEVP lavas, I tried to decipher the origin of the Hocheifel magmas and to evaluate whether they are related to the Eifel plume activity or to extension.

2.2 - Ko'olau volcano, Oahu, Hawaii

Ko'olau volcano is located on the Oahu Island, Hawaii in the Pacific ocean (Fig. 1, Fig. 9). Hawaiian Islands represent one of the most actively studied hot-spot occurrences on Earth. The alignment of volcanoes records the movement of the Pacific plate over the Hawaiian mantle plume. Composition of magma which erupts on the oceanic floor above the hot-spot reveals the geochemical signature of the mantle plume below. As the Pacific plate moves over the hot-spot, Hawaiian volcanoes evolve through four stages of volcanic activity: pre-shield, shield, post-shield and rejuvenated stage (Fig. 10) (Clague and Dalrymple, 1987). The alkalic preshield stage is usually not seen because it is buried under the shield stage. Loihi would represent this first evolution step. Most of the volcano's volume is erupted during the tholeiitic shield stage which is followed by the postshield alkalic stage. The volcanic activity stops for 0.25-2.5 Ma before the rejuvenated stage takes place to produce small volumes of silica poor lavas. The changes in the chemical composition of the mantle plume are expressed in the compositional variations of erupting lavas. Thus, a study of the geochemical and isotopic evolution of a single Hawaiian volcano can reveal crucial information about the evolution of the Hawaiian mantle plume.

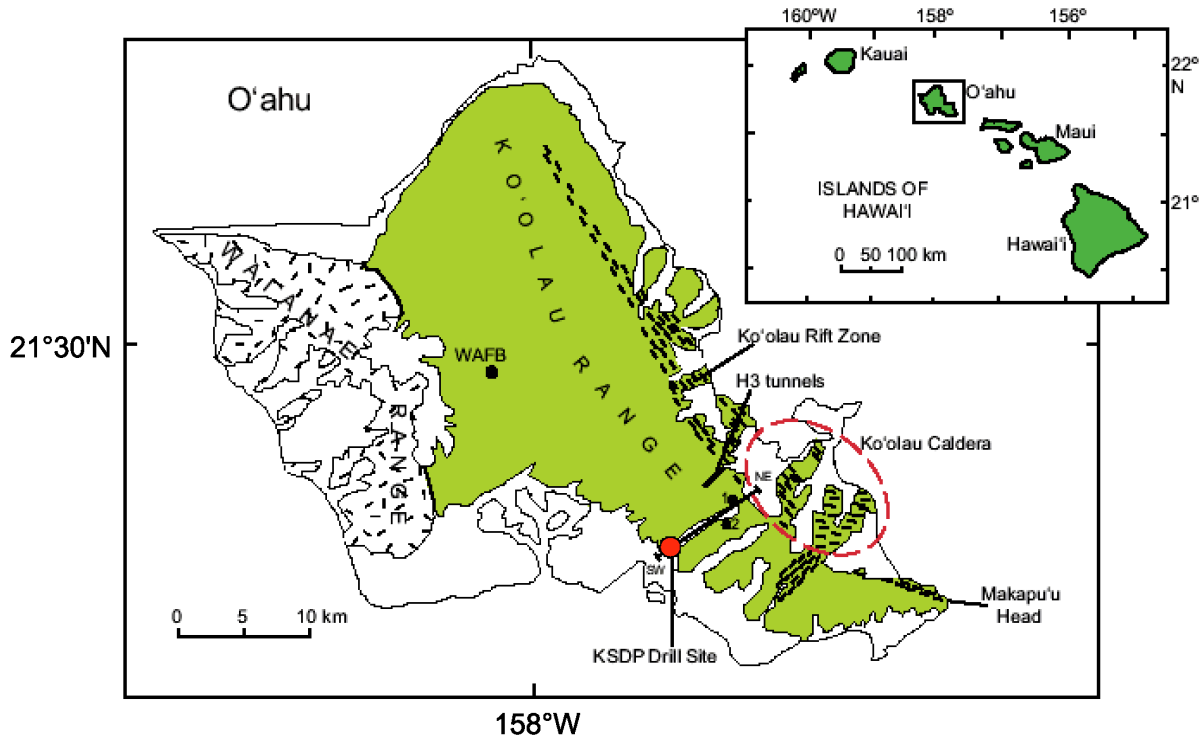


Figure 9: Location of the Ko'olau volcano on the Oahu Island, Hawaii. Red dot indicates the location of the Ko'olau Scientific Drilling Project (KSDP) site. Figure from Haskins (2002) (Haskins, 2002)

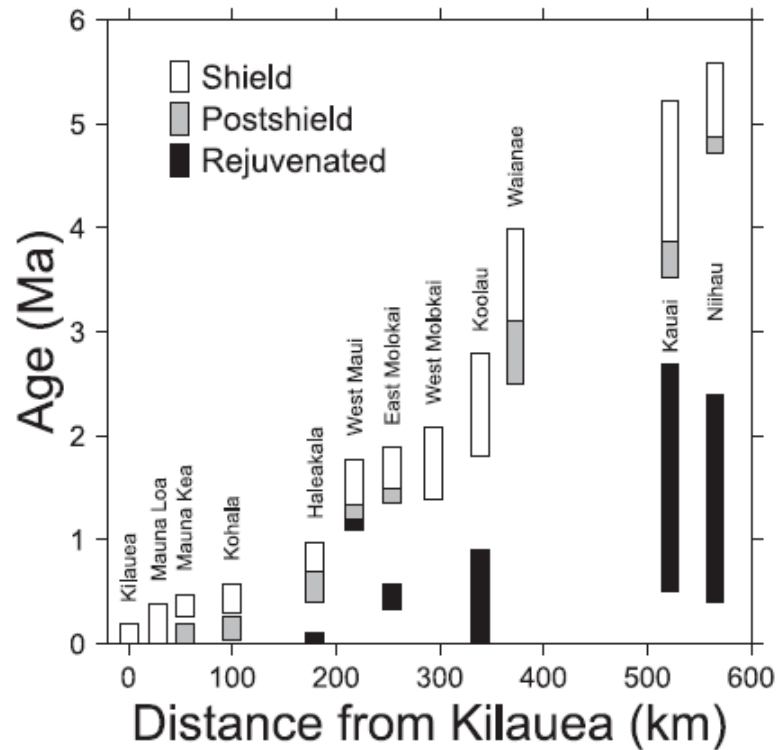


Figure 10: K-Ar age ranges of the last three volcanic stages of 12 Hawaiian volcanoes as a function of the distance of the Kilauea. From (Ribe and Christensen, 1999).

The main goal of my project was to analyse the Pb isotopic compositions of the different evolutionary stages of Ko'olau using the Pb triple spike technique to correct for instrumental mass fractionation (Galer, 1999). The high precision Pb isotopic compositions obtain by this technique, together with the Sr and Nd isotopic compositions, have been used to evaluate the compositional changes within Ko'olau lavas. The objective of this study was to decipher changes within the Hawaiian mantle plume. In this report I will present the methods used in this study, the results of this work, and the conclusions that were drawn. Finally, I will present potential projects for future investigations.

3 - Contribution to this thesis

The results of my three-years work brought me to write three manuscripts. Two of them will be submitted to a scientific book, which summarizes the results of the Hocheifel volcanism project funded by Deutsche Forschungsgemeinschaft (DFG). The third manuscript (Ko'olau project) will be submitted to a scientific journal. These three manuscripts contain detailed presentation of the studied areas, collected samples and used methods of investigation as well as the results and conclusions which have arisen from the studies. In this report I will present the three publications, in the following order:

1/ Fekiacova, Z; Mertz, D., Renne, P.: Geodynamic setting of the Tertiary Hocheifel Volcanism (Germany), Part I: $^{40}\text{Ar}/^{39}\text{Ar}$ dating.

This manuscript is submitted to: Ritter, J. and Christensen, U. (Eds), *Mantle Plumes: A Multidisciplinary Approach*.

2/ Fekiacova, Z and Mertz, D.: Geodynamic setting of the Tertiary Hocheifel Volcanism (Germany), Part II: Geochemistry and Sr, Nd and Pb isotopic compositions.

This manuscript will be submitted to: Ritter, J. and Christensen, U. (Eds), *Mantle Plumes: A Multidisciplinary Approach*.

3/ Fekiacova, Z and Abouchami, W.: Evolution of the Pb isotopic compositions of Ko'olau volcano, Oahu, Hawaii.

This manuscript will be submitted to *Earth and Planetary Science Letters*

References

- Bassi, G., C. E. Keen and P. Potter (1993). Contrasting styles of rifting: Models and examples from the eastern Canadian margin. Tectonics **12**: 639-655.
- Ben Othman, D., W. M. White and J. Patchett (1989). The geochemistry of marine sediments, island arc magma genesis, and crust-mantle recycling. Earth Planet. Sci. Lett. **94**: 1-21.
- Braun, J. and C. Beaumont (1989). Dynamical models of the role of crustal shear zones in asymmetric continental extension. Earth Planet. Sci. Lett. **93**: 405-423.
- Chase, C. G. (1981). Oceanic island Pb: two stage histories and mantle evolution. Earth Planet. Sci. Lett. **52**: 277-284.
- Chauvel, C., A. W. Hofmann and P. Vidal (1992). HIMU-EM: the French Polynesian connection. Earth Planet. Sci. Lett. **110**: 99-119.
- Christensen, U. R. (1992). An Eulerian technique for thermomechanical modeling of lithospheric extension. J. Geoph. Res. **97**: 2015-2036.
- Clague, D. A. and G. B. Dalrymple (1987). The Hawaiian-Emperor volcanic chain. Part I, Geologic evolution. Volcanism in Hawaii. P. H. Stauffer: 5-73.
- Cloetingh, S. A. P. L. and M. J. R. Wortel (1988). On the mechanics of the plate boundary formation. Mathematical Geophysics. S. A. P. L. Cloetingh, D. Reidel: 363-287.
- DePaolo, D. J., J. B. Bryce, A. Dodson, D. L. Shuster and M. B. Kennedy (2001). Isotopic evolution of Mauna Loa and the chemical structure of the Hawaiian plume. Geochem. Geophys. Geosyst. **2**.
- DePaolo, D. J. and E. M. Stolper (1996). Models of Hawaiian volcano growth and plume structure: Implications of results from Hawaiian Scientific Drilling Project. J. Geoph. Res. **101**: 11,643-11,654.
- Dunbar, J. A. and D. S. Sawyer (1989b). Patterns of continental extension along the conjugate margins of the central and North Atlantic Oceans and Labrador Sea. Tectonics **8**: 1059-1077.
- Eaton, G. P. (1979). A plate-tectonic model for late Cenozoic crustal spreading in the western United States. Rio Grande Rift: Tectonics and Magmatism. R. E. Riecker. Washington, D. C., AGU: 1-12.
- Eisele, J., M. Sharma, S. J. G. Galer, J. Blichert-Toft, C. W. Devey and A. W. Hofmann (2002). The role of sediment recycling in EM-1 inferred from Os, Pb, Hf, Nd, Sr isotope and trace element systematics of the Pitcairn hotspot. Earth Planet. Sci. Lett. **196**: 197-212.
- Fekiacova, Z., D. F. Mertz and P. R. Renne (submit.). Geodynamic setting of the Tertiary Hoheifel volcanism (Germany), Part I: $^{40}\text{Ar}/^{39}\text{Ar}$ dating. Mantle plumes - A multidisciplinary approach. U. R. Christensen, Springer Verlag.
- Forsyth, D. and S. Uyeda (1975). On the relative importance of the driving forces of plate motion. Geophys. J. R. Astron. Soc. **43**: 163-200.
- Galer, S. J. G. (1999). Optimal double and triple spiking for high precision lead isotopic measurements. Chem. Geol. **157**: 255-274.
- Griffiths, R. and I. Campbell (1991). Interaction of mantle plume heads with the Earth's surface and onset of small-scale convection. J. Geoph. Res. **96**: 18,295-18,310.

- Gripp, A. E. and R. G. Gordon (2002). Young tracks of hotspots and current plate velocities. Geophys. J. Int. **150**: 321-361.
- Hanan, B. B. and D. W. Graham (1996). Lead and Helium isotope evidence from oceanic basalts for a common deep source of mantle plumes. Science **272**(991-995).
- Harry, D. L. and D. S. Sawyer (1992). Basaltic volcanism, mantle plumes, and the mechanics of rifting: The Parana flood basalt province of South America. Geology **20**: 207-210.
- Hart, S. (1988). Heterogeneous mantle domains: signatures, genesis and mixing chronologies. Earth Planet. Sci. Lett. **90**: 273-296.
- Hart, S., E. H. Hauri, L. A. Oschmann and J. A. Whitehead (1992). Mantle Plumes and Entrainment: Isotopic Evidence. Science **256**: 517-520.
- Haskins, E. H. (2002). Core drilling of Ko'olau volcano reveals a rapid change in shield-stage geochemistry: implications for compositional variability of the Hawaiian source, University of Hawaii.
- Hauri, E., J. A. Whitehead and S. Hart (1994). Fluid dynamic and geochemical aspects of entrainment in mantle plumes. J. Geoph. Res. **99**(B12): 24,275-24,300.
- Hawkesworth, C. J., M. S. M. Mantovani, P. N. Taylor and Z. Palacs (1986). Evidence from the Parana of South Brazil for a continental contribution to Dupal basalts. Nature **322**: 356-359.
- Hill, R. I. (1991). Starting plumes and continental breakup. Earth Planet. Sci. Lett. **104**: 398-416.
- Hofmann, A. W. (1988). Chemical differentiation of the Earth: the relationship between mantle, continental crust and oceanic crust. Earth Planet. Sci. Lett. **90**: 297-314.
- Hofmann, A. W. (1997). Mantle geochemistry: the message from oceanic volcanism. Nature **385**: 219-229.
- Hofmann, A. W. (2003). Sampling mantle heterogeneity through oceanic basalts: isotopes and trace elements. Treatise on Geochemistry, Elsevier. **2**: 61-1001.
- Hofmann, A. W. and W. M. White (1980). The role of subducted oceanic crust in mantle evolution. Carnegie Inst. Wash. Year Book **79**: 477-483.
- Hofmann, A. W. and W. M. White (1982). Mantle plumes from ancient oceanic crust. Earth Planet. Sci. Lett. **57**: 421-436.
- Houseman, G. and P. England (1986a). A dynamical model of lithosphere extension and sedimentary basin formation. J. Geoph. Res. **91**: 719-729.
- Houseman, G. and P. England (1986b). Finite strain calculations of continental deformation, 1, Method and general results for convergent zones. J. Geoph. Res. **91**: 3651-3663.
- Illies, J. H. (1981). Mechanism of graben formation. Tectonophysics **73**: 249-266.
- Ingersoll, R. V., W. Cavazza, W. S. Baldrige and M. Shafiqullah (1990). Cenozoic sedimentation and paleotectonics of north-central New Mexico: Implications for initiation and evolution of the Rio Grande rift. Geol. Soc. Am. Bull.
- Keen, C. E. (1985). The dynamics of rifting: deformation of the lithosphere by active and passive driving forces. Geophys. J. R. Astron. Soc. **80**: 95-120.
- Lister, G. S., M. A. Etheridge and P. A. Symonds (1991). Detachment models for the formation of passive continental margins. Tectonics **10**: 1038-1064.
- Logatchev, N. A., V. A. Rogozhina, V. P. Solonenko and Y. A. Zorin (1978). Deep structure and evolution of the Baikal rift zone. Tectonics and geophysics of continental rifts. E. R. Neumann. Norwell, Mass., D. Reidel: 49-62.

- Mahoney, J., C. Nicollet and C. Dupuy (1991). Madagascar basalts: tracking oceanic and continental sources. Earth Planet. Sci. Lett. **104**: 350-363.
- McKenzie, D. and M. J. Bickle (1988). The volume and composition of melt generated by extension of the lithosphere. J. Petrol. **29**: 625-679.
- McKenzie, D. and R. K. O'Nions (1983). Mantle reservoirs and ocean island basalts. Nature **301**: 229-231.
- Milner, S. C. and A. P. le Roex (1996). Isotope characteristics of the Okenyena igneous complex, northwestern Namibia: constraints on the composition of the early Tristan plume and the origin of the EM 1 mantle component. Earth Planet. Sci. Lett. **141**: 277-291.
- Moretti, I. and C. Froidevaux (1986). Thermomechanical models of active rifting. Tectonics **5**: 501-511.
- Morgan, W. J. (1972a). Plate motions and deep mantle convection. Geol. Soc. Am. Mem.: 7-22.
- Morgan, W. J. (1972b). Deep mantle convection plumes and plate motions. AAPG Bull. **56**(203-213).
- Olson, P., G. Schubert, C. Anderson and P. Goldman (1988). Plume formation and lithosphere erosion: A comparison of laboratory and numerical experiments. J. Geoph. Res. **93**: 15,065-15,084.
- Oxburgh, E. R. and D. L. Turcotte (1974). Membrane tectonics and the East African Rift. Earth Planet. Sci. Lett. **22**: 133-140.
- Parker, E. C., P. M. Davis, J. R. Evans, H. M. Iyer and K. H. Olson (1984). Upwarp of anomalous asthenosphere beneath the Rio Grande Rift. Nature **312**: 354-356.
- Plank, T. and C. H. Langmuir (1998). The chemical composition of subducting sediment and its consequences for the crust and mantle. Chem. Geol. **145**: 325-394.
- Rehkämper, M. and A. W. Hofmann (1997). Recycled ocean crust and sediment in Indian Ocean MORB. Earth Planet. Sci. Lett. **147**: 93-106.
- Ribe, N. M. and U. R. Christensen (1999). The dynamical origin of Hawaiian volcanism. Earth Planet. Sci. Lett. **171**: 517-531.
- Ritter, J. R. R., M. Jordan, U. R. Christensen and U. Achauer (2001). A mantle plume below the Eifel volcanic fields, Germany. Earth Planet. Sci. Lett. **186**: 7-14.
- Ruppel, C. (1995). Extensional processes in continental lithosphere. J. Geoph. Res. **100**(B12): 24,187-24,215.
- Sengör, A. M. C. and K. Burke (1978). Relative timing of rifting and volcanism on earth and its tectonic implications. Geoph. Res. Lett. **5**: 419-421.
- Spohn, T. and G. Schubert (1982). Convective thinning of the lithosphere: A mechanism for initiation of continental rifting. J. Geoph. Res. **87**: 4669-4681.
- Strecker, M. R., P. M. Blisniuk and G. H. Eisbacher (1990). Rotation of extension direction in the central Kenya rift. Geology **18**: 229-302.
- Tapponnier, P. and P. Molnar (1979). Active faulting and Cenozoic tectonics on the Tien Shan, Mongolia and Baikal regions. J. Geoph. Res. **84**: 3425-3459.
- Thompson, R. N. and M. B. Fowler (1986). Subduction-related shoshonitic and ultrapotassic magmatism: a study of Siluro-Ordovician syenites from the Scottish Caldonides. Contrib. Mineral. Petrol. **94**: 507-522.
- Turcotte, D. L. and S. H. Emermen (1983). Mechanism of active and passive rifting. Tectonophysics **94**: 39-50.

- Weaver, B. L. (1991). The origin of ocean island basalt end-member compositions: trace-element end isotopic constraints. Earth Planet. Sci. Lett. **104**: 381-397.
- Wendlandt, R. F. and P. Morgan (1982). Lithospheric thinning associated with rifting in East Africa. Nature **298**: 734-736.
- Westaway, R. (1993). Forces associated with mantle plumes. Earth Planet. Sci. Lett. **11c**: 331-348.
- White, W. M. (1985). Sources of oceanic basalts: radiogenic isotope evidence. Geology **13**: 115-118.
- White, W. M. and D. McKenzie (1989). Magmatism at rift zones: The generation of volcanic continental margins and flood basalts. J. Geoph. Res. **94**: 7685-7729.
- White, W. M., S. R. Spence, S. R. Fowler, D. P. McKenzie, G. K. Westbrook and A. N. Brown (1987b). Hatton Bank (northwest U.K) continental margin structure. Geophys. J. R. Astron. Soc. **89**: 265-272.
- Wilson, J. T. (1963). Evidence from islands on the spreading of ocean floors. Nature **197**: 536-538.
- Wilson, M. (1989). Igneous Petrogenesis. A global tectonic approach. Oxford, Chapman & Hall.
- Withjack, M. (1979). A convective heat transfer model for lithospheric thinning and crustal uplift. J. Geoph. Res. **84**(983-995).
- Workman, R. K., S. Hart, M. Jackson, M. Regelous, K. A. Farley, J. Bluzstajn, M. Kurz and H. Staudigel (2004). Recycled metasomatized lithosphere as the origin of the Enriched Mantle II (EM2) end-member: Evidence from the Samoan Volcanic Chain. Geochem. Geophys. Geosyst. **5**(4).
- Zindler, A. and S. Hart (1986). Chemical geodynamics. Ann. Rev. Earth Planet Sci. **14**: 493-571.
- Zorin, Y. A. (1981). The Baikal Rift: An example of the intrusion of asthenospheric material into the lithosphere as the cause of disruption of lithospheric plates. Tectonophysics **73**: 91-104.

Chapter 2

Fekiacova, Z., Mertz, D., Renne, P.: Geodynamic setting of the Tertiary Hocheifel Volcanism (Germany), Part I: $^{40}\text{Ar}/^{39}\text{Ar}$ dating.

This manuscript is submitted to: Ritter, J. and Christensen, U. (Eds), Mantle Plumes: A Multidisciplinary Approach.

**Geodynamic setting of the Tertiary Hoheifel volcanism (Germany),
Part I: $^{40}\text{Ar}/^{39}\text{Ar}$ dating**

by

Zuzana Fekiacova¹, Dieter F. Mertz^{1,2} and Paul R. Renne²

Abstract

The Eifel volcanism is part of the Cenozoic Central European Volcanic Province and is located close to Rhine and Leine Graben structures, which have been formed by rifting and subsidence since the Eocene. Whereas the Quaternary volcanism of the Eifel appears to be genetically related to mantle plume activity the cause of the Tertiary volcanism of the Hocheifel field is less clear. Here, we present geochronological evidence for the geotectonic setting of the Tertiary Eifel volcanism based on $^{40}\text{Ar}/^{39}\text{Ar}$ dating of 27 samples from 25 volcanic occurrences. Included are also samples from the northern Upper Rhine Graben in order to evaluate a possible relationship between Hocheifel volcanism and Rhine Graben taphrogenesis.

The geological relevance of the age data used for the geological discussion is indicated by plateau-type age spectra and tested by inverse isochron calculations. For the Hocheifel, two periods of activity at 43.6.0 to 39.0 Ma and 37.5 to 35.0 Ma were measured. Both age groups are represented by basanites as well as by more evolved rocks and there is no clear relation between age and chemical composition. The time span dated for the northernmost Upper Rhine Graben volcanism is 59 to 47 Ma indicating fooiditic to basanitic activity up to ca. 15 m.y. prior to the onset of rifting and subsidence.

The Hocheifel volcanism is interpreted to represent the propagation of the pre-rifting volcanism of the northern Upper Rhine Graben to the NW because Hocheifel volcanism closely follows in time pre-rifting northern Upper Rhine Graben volcanism, the older period of Hocheifel activity shows propagation of younger volcanism to the north and the Hocheifel tectonic pattern derived from the time - space relation of volcanism corresponds to stress field conditions identical to those of the Upper Rhine Graben at the time of Hocheifel volcanic activity. Magma generation therefore appears to be related to decompression by extension during Middle to Late Eocene. However, in contrast to the northern Upper Rhine Graben with graben formation subsequent to pre-rifting volcanism, no relevant rifting or subsidence occurred in the Hocheifel. The taphrogenetic evolution in between the Upper and Lower Rhine Graben regions got stuck in a very early stage.

1 Introduction

The Hocheifel volcanic field is located in the Hercynian Rhenish Massif in Germany (Figure 1) and consists of about 300 occurrences representing relics of Tertiary volcanism. To the East and West of the Hocheifel, the Quaternary Eifel volcanic fields border. The Eifel volcanism represents the westernmost site of the Central European Volcanic Province (CEVP), a generally W - E striking volcanic belt of Cenozoic age extending from West Germany to Poland.

The geodynamic setting of the Tertiary Hocheifel volcanism is not clear. The Eifel together with neighbouring volcanic fields of Siebengebirge, Westerwald and Vogelsberg (western part of CEVP) are located close to a Tertiary rift system (Figure 1). Therefore, on one hand magma generation by decompression melting related to lithospheric extension has been suggested (e.g. Wilson and Downes 1991; Ziegler 1992). On the other hand, there is seismic (e.g. Ritter, et al. 2001) combined with isotopic evidence (e.g. Hoernle, et al. 1995) that at least partly CEVP volcanism is related to mantle plume activity. The setting of the Eifel volcanism is in so far unique within the CEVP as there is Tertiary and Recent volcanic activity at more or less the same site. Thus, the evolution of volcanism over a long time span can be evaluated.

Aim of this contribution is to decipher the geodynamic setting of the Tertiary Hocheifel volcanism using geochronological, geochemical and isotope data. We present evidence from $^{40}\text{Ar}/^{39}\text{Ar}$ dating (Part I) as well as from major and trace element concentrations and Sr, Nd, Pb isotope ratios (Part II).

2 Geological setting and sampling

The Tertiary Hocheifel volcanic field together with the neighbouring volcanic fields of Siebengebirge, Westerwald, Vogelsberg and Rhön (Figure 1) represent the western part of the Cenozoic CEVP. These volcanic fields developed close to an extensive Central and West European Cenozoic rift system which originated in the Alpine foreland and which is interpreted as a result of tensional reactivation of originally Late Hercynian fractures (Ziegler 1992). The Hocheifel is situated within a complex triple junction-type constellation in between Upper Rhine Graben, Lower Rhine Graben and Leine Graben representing a central part of the Cenozoic rift

system (Figure 1). In addition to the Hocheifel volcanic rocks we collected samples from the northern Upper Rhine Graben flanks in order to evaluate a possible relationship between Hocheifel volcanism and Rhine Graben taphrogenesis during the Tertiary. Table 1 lists the grid coordinates of the Hocheifel and Rheingraben sampling locations.

The Hocheifel volcanism is formed by about 300 volcanic occurrences spread over ~1000 km² in between the Quaternary West and East Eifel volcanic fields and produced mostly more primitive alkali basaltic rocks and fewer differentiated lavas. A systematic compositional zoning within the Tertiary Hocheifel field has been suggested with the most differentiated lavas erupting in the centre and the less evolved lavas mostly occurring in the outer region (Huckenholz 1983). The Hocheifel lavas mostly intruded weakly metamorphosed Devonian and Carboniferous sediments of the Hercynian Rhenish Massif. Major tectonic elements of parts of the Hocheifel area were mapped by, e.g., Fuchs (Fuchs 1974). Figure 2 shows that NE striking host rock syncline and anticline structures are cut by N striking cross faults. These faults are interpreted as being of late Hercynian age with later reactivation since locally Tertiary intrusions appear to have used the faults as pathways. The basaltic to trachytic samples taken for our Hocheifel study cover the complete range of chemical compositions known from this region. Also, various geographic areas were sampled with emphasis on the centre of the Hocheifel field with major volcanic activity around the village of Kelberg. This sampling pattern is shown in Figure 2. Informations on the geology of several of these occurrences as well as on their petrography and geochemistry are given in Huckenholz & Büchel (Huckenholz and Büchel 1988) together with further references.

Foiditic to basaltic rocks were taken from three geological units forming the northernmost Upper Rhine Graben flanks (Figure 1): Taunus Mountains (weakly metamorphic rocks of the Hercynian Rhenish Massif), Spredlingen Horst (Paleozoic metamorphic and magmatic basement with Rotliegend sediment cover) and Mainz Basin (Tertiary sediments). (Negendank 1969) describes occurrences and petrography of Tertiary volcanic rocks of the northern Upper Rhine Graben.

3 Sample preparation and analytical method

For sample preparation fresh hand specimen were selected by thin section microscopy. Altered domains manifested by olivine phenocrysts with iddingsite rims and fracture fillings were removed. 2 -3 kg fresh rock material of each sample was crushed into pieces < 5mm using a hydraulic press and aliquots were prepared. Further crushing and sieving yield different grain size fractions in the range < 1mm. They were rinsed with tap water and dried down in an oven, at a temperature of ca. 60 °C. The fractions 250 – 355 mm and 355 – 500 mm were used for $^{40}\text{Ar}/^{39}\text{Ar}$ dating. For producing magnetic ground mass and phenocryst (sanidine, plagioclase, amphibole) dating separates an isodynamic Frantz magnetic separator was used. We checked each of our ground mass separates through binocular microscope hand picking in order to ensure that there is no contamination by xenolithic material. Microprobe analyses on selected ground mass separates show that plagioclase containing some mol-% orthoclase mostly represent a relevant component.

$^{40}\text{Ar}/^{39}\text{Ar}$ analysis samples were loaded in Cu foil packages and irradiated in the cadmium shielded port (CLICIT) at the Triga reactor at University of Oregon and analyzed at Berkeley Geochronology Center. Values of J (a measure of neutron dosage) were determined from the mean of 12 single-crystal laser fusion analyses of co-irradiated Fish Canyon sanidine based on an age of 28.02 Ma (Renne, et al. 1998). Corrections for interfering nucleogenic isotopes of Ar were determined from analyses of irradiated CaF_2 and a synthetic K-bearing glass (KFeSiO_4) using the values given by Renne (Renne 1995). The samples were baked out at ca. 200 °C for about 12 hours prior to analysis and heated incrementally with a CO_2 laser by up to 24 degassing steps for each sample. Extraction line operation, including sample heating, is fully automated. Blanks for the extraction line were measured and blank correction was applied as described by Sharp et al. (Sharp, et al. 1996). Reactive components, such as H_2O , CO_2 , CO , and N_2 , were removed from the sample gas in two sequential stages using SAES GP-50 Zr-Al getters operated at 400°C. The purified gas was analyzed using a Mass Analyser Products 215-50 mass spectrometer, configured for a resolution of 450. Mass discrimination was determined from repeated analyses of air Ar using an on-line pipette, yielding a mean value of $1.0058 \pm 0.0012/\text{a.m.u.}$ during the course of this study. The decay constants and isotopic ratios used are those given by Steiger and Jäger (Steiger and

Jäger 1977). Uncertainties for ages are given at the 2 σ level and include errors arising from irradiation and Ar analysis but do not include errors in decay constants or isotopic abundances of K and atmospheric Ar.

4 Results

The $^{40}\text{Ar}/^{39}\text{Ar}$ incremental heating technique results on volcanic rocks from 19 occurrences of the Hocheifel and from 6 occurrences of the northern Upper Rhine Graben are presented in Table 2. Figures 3 a-d show the corresponding age spectra. Principally, there are three types of age spectra: 1) flat spectra forming age plateau matching the criteria given by Fleck et al. (Fleck, et al. 1977), 2) flat spectra forming age plateau with step ages scattering slightly more than allowed by the Fleck et al. (1977) definition, 3) discordant spectra.

Type 1 age spectra are represented by mineral as well as ground mass separates. Figure 3 a indicates the type 1 minerals comprising trachyte from Reimerath (sanidine plateau age = 40.1 ± 0.3 Ma), basanite from Vogelsherdchen (sanidine/plagioclase plateau age = 35.2 ± 0.3 Ma) as well as latites from Quiddelbach and Bocksberg (amphibole plateau ages = 37.0 ± 0.3 and 39.7 ± 0.3 Ma, respectively). Figure 3 b indicates the type 1 ground masses comprising basanites from Hoch-Bermel, Staufskopf, Bad Neuenahr Berg, Hohe Acht, Kopp, Nürburg, Rabenkopf, Stetteritz and Forstberg (plateau ages = 35.9 ± 0.3 , 37.0 ± 0.3 , 35.2 ± 0.3 , 36.3 ± 0.3 , 35.9 ± 0.3 , 35.0 ± 0.3 Ma, 58.7 ± 0.4 Ma, 48.7 ± 0.2 Ma and 47.2 ± 0.3 Ma, respectively), hawaiiite from Steimelskopf (plateau age = 37.5 ± 0.3 Ma) and latite from Quiddelbach (plateau age = 37.0 ± 0.3 Ma). Plateau and integrated ages of the mineral separates are identical within analytical error in each case. The ground mass separates also yield identical plateau and integrated ages or show minor deviation up to ca. 4%. A duplicate analysis on the Reimerath trachyte (Figure 3 a) yield identical sanidine plateau ages of 40.1 ± 0.3 Ma for separates #33239-01 and #33239-02, respectively, indicating that our results are reproducible and thus analytically significant. Also, amphibole and ground mass separates prepared from the Quiddelbach latite yield identical plateau ages of 37.0 ± 0.3 and 37.1 ± 0.3 Ma, respectively. This concordance in addition shows that mineral as well as ground mass plateau ages can be regarded as geologically meaningful.

Type 2 age spectra (Figure 3 c) are represented by ground masses comprising basalt from Scharfer Kopf (forced plateau age = 37.0 ± 1.1 Ma) and basanites from Reifferscheid, Nollenbachtal, Steineberger Ley, Kastelberg and Forst (forced plateau ages = 39.0 ± 0.6 , 41.9 ± 1.0 , 35.2 ± 0.5 , 37.3 ± 0.7 Ma and 50.6 ± 0.4 Ma, respectively). „Forced“ means that the plateau ages are calculated accepting 3s instead of 2s for the confidence interval of the $^{40}\text{Ar}_{\text{rad}}/^{39}\text{Ar}_{\text{K}}$ ratios of the plateau steps. Forced plateau ages and integrated ages are identical within analytical errors given, except for the Steineberger Ley, Kastelberg and Forst basanites with a maximum deviation up to ca. 7%. In most cases, the forced plateau is related to high-temperature degassing steps, which are correlated with relatively low Cl/K and high Ca/K ratios (Figure 3 c). This indicates that during high-temperature degassing most probably Ar from groundmass plagioclase is released predominantly. In contrast, the forced plateau of the Kastelberg and Steineberger Ley basanites are related to low-temperature or medium-temperature degassing, respectively, comprising step ages with relatively low Ca/K ratios. The Ar released most likely preferentially comes from groundmass nepheline (high Cl/K) in case of Kastelberg and from groundmass K-feldspar (low Cl/K) in case of Steineberger Ley. Since volcanic feldspars as well as nepheline are regarded as suitable Ar chronometer, we consider the outlined relation between degassing temperature, step age and geochemical composition as additional evidence that the forced plateau ages are geologically meaningful. Type 2 age spectrum shapes indicate minor disturbances of the Ar isotope system, however, we suggest that these disturbances do not affect the determination of the geological age significantly. We conclude that the forced plateau age is the best available date for the age of these lavas.

Type 3 age spectra (Figure 3 d) are represented by ground masses comprising basanites from Barsberg, Rote Heck, Hörkopf and Steinbuckel (integrated ages = 33.8 ± 0.3 Ma, 35.8 ± 0.3 Ma, 54.5 ± 0.3 Ma and 47.3 ± 0.2 Ma, respectively). The shapes of the spectra reflect relevant disturbances of the Ar isotope system probably largely caused by Ar redistribution related to recoil effects during neutron irradiation. Assuming that there is no ^{39}Ar loss caused by recoil, the integrated ages can be regarded as a good approximation to the geological age. However, such an estimate does not consider that there could in addition be geologically caused disturbances of the

Ar isotope system, e.g., Ar loss by alteration. Because of these uncertainties we do not include the type 3 age spectra in the geological discussion.

All samples were evaluated by inverse isochron calculations. In each case, the calculated isochrons define trapped $^{40}\text{Ar}/^{36}\text{Ar}$ ratios identical within analytical errors with or lower than the atmospheric ratio of 295.5. Since no initial $^{40}\text{Ar}/^{36}\text{Ar}$ ratio > 295.5 was detected, we conclude that no excess Ar is related to the samples measured. In order to demonstrate typical results on samples regarded to yield geological meaningful ages, Figure 4 shows inverse isochrons calculated on samples of age spectrum type 1 (minerals: sanidine Reimerath trachyte, sanidine/plagioclase Vogelsherdchen basanite, amphibole Bocksberg basanite; ground mass Quiddelbach latite) and type 2 (ground mass Reifferscheid basanite). The $^{40}\text{Ar}/^{36}\text{Ar}$ intercepts of 289 ± 19 for the sanidine, of 296 ± 3 for the sanidine/plagioclase separate and of 298 ± 7 for the amphibole are atmospheric. The $^{40}\text{Ar}/^{36}\text{Ar}$ intercepts of the ground masses are slightly lower than atmospheric with 289 ± 3 for the Reifferscheid basanite or substantially lower with 240 ± 5 for the Quiddelbach latite, which could be caused by fractionated Ar (e.g. Lippolt, et al. 1990). However, for both occurrences isochron ages (38.9 ± 0.3 Ma and 37.5 ± 0.3 Ma, respectively) and plateau ages (39.0 ± 0.4 Ma and 37.1 ± 0.3 Ma, respectively) are identical. Therefore, it appears that the lower-than-atmospheric intercepts are not a significant source of error in K-Ar dating for the Tertiary Hocheifel samples.

Summarizing, we interpret the plateau and forced plateau ages to represent geologically meaningful ages of the lavas dated.

5 Discussion

5.1 Comparison with conventional K-Ar ages

Several of the occurrences we measured by the $^{40}\text{Ar}/^{39}\text{Ar}$ incremental heating technique were dated previously using the conventional K-Ar method (Cantarel and Lippolt 1977; Horn, et al. 1972; Lippolt and Fuhrmann 1980; Müller-Sohnius, et al. 1989). Table 1 compares the $^{40}\text{Ar}/^{39}\text{Ar}$ plateau ages regarded to be geologically significant with conventional K-Ar ages on total rock, mineral or mineral mixture separates. Eight out of 14 occurrences show either up to ca. 20% younger or up to ca. 7% older conventional K-Ar total rock ages compared to $^{40}\text{Ar}/^{39}\text{Ar}$

groundmass, amphibole or sanidine plateau ages. This discrepancy can be explained by Ar loss or excess Ar related to the younger or the older total rock separates, respectively. For example, Lippolt et al. (Lippolt, et al. 1976) have argued that Tertiary total rocks from Sprenndlingen Horst and Odenwald (Northern Upper Rhine Graben) volcanic occurrences are affected by Ar loss, because they yield up to 20% younger K-Ar ages than separates of minerals regarded to be Ar retentive and therefore suitable for K-Ar dating. Also, excess Ar contamination is a known feature of phonolitic, foiditic and alkaline volcanic rocks from the Quarternary Eifel (e.g. Fuhrmann and Lippolt 1986; Fuhrmann and Lippolt 1987) or from Tertiary fields (Rittmann and Lippolt 1998) of the western CEVP. Generally, our data confirm the results of Lippolt et al. (1976). Therefore, we conclude that total rock conventional K-Ar ages published from CEVP volcanic fields can give an order-of-magnitude sense of the geological age, however, they are not useful for high-precision geochronology purposes.

Six occurrences show identical conventional total rock K-Ar and $^{40}\text{Ar}/^{39}\text{Ar}$ plateau ages considering analytical error. In these cases, the total rocks contain negligible rock or mineral components with insufficient Ar retentivity or with excess Ar. As an example, the total rock separate from the location Reimerath represents a trachytic composition and the Ar measured on the total rock most likely almost exclusively originates from sanidine. This leads to a concordance between the $^{40}\text{Ar}/^{39}\text{Ar}$ sanidine plateau age and the K-Ar total rock age of 40.1 ± 0.3 and 40.1 ± 1.1 Ma, respectively. However, there are no criteria in order to decide whether a K-Ar total rock separate yield a geologically meaningful age, especially if Ar-retentive minerals are not an essential component of the separate.

For the sample locations Kastelberg and Steineberger Ley the K-Ar ages on feldspar and nepheline mineral mixture separates are up to ca. 15% higher than the corresponding $^{40}\text{Ar}/^{39}\text{Ar}$ groundmass plateau. This discordance is in so far unusual as volcanic feldspars are commonly suitable K-Ar chronometer. In addition, for the Steineberger Ley $^{40}\text{Ar}/^{39}\text{Ar}$ ground mass separate from petrography and the distribution of Ar-derived K, Ca and Cl during degassing we conclude that the Ar of the plateau steps mainly originates from ground mass K-feldspar. Conventional K-Ar and $^{40}\text{Ar}/^{39}\text{Ar}$ ages are consequently measured on mineralogically similar material from the

same occurrence. A suitable approach in order to explain the higher K-Ar ages would be to measure the mineral separate ages using the $^{40}\text{Ar}/^{39}\text{Ar}$ technique so that possible disturbances of the Ar isotope system can be identified. Until then, we suggest to treat the high conventional K-Ar ages with care.

In contrast to the feldspar and nepheline separates, all conventional K-Ar ages on amphiboles are identical with the $^{40}\text{Ar}/^{39}\text{Ar}$ plateau ages within analytical error, which is larger by a factor of 2 to 3 for the K-Ar ages. Based on the age concordance, we consider the K-Ar amphibole ages to be geologically significant and we therefore use the published data (Müller-Sohnius, et al. 1989) in our geological discussion.

The samples showing disturbed $^{40}\text{Ar}/^{39}\text{Ar}$ age spectra yield integrated $^{40}\text{Ar}/^{39}\text{Ar}$ ages up to 28% older than the corresponding conventional K-Ar total rock ages (locations Barsberg, Am Hörkopf, Traisa). Since the inverse isochron calculations give no indication of excess Ar and assuming that the age spectrum disturbances are mainly caused by Ar isotope redistribution from recoil, than the conventional K-Ar total rock ages appear to be affected by Ar loss.

5.2 Hocheifel age distribution and relation to tectonics

The evaluation of the Tertiary Hocheifel volcanism is based on 22 age determinations, comprising the $^{40}\text{Ar}/^{39}\text{Ar}$ ages presented in Table 1 and 4 conventional K-Ar amphibole ages from Müller-Sohnius et al. (Müller-Sohnius, et al. 1989). There is a younger age group ranging from 35.0 to 37.5 Ma and an older broader age group ranging from 39.0 to 43.6 Ma, which show a maximum of volcanic activity at ca. 40 Ma. Using the time scale of Bergren et al. (Bergren, et al. 1995) with the boundary Middle Eocene/Late Eocene defined at 37 Ma most of the volcanic activity of the younger phase is of Late Eocene age, whereas the older phase is of Middle Eocene age. Published Oligocene (< 34 Ma) conventional K-Ar ages by comparison with $^{40}\text{Ar}/^{39}\text{Ar}$ ages turned out to be geologically not meaningful and in fact of Eocene age (Table 1). However, since our data set represent a random test volcanism younger than Eocene can not definitively ruled out for the Tertiary Hocheifel.

There is no clear relation between age and chemical composition. Both age groups are represented by less evolved basanites as well as by more evolved rocks (hawaiite, shoshonite, latite, trachyte). However, basanites are the youngest rocks with a maximum of volcanic activity at 35 to 36 Ma, whereas the more evolved rocks show maxima at ca. 37 Ma and 40 Ma.

The volcanism represented by the older age group generally becomes younger from south to north (Figure 5 a). Volcanic activity propagated from occurrence Hillscheid at 43.6 Ma via Nollenbachtal at ca. 42 Ma and Darscheid, Brinkenkopf as well as Reimerath at ca. 40 Ma to Nürburg as well as Reifferscheid at ca. 39 Ma, resulting in a fast average propagation velocity of 6.7 mm/a. For the distribution of the volcanism of the younger age group no systematic pattern with geography can be identified (Figure 5 b).

Defining tectonic lineaments by connecting occurrences with identical ages indicate discrete pathways for magma ascent active during phases at ca. 40, 39, 38-36 and 35 Ma (Figure 5 c). These lineaments form a pattern which corresponds to the stress field derived for the Upper Rhine Graben for the time span ca. 40 - 35 Ma (e.g. Schumacher 2002) with NNE - SSW compression and ESE - WNW extension. In this case, the ESE striking lineaments represent transform zones between NNE striking extension zones. The N-S faults mapped by Fuchs (Fuchs 1974) appear to be steep dextrale strike-slip faults.

5.3 Relation to Upper Rhine Graben Taphrogenesis

The volcanic rocks measured from the northern Upper Rhine Graben (47 - 59 Ma, early Middle Eocene to middle Late Paleocene) are older than those from the Hocheifel. Initial Upper Rhine Graben rifting and starting subsidence is derived from composition and succession of lacustrine sediments from the basis of the Rhine Graben trough (e.g. Sittler 1969) for the time since Middle to late Middle Eocene (< ca. 45 Ma). Therefore, for the northern Upper Rhine Graben region (Sprendlingen Horst, Taunus Mountains, Mainz Basin) the major volcanic phase occurred prior to the onset of rifting. In contrast, the most intense Upper Rhine Graben formation in the north with major subsidence and rifting in the Early Oligocene, if at all appears to be accompanied only by sporadic volcanism (Mertz, et al. 2004) Although there are more suitable

conditions for magma generation and ascent by decompression and pathway formation during the phase of extensive rifting compared to pre-rifting times, at least intrusions fail to come.

The Hocheifel volcanism closely follows in time the pre-rifting volcanism of the northern Upper Rhine Graben and the older Hocheifel volcanic phase shows propagation of younger volcanism to the north. Also, the Hocheifel tectonic pattern derived from the time - space relation of the volcanism corresponds to the stress field of the Upper Rhine Graben at that time. These indications suggest that in terms of geodynamic setting the Hocheifel volcanism is the northwestern propagation of the pre-rifting volcanism of the northern Upper Rhine Graben. However, in contrast to the Upper Rhine Graben, no relevant rifting or subsidence occurred subsequent to volcanic activity so that the taphrogenetic evolution in between the Upper and Lower Rhine Graben regions appears to got stuck in a very early stage.

5.4 Relation to neighbouring Tertiary volcanism

For the neighbouring western part CEVP volcanic fields to the NE or E (Siebengebirge, Westerwald, Vogelsberg, Rhön) of the Hocheifel (Figure 1), several of the available geochronological data are conventional total rock K-Ar ages. These ages are not suitable for high-precision geochronology as outlined above, however, together with published conventional mineral K-Ar ages and few $^{40}\text{Ar}/^{39}\text{Ar}$ ages, enable at least a useful first approach-type discussion.

For the Siebengebirge volcanism conventional K-Ar ages on sanidine, biotite and total rock yield an age range 26 - 22 Ma (Todt and Lippolt 1980). Conventional K-Ar ages on feldspar, hornblende and total rock from the Westerwald indicate major volcanic activity between ca. 28 and 17 Ma as well as volcanism at ca. 6 Ma and in the range < 1Ma (Lippolt and Todt 1978). For the Rhön, based on conventional total rock K-Ar ages, Lippolt (Lippolt 1982; Lippolt and Todt 1978) suggested a major older phase at 26 – 18 Ma and a subordinate younger phase of activity at 14 – 11 Ma. $^{40}\text{Ar}/^{39}\text{Ar}$ plateau ages on groundmass and plagioclase-enriched separates yield an age range of 14.8 - 16.3 Ma for the Main trap tholeiites (Fuhrmann and Lippolt 1987), which are located few tens of km south of the Vogelsberg volcanic field and are thought to be genetically related with the Vogelsberg volcanism. $^{40}\text{Ar}/^{39}\text{Ar}$ spectra on ground masses from the Vogelsberg

volcanic centre show disturbances of the Ar isotope system (Bogaard and Wörner 2003), however, their integrated ages at ca. 17 and 15 Ma confirm the age range indicated by the Main trap tholeiites.

The Hocheifel volcanism was active from ca. 44 - 35 Ma subsequent to pre-rifting > 47 Ma old volcanism of the northern Upper Rhine Graben flanks. Siebengebirge, Westerwald and Rhön major volcanic activity occurred to a large extent contemporaneously within the time span ca. 28 - 17 Ma (Late Oligocene - Early Miocene) followed by Vogelsberg volcanism at about 17-15 Ma. Except of the pre-rifting volcanism related to the northern Upper Rhine Graben, the Hocheifel volcanism represents the oldest volcanism within the western part of the Cenozoic CEVP. Based on the compilation of geochronological data by Lippolt (Lippolt 1983) this appears also to be the case considering the volcanic fields of the eastern part of the CEVP. There are Eocene conventional K-Ar ages from the east CEVP Heldburg dyke swarm. However, these ages are possibly caused by excess Ar (Lippolt 1983) and therefore appear not to be geologically meaningful. Although the Hocheifel as the oldest volcanic centre also represents the westernmost field of the CEVP, no systematic time - space relation regarding the distribution of volcanism can be derived based on the available data. This confirms the conclusion of Lippolt (Lippolt 1982) that hotspot-type activity is unlikely for the CEVP. The overlap in time for volcanic activity of Siebengebirge, Westerwald and Rhön could indicate similar tectonic setting and cause of volcanism. Since the Hocheifel activity is substantially older, the tectonic setting of these neighbouring CEVP fields does not need to be comparable to that suggested for the Hocheifel.

6 Conclusions

Based on the $^{40}\text{Ar}/^{39}\text{Ar}$ dating technique with incremental heating two periods of activity of Hocheifel volcanism from 43.6.0 to 39.0 Ma and 37.5 to 35.0 Ma were measured. There is no clear relation between age and chemical composition. Both age groups are represented by less evolved basanites as well as by more evolved rocks (hawaiite, shoshonite, latite, trachyte). However, basanites are the youngest rocks with a maximum of volcanic activity at 35 to 36 Ma, whereas the

more evolved rocks show maxima at ca. 37 Ma and 40 Ma. The northern Upper Rhine Graben samples yield a period of foiditic to basanitic activity from 59 to 47 Ma.

The geological relevance of the age data used to define these periods is indicated by plateau-type age spectra as well as inverse isochron calculations showing that there are no age-significant disturbances of the Ar isotope system. Discrepancy between $^{40}\text{Ar}/^{39}\text{Ar}$ plateau ages and previously determined conventional total rock K-Ar ages confirm that the conventional K-Ar ages can be affected by excess Ar or loss of Ar and are therefore considered of only limited use for high-precision geochronology.

The northern Upper Rhine Graben foiditic to basanitic volcanism started up to ca. 15 m.y. prior to initial rifting and onset of subsidence derived from Rhine Graben trough sediments. In contrast, the most intense phase of Upper Rhine Graben formation in the north with major subsidence and rifting in the Early Oligocene, if at all appears to be accompanied only by sporadic volcanism. Although there are more suitable conditions for magma generation and ascent by decompression and pathway formation during the phase of extensive rifting compared to pre-rifting times, at least intrusions fail to come.

In terms of geodynamic setting of the Hocheifel activity we suggest that it represents the northwestern propagation of the pre-rifting volcanism of the northern Upper Rhine Graben based on the following indications: a) The Hocheifel volcanism closely follows in time the pre-rifting volcanism of the northern Upper Rhine Graben. b) The older period of Hocheifel activity shows propagation of younger volcanism to the north. c) The Hocheifel tectonic pattern derived from the time - space relation of the volcanism corresponds to stress field conditions identical to those of the Upper Rhine Graben at the time of Hocheifel volcanic activity.

Thus, a plausible cause for the generation of the Hocheifel magmas is decompression related to Middle to Late Eocene extension processes. In contrast to the Upper and Lower Rhine Graben, however, no relevant rifting or subsidence occurred subsequent to volcanic activity indicating that the taphrogenetic evolution in between the Upper and Lower Rhine Graben regions got stuck in a very early stage.

7 Acknowledgement

We thank I. van der Zander for support with sampling. This project was funded by the Deutsche Forschungsgemeinschaft (DFG, Bonn) via grant Me 1155/4-1 to D.F.M.

References

- Bergren WA, Kent DV, Aubry M-P, Hardenbol J (1995) Geochronology, Time Scales, and Global Stratigraphic Correlation. In: Mineralogists SoEPa (ed), Special Publication No. 54. pp 95-126
- Bogaard PJF, Wörner G (2003) Petrogenesis of basanitic to tholeiitic volcanic rocks from the Miocene Vogelsberg, Central Germany. *J. Petrol.* 44(3):569 - 602
- Cantarel P, Lippolt HJ (1977) Alter und Abfolge des Vulkanismus der Hocheifel. *Neues Jahrb. Geol. Paläontol. Monatsh.* 10:600-612
- Fleck RJ, Sutter JF, Elliot DH (1977) Interpretation of discordant $^{40}\text{Ar}/^{39}\text{Ar}$ age spectra of Mesozoic tholeiites from Antarctica. *Geochem. Cosmochim. Acta* 41:15-32
- Fuchs G (1974) Das Unterdevon am Ostrand der Eifeler Nord-süd-Zone. *Beitr. Naturkd. Forsch. Südwestdtshl. Beih.* 3:3-163
- Fuhrmann U, Lippolt HJ (1986) Excess argon and dating of Quaternary Eifel volcanism. II. Phonolithic and foiditic rocks near Rieden. *N. Jb. Geol. Paläont. Abh.* 172(1):1-19
- Fuhrmann U, Lippolt HJ (1987) Excess argon and dating of Quaternary Eifel volcanism: III. Alkali basaltic rocks of the Central West Eifel/FR Germany. *N. Jb. Geol. Paläont. Mh.* 4:213-236
- Hoernle K, Zhang YS, Graham D (1995) Seismic and geochemical evidence for large-scale mantle upwelling beneath the eastern Atlantic and western and central Europe. *Nature* 374(2):34-39
- Horn P, Lippolt HJ, Todt W (1972) Kalium-Argon-Alterbestimmungen an tertiären Vulkaniten des Oberrheingrabens I. *Gesamtgesteinsalter. Ecl. geol. Helv.* 65(1):131-156
- Huckenholz HG (1983) Tertiary volcanism of the Hocheifel area. In: Fuchs K, von Gehlen, K., Mälzer, H., Murawski, H., Semmel, A. (ed) *Plateau Uplift - Rhenish Shield - A case History*, vol. Springer Verlag, Berlin, pp 121-128
- Huckenholz HG, Büchel G (1988) Tertiären Vulkanismus der Hocheifel. *Fortschr. Miner.* 66:43-82
- Lippolt HJ (1982) K/Ar Age Determinations and the Correlation of Tertiary Volcanic Activity in Central Europe. *Geol. Jb.* D52:113-135
- Lippolt HJ (1983) Distribution of volcanic activity in space and time. In: Fuchs K, von Gehlen, K., Mälzer, H., Murawski, H., Semmel, A. (ed) *Plateau uplift - Rhenish Shield - A case history*, Spinger Verlag, Berlin, pp 112-120
- Lippolt HJ, Fuhrmann U (1980) Vulkanismus der Nordeifel: Datierung von Gang- und Schlotbasalten. *Aufschluss* 31:540-547
- Lippolt HJ, Horn P, Todt W (1976) Kalium-Argon-Alter von Mineralien und Einschlüssen der Basalt-Vorkommen Katzenbuckel und Roßberg. *N. Jb. Miner., Abh.* 127(3):242-260
- Lippolt HJ, Todt W (1978) Isotopische Alterbestimmungen an Vulkaniten des Westerwaldes. *N. Jahrbuch. Geol. Paläontol. Abh.*:332-352
- Lippolt HJ, Troesch M, Hess JC (1990) Excess argon and dating of Quaternary Eifel volcanism, IV. Common argon with high and lower-than-atmospheric $^{40}\text{Ar}/^{39}\text{Ar}$ ratios in phonolithic rocks, East Eifel, F.R.G. *Earth Planet. Sci. Letters* 101:19-33
- Mertz DF, Fekiacova Z, Renne PR (2004) A major volcanic pulse at 47-49 Ma triggered origin of Eocene Sprenglingen Horst (Germany) fossil deposits. *Courier Forschungsinstitut Senckenberg* 218, in press
- Müller-Sohnius D, Horn P, Huckenholz HG (1989) Kalium-Argon-Datierungen an tertiären Vulkaniten der Hocheifel. *Chem. Erde* 49:119-136

- Negendank J (1969) Beschreibung einiger tertiärer Alkali-Basalte im nördlichen Oberrheingraben. Notizbl. hess. L.-Amt Bodenforsch. 97:283-295
- Renne PR (1995) Excess ^{40}Ar in biotite and hornblende from the Noril'sk 1 intrusion: Implications for the age of the Siberian Traps. *Earth Planet. Sci. Letters* 131:165-176
- Renne PR, Swisher CC, Deino AL, Karner DB, Owens TL, DePaolo DJ (1998) Intercalibration of standards, absolute ages and uncertainties in $^{40}\text{Ar}/^{39}\text{Ar}$ dating. *Chem. Geol.* 145:117-152
- Ritter JRR, Jordan M, Christensen UR, Achauer U (2001) A mantle plume below the Eifel volcanic fields, Germany. *Earth Planet. Sci. Lett.* 186:7-14
- Rittmann U, Lippolt HJ (1998) Evidence for distortion of Tertiary K/Ar ages by excess argon-example given by three alkali olivine basalts from Northern Hesse, Germany. *Eur. J. Mineral* 10:95-110
- Schumacher ME (2002) Upper Rhine Graben: Role of preexisting structures during rift evolution. *Tectonics* 21(NO. 1):1-17
- Sharp WD, Turrin BD, Renne PR, Lanphere MA (1996) $^{40}\text{Ar}/^{39}\text{Ar}$ and K/Ar dating of lavas from the Hilo 1-km core hole, Hawaii Scientific Drilling Project. *J. Geophys. Res. B, Solid Earth and Planets* 101(5):607-611,616
- Sittler C (1969) The sedimentary trough of the Rhine Graben. *Tectonophysics* 8:543-560
- Steiger RH, Jäger E (1977) Subcommittee on geochronology: Convention on the use of decay constants in geo- and cosmochronology. *Earth Planet. Sci. Lett.* 36:359-3692
- Todt W, Lippolt HJ (1980) K-Ar- Age Determinations on Tertiary Volcanic Rocks: V. Siebengebirge und Siebengebirgs-Graben. *J. Geophysics* 48:8-23
- Wilson M, Downes H (1991) Tertiary-Quaternary extension related alkaline magmatism in Western and Central Europe. *J.petro.* 32:811-849
- Ziegler PA (1992) European Cenozoic rift system. *Tectonophysics* 208:91-111

Figure captions

Figure 1: Tectonic setting of Cenozoic volcanic fields (WE=West Eifel, EE=East Eifel, WW=Westerwald, VG=Vogelsberg, RH=Rhön) close to the Tertiary Upper Rhine Graben-Lower Rhine Graben-Leine Graben rift system. Inset “Hocheifel“ refers to the map in Figures 2 and 5. The northwestern and northeastern flanks of the northern Upper Rhine Graben are formed by the geological units of Mainz Basin (MB), Taunus Mountains (TM), Sprenzligen Horst (SH) and Odenwald (OW).

Figure 2: Hocheifel sampling locations. Tectonic elements are taken from the geological map of Fuchs (1974). For geographic orientation the villages of Reifferscheid, Kelberg, Ulmen and Daun are shown.

Figure 3: $^{40}\text{Ar}/^{39}\text{Ar}$ age spectra showing incremental heating results on mineral plateau (a), ground mass plateau (b), ground mass forced plateau (c) and disturbed spectra (d). Subscript f in (c) indicates forced plateau.

Figure 4: Inverse isochrons calculated on selected samples representing different age spectrum types with $^{40}\text{Ar}/^{39}\text{Ar}$ ages regarded to be geologically meaningful.

Figure 5: Hocheifel volcanic pulses based on $^{40}\text{Ar}/^{39}\text{Ar}$ ages of this work together with conventional K-Ar ages on amphibole from literature and their spatial distribution. (a) shows the older phase of activity, (b) the older together with the younger phase of activity and (c) the relation between space – time distribution of volcanism and tectonic pattern. Filled and open arrows of stress field symbol in (c) represent directions of compression and extension, respectively. Greyed lines are tectonic lineaments derived from the distribution of contemporaneous volcanic activity indicating distinct pathways for magma ascent at discrete times of magma production.

Appendix

Figures and tables

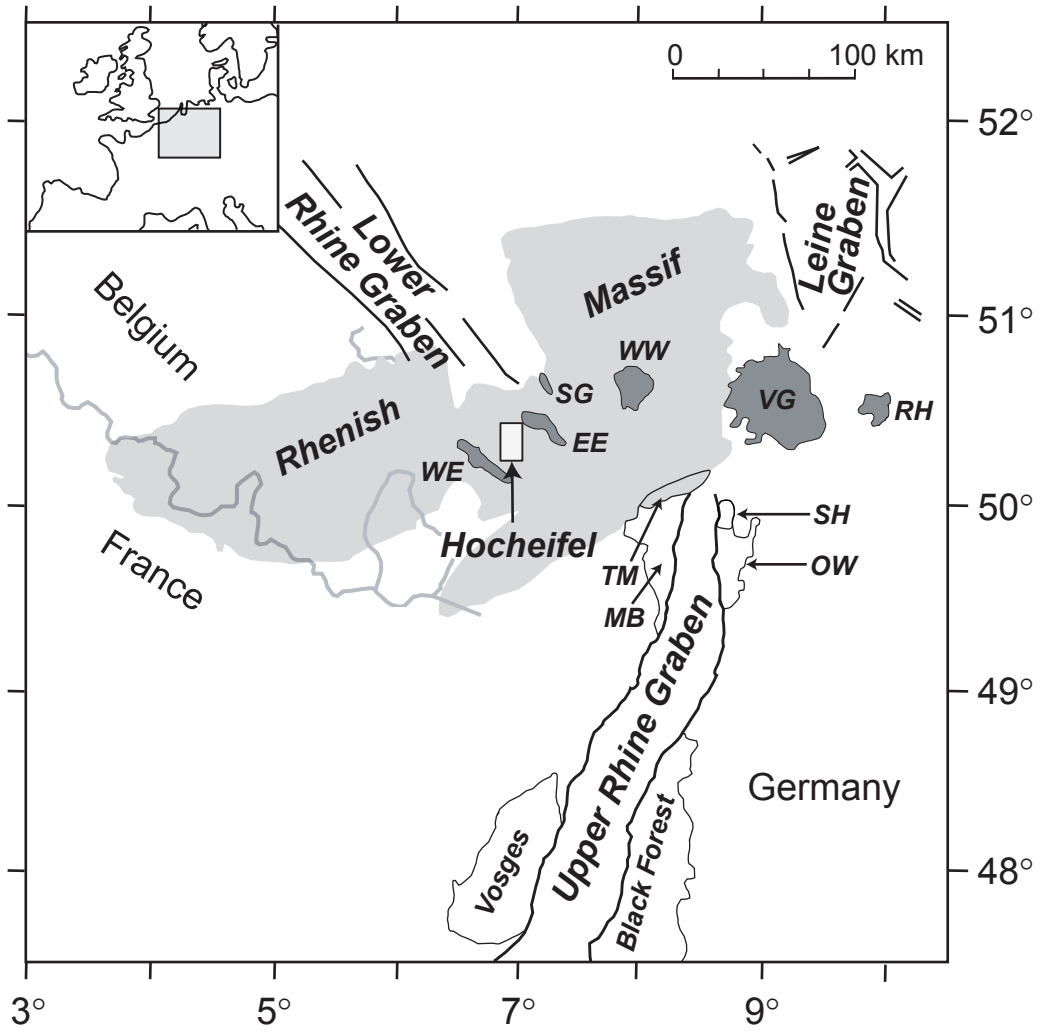


Figure 1

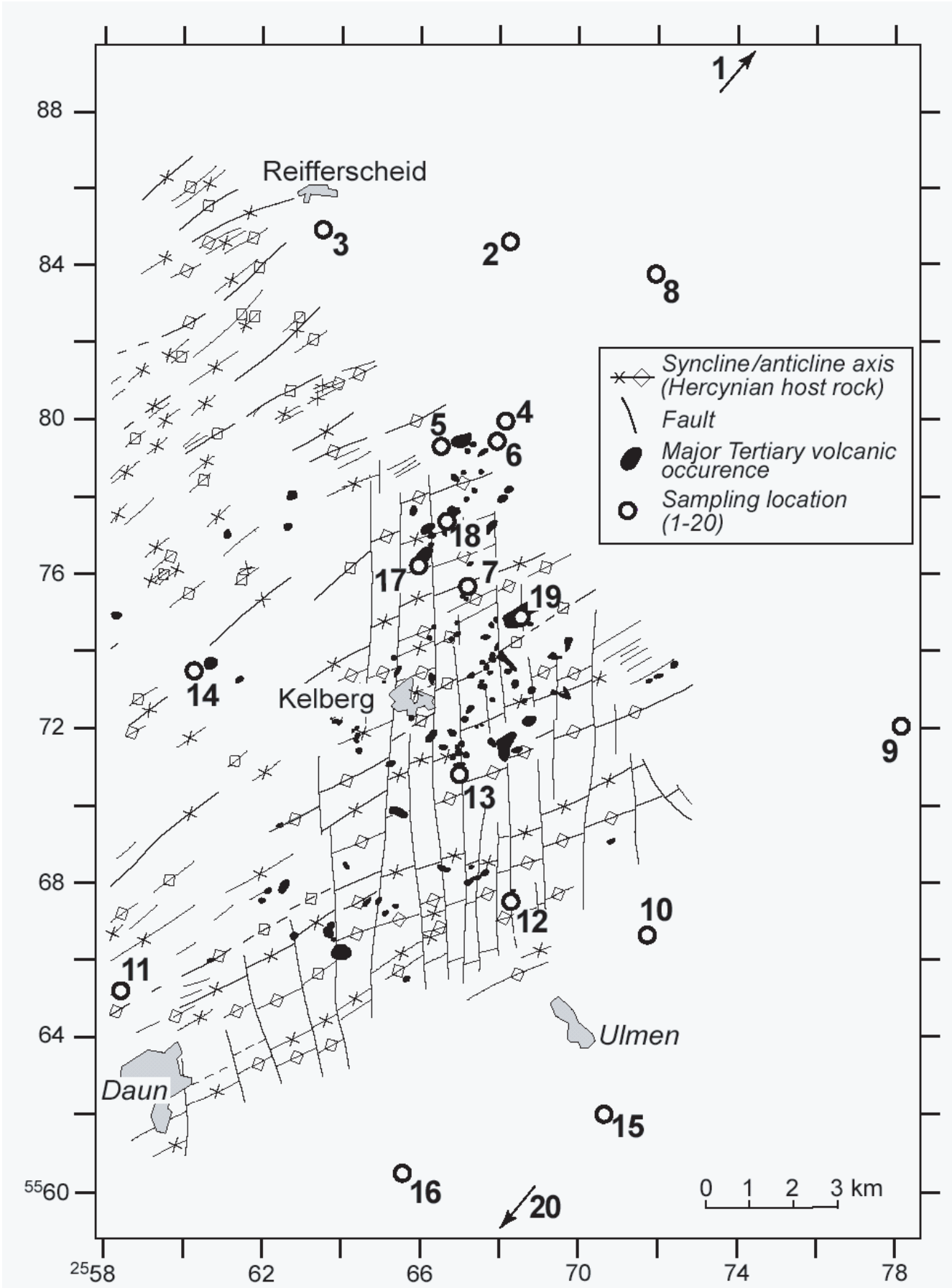


Figure 2

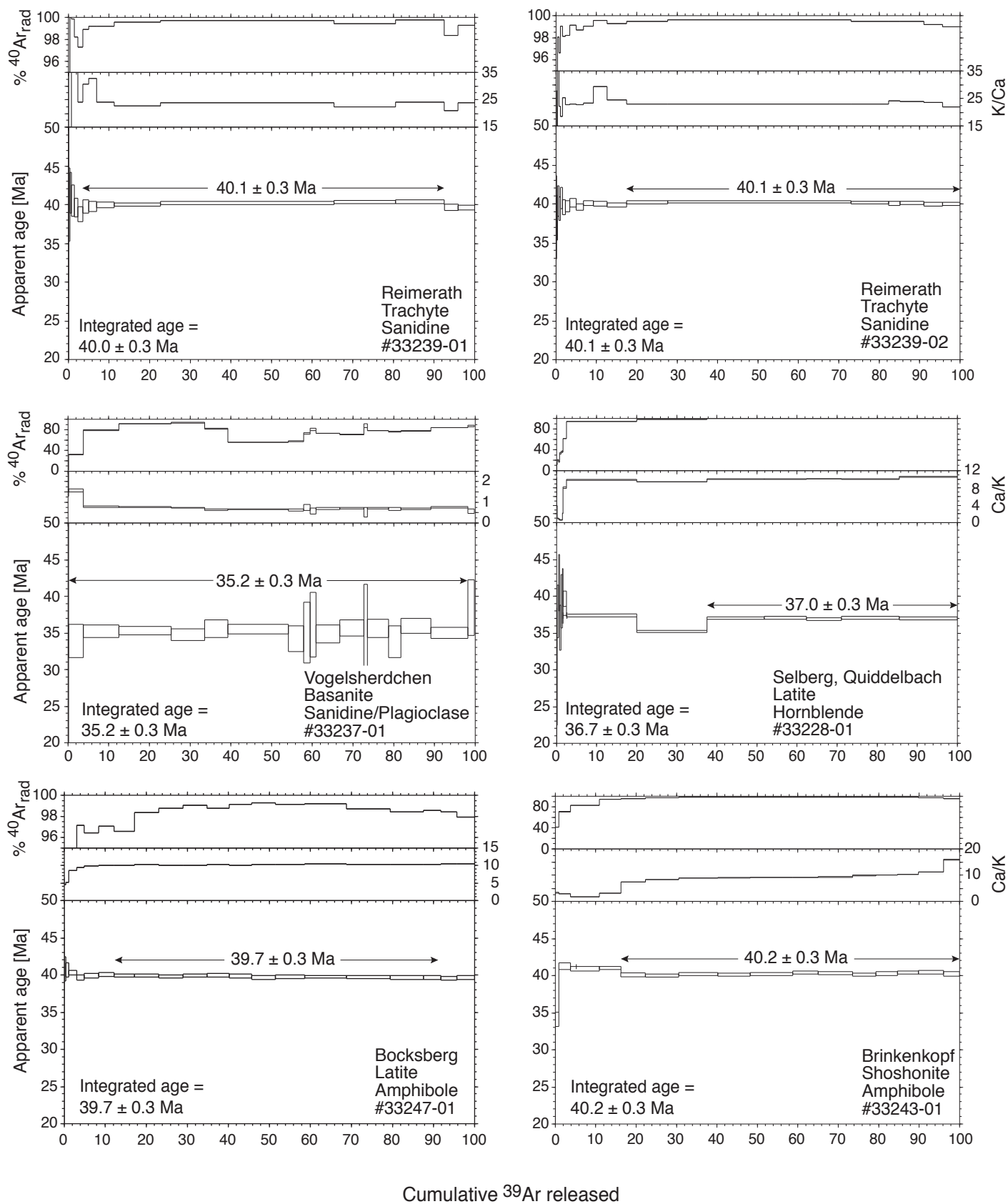


Figure 3a

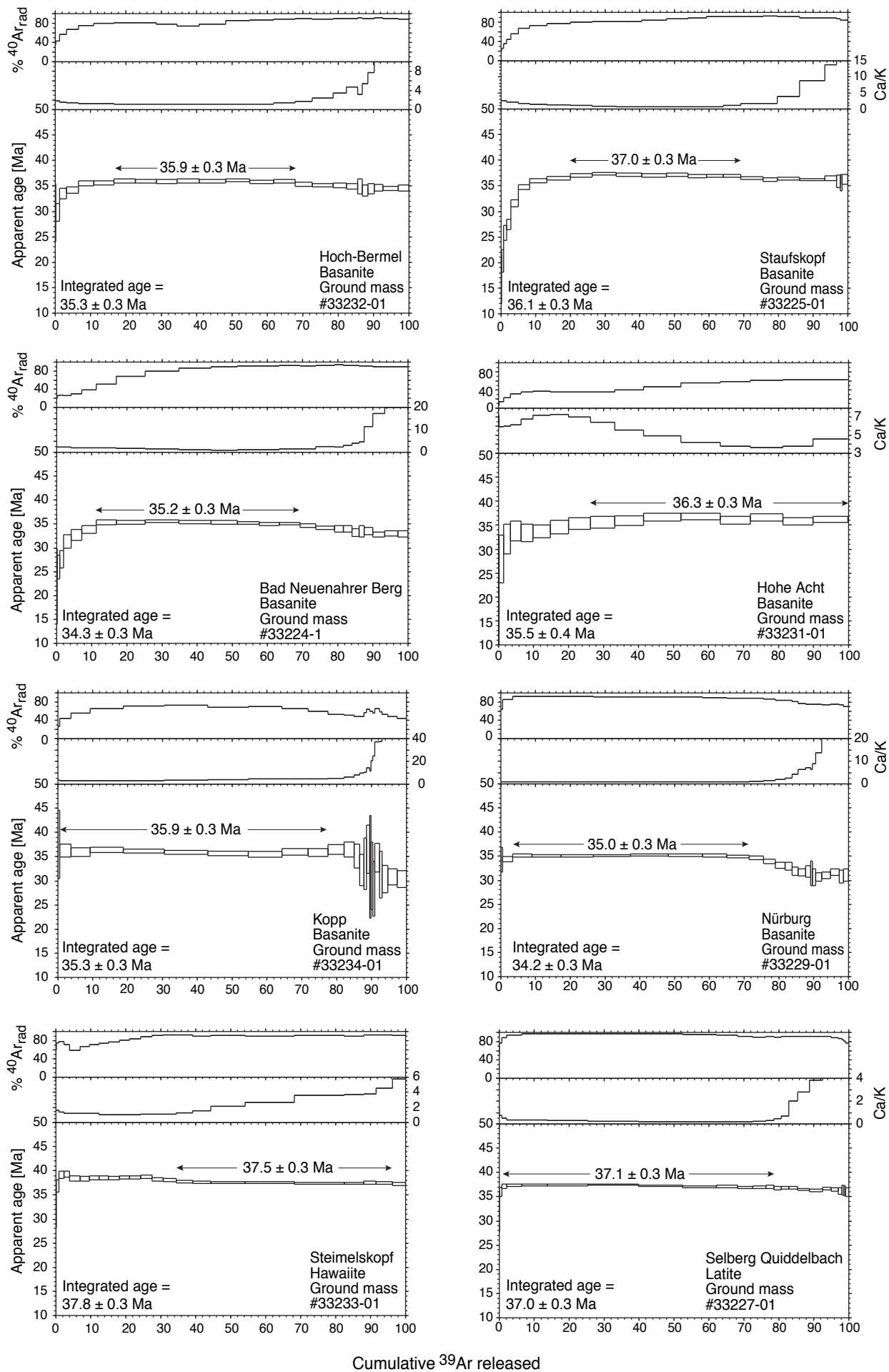
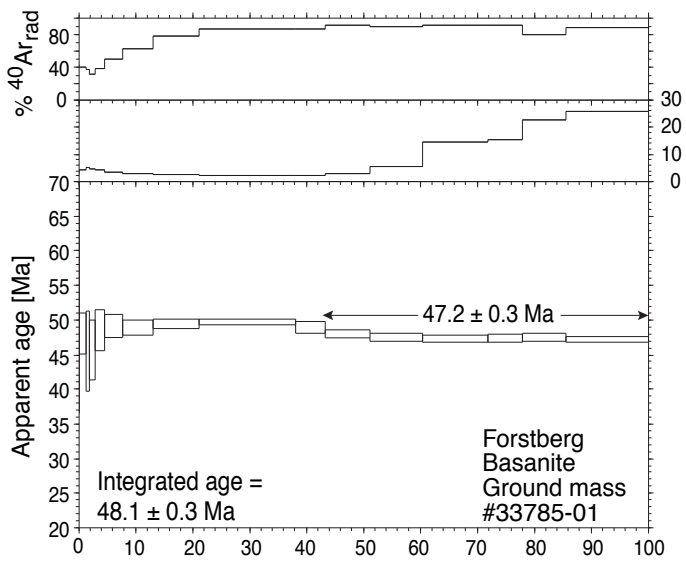
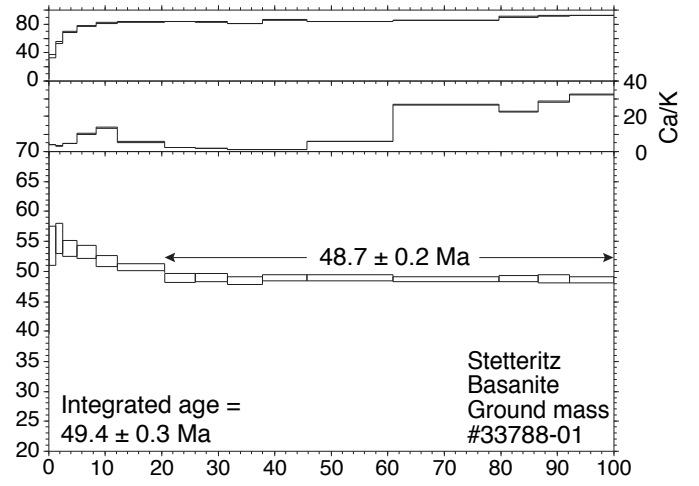
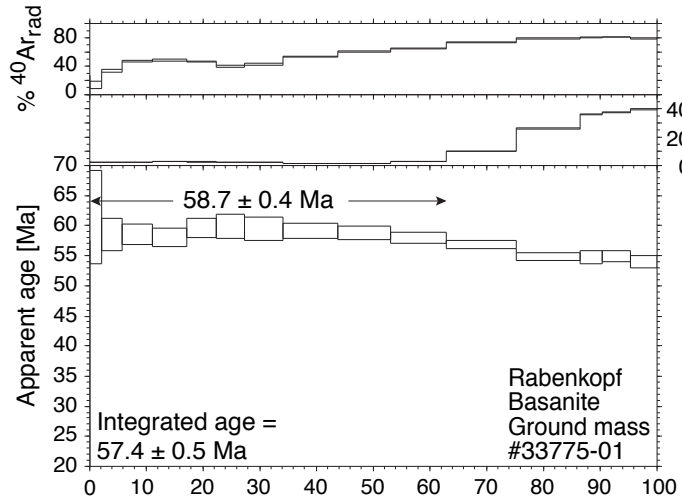


Figure 3b-1



Cumulative ^{39}Ar released

Figure 3b-2

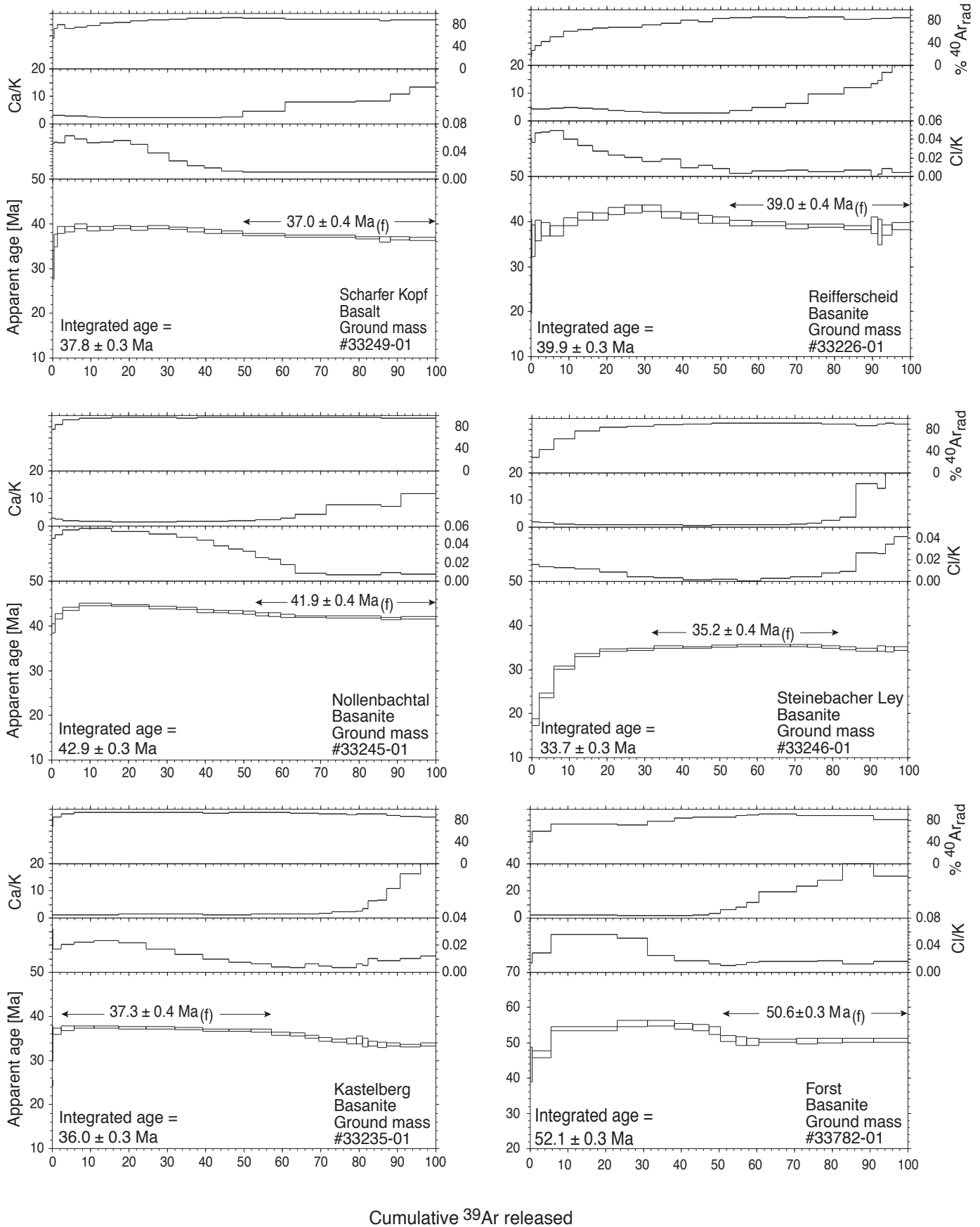


Figure 3c

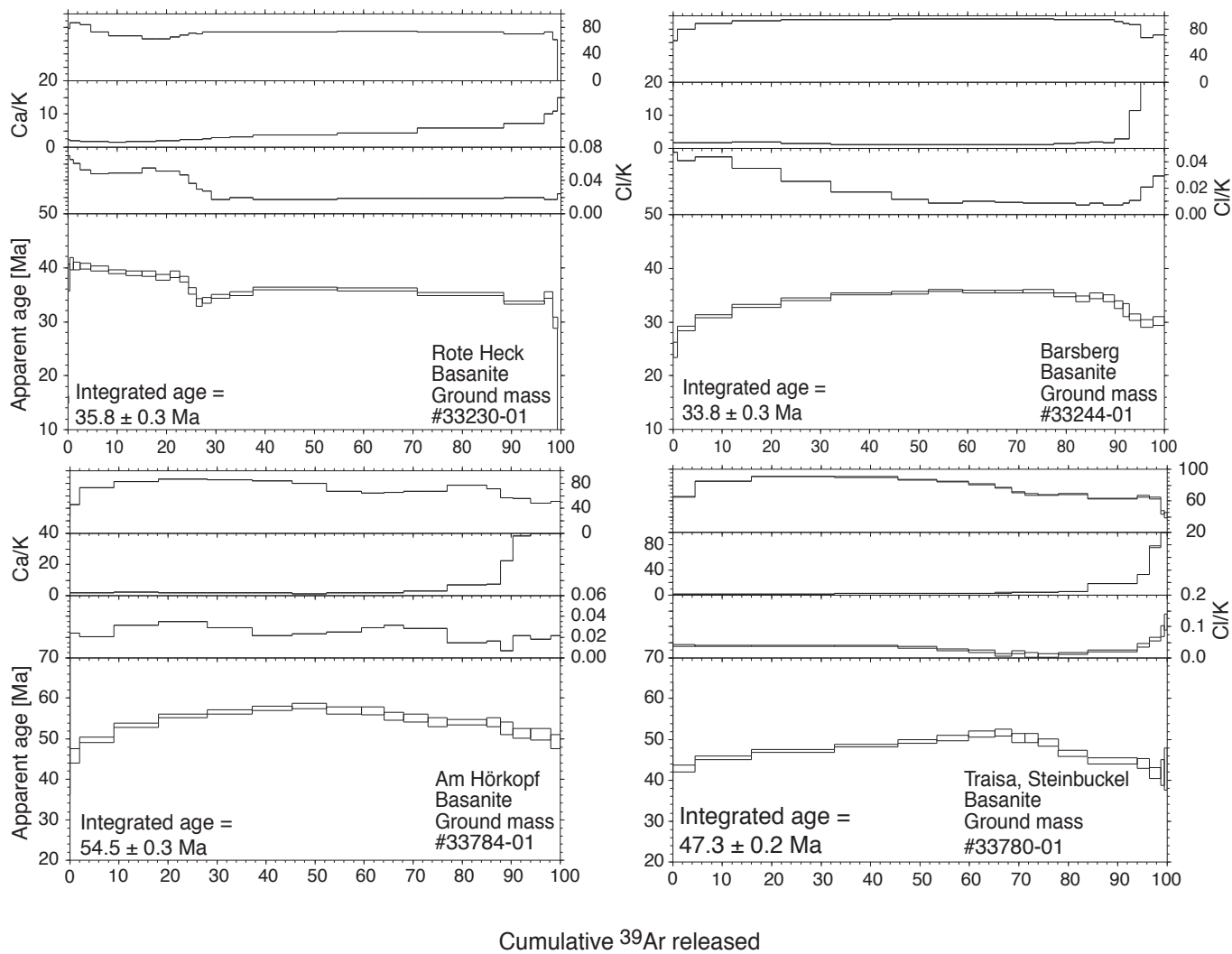


Figure 3d

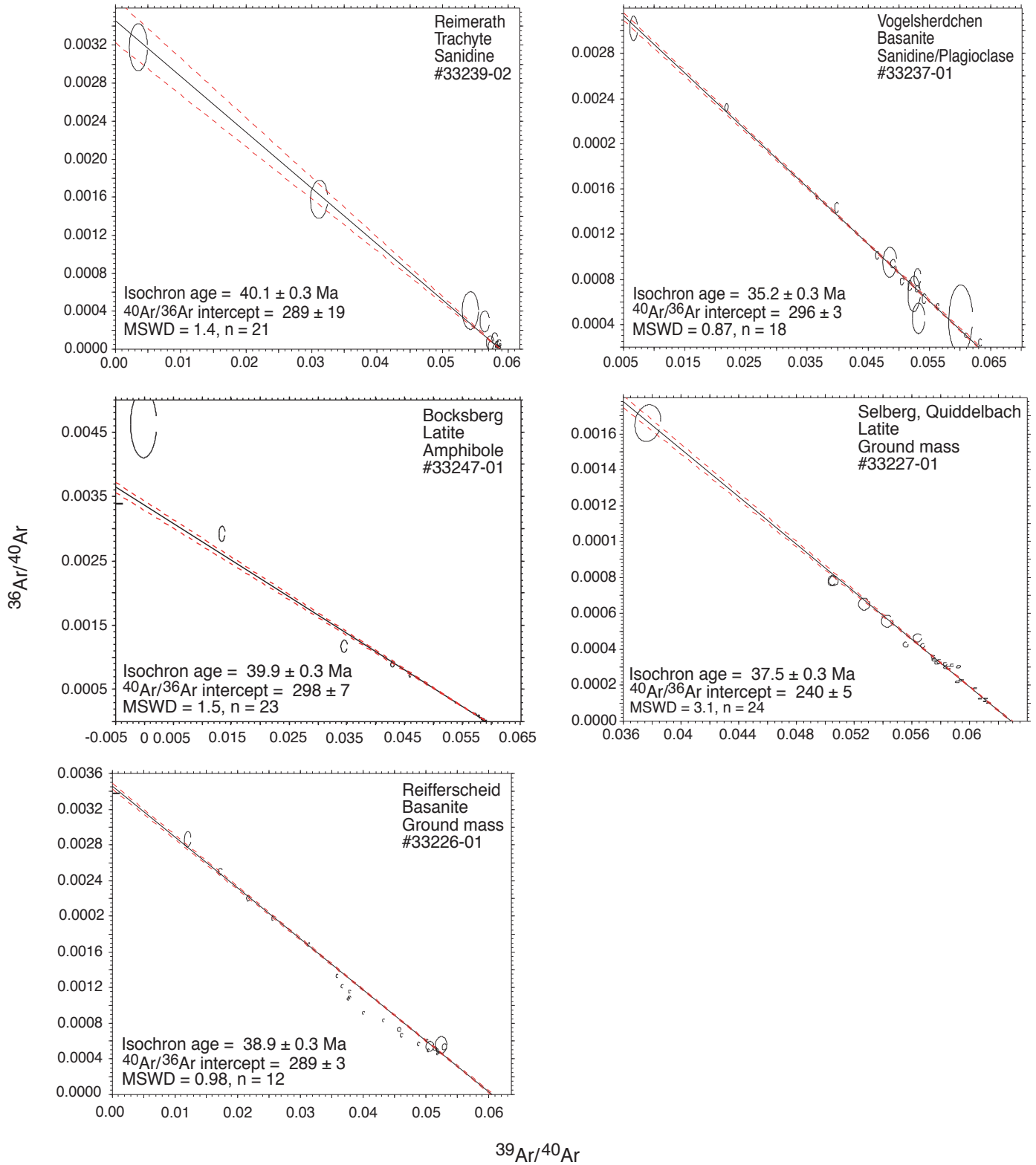


Figure 4

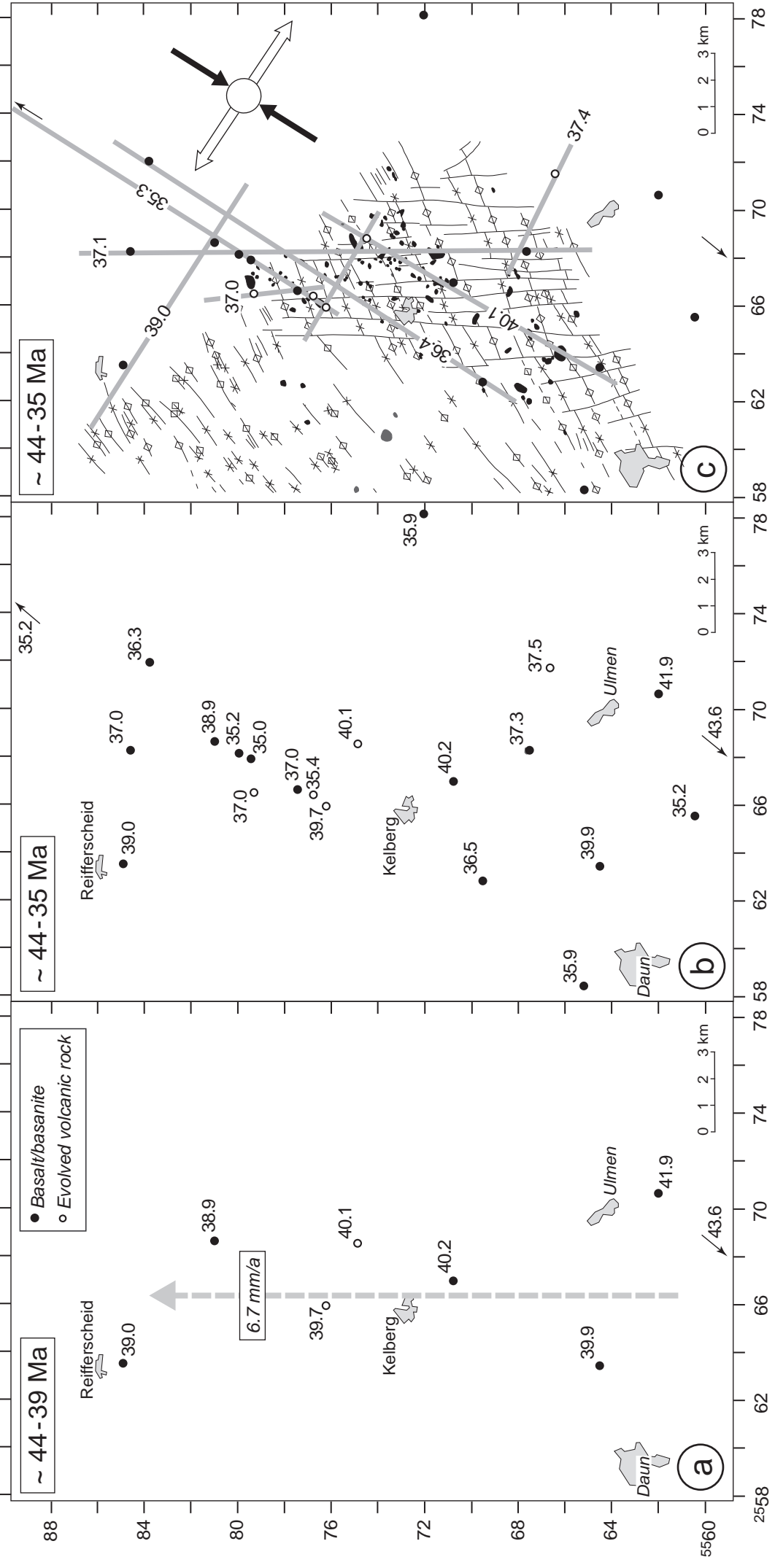


Figure 5

Table 1: Sampling data and TAS classification on samples from the Hocheifel and the Northern Upper Rhine Graben as well as a comparison of $^{40}\text{Ar}/^{39}\text{Ar}$ ages of this work regarded to be geologically significant with previously published conventional K-Ar ages.

Sample#	Sample location Topographic map 1: 25000, Grid coordinates	TAS*	Suggested age [Ma] This work**	Previous K-Ar ages [Ma]
Hocheifel				
1	Bad Neuenahrer Berg (hill top) 5408 Bad Neuenahr-Ahrweiler, 25 80 64/56 00 05	Basanite	35.2±0.3 gm	34±2 tr (3)
2	Staufskopf (hill top in Näßbachtal) 5607 Adenau, 25 68 30/55 84 69	Basanite	37.0±0.3 gm	
3	Reifferscheid (quarry at Alte Burg) 5607 Adenau, 25 63 48/55 84 90	Basanite	39.0±0.4 gm	39.3±0.8 amph (4)
4	Vogelsherdchen (quarry Bruchtal) 5607 Adenau, 25 68 08/55 79 88	Basanite	35.2±0.3 san/plag	35.5±1.3 tr (4)
5	Quiddelbach (Selberg, quarry at street) 5607 Adenau, 25 66 63/55 79 30	Latite	37.0±0.3 amph	29.5±0.8 tr (2), 36.6±0.7 amph (4)
6	Nürburg (castle hill, small quarry) 5607 Adenau, 25 67 90/55 79 45	Basanite	35.0±0.3 gm	33.0±1.0 tr (2), 31.9±1.1/32.3±1.1 tr (4)
7	Rote Heck (hill top) 5607 Adenau, 25 67 08/55 7555	Basalt		
8	Hohe Acht (at the top, view point) 5608 Virneburg, 25 71 90/55 83 85	Basanite	36.3±0.3 gm	37.3±1.1 tr (2)
9	Hoch-Bermel (quarry, south wall) 5708 Kaisersesch, 25 78 13/55 72 13	Basanite	35.9±0.3 gm	32.3±1.2 tr (4)
10	Steimelskopf (hill top) 5708 Kaisersesch, 25 71 70/55 66 75	Hawaiite	37.5±0.3 gm	39.4±1.4 tr (4)
11	Kopp (small hill top E of road Daun – Dockweiler) 5706 Hillesheim, 25 58 40/55 65 20	Basanite	35.9±0.3 gm	
12	Kastelberg (small quarry, west flank of hill top) 5707 Kelberg, 25 68 20/55 67 50	Basanite	37.3±0.4 gm	40.3±0.8 neph/plag/kf (4)
13	Brinkenkopf (quarry SW of Brinkenkopf) 5707 Kelberg, 25 66 96/55 70 82	Shoshonite	40.2±0.3 amph	40.4±0.8 tr (2), 39.0±0.9 amph (4)
14	Barsberg (little hill top E of Bongard) 5707 Kelberg, 25 60 40/55 73 55	Basanite		26.7±1.0 tr (4)
15	Nollenbachtal (cliff close to Auderath mill) 5807 Gillenfeld, 25 70 60/55 61 88	Basanite	41.9±0.4 gm	37.5±1.4 tr (4)
16	Steineberger Ley (boulders at hill top slope) 5807 Gillenfeld, 25 65 60/55 60 53	Basanite	35.2±0.4 gm	41.5±0.8 plag/kf (4)
17	Bocksberg (SE of Nürburgring racing course) 5607 Adenau, 25 65 95/55 76 30	Latite	39.7±0.3 amph	41.9±1.1 tr (2)
18	Scharfer Kopf (at Nürburgring racing course) 5607 Adenau, 25 66 65/55 77 43	Basalt	37.0±0.4 gm	
19	Reimerath (quarry) 5607 Adenau, 25 68 50/55 74 83	Trachyte	40.1±0.3 san	40.1±1.1 tr (2)
20***	Hillscheid (occurrence at upper hill top slope) 5806 Daun, 25 58 75/55 54 26	Basanite	43.6±0.2 gm	
Northern Upper Rhine Graben				
20	Rabenskapf (quarry at NW flank of hill top) 5913 Presberg/Taunus Mountains	Basanite	58.7±0.4 gm	

Table 1 cont.

21	Am Hörkopf (quarry at hill top) 5913 Presberg/Taunus Mountains	Basanite		40.4±1.6 tr (1)
22	Forst (quarry ca. 1.5km W of Forst) 6514 Bad Dürkheim/Mainz Basin	Basanite	50.6±0.3 gm	52.4±2.0 tr (1)
23	Stetteritz (construction site at Stetteritzer Ring #36) 6118 Darmstadt-Ost (Roßdorf)/Sprendlingen Horst	Foidite	48.7±0.2 gm	43.5±1.7 tr (1)
24	Traisa (Steinbuckel, quarry N of Ramstadter Straße) 6118 Darmstadt-Ost (Roßdorf)/Sprendlingen Horst	Basanite		34.0±1.4 tr (1)
25	Forstberg (small quarry at W flank of hill top) 6119 Groß-Umstadt/Sprendlingen Horst	Basanite	47.2±0.3 gm	44.4±1.8 tr (1)

* Data used for TAS classification are from Fekiacova & Mertz (2005).

** Samples without age indication do not yield geologically significant $^{40}\text{Ar}/^{39}\text{Ar}$ ages or there are no conventional K-Ar ages published, respectively.

*** $^{40}\text{Ar}/^{39}\text{Ar}$ Ar age from Mertz et al. (2000)

amph = amphibole, gm = ground mass (magnetic), kf = K-feldspar, neph = nepheline, plag = plagioclase, tr = total rock.
(1) Horn et al. (1972), (2) Cantarel & Lippolt (1977), (3) Lippolt & Fuhrmann (1980), (4) Müller-Sohnius et al. (1989).
Data from references (1), (2), (3) are recalculated to IUGS constants, renormalized to an age of standard LP6 = 128.9 Ma and rounded.

Table 2: Step heating $^{40}\text{Ar}/^{39}\text{Ar}$ data of volcanic rocks from Hocheifel and Upper Rhine Graben regions.

Sample	Power [W]	^{39}Ar [Mo]	$^{40}\text{Ar}/^{39}\text{Ar}$	$^{37}\text{Ar}_{Ca}/^{39}\text{Ar}_{K}$	$^{38}\text{Ar}_{Ca}/^{39}\text{Ar}_{K}$	$^{36}\text{Ar}/^{39}\text{Ar}$	$^{40}\text{Ar}_{rad}/^{39}\text{Ar}_{K}$	$^{40}\text{Ar}_{int}$ [%]	Age [Ma]	$\pm 2\sigma$
Hocheifel samples: J = 0.001320										
Bad Neuenahr Berg Run# 33224-1	1.0	0.0033	48.85	2.098	0.0316	0.1340	9.23	18.90	21.84	3.96
	1.5	0.0116	43.86	2.264	0.0176	0.1114	10.95	25.00	25.88	1.26
	2.0	0.0175	44.70	2.124	0.0137	0.1119	11.65	26.10	27.53	0.92
	2.5	0.0326	51.63	2.168	0.0205	0.1298	13.25	25.70	31.28	0.69
	3.0	0.0475	47.89	1.966	0.0228	0.1153	13.83	28.90	32.63	0.57
	3.5	0.0653	37.47	1.781	0.0246	0.0783	14.34	38.30	33.83	0.41
	4.0	0.0891	29.33	1.777	0.0245	0.0488	14.94	51.00	35.24	0.29
	4.5	0.1297	21.90	1.508	0.0210	0.0237	14.94	68.20	35.23	0.18
	5.0	0.1504	18.95	1.247	0.0143	0.0133	15.08	79.60	35.56	0.15
	5.5	0.1439	17.48	1.073	0.0110	0.0086	14.98	85.70	35.34	0.17
	6.0	0.1165	16.69	0.856	0.0086	0.0060	14.95	89.50	35.25	0.17
	6.5	0.0987	16.43	0.873	0.0078	0.0053	14.89	90.60	35.12	0.16
	7.0	0.0884	16.31	0.939	0.0096	0.0052	14.82	90.90	34.94	0.16
	7.5	0.0925	16.14	1.160	0.0072	0.0046	14.84	91.90	35.00	0.16
	8.0	0.0722	16.09	1.395	0.0063	0.0050	14.66	91.10	34.58	0.19
	9.0	0.0830	15.80	2.486	0.0077	0.0048	14.48	91.70	34.16	0.17
	10.0	0.0379	15.47	2.003	0.0064	0.0039	14.39	93.00	33.94	0.35
	11.0	0.0412	15.56	3.136	0.0110	0.0045	14.37	92.30	33.89	0.34
	12.0	0.0302	15.30	3.934	0.0069	0.0048	14.03	91.70	33.10	0.43
	14.0	0.0223	15.60	4.507	0.0089	0.0055	14.15	90.70	33.39	0.59
	16.0	0.0395	15.58	11.229	0.0102	0.0063	14.17	90.90	33.42	0.35
	18.0	0.0543	15.42	17.048	0.0123	0.0076	13.87	89.90	32.72	0.26
21.0	0.0564	15.58	25.491	0.0150	0.0089	13.97	89.70	32.95	0.25	
25.0	0.0446	15.66	29.770	0.0148	0.0099	13.92	88.90	32.84	0.31	
Staufskopf Run# 33225-01	1.0	0.0054	37.79	2.604	0.0119	0.1042	7.03	18.60	16.65	2.43
	1.5	0.0125	34.32	2.425	0.0099	0.0873	8.56	24.90	20.27	1.12
	2.0	0.0208	31.14	2.412	0.0124	0.0688	10.85	34.80	25.66	0.73
	2.5	0.0293	26.94	1.932	0.0082	0.0520	11.60	43.10	27.42	0.51
	3.0	0.0455	24.06	2.096	0.0017	0.0365	13.33	55.40	31.47	0.36
	3.5	0.0743	22.32	1.558	0.0036	0.0260	14.69	65.80	34.64	0.23
	4.0	0.1099	21.00	1.348	0.0011	0.0197	15.23	72.50	35.91	0.20
	4.5	0.1505	20.14	1.114	0.0014	0.0160	15.44	76.70	36.40	0.15
	5.0	0.1427	19.73	0.912	0.0009	0.0138	15.67	79.40	36.93	0.16
	5.5	0.1540	19.62	0.762	0.0005	0.0130	15.81	80.60	37.27	0.15
	6.0	0.1652	19.39	0.623	0.0012	0.0124	15.73	81.20	37.09	0.15
	6.5	0.1585	18.81	0.543	-0.0005	0.0107	15.67	83.30	36.94	0.14
	7.0	0.1409	18.25	0.570	0.0008	0.0086	15.73	86.20	37.07	0.14
	7.5	0.1179	17.70	0.552	0.0012	0.0072	15.60	88.20	36.78	0.15
	8.0	0.1082	17.33	0.603	0.0014	0.0058	15.63	90.20	36.85	0.15
	9.0	0.1114	17.23	0.920	0.0001	0.0056	15.62	90.70	36.82	0.14
	10.0	0.1453	16.98	1.505	0.0014	0.0057	15.35	90.40	36.19	0.12
	11.0	0.0906	16.74	1.682	0.0008	0.0050	15.33	91.50	36.14	0.17
	12.0	0.1436	16.97	3.838	0.0027	0.0057	15.42	90.90	36.35	0.13
	14.0	0.1649	17.37	8.721	0.0033	0.0081	15.32	88.20	36.12	0.12
	16.0	0.0735	17.61	13.557	0.0042	0.0092	15.43	87.60	36.37	0.22
	18.0	0.0231	17.65	16.177	0.0018	0.0106	15.17	86.00	35.77	0.60
21.0	0.0156	17.90	16.584	0.0034	0.0118	15.06	84.10	35.50	0.83	
25.0	0.0323	18.23	24.471	0.0044	0.0130	15.35	84.20	36.18	0.45	
Reifferscheid Run# 33226-01	1.0	0.0025	83.40	4.679	0.0404	0.2391	12.66	15.20	29.90	5.26
	1.5	0.0080	58.24	4.145	0.0367	0.1460	15.12	26.00	35.66	1.79
	2.0	0.0135	46.25	4.194	0.0466	0.1022	16.11	34.80	37.95	1.13
	2.5	0.0198	39.15	4.128	0.0472	0.0779	16.24	41.50	38.26	0.75
	3.0	0.0299	31.97	4.475	0.0493	0.0543	16.05	50.20	37.81	0.56
	3.5	0.0324	27.93	4.678	0.0401	0.0378	16.92	60.60	39.84	0.46
	4.0	0.0349	27.32	4.533	0.0332	0.0338	17.48	64.00	41.14	0.45
	4.5	0.0353	26.46	4.125	0.0272	0.0310	17.42	65.90	41.02	0.43
	5.0	0.0366	26.47	3.558	0.0229	0.0293	17.94	67.80	42.22	0.42
	5.5	0.0388	26.60	3.186	0.0202	0.0290	18.13	68.10	42.65	0.43
	6.0	0.0429	25.01	2.871	0.0158	0.0233	18.21	72.80	42.85	0.37
	6.5	0.0457	23.15	2.669	0.0181	0.0196	17.45	75.40	41.09	0.33
	7.0	0.0393	21.71	2.595	0.0093	0.0148	17.43	80.30	41.04	0.36
	7.5	0.0324	21.89	2.627	0.0116	0.0164	17.15	78.30	40.38	0.45
	8.0	0.0363	20.51	2.813	0.0077	0.0120	17.05	83.20	40.16	0.37
	9.0	0.0508	19.87	3.506	0.0031	0.0103	16.98	85.40	39.98	0.28
	10.0	0.0763	19.33	4.763	0.0055	0.0094	16.73	86.50	39.40	0.20
	11.0	0.0507	19.32	6.243	0.0062	0.0104	16.49	85.40	38.86	0.28
	12.0	0.0804	19.24	9.601	0.0050	0.0104	16.53	85.90	38.95	0.20
	14.0	0.0622	19.96	11.872	0.0065	0.0137	16.37	82.00	38.57	0.25
	16.0	0.0143	19.77	13.371	-0.0001	0.0125	16.60	84.00	39.11	0.91
	18.0	0.0088	19.09	14.490	0.0022	0.0125	15.95	83.60	37.60	1.44
21.0	0.0242	18.91	17.332	0.0080	0.0125	15.91	84.10	37.50	0.55	
25.0	0.0399	19.46	23.455	0.0036	0.0131	16.50	84.80	38.88	0.39	
Quiddelbach Run# 33227-01	1.0	0.0060	26.52	1.444	-0.0062	0.0442	13.50	50.90	31.86	2.13
	1.5	0.0301	19.81	0.724	0.0012	0.0156	15.23	76.80	35.90	0.45
	2.0	0.0633	17.99	0.486	-0.0014	0.0077	15.73	87.40	37.08	0.23
	2.5	0.1888	16.91	0.341	-0.0018	0.0037	15.81	93.50	37.27	0.11
	3.0	0.3288	16.46	0.303	-0.0012	0.0021	15.85	96.30	37.36	0.09
	3.5	0.5092	16.31	0.248	-0.0011	0.0017	15.83	97.00	37.31	0.09
	4.0	0.6398	16.38	0.195	-0.0009	0.0018	15.85	96.80	37.36	0.07
	4.5	0.5617	16.36	0.168	-0.0007	0.0021	15.74	96.20	37.11	0.08
	5.0	0.4314	16.56	0.145	-0.0007	0.0030	15.66	94.60	36.92	0.09
	5.5	0.2626	16.83	0.171	-0.0017	0.0039	15.69	93.30	36.99	0.12
	6.0	0.1889	17.14	0.153	-0.0016	0.0051	15.63	91.20	36.84	0.11
	6.5	0.1683	17.38	0.199	-0.0010	0.0059	15.63	89.90	36.84	0.13
	7.0	0.0996	17.32	0.238	-0.0014	0.0057	15.64	90.30	36.88	0.16
	7.5	0.0972	17.40	0.416	0.0000	0.0063	15.56	89.40	36.68	0.16
	8.0	0.0931	17.27	0.682	0.0004	0.0058	15.58	90.20	36.72	0.16
	9.0	0.1157	17.09	1.955	0.0009	0.0053	15.58	91.20	36.73	0.14
	10.0	0.1503	17.01	2.780	0.0014	0.0057	15.44	90.80	36.40	0.12
	11.0	0.1643	16.88	3.802	0.0005	0.0056	15.37	91.00	36.23	0.13
	12.0	0.1106	17.15	4.882	0.0012	0.0061	15.54	90.60	36.62	0.14
	14.0	0.0885	17.62	7.857	0.0015	0.0085	15.43	87.60	36.37	0.18
	16.0	0.0421	17.74	5.771	0.0012	0.0090	15.31	86.30	36.09	0.34
	18.0	0.0272	18.42	5.839	0.0042	0.0110	15.38	83.50	36.26	0.51
21.0	0.0265	18.98	7.684	0.0043	0.0134	15.32	80.70	36.11	0.52	
25.0	0.0326	19.77	8.633	0.0013	0.0166	15.20	76.90	35.84	0.44	

Table 2 cont./-2-

Quiddelbach	1.0	0.0008	165.56	8.345	-0.0390	0.5454	3.94	2.40	9.35	14.50
Run# 33228-01	2.5	0.0061	93.46	3.655	-0.0012	0.2773	11.44	12.20	27.03	2.33
	3.5	0.0083	83.82	0.906	0.0182	0.2289	16.07	19.20	37.86	1.80
	4.5	0.0092	109.17	0.607	0.0239	0.3090	17.74	16.20	41.76	1.94
	5.3	0.0084	46.73	0.507	-0.0003	0.1068	15.12	32.40	35.64	1.55
	6.5	0.0070	47.06	0.582	0.0106	0.1027	16.66	35.40	39.25	1.81
	8.5	0.0067	47.04	2.073	-0.0045	0.1018	16.96	36.10	39.93	1.86
	12.0	0.0249	27.62	7.968	0.0093	0.0375	16.81	60.90	39.60	0.55
	15.0	0.4779	16.84	9.724	0.0049	0.0048	15.82	94.00	37.29	0.10
	15.5	0.4837	15.22	9.339	0.0053	0.0024	14.90	97.90	35.15	0.07
	16.0	0.3885	15.88	9.931	0.0057	0.0020	15.68	98.70	36.97	0.09
	16.5	0.2911	15.89	9.983	0.0046	0.0020	15.71	98.90	37.02	0.09
	17.0	0.2406	15.78	10.019	0.0042	0.0020	15.61	98.90	36.81	0.12
	18.0	0.3967	15.88	10.002	0.0045	0.0020	15.70	98.90	37.00	0.10
	20.0	0.3928	15.82	10.483	0.0040	0.0019	15.67	99.10	36.94	0.11
Nürburc	1.0	0.0102	22.58	0.618	0.0266	0.0275	14.47	64.10	34.13	1.28
Run# 33229-01	1.5	0.0479	17.00	0.590	0.0199	0.0084	14.54	85.50	34.29	0.29
	2.0	0.0930	16.11	0.584	0.0219	0.0044	14.85	92.20	35.02	0.16
	2.5	0.1401	16.08	0.615	0.0205	0.0043	14.84	92.30	35.00	0.12
	3.0	0.1540	16.13	0.608	0.0206	0.0045	14.81	91.90	34.94	0.13
	3.5	0.1816	16.33	0.627	0.0194	0.0051	14.85	90.90	35.01	0.12
	4.0	0.1800	16.47	0.710	0.0144	0.0054	14.91	90.50	35.17	0.11
	4.5	0.1668	16.53	0.653	0.0123	0.0056	14.90	90.10	35.13	0.12
	5.0	0.1146	16.73	0.704	0.0103	0.0064	14.86	88.80	35.05	0.14
	5.5	0.1069	16.71	0.805	0.0100	0.0066	14.78	88.50	34.87	0.15
	6.0	0.0709	16.81	0.903	0.0092	0.0074	14.65	87.20	34.55	0.20
	6.5	0.0571	16.56	1.194	0.0127	0.0076	14.35	86.70	33.86	0.24
	7.0	0.0453	16.74	1.903	0.0179	0.0095	14.01	83.70	33.05	0.30
	7.5	0.0328	16.72	2.569	0.0166	0.0098	13.91	83.20	32.82	0.42
	8.0	0.0308	16.73	4.253	0.0205	0.0116	13.47	80.50	31.79	0.44
	9.0	0.0375	17.50	6.039	0.0265	0.0148	13.36	76.30	31.54	0.36
	10.0	0.0221	18.03	6.936	0.0237	0.0164	13.46	74.60	31.76	0.62
	11.0	0.0098	17.59	6.020	0.0274	0.0154	13.28	75.50	31.36	1.28
	12.0	0.0148	17.10	8.654	0.0279	0.0152	12.94	75.70	30.56	0.86
	14.0	0.0307	17.27	13.632	0.0317	0.0163	12.98	75.10	30.64	0.44
	16.0	0.0426	17.78	20.490	0.0427	0.0186	13.08	73.60	30.88	0.34
	18.0	0.0405	17.71	26.719	0.0538	0.0181	13.39	75.60	31.60	0.35
	21.0	0.0201	17.55	38.355	0.0635	0.0205	12.98	73.90	30.64	0.67
	25.0	0.0237	19.09	64.522	0.0882	0.0285	13.14	68.80	31.03	0.62
Rote Heck	1.0	0.0037	20.56	2.428	0.0372	0.0311	11.46	55.70	27.08	3.34
Run# 33230-01	1.5	0.0103	20.63	2.242	0.0696	0.0154	16.16	78.30	38.08	1.24
	2.0	0.0250	20.08	1.991	0.0645	0.0098	17.26	85.90	40.64	0.55
	2.5	0.0431	19.81	1.789	0.0598	0.0095	17.07	86.20	40.20	0.33
	3.0	0.0660	20.40	1.575	0.0521	0.0113	17.10	83.90	40.28	0.26
	3.5	0.1077	23.29	1.474	0.0471	0.0219	16.87	72.40	39.73	0.21
	4.0	0.1126	25.28	1.418	0.0484	0.0294	16.62	65.70	39.16	0.21
	4.5	0.0985	24.69	1.486	0.0486	0.0279	16.48	66.80	38.83	0.23
	5.0	0.0906	26.47	1.696	0.0538	0.0339	16.49	62.30	38.84	0.24
	5.5	0.0859	26.04	1.802	0.0512	0.0336	16.17	62.10	38.09	0.24
	6.0	0.0648	25.03	1.885	0.0508	0.0293	16.43	65.60	38.72	0.27
	6.5	0.0562	23.52	2.038	0.0461	0.0256	16.01	68.10	37.73	0.30
	7.0	0.0480	21.13	2.189	0.0361	0.0207	15.08	71.40	35.55	0.51
	7.5	0.0401	20.22	2.244	0.0294	0.0209	14.13	69.90	33.33	0.37
	8.0	0.0540	19.99	2.455	0.0270	0.0194	14.36	71.80	33.87	0.29
	9.0	0.1159	20.33	2.777	0.0166	0.0195	14.67	72.10	34.59	0.18
	10.0	0.1451	20.81	2.949	0.0192	0.0204	14.89	71.60	35.13	0.16
	11.0	0.5333	21.05	3.546	0.0168	0.0198	15.33	72.90	35.15	0.13
	12.0	0.5031	20.64	4.285	0.0179	0.0188	15.23	73.80	35.92	0.13
	14.0	0.5400	20.52	5.436	0.0176	0.0199	14.83	72.30	34.98	0.13
	16.0	0.2590	20.31	6.909	0.0183	0.0219	14.09	69.40	33.24	0.15
	18.0	0.0521	20.46	9.735	0.0165	0.0205	14.77	72.20	34.83	0.28
	21.0	0.0265	20.49	10.620	0.0168	0.0282	12.55	61.20	29.64	0.53
	25.0	0.0218	21.05	14.790	0.0235	0.0834	-3.16	-15.00	-7.55	0.72
Hohe Acht	1.0	0.0015	118.20	7.092	0.0237	0.3789	6.01	5.10	14.25	8.48
Run# 33231-01	1.5	0.0059	83.06	5.888	0.0578	0.2411	11.77	14.20	27.82	2.48
	2.0	0.0097	59.42	5.958	0.0472	0.1554	13.56	22.80	31.99	1.53
	2.5	0.0143	45.72	6.080	0.0645	0.1068	14.28	31.20	33.69	1.03
	3.0	0.0167	40.42	6.742	0.0688	0.0895	14.12	34.90	33.31	0.91
	3.5	0.0236	38.79	7.149	0.0896	0.0836	14.27	36.80	33.67	0.69
	4.0	0.0244	41.02	7.235	0.0847	0.0899	14.63	35.70	34.51	0.69
	4.5	0.0307	43.44	6.995	0.0764	0.0970	14.96	34.40	35.28	0.61
	5.0	0.0335	43.69	6.375	0.0691	0.0974	15.06	34.50	35.50	0.61
	5.5	0.0389	39.28	5.561	0.0507	0.0819	15.20	38.70	35.85	0.51
	6.0	0.0519	33.81	4.924	0.0354	0.0623	15.53	45.90	36.60	0.39
	6.5	0.0537	28.34	4.207	0.0184	0.0435	15.60	55.10	36.78	0.34
	7.0	0.0409	26.09	3.741	0.0115	0.0371	15.23	58.40	35.91	0.39
	7.5	0.0445	25.62	3.632	0.0108	0.0346	15.51	60.50	36.55	0.36
	8.0	0.0411	24.44	3.762	0.0106	0.0318	15.16	62.00	35.75	0.38
	9.0	0.0487	24.37	4.504	0.0096	0.0312	15.32	62.90	36.12	0.32
Hoch-Bermel	1.0	0.0045	36.46	1.814	0.0225	0.0809	12.56	34.50	29.67	2.86
Run# 33232-01	1.5	0.0157	30.14	1.767	0.0150	0.0595	12.59	41.80	29.75	0.87
	2.0	0.0290	25.28	1.435	0.0223	0.0378	14.15	56.00	33.38	0.51
	2.5	0.0497	21.74	1.289	0.0185	0.0248	14.46	66.50	34.11	0.31
	3.0	0.0637	19.88	1.181	0.0189	0.0165	15.04	75.70	35.47	0.26
	3.5	0.0847	18.84	1.154	0.0168	0.0129	15.06	79.90	35.51	0.20
	4.0	0.0897	18.72	1.101	0.0112	0.0119	15.23	81.40	35.92	0.19
	4.5	0.0869	18.88	1.042	0.0087	0.0125	15.21	80.50	35.85	0.20
	5.0	0.0868	19.63	1.024	0.0075	0.0152	15.17	77.30	35.78	0.19
	5.5	0.0955	20.63	1.014	0.0052	0.0183	15.25	73.90	35.96	0.20
	6.0	0.1110	19.38	1.031	0.0056	0.0142	15.21	78.50	35.85	0.18
	6.5	0.0995	17.99	1.035	0.0027	0.0092	15.30	85.00	36.07	0.16
	7.0	0.1002	17.45	1.121	0.0019	0.0078	15.18	87.00	35.79	0.17
	7.5	0.0911	17.24	1.326	0.0019	0.0071	15.20	88.20	35.84	0.18
	8.0	0.0713	16.88	1.580	0.0026	0.0067	14.96	88.60	35.29	0.20
	9.0	0.0851	16.80	2.364	0.0013	0.0068	14.87	88.50	35.07	0.17
	10.0	0.0574	16.68	3.291	0.0033	0.0066	14.86	89.10	35.06	0.24
	11.0	0.0471	16.51	4.672	0.0044	0.0065	14.78	89.50	34.86	0.29
	12.0	0.0175	16.39	3.119	0.0044	0.0059	14.77	90.10	34.83	0.73
	14.0	0.0237	16.24	5.398	0.0021	0.0068	14.44	88.90	34.06	0.54
	16.0	0.0275	16.27	7.642	0.0042	0.0067	14.58	89.60	34.40	0.49

Table 2 cont./-3-

Steimelskopf	1.0	0.0016	24.38	1.793	0.0231	0.0566	7.70	31.60	18.24	7.97
Run# 33233-01	1.5	0.0091	21.79	1.600	0.0427	0.0297	13.07	60.00	30.86	1.39
	2.0	0.0210	20.90	1.593	0.0444	0.0180	15.63	74.80	36.85	0.63
	2.5	0.0405	21.32	1.311	0.0483	0.0161	16.61	77.90	39.12	0.37
	3.0	0.0544	23.57	1.149	0.0476	0.0235	16.65	70.60	39.22	0.30
	3.5	0.0883	28.28	1.180	0.0681	0.0407	16.28	57.60	38.35	0.27
	4.0	0.0826	24.28	1.158	0.0581	0.0272	16.27	67.00	38.34	0.23
	4.5	0.0869	23.21	1.115	0.0592	0.0234	16.33	70.30	38.47	0.21
	5.0	0.0817	22.27	1.000	0.0553	0.0201	16.36	73.50	38.53	0.21
	5.5	0.0951	21.19	1.022	0.0532	0.0167	16.29	76.90	38.38	0.18
	6.0	0.0915	20.21	1.012	0.0500	0.0131	16.36	81.00	38.55	0.18
	6.5	0.0949	19.43	1.027	0.0420	0.0105	16.37	84.20	38.56	0.17
	7.0	0.1006	18.58	1.055	0.0352	0.0074	16.42	88.40	38.70	0.15
	7.5	0.1008	17.91	1.031	0.0284	0.0059	16.20	90.40	38.18	0.17
	8.0	0.1114	17.63	1.079	0.0183	0.0052	16.14	91.50	38.03	0.15
	9.0	0.1438	17.44	1.218	0.0094	0.0051	15.99	91.70	37.88	0.14
	10.0	0.1584	17.73	1.461	0.0091	0.0062	15.95	90.00	37.59	0.13
	11.0	0.3049	17.65	2.071	0.0065	0.0062	15.90	90.10	37.48	0.11
	12.0	0.4327	17.69	2.652	0.0058	0.0064	15.89	89.80	37.45	0.10
	14.0	0.4364	17.53	3.521	0.0050	0.0061	15.87	90.50	37.40	0.11
	16.0	0.1742	17.66	3.647	0.0053	0.0066	15.84	89.70	37.33	0.11
	18.0	0.1083	17.31	3.744	0.0042	0.0052	15.90	91.90	37.48	0.15
	21.0	0.1447	17.28	4.534	0.0052	0.0054	15.85	91.70	37.36	0.13
	25.0	0.1109	17.37	5.678	0.0045	0.0061	15.78	90.90	37.20	0.15
Kopp	1.0	0.0038	61.58	2.971	0.0053	0.1546	15.89	25.80	37.44	3.54
Run# 33234-01	1.5	0.0215	35.12	2.529	-0.0028	0.0671	15.35	43.70	36.19	0.70
	2.0	0.0360	27.78	2.320	0.0031	0.0428	15.19	54.70	35.81	0.43
	2.5	0.0614	23.51	2.383	0.0003	0.0277	15.41	65.60	36.33	0.28
	3.0	0.0772	21.47	2.606	0.0011	0.0212	15.29	71.20	36.06	0.22
	3.5	0.0812	21.10	3.190	-0.0009	0.0205	15.17	71.90	35.77	0.21
	4.0	0.0753	22.04	3.736	-0.0013	0.0239	15.11	68.60	35.64	0.23
	4.5	0.0617	21.66	4.121	0.0005	0.0235	14.87	68.70	35.07	0.26
	5.0	0.0489	23.60	4.184	-0.0014	0.0287	15.26	64.60	35.98	0.33
	5.5	0.0370	25.78	4.093	0.0011	0.0363	15.18	58.90	35.80	0.42
	6.0	0.0300	29.59	4.864	0.0029	0.0485	15.41	52.10	36.34	0.50
	6.5	0.0186	30.86	6.103	0.0042	0.0528	15.46	50.10	36.44	0.77
	7.0	0.0109	31.03	7.924	0.0063	0.0555	14.86	47.90	35.06	1.24
	7.5	0.0080	28.18	9.490	0.0126	0.0503	13.63	48.30	32.16	1.64
	8.0	0.0048	25.18	10.032	0.0100	0.0384	14.18	56.30	33.45	2.66
	9.0	0.0051	24.43	14.041	0.0103	0.0321	15.46	63.30	36.45	2.51
	10.0	0.0024	23.26	11.102	0.0407	0.0330	13.91	59.80	32.83	5.35
	11.0	0.0036	22.35	20.209	0.0127	0.0338	13.11	58.70	30.94	3.48
	12.0	0.0045	21.46	24.053	0.0131	0.0351	11.95	55.70	28.23	2.81
	14.0	0.0087	22.64	36.780	0.0134	0.0314	14.73	65.00	34.73	1.50
	16.0	0.0052	22.96	37.633	0.0325	0.0376	13.22	57.60	31.22	2.42
	18.0	0.0095	24.33	50.735	0.0212	0.0451	12.81	52.70	30.25	1.39
	21.0	0.0176	27.22	78.577	0.0231	0.0573	13.03	47.90	30.77	0.84
	25.0	0.0172	29.82	86.153	0.0220	0.0675	12.80	42.90	30.23	0.87
Kastelberg	1.0	0.0064	21.08	0.762	0.0318	0.0231	14.27	67.70	33.67	2.00
Run# 33235-01	1.5	0.0411	18.12	0.871	0.0170	0.0090	15.49	85.50	36.51	0.33
	2.0	0.0664	17.39	0.871	0.0202	0.0055	15.80	90.90	37.24	0.23
	2.5	0.1042	17.13	0.944	0.0222	0.0042	15.91	92.90	37.51	0.14
	3.0	0.1295	17.01	1.106	0.0230	0.0039	15.91	93.50	37.49	0.14
	3.5	0.1415	16.82	1.244	0.0216	0.0035	15.82	94.10	37.30	0.13
	4.0	0.1487	16.86	1.309	0.0169	0.0036	15.86	94.10	37.38	0.12
	4.5	0.1426	16.86	1.219	0.0130	0.0038	15.78	93.60	37.19	0.13
	5.0	0.1372	16.85	1.137	0.0096	0.0043	15.63	92.80	36.84	0.14
	5.5	0.1112	16.79	1.097	0.0073	0.0042	15.59	92.90	36.76	0.14
	6.0	0.1087	16.74	1.152	0.0061	0.0041	15.57	93.00	36.71	0.14
	6.5	0.0944	16.43	1.167	0.0038	0.0041	15.26	92.90	35.97	0.17
	7.0	0.0786	16.37	1.201	0.0030	0.0041	15.20	92.80	35.84	0.18
	7.5	0.0693	16.15	1.297	0.0063	0.0042	14.98	92.70	35.32	0.20
	8.0	0.0659	16.15	1.499	0.0043	0.0050	14.72	91.20	34.73	0.22
	9.0	0.0804	16.07	2.263	0.0030	0.0054	14.57	90.70	34.37	0.19
	10.0	0.0474	16.23	2.181	0.0034	0.0060	14.54	89.60	34.30	0.28
	11.0	0.0343	16.11	2.497	0.0062	0.0053	14.65	90.90	34.54	0.42
	12.0	0.0263	15.86	3.151	0.0049	0.0054	14.38	90.70	33.92	0.50
	14.0	0.0511	15.78	6.046	0.0098	0.0057	14.32	90.80	33.78	0.26
	16.0	0.0445	15.59	6.540	0.0083	0.0057	14.16	90.90	33.42	0.32
	18.0	0.0697	16.13	10.668	0.0085	0.0079	14.21	88.10	33.52	0.21
	21.0	0.1087	16.24	16.006	0.0101	0.0094	14.10	86.80	33.27	0.16
	25.0	0.0751	16.58	24.165	0.0120	0.0113	14.20	85.70	33.51	0.21
Vogelsherdchen	2.0	0.0010	150.60	2.038	-0.0261	0.4554	15.90	10.60	37.48	11.82
Run# 33237-01	4.0	0.0124	45.91	1.551	0.0097	0.1068	14.34	31.20	33.84	1.15
	6.0	0.0312	18.91	0.771	-0.0017	0.0136	14.91	78.80	35.17	0.43
	8.0	0.0460	16.43	0.740	-0.0019	0.0051	14.96	91.00	35.27	0.28
	10.0	0.0292	15.82	0.716	-0.0012	0.0039	14.70	92.90	34.67	0.41
	12.0	0.0200	18.50	0.634	0.0031	0.0117	15.07	81.40	35.52	0.61
	13.0	0.0527	27.39	0.649	0.0002	0.0418	15.04	54.90	35.46	0.33
	14.0	0.0138	25.14	0.614	-0.0047	0.0361	14.47	57.50	34.13	0.88
	15.0	0.0057	20.65	0.734	0.0125	0.0197	14.84	71.80	34.99	2.08
	16.0	0.0052	19.09	0.555	0.0028	0.0129	15.30	80.20	36.08	2.21
	17.0	0.0206	20.43	0.681	-0.0011	0.0193	14.76	72.20	34.81	0.62
	18.0	0.0215	21.57	0.700	-0.0007	0.0219	15.11	70.10	35.62	0.57
	19.0	0.0030	16.67	0.505	-0.0194	0.0075	14.48	86.90	34.16	3.72
	20.0	0.0183	19.34	0.707	0.0017	0.0145	15.08	78.00	35.56	0.65
	21.0	0.0110	18.89	0.650	-0.0020	0.0155	14.32	75.80	33.77	1.08
	23.0	0.0260	19.83	0.674	0.0022	0.0156	15.24	76.80	35.93	0.50
	25.0	0.0323	17.77	0.731	-0.0009	0.0101	14.83	83.40	34.97	0.37
	27.0	0.0062	18.83	0.561	0.0029	0.0086	16.29	86.60	38.39	1.90

Table 2 cont./-4-

Reimerath	0.5	0.0001	55.59	-4.769	-0.1822	0.3310	-42.39	-76.30	-103.88	109.02
Run# 33239-01	1.0	0.0002	288.18	-0.884	0.3245	1.0986	-36.94	-12.80	-90.19	87.81
	2.0	0.0007	90.91	0.025	0.0677	0.2807	7.84	8.60	18.58	15.61
	3.0	0.0022	19.70	-0.045	0.0161	0.0081	17.30	87.80	40.74	5.27
	4.0	0.0049	18.07	-0.002	-0.0004	0.0037	16.96	93.90	39.94	2.36
	5.0	0.0088	17.52	-0.032	-0.0114	-0.0003	17.60	100.50	41.43	1.31
	6.0	0.0115	17.21	0.017	-0.0043	0.0001	17.18	99.80	40.45	1.01
	7.0	0.0193	17.12	0.020	0.0035	0.0011	16.80	98.10	39.57	0.61
	8.0	0.0243	16.89	0.042	0.0016	0.0016	16.43	97.20	38.70	0.49
	9.0	0.0286	17.03	0.033	0.0007	0.0006	16.84	98.90	39.66	0.42
	10.0	0.0387	16.99	0.031	0.0000	0.0005	16.85	99.20	39.68	0.32
	12.0	0.0844	17.09	0.042	0.0001	0.0005	16.94	99.10	39.91	0.16
	14.0	0.2254	17.05	0.044	0.0004	0.0003	16.97	99.50	39.96	0.12
	16.0	0.8402	17.11	0.042	-0.0004	0.0002	17.05	99.70	40.16	0.08
	18.0	0.3004	17.19	0.045	-0.0014	0.0003	17.09	99.40	40.25	0.08
	21.0	0.2361	17.14	0.042	-0.0004	0.0001	17.10	99.80	40.27	0.13
	24.0	0.0663	17.06	0.048	-0.0002	0.0010	16.77	98.30	39.51	0.20
	27.0	0.0791	16.92	0.042	-0.0019	0.0004	16.80	99.30	39.56	0.17
Reimerath	2.0	0.0002	285.71	-1.588	0.0150	0.9077	16.86	5.90	39.71	51.62
Run# 33239-02	4.0	0.0025	32.15	0.094	0.0194	0.0507	17.14	53.30	40.35	4.80
	5.0	0.0042	18.45	0.036	-0.0129	0.0075	16.24	88.00	38.26	2.69
	6.0	0.0081	17.73	0.074	0.0006	0.0052	16.20	91.40	38.18	1.43
	7.0	0.0117	17.47	0.017	-0.0012	0.0012	17.12	98.00	40.32	0.99
	8.0	0.0155	17.27	0.045	-0.0032	0.0020	16.68	96.60	39.30	0.76
	9.0	0.0175	17.45	0.054	-0.0068	0.0006	17.28	99.00	40.68	0.68
	10.0	0.0248	17.07	0.040	-0.0024	0.0011	16.75	98.10	39.46	0.48
	12.0	0.0392	17.15	0.044	0.0005	0.0011	16.84	98.20	39.67	0.34
	13.0	0.0537	17.19	0.044	-0.0003	0.0005	17.03	99.10	40.10	0.26
	14.0	0.0628	17.01	0.044	-0.0007	0.0008	16.79	98.70	39.54	0.20
	15.0	0.0847	17.17	0.043	0.0001	0.0006	17.00	99.00	40.03	0.16
	16.0	0.1190	17.04	0.034	0.0006	0.0003	16.96	99.50	39.94	0.14
	17.0	0.1726	17.04	0.041	-0.0005	0.0005	16.91	99.20	39.83	0.12
	18.0	0.3529	17.16	0.044	-0.0004	0.0003	17.06	99.50	40.18	0.10
	19.0	1.5874	17.14	0.044	-0.0006	0.0002	17.07	99.60	40.21	0.06
	20.0	0.3234	17.11	0.044	-0.0003	0.0003	17.02	99.50	40.08	0.09
	21.0	0.0964	17.08	0.041	0.0001	0.0003	16.98	99.40	40.00	0.14
	23.0	0.2092	17.11	0.042	-0.0008	0.0003	17.02	99.50	40.08	0.09
	25.0	0.1612	17.09	0.043	-0.0013	0.0005	16.96	99.20	39.93	0.13
	27.0	0.1454	17.16	0.046	-0.0003	0.0006	16.98	98.90	39.98	0.11
Brinkenkopf	1.0	0.0023	86.88	2.648	-0.0006	0.2594	10.09	11.60	23.88	5.31
Run# 33243-01	3.0	0.0338	35.55	3.186	0.0081	0.0717	14.43	40.60	34.04	0.50
	5.0	0.0971	25.06	2.715	-0.0007	0.0259	17.51	69.90	41.21	0.20
	8.0	0.2584	21.20	1.518	0.0000	0.0132	17.35	81.80	40.85	0.16
	11.0	0.1857	18.67	2.965	0.0007	0.0047	17.40	93.20	40.96	0.12
	12.0	0.2169	17.80	7.221	0.0045	0.0038	16.97	95.30	39.98	0.14
	12.5	0.2928	17.52	8.147	0.0050	0.0030	16.96	96.80	39.95	0.09
	13.0	0.3377	17.47	8.703	0.0054	0.0026	17.05	97.60	40.15	0.10
	13.5	0.2885	17.37	8.902	0.0063	0.0024	17.01	98.00	40.07	0.11
	14.0	0.3732	17.49	9.009	0.0057	0.0027	17.05	97.50	40.16	0.09
	14.5	0.2171	17.54	9.052	0.0062	0.0026	17.14	97.70	40.37	0.11
	15.2	0.3055	17.46	9.139	0.0055	0.0025	17.09	97.90	40.25	0.12
	15.8	0.2002	17.37	9.773	0.0061	0.0026	16.99	97.80	40.00	0.10
	16.6	0.1942	17.39	9.920	0.0061	0.0025	17.07	98.10	40.19	0.12
	18.0	0.1788	17.58	10.106	0.0063	0.0029	17.13	97.40	40.33	0.11
	22.0	0.2272	17.90	11.303	0.0053	0.0040	17.15	95.80	40.39	0.14
	28.0	0.1334	17.91	15.705	0.0079	0.0050	17.06	95.20	40.17	0.14
Barsberg	1.0	0.0174	16.78	1.613	0.0468	0.0216	10.45	62.30	24.72	0.69
Run# 33244-01	1.5	0.0603	15.33	1.555	0.0406	0.0111	12.11	79.00	28.60	0.22
	2.0	0.1306	14.87	1.667	0.0433	0.0061	13.12	88.30	30.97	0.12
	2.5	0.1753	15.21	1.718	0.0349	0.0045	13.96	91.80	32.95	0.11
	3.0	0.1744	15.47	1.425	0.0250	0.0036	14.47	93.50	34.14	0.10
	3.5	0.2139	15.63	1.098	0.0170	0.0032	14.91	94.20	35.17	0.09
	4.0	0.1312	15.87	0.907	0.0110	0.0030	15.00	94.50	35.38	0.12
	4.5	0.1203	15.99	0.876	0.0084	0.0028	15.18	95.00	35.80	0.12
	5.0	0.1153	15.93	0.901	0.0094	0.0030	15.07	94.60	35.53	0.13
	5.5	0.1004	15.84	0.930	0.0091	0.0028	15.06	95.10	35.51	0.15
	6.0	0.1073	15.90	1.000	0.0080	0.0028	15.11	95.00	35.62	0.15
	6.5	0.0791	15.78	1.153	0.0085	0.0033	14.84	94.00	35.00	0.18
	7.0	0.0482	15.53	1.449	0.0069	0.0035	14.54	93.60	34.29	0.27
	7.5	0.0465	15.73	1.769	0.0082	0.0035	14.76	93.80	34.80	0.28
	8.0	0.0403	15.59	1.690	0.0070	0.0038	14.54	93.20	34.30	0.32
	9.0	0.0316	15.27	2.573	0.0064	0.0050	13.89	90.90	32.77	0.37
	10.0	0.0207	15.40	2.607	0.0085	0.0064	13.60	88.40	32.11	0.58
	14.0	0.0401	15.13	11.222	0.0105	0.0086	13.02	86.10	30.75	0.30
	19.0	0.0454	18.95	40.382	0.0207	0.0269	12.54	66.20	29.61	0.33
	25.0	0.0374	17.92	60.172	0.0287	0.0254	12.74	71.10	30.09	0.39
Nollenbachtal	1.0	0.0215	22.20	2.673	0.0462	0.0189	16.70	75.20	39.34	0.57
Run# 33245-01	1.5	0.0403	21.39	2.467	0.0505	0.0121	17.90	83.70	42.13	0.32
	2.0	0.0901	20.29	1.877	0.0555	0.0060	18.59	91.60	43.74	0.17
	2.5	0.1760	19.90	1.545	0.0568	0.0032	19.00	95.50	44.69	0.13
	3.0	0.2039	19.64	1.415	0.0534	0.0027	18.90	96.20	44.45	0.11
	3.5	0.1521	19.50	1.409	0.0507	0.0030	18.69	95.80	43.96	0.12
	4.0	0.1092	19.55	1.532	0.0475	0.0034	18.61	95.20	43.77	0.14
	4.5	0.0906	19.17	1.609	0.0441	0.0029	18.38	95.90	43.25	0.16
	5.0	0.0917	19.06	1.686	0.0379	0.0027	18.33	96.20	43.12	0.17
	5.5	0.0789	18.93	1.790	0.0350	0.0024	18.29	96.60	43.04	0.17
	6.0	0.0688	18.80	1.921	0.0318	0.0022	18.23	97.00	42.90	0.19
	6.5	0.0705	18.62	2.027	0.0255	0.0021	18.08	97.10	42.55	0.19
	7.0	0.0665	18.63	2.217	0.0232	0.0023	18.02	96.80	42.42	0.20
	8.0	0.0789	18.53	2.746	0.0172	0.0024	17.92	96.70	42.17	0.17
	10.0	0.1656	18.47	4.187	0.0078	0.0027	17.83	96.60	41.98	0.12
	13.0	0.3006	18.41	7.704	0.0066	0.0031	17.80	96.70	41.90	0.12
	17.0	0.1093	18.54	7.003	0.0090	0.0041	17.62	95.00	41.47	0.14
	23.0	0.1868	18.67	11.571	0.0072	0.0047	17.74	95.00	41.75	0.13

Table 2 cont./-5-

Steineberger Lev	1.0	0.0428	27.43	1.888	0.0154	0.0674	7.54	27.50	17.88	0.41
Run# 33246-01	1.5	0.0798	23.88	1.527	0.0133	0.0465	10.15	42.50	24.01	0.28
	2.0	0.1122	20.51	0.951	0.0127	0.0260	12.84	62.60	30.33	0.19
	2.5	0.1322	18.36	0.785	0.0110	0.0147	14.05	76.50	33.16	0.14
	3.0	0.1496	17.46	0.640	0.0083	0.0100	14.52	83.20	34.25	0.13
	3.5	0.1468	17.17	0.602	0.0039	0.0087	14.63	85.20	34.50	0.13
	4.0	0.1548	16.98	0.595	0.0029	0.0073	14.83	87.40	34.98	0.12
	4.5	0.1552	16.70	0.570	0.0012	0.0064	14.82	88.70	34.95	0.12
	5.0	0.1402	16.55	0.624	0.0018	0.0056	14.91	90.10	35.17	0.13
	5.5	0.1249	16.45	0.635	0.0005	0.0051	14.98	91.00	35.32	0.13
	6.0	0.1608	16.44	0.735	0.0025	0.0049	15.01	91.30	35.40	0.12
	6.5	0.0896	16.47	0.962	0.0039	0.0052	14.98	91.00	35.33	0.15
	7.0	0.0800	16.56	1.292	0.0042	0.0056	14.96	90.30	35.28	0.18
	8.0	0.0988	16.64	2.286	0.0074	0.0064	14.83	89.10	34.97	0.15
	10.0	0.0870	16.52	3.507	0.0089	0.0065	14.72	89.10	34.73	0.16
	13.0	0.1167	16.80	15.831	0.0262	0.0096	14.58	86.80	34.40	0.14
	17.0	0.0416	16.37	14.066	0.0256	0.0076	14.67	89.60	34.61	0.30
	20.0	0.0477	16.20	23.430	0.0337	0.0085	14.62	90.20	34.48	0.27
	26.0	0.0710	16.40	38.448	0.0410	0.0110	14.68	89.50	34.62	0.23

Bocksberg	1.0	0.0000	-1960.78	-11.273	2.5157	-6.5085	-26.46	1.40	-64.15	948.32
Run# 33247-01	3.0	0.0019	75.36	6.614	0.0143	0.2107	13.09	17.40	39.92	6.08
	5.0	0.0053	28.94	6.323	0.0158	0.0387	17.72	61.20	41.70	2.26
	8.0	0.0156	23.40	4.427	0.0277	0.0212	17.31	74.00	40.75	0.80
	11.0	0.0296	22.07	4.993	0.0155	0.0170	17.24	78.10	40.59	0.46
	12.0	0.0998	18.63	8.370	0.0116	0.0064	17.08	91.70	40.21	0.15
	12.5	0.0878	17.33	9.415	0.0065	0.0030	16.82	97.10	39.62	0.17
	13.0	0.1685	17.56	9.771	0.0066	0.0035	16.93	96.40	39.88	0.14
	13.5	0.1897	17.50	10.008	0.0082	0.0031	16.99	97.10	40.01	0.10
	14.0	0.2425	17.53	10.035	0.0076	0.0034	16.93	96.60	39.87	0.10
	14.5	0.2843	17.20	10.103	0.0060	0.0024	16.91	98.30	39.84	0.12
	15.0	0.2869	17.09	10.048	0.0066	0.0021	16.88	98.80	39.76	0.11
	15.5	0.2821	17.09	10.068	0.0056	0.0020	16.92	99.00	39.85	0.12
	16.0	0.2631	17.15	10.124	0.0051	0.0021	16.94	98.80	39.89	0.12
	16.5	0.2677	17.04	9.994	0.0062	0.0019	16.88	99.10	39.76	0.12
	17.0	0.2824	16.94	10.129	0.0055	0.0018	16.81	99.20	39.60	0.11
	18.0	0.3450	17.02	10.249	0.0066	0.0019	16.86	99.10	39.71	0.11
	19.0	0.5028	16.98	10.322	0.0067	0.0019	16.84	99.20	39.67	0.08
	20.0	0.5185	17.06	10.193	0.0056	0.0022	16.84	98.70	39.66	0.09
	20.6	0.3889	17.09	10.198	0.0063	0.0023	16.81	98.40	39.59	0.11
	21.2	0.2174	17.05	10.207	0.0066	0.0022	16.80	98.60	39.58	0.12
	22.2	0.1843	17.06	10.363	0.0077	0.0024	16.78	98.40	39.52	0.12
	24.2	0.2081	17.18	10.378	0.0076	0.0027	16.81	97.90	39.60	0.12

Scharfer Kopf	1.0	0.0072	23.60	3.088	0.0509	0.0361	13.02	55.20	30.75	1.61
Run# 33249-01	1.5	0.0163	21.45	3.090	0.0534	0.0211	15.34	71.50	36.17	0.73
	2.0	0.0317	20.80	2.942	0.0525	0.0154	16.36	78.70	38.56	0.41
	2.5	0.0424	23.00	2.695	0.0623	0.0225	16.44	71.50	38.73	0.35
	3.0	0.0521	22.08	2.590	0.0579	0.0186	16.67	75.50	39.27	0.27
	3.5	0.0584	21.01	2.398	0.0520	0.0156	16.48	78.50	38.83	0.24
	4.0	0.0602	20.00	2.244	0.0535	0.0121	16.51	82.60	38.90	0.24
	4.5	0.0731	19.74	2.261	0.0552	0.0108	16.63	84.20	39.16	0.20
	5.0	0.0761	19.22	2.207	0.0500	0.0094	16.52	85.90	38.91	0.19
	5.5	0.0924	18.98	2.174	0.0374	0.0082	16.63	87.60	39.17	0.17
	6.0	0.0797	18.60	2.168	0.0256	0.0073	16.51	88.80	38.90	0.18
	6.5	0.0744	18.20	2.129	0.0194	0.0064	16.38	90.00	38.58	0.20
	7.0	0.0755	17.83	2.113	0.0149	0.0058	16.20	90.90	38.18	0.20
	8.0	0.0931	17.42	2.419	0.0110	0.0047	16.13	92.50	38.00	0.17
	10.0	0.1851	17.42	4.484	0.0099	0.0058	15.89	91.20	37.46	0.11
	12.0	0.3090	17.57	7.765	0.0098	0.0072	15.74	89.60	37.09	0.11
	14.0	0.1056	17.57	8.260	0.0092	0.0077	15.62	88.90	36.81	0.15
	17.0	0.0471	18.03	8.067	0.0100	0.0098	15.46	85.70	36.45	0.29
	21.0	0.0834	17.85	10.628	0.0099	0.0091	15.59	87.30	36.74	0.17
	25.0	0.1127	17.57	13.340	0.0097	0.0088	15.51	88.30	36.56	0.15

Upper Rhine Graben samples: J = 0.000805

Rabenkopf	0.5	0.0031	1052.63	2.032	0.0650	3.4941	15.80	1.50	22.78	17.35
Run# 33775-01	1.0	0.0348	332.23	1.953	0.0240	0.9776	42.99	12.90	61.34	3.84
	1.5	0.0607	124.22	1.952	0.0254	0.2815	40.97	33.00	58.50	1.35
	2.0	0.0926	88.03	1.807	0.0136	0.1591	40.95	46.50	58.48	0.83
	2.5	0.1030	84.96	2.218	0.0150	0.1498	40.64	47.80	58.04	0.76
	3.0	0.0855	91.32	2.228	0.0146	0.1676	41.72	45.70	59.56	0.79
	3.5	0.0873	105.71	1.966	0.0167	0.2156	41.94	39.70	59.86	1.03
	4.0	0.1138	99.21	1.610	0.0094	0.1946	41.59	41.90	59.38	0.94
	4.5	0.1632	78.00	1.351	0.0084	0.1238	41.40	53.10	59.11	0.63
	5.0	0.1596	68.07	1.388	0.0061	0.0913	41.12	60.40	58.71	0.52
	6.0	0.1662	62.81	2.263	0.0033	0.0755	40.55	64.50	57.91	0.47
	9.0	0.2090	54.50	9.697	0.0054	0.0509	39.77	73.00	56.82	0.33
	15.0	0.1927	48.80	25.756	0.0056	0.0387	38.28	78.40	54.71	0.33
	20.0	0.0658	47.53	35.873	0.0021	0.0358	38.24	80.50	54.66	0.54
	24.0	0.0877	47.51	37.281	0.0119	0.0356	38.34	80.70	54.81	0.45
	28.0	0.0780	48.31	39.247	0.0095	0.0406	37.72	78.10	53.94	0.49
	32.0	0.0529	48.12	39.436	0.0066	0.0417	37.19	77.30	53.19	0.65

Traisa, Steinbuckel	0.5	0.0039	83.61	0.735	0.0334	0.1631	35.35	42.30	50.59	6.62
Run# 33780-01	1.0	0.1122	46.00	1.016	0.0388	0.0548	29.81	64.80	42.75	0.42
	1.5	0.2864	37.52	1.037	0.0368	0.0197	31.72	84.50	45.46	0.21
	1.8	0.4234	36.47	1.252	0.0373	0.0123	32.88	90.20	47.10	0.18
	2.1	0.3239	37.78	1.867	0.0377	0.0136	33.84	89.60	48.46	0.19
	2.4	0.1991	40.00	2.365	0.0322	0.0189	34.51	86.30	49.41	0.25
	2.7	0.1609	41.86	2.608	0.0238	0.0231	35.13	83.90	50.28	0.29
	3.0	0.1376	44.35	2.740	0.0198	0.0291	35.83	80.80	51.26	0.34
	3.3	0.0838	47.64	2.905	0.0096	0.0396	36.03	75.60	51.55	0.46
	3.6	0.0701	49.90	3.103	0.0166	0.0500	35.19	70.50	50.37	0.54
	4.0	0.0662	52.00	3.257	0.0092	0.0574	35.10	67.50	50.24	0.57
	5.0	0.1031	51.52	3.505	0.0068	0.0584	34.35	66.70	49.18	0.47
	7.0	0.1522	47.66	5.369	0.0118	0.0521	32.43	68.10	46.47	0.38
	10.0	0.2494	49.88	17.567	0.0205	0.0652	31.16	62.50	44.67	0.38
	15.0	0.0652	47.08	32.317	0.0388	0.0593	30.65	65.10	43.94	0.60
	20.0	0.0557	46.45	76.368	0.0586	0.0674	29.07	62.60	41.71	0.63
	25.0	0.0195	64.77	173.031	0.0843	0.1364	29.13	45.00	41.79	1.60
	30.0	0.0115	72.31	221.180	0.1117	0.1625	29.73	41.10	42.64	2.61

Table 2 cont./-6-

Forst										
Run# 33782-01	0.5	0.0099	77.28	2.206	0.0137	0.1579	30.56	39.60	43.82	2.49
	1.0	0.0741	55.19	1.891	0.0281	0.0768	32.52	58.90	46.59	0.51
	3.0	0.2652	52.63	2.006	0.0555	0.0507	37.70	71.60	53.91	0.31
	3.5	0.1243	54.61	1.422	0.0501	0.0539	38.73	70.90	55.35	0.40
	4.0	0.1072	49.43	1.233	0.0244	0.0361	38.81	78.50	55.47	0.36
	4.5	0.0727	46.13	1.451	0.0165	0.0268	38.22	82.90	54.64	0.40
	5.0	0.0642	44.88	2.049	0.0171	0.0239	37.88	84.40	54.15	0.44
	5.5	0.0478	43.55	2.906	0.0119	0.0215	37.30	85.60	53.33	0.54
	6.5	0.0625	42.37	5.841	0.0101	0.0230	35.79	84.50	51.21	0.44
	7.5	0.0428	40.23	7.873	0.0113	0.0179	35.22	87.60	50.41	0.59
	10.0	0.0484	39.20	11.099	0.0146	0.0154	35.08	89.50	50.21	0.52
	14.0	0.1526	39.17	19.153	0.0153	0.0155	35.33	90.20	50.56	0.24
	18.0	0.0820	40.24	22.857	0.0159	0.0199	35.23	87.50	50.41	0.36
	24.0	0.0996	40.19	27.962	0.0169	0.0201	35.31	87.80	50.54	0.31
	28.0	0.1261	40.10	40.719	0.0118	0.0211	35.40	88.30	50.66	0.26
	33.0	0.1359	43.71	30.295	0.0150	0.0320	35.37	80.90	50.62	0.29
	10.0	0.2067	49.55	6.316	0.0140	0.0406	37.77	76.20	54.01	0.32
	14.0	0.0720	53.53	7.063	0.0157	0.0539	37.82	70.60	54.07	0.55
	18.0	0.0616	64.77	22.051	0.0064	0.0971	36.69	56.60	52.48	0.73
	24.0	0.0929	64.56	37.915	0.0209	0.1008	35.84	55.50	51.29	0.62
	28.0	0.1008	74.24	65.510	0.0178	0.1361	35.67	48.00	51.04	0.70
	32.0	0.0489	68.12	48.662	0.0211	0.1185	34.41	50.50	49.27	0.88
Am Hörkopf										
Run# 33784-01	0.5	0.0029	141.84	1.402	-0.0466	0.3493	38.51	27.10	55.04	9.38
	1.0	0.0508	70.47	1.594	0.0234	0.1304	31.89	45.30	45.70	0.88
	1.5	0.1702	48.22	1.509	0.0203	0.0461	34.63	71.80	49.57	0.35
	2.0	0.2292	45.35	1.783	0.0315	0.0279	37.18	82.00	53.16	0.28
	2.5	0.2508	45.39	1.703	0.0349	0.0221	38.92	85.70	55.62	0.25
	3.0	0.2299	46.51	1.363	0.0289	0.0234	39.63	85.20	56.61	0.27
	3.5	0.2049	47.73	1.189	0.0211	0.0257	40.16	84.10	57.37	0.29
	4.0	0.1753	51.12	1.133	0.0225	0.0358	40.59	79.40	57.97	0.31
	4.5	0.1807	59.56	1.243	0.0246	0.0667	39.84	66.90	56.92	0.42
	5.0	0.1136	62.19	1.413	0.0288	0.0758	39.80	64.00	56.86	0.51
	5.5	0.0983	59.38	1.694	0.0309	0.0696	38.84	65.40	55.50	0.51
	6.5	0.1298	58.38	2.302	0.0278	0.0674	38.51	66.00	55.05	0.48
	7.5	0.0946	56.47	2.711	0.0280	0.0634	37.80	66.90	54.04	0.51
	10.0	0.2067	49.55	6.316	0.0140	0.0406	37.77	76.20	54.01	0.32
	14.0	0.0720	53.53	7.063	0.0157	0.0539	37.82	70.60	54.07	0.55
	18.0	0.0616	64.77	22.051	0.0064	0.0971	36.69	56.60	52.48	0.73
	24.0	0.0929	64.56	37.915	0.0209	0.1008	35.84	55.50	51.29	0.62
	28.0	0.1008	74.24	65.510	0.0178	0.1361	35.67	48.00	51.04	0.70
	32.0	0.0489	68.12	48.662	0.0211	0.1185	34.41	50.50	49.27	0.88
Forstberg										
Run# 33785-01	0.5	0.0022	96.99	2.295	-0.0201	0.1911	40.48	41.70	57.81	10.72
	1.0	0.0185	84.25	3.962	0.0319	0.1720	33.43	39.70	47.88	1.47
	1.5	0.0083	88.65	4.932	0.0589	0.1927	31.68	35.80	45.41	2.93
	2.0	0.0163	103.73	4.508	0.0586	0.2433	31.82	30.70	45.60	2.18
	2.5	0.0273	89.85	4.025	0.0626	0.1894	33.82	37.70	48.43	1.45
	3.0	0.0508	69.98	3.044	0.0672	0.1210	34.25	48.90	49.04	0.87
	3.5	0.0836	54.79	2.603	0.0662	0.0703	34.07	62.20	48.79	0.55
	4.0	0.1290	44.54	2.157	0.0659	0.0341	34.52	77.50	49.41	0.35
	4.5	0.2674	39.82	1.854	0.0519	0.0176	34.68	87.10	49.65	0.20
	5.0	0.0827	39.34	1.953	0.0566	0.0178	34.13	86.80	48.87	0.44
	6.0	0.1227	37.76	2.779	0.0386	0.0128	34.08	90.20	48.80	0.31
	8.0	0.1488	36.86	5.313	0.0331	0.0134	33.11	89.80	47.42	0.28
	12.0	0.1791	36.01	14.307	0.0232	0.0123	32.91	91.40	47.15	0.25
	16.0	0.0982	36.14	15.357	0.0228	0.0127	32.97	91.20	47.23	0.30
	22.0	0.1197	42.05	22.307	0.0229	0.0329	33.14	78.80	47.46	0.30
	30.0	0.2297	37.27	25.665	0.0186	0.0181	32.89	88.20	47.12	0.21
Stetteritz										
Run# 33788-01	0.5	0.0036	281.69	4.295	0.0289	0.8181	39.66	14.10	56.67	8.61
	1.0	0.0260	110.50	3.631	0.0014	0.2457	37.89	34.30	54.17	1.64
	1.5	0.0256	72.20	2.791	-0.0099	0.1130	38.84	53.80	55.50	1.26
	2.0	0.0518	54.85	4.439	0.0038	0.0589	37.58	68.50	53.74	0.68
	2.5	0.0687	47.96	9.589	0.0027	0.0376	37.18	77.50	53.17	0.54
	3.0	0.0798	44.66	13.056	-0.0013	0.0304	36.15	81.00	51.72	0.46
	3.5	0.1741	42.55	5.087	0.0005	0.0248	35.39	83.20	50.65	0.29
	4.0	0.1108	40.88	2.022	0.0026	0.0229	34.19	83.60	48.95	0.35
	4.5	0.1200	41.14	1.308	0.0009	0.0238	34.14	83.00	48.88	0.33
	5.0	0.1336	41.79	0.920	0.0057	0.0271	33.81	80.90	48.41	0.32
	6.0	0.1628	39.95	0.995	0.0025	0.0198	34.14	85.40	48.89	0.27
	8.0	0.3141	40.80	5.440	0.0072	0.0232	34.13	83.70	48.87	0.24
	12.0	0.3928	40.13	26.337	0.0087	0.0242	33.96	84.60	48.63	0.21
	16.0	0.1463	37.65	22.486	0.0142	0.0153	34.01	90.30	48.70	0.28
	23.0	0.1156	37.33	28.003	0.0145	0.0150	33.99	91.10	48.66	0.32
	30.0	0.1628	36.71	32.253	0.0214	0.0138	33.89	92.30	48.53	0.24

Chapter 3

Fekiacova, Z. and Mertz, D.: Geodynamic setting of the Tertiary Hocheifel Volcanism (Germany), Part II: Geochemistry and Sr, Nd and Pb isotopic compositions.

This manuscript will be submitted to: Ritter, J. and Christensen, U. (Eds), Mantle Plumes: A Multidisciplinary Approach.

**Geodynamic setting of the Tertiary Hocheifel volcanism (Germany),
Part II: Geochemistry and Sr, Nd and Pb isotopic compositions.**

Zuzana Fekiacova^{1,2} and Dieter F. Mertz¹

Abstract

The Eifel volcanic fields are located in the Hercynian Rhenish Massif, Western Germany and belong to the Central European Volcanic Province (CEVP).

Seismic tomography has shown that there is a low velocity anomaly in the upper mantle underneath the Eifel (Ritter et al. 2001). This anomaly extends at least to a depth of 400 km and is interpreted as a mantle plume. The activity of the Quaternary East and West Eifel volcanism appears to be related to this so-called Eifel mantle plume. Because of a lack of studies, the geodynamic settings of the Tertiary Hocheifel volcanism remains unclear. In particular, the relationships with mantle dynamics are not established. The results of the $^{40}\text{Ar}/^{39}\text{Ar}$ dating, together with regional tectonic observations show that the Hocheifel volcanic activity is likely to be related to extension and pre-rift tectonic activity in the Upper Rhine Graben area (Fekiacova et al. submit.). In this study, we present geochemical results in order to establish the relationships of the Tertiary Hocheifel volcanic activity with mantle dynamics.

Major elements data show that the Hocheifel volcanic activity was dominated by basanitic and basaltic and only few differentiated magmas. They were produced by partial melting of garnet peridotite at about 75-90 km depth. Although they erupted through relatively thick continental lithosphere, they remained uncontaminated or were only slightly contaminated by crustal material. Trace element data of the Hocheifel magmas show features of typical Ocean Island Basalts (OIB), i.e. the incompatible elements are enriched compared to compatible elements and the primitive-mantle normalized patterns exhibit negative Cs, Pb, K and Ti

anomalies. The source of the Tertiary Hocheifel magmas appear to be more depleted in trace elements compared to the source of the Quaternary Eifel plume-related magmas.

Sr, Nd and Pb isotopic compositions of the Tertiary Hocheifel magmas indicate a mixing between a depleted end-member characterized by relatively high Pb isotopic compositions, similar to those of the Focal Zone (FOZO) or high- μ (HIMU) and an enriched end-member with enriched mantle 2 (EM 2) isotopic characteristics. The potential involvement of FOZO-like material would tend to show the contribution of the deep lower mantle.

Although, the Sr and Nd isotopic compositions of the Tertiary Hocheifel and the Quaternary Eifel-plume related lavas suggest that they were probably influenced by similar enriched component, trace elements and Pb isotope data indicate that they sampled distinct sources. In contrast to this observation the Sr, Nd and Pb isotopic compositions suggest that the Hocheifel lavas shared a common depleted component with other Tertiary CEVP lavas.

On the basis of the geochemical and isotope data, we cannot rule out the hypothesis that the Hocheifel volcanism was related to mantle dynamics and eventually to a mantle plume activity. We suggest, that the previously with plume material contaminated mantle source is tapped by Eocene volcanism generated by lithospheric extension.

1. Introduction

The Tertiary Hocheifel volcanic area is located in between the Quaternary West and East Eifel volcanic fields, in the Rhenish Massif, Western Germany. This area belongs to the Central European Volcanic Province (CEVP), a volcanic belt which has developed during the Cenozoic across Europe. The ages of volcanic products from the different areas of the CEVP were determined mostly by the conventional K/Ar method (Huckenholz 1983; Lippolt H. 1982; Lippolt H. and Todt 1978; Lippolt 1983; Lippolt, et al. 1990; Mertes and Schminke 1983; Müller-Sohnius, et al. 1989; Rittmann and Lippolt 1998). The geochemical and isotopic characteristics of magmas from individual volcanic areas of the CEVP have been studied and described by several authors (Cebriá and Wilson 1995; Jung 1995; Jung and Hoernes 2000; Lippolt 1983; Mertes 1985; Wedepohl and Baumann 1999; Wedepohl, et al. 1994; Wilson and Downes 1991; Wörner, et al. 1986). Two hypotheses have been proposed to explain the origin of the CEVP magmas: (1) magmas originating from a mantle plume (Duncan 1972; Wedepohl and Baumann 1999) or (2) magmas generation related to extension (Wilson and Downes 1992; Ziegler 1992).

An extensive geophysical investigation was performed in the area of the Quaternary West and East Eifel volcanic fields. The seismic tomography experiments revealed the presence of a low-velocity anomaly in the upper mantle down to a depth of about 400 km, which has been interpreted as a mantle plume (Ritter, et al. 2001). Although the estimated average magma flux for this plume is significantly lower than, for example, the one of the Hawaiian hot-spot (White 1993), there are several additional pieces of evidence that favour the presence of a mantle plume beneath the Eifel during the Quaternary: (1) the uplift of the area contemporaneous with the

Quaternary volcanic activity (Meyer and Stets 1998), (2) the exhalations of He with mantle characteristics (Griesshaber 1992) and (3) the similarity of the geochemical and isotopic characteristics of the volcanic products with those of typical Ocean Island Basalts (OIBs) (Hoernle, et al. 1995; Wedepohl and Baumann 1999). On the basis of this evidence, the origin of the Quaternary West and East Eifel volcanism was attributed to the activity of the so-called Eifel mantle plume (Ritter, et al. 2001). Compared to the well-studied Quaternary volcanic fields, only a few studies have been made so far on the Tertiary Hocheifel volcanic area (Cantarel and Lippolt 1977; Huckenholz 1983; Lippolt 1983; Wörner, et al. 1986). The specific origin of the Tertiary Hocheifel volcanic activity remains a matter of debate.

In this paper we present new major and trace elements data on the Tertiary Hocheifel and Upper Rhine Graben volcanic rocks, as well as Sr, Nd and Pb isotopic compositions on the Tertiary Hocheifel lavas.

2. Geologic setting

The Tertiary Hocheifel volcanism has developed in the Hercynian Rhenish Massif as a part of the large Cenozoic Central European Volcanic Province (CEVP). CEVP forms a belt that extends from France through Germany towards Czech Republic and Poland. The volcanic activity was highly concentrated in the central part of the belt, i.e. Western Germany. It includes the Quaternary West and East Eifel, Tertiary Hocheifel, Siebengebirge, Westerwald, Hessian Depression, Rhön and Heldburger Dyke swarm (Fig. 1). The CEVP has developed close to the Cenozoic European Rift system which is a major tectonic feature of Europe (Ziegler 1992). The Cenozoic European Rift system is about 1100 km long and consists of the Spanish Valencia

Trough, the Gulf of Lions, Saône, Limagne and Bresse grabens, the Rhine, Ruhr and Leine grabens which crosscut the Rhenish Shield, and the Eger Graben. This extensive rift system has developed in the Alpine foreland as a result of tensional reactivation of the Late Hercynian fractures (Ziegler 1992). The Rhine Graben, the Leine Graben and the Ruhr Valley Graben form a complex triple junction (Fig. 1), which is located close to the principal center of the volcanic activity in the Rhenish Massif (Ziegler 1992).

The Tertiary Hocheifel volcanic area contains about 300 volcanic occurrences spread over ~1000 km² in between the Quaternary West and East Eifel volcanic fields (Huckenholz 1983). The Hocheifel volcanic edifices, which are at present deeply eroded, produced mostly basaltic and only few differentiated lavas. A systematic zoning within the Tertiary Hocheifel area has been observed (Huckenholz 1983): the most differentiated lavas erupted in the central part of the Hocheifel area and the basaltic products are spread mostly towards the outside of the area. Conventional K/Ar dating led to the conclusion that the volcanic activity in the Hocheifel area was restricted between 45 and 18 My (Cantarel and Lippolt 1977; Lippolt and Fuhrmann 1980). However, it has been demonstrated that the ages obtained by the conventional K/Ar dating of volcanic rocks from several CEVP have been affected by a significant Ar-excess (Lippolt, et al. 1990; Rittmann and Lippolt 1998). Therefore, the age data of the individual volcanic occurrences should be reviewed.

3 Methods

3.1 Samples

We collected 20 samples in the Hocheifel and 6 samples in the Upper Rhine Graben volcanic areas. The majority of the volcanic rocks are mafic, non-differentiated lavas, only 4 Hocheifel samples represent more differentiated volcanic rocks. The samples are generally fresh, although the olivine phenocrysts exhibit iddingsite rims and fillings in the fractures. The most primitive samples have finely crystallised to glassy matrix and are rich in olivine and clinopyroxene phenocrysts (from 10 to 60%). Olivine crystals, ranging from 0.5 to 3 mm, are mostly euhedral and fractured. The clinopyroxenes are brown Ti-augites with zoning: a dark-brown rim surrounding a light-brown core. Rarely, the clinopyroxenes exhibit greenish core and brown rim. The primitive samples are characterized by abundance of oxides, from 0.1 to 0.5 mm. The evolved lavas contain variable amounts of the phenocrysts of hornblendes, plagioclases and biotites, in addition to clinopyroxenes and oxides.

3.2 Analytical methods

Samples were crushed into small pieces using a hydraulic press and separated in two aliquots: one aliquot was used for the $^{40}\text{Ar}/^{39}\text{Ar}$ dating and the other aliquot for geochemical and isotopic analyses. Details on the $^{40}\text{Ar}/^{39}\text{Ar}$ dating method and results on the Tertiary Hocheifel and Upper Rhine Graben volcanic occurrences were presented and discussed in (Fekiacova, et

al. submit.). For the geochemical and isotopic analyses, the samples were milled into fine powders using an agate mill.

Bulk rock analyses for major elements were determined by Professor Matthew Thirlwall using the Philips PW1480 XRF spectrometer of the London University XRF facility at Royal Holloway. Major elements were analyzed on glass discs prepared from sample powder ignited at 1100°C, providing the loss on ignition (LOI) value. Major elements 2σ range from 0.005 to 0.15. The accuracy is estimated to be similar to the 2σ based on the conformity of standard results to recommended values and on isotope dilution studies (Thirlwall, et al. 2000).

Trace elements were analyzed by Laser Ablation Inductively-Coupled Plasma Mass-Spectrometer (ICP MS) using an Element 2 (Finnigan) connected to a 213 nm laser (Merchantek) at the Max-Planck-Institute for Chemistry, Germany. We used the NIST 612, KL2 and T1 glasses as standard reference material. They were analyzed repeatedly together with the samples. The average relative standard deviation (RSD) based on the repeated measurements of the standard materials range from 2 to 4%.

Sr, Nd and Pb isotopic compositions were measured using a Thermal Ionisation Mass Spectrometer (TIMS) MAT 261 (Finnigan), at the Max-Planck-Institute for Chemistry, Mainz. The sample powders were dissolved in a mixture of concentrated HF and HNO₃. Sr was separated using a cationic exchange column (BioRad AG 50x80, 100 - 200 mesh, 1 column volume (1 cv) =5 ml) with 2.5N HCl used as eluant. Nd was separated by reversed-phase chromatography on HDEHP (di(2-ethylhexyl) phosphoric acid) coated on Teflon columns (1 cv =2 ml) with 0.18N HCl used as eluant. The total blanks ranged from 0.2 to 0.8 ng for Sr and from 27 to 36 pg for Nd, which is negligible compared to total amounts measured (typically ~400 ng for Sr and ~ 300 pg for Nd). The measured values were referenced to the standard reference

material NIST SRM 987 for Sr ($^{87}\text{Sr}/^{86}\text{Sr}=0.71024$) and to the La Jolla value of $^{143}\text{Nd}/^{144}\text{Nd}=0.51186$ for Nd. The Pb fractions were separated using an anion exchange resin (AG 1X8, 100-200 mesh, 1 cv=100 ml) and the eluent was a mixture of HBr and HNO_3 (Abouchami, et al. 1999a; Lugmair and Galer 1992). Pb isotopic compositions were measured using the triple spike technique to correct for instrumental mass fractionation (Galer 1999). The measured values were referenced to the values of the standard reference material NIST SRM 981 Pb standard, with $^{206}\text{Pb}/^{204}\text{Pb}$, $^{207}\text{Pb}/^{204}\text{Pb}$ and $^{208}\text{Pb}/^{204}\text{Pb}$ of 16.9401 ± 23 , 15.4968 ± 29 and 36.7234 ± 44 (2 σ), respectively. The total Pb blanks ranged from 12 to 17 pg and are negligible compared to the total amount of Pb (typically ~ 300 pg).

4. Results

4.1. Major and trace elements

Major and trace element concentrations are reported in Table 1. Based on the TAS classification (LeMaitre 1989) the majority of the Hocheifel lavas are basanites (13 samples) which together with two basalts are termed “less differentiated group” herein for brevity. A “more differentiated groupe ” of five Hocheifel lavas represent hawaiitic, shoshonitic, latitic and trachytic compositions. The Upper Rhine Graben lavas are of basanites and foidites (Figure 2a).

Figure 2 (b-i) shows the major element oxides variations of the Hocheifel and Upper Rhine Graben lavas. In addition, data on the neighboring Westerwald, Vogelsberg and Quaternary West and East Eifel lavas are shown, for comparison (Bogaard and Wörner 2003; Haase 2004; Mertes 1985). Hocheifel basanites and basalts have high Mg# ranging from 57 to 72 and relatively high sodium content ($\text{Na}_2\text{O}>2.27$ wt.%). Their TiO_2 (2.15 – 3.1 wt.%), Fe_2O_3^* (10.45 –

13.78 wt.%) and CaO (10.98 – 13.02 wt.%) concentrations decrease with the increasing SiO₂ contents. The Hocheifel lavas have, in general, similar ranges of major element contents compared to the Tertiary Westerwald and Vogelsberg. The Westerwald lavas have however, higher Fe₂O₃ (up to 14.51 wt.%) and TiO₂ (up to 3.71 wt.%) contents compared to the Hocheifel basanites and basalts. The Quaternary Eifel lavas show larger ranges of major element compositions. Although the East Eifel lavas are, in general similar to the Hocheifel basanites and basalts, the West Eifel lavas have lower Al₂O₃ and MnO contents. Both, Quaternary West and East Eifel lavas have significantly higher potassium content (up to 4.1 wt. %) compared to the Tertiary Hocheifel basanites and basalts (0.6-2.01 wt. %). The Upper Rhine Graben lavas exhibit similar major element compositions to those of the Hocheifel basanites and basalts except that the Upper Rhine Graben rocks generally have lower Al₂O₃ concentrations.

The differentiated Hocheifel samples range from trachybasalt to trachyte and have high SiO₂ (51 to 66 %), Al₂O₃ (>17.5 wt.%) and Na₂O (>4.2 wt.%) contents. They are characterized by lower Mg# (24-49) compared to the less differentiated Hocheifel lavas. According to a TAS classification (LeMaitre 1989), the differentiated Hocheifel samples are shoshonites and latites. This is in contrast to the previously published description by Huckenholz and Büchel, (Huckenholz and Büchel 1988) who described occurrences of mugearites and benmoreites. This nomenclature refers to relative potassium and sodium contents. While shoshonites and latites have Na₂O-2 □K₂O, benmoreites and mugearites have Na₂O-2 ≥ K₂O (LeMaitre 1989).

The Hocheifel and Upper Rhine Graben volcanic rocks have similar chondrite-normalized Rare Earth Element (REE) patterns (Figure 3). The light Rare Earth Elements (LREE) are enriched relative to the middle REE (MREE) and heavy REE (HREE). Chondrite-normalized (La/Sm)_n and (La/Lu)_n ratios range from 3.42 to 12.74 and from 14.42 to 35.89, respectively.

Two differentiated Hocheifel samples (#19, trachyte from Reimerath and #17, latite from Bocksberg) have substantially higher REE concentrations compared to all other samples. For example, their La content is about 1 order of magnitude higher compared to the remaining 24 samples.

Primitive mantle-normalized trace element patterns of the Hocheifel and Upper Rhine Graben lavas are shown on a figure 4 a, b. The Upper Rhine Graben lavas have similar PM-normalized trace element patterns to those of the undifferentiated Hocheifel lavas. The incompatible elements, such as Ba, Th, U, Nb are about 9 to 15 times enriched relative to less incompatible elements, such as Y, Tb. The samples exhibit large negative Cs, Pb, K and Ti anomalies, up to 3 times for Cs, 100 times for Pb, 14 times for K and 4 times more depleted compared to their surrounding elements. In addition, all samples exhibit a slight negative Hf anomaly, up to 2 times less than the surrounding elements. Samples #24, #25, #23 and #11 show significantly higher Cs concentrations compared to the other samples

The differentiated Hocheifel samples have similar general shape of the trace elements patterns compared to the basanites and basalts, i.e. the incompatible elements are enriched compared to the compatible elements and they exhibit more or less important negative K, Pb and Ti anomalies (Fig. 4b). However, the most evolved rocks (especially #19, trachyte from Reimerath and #17, latite from Bocksberg) are 10 to 30 times more enriched compared to the less differentiated Hocheifel lavas. In addition to the negative K, Pb and Ti anomalies, the differentiated lavas show also a negative Ba and Sm anomalies in their trace element patterns. The latite from Quiddelbach (#5) has trace element pattern slightly distinct from all the other samples.

The undifferentiated Hocheifel and Upper Rhine Graben lavas have primitive mantle-normalized trace element patterns exhibit typical features of the Ocean Island Basalts (Hofmann 1997; Weaver 1991) which are often associated with hot-spots (Fig. 4c). They are up to 100 times enriched compared to the primitive upper mantle, with the highest normalized concentrations at the highly incompatible elements (Rb, Ba, Th). In addition, they bear significant negative Pb and K anomalies which is a feature that can be used to distinguish between the oceanic basalts on one side and continental crust and island arc basalts on the other (Hofmann 1997).

Comparison of the Tertiary Hocheifel and Quaternary West and East Eifel lavas shows that they have similar general shape of the primitive mantle-normalized trace element patterns Fig. 4d). However, the Quaternary Eifel lavas are, on average (with exception of Pb) 2 times more enriched in trace elements compared to the Tertiary lavas.

4.2 Sr, Nd and Pb isotopic compositions

Table 2 presents the measured Sr, Nd and Pb isotopic compositions of the Hocheifel lavas as well as the calculated initial ratios based on the $^{40}\text{Ar}/^{39}\text{Ar}$ ages (Fekiacova, et al. submit.). The ranges of initial ratios are 0.7032 to 0.7047 for $^{87}\text{Sr}/^{86}\text{Sr}$, 0.512647 to 0.512847 for $^{143}\text{Nd}/^{144}\text{Nd}$, 19.3971 to 19.7390 for $^{206}\text{Pb}/^{204}\text{Pb}$, 15.6171 to 15.6477 for $^{207}\text{Pb}/^{204}\text{Pb}$ and 39.1170 to 39.5303 for $^{208}\text{Pb}/^{204}\text{Pb}$ ratios.

Sr, Nd and Pb isotopic compositions of the Hocheifel lavas are shown in figure 5. The differentiated Hocheifel lavas have, with exception of one sample (#5, see Table 1) higher $(^{87}\text{Sr}/^{86}\text{Sr})_i$ and lower $(^{143}\text{Nd}/^{144}\text{Nd})_i$ ratios (i refers to initial) compared to the basanites and basalts. There is a relationship between the initial isotopic compositions and age of the

Hocheifel volcanic activity. The older age group (ca. 44 to 39 Ma) distinguished by (Fekiacova, submit. #115) has, in general, higher Sr and lower Nd isotopic compositions compared to the younger group (ca. 38 to 35 Ma). Whereas the younger Hocheifel lavas have relatively constant $(^{87}\text{Sr}/^{86}\text{Sr})_i \sim 0.7032$, Sr and Nd isotopic compositions of the older lavas are negatively correlated. Sr and Nd isotopic compositions of the Quaternary West and East Eifel lavas (Wedepohl, et al. 1994; Wörner, et al. 1986) are shown, for comparison. They exhibit distinct Sr and Nd isotopic compositions from those of the Tertiary Hocheifel lavas (Fig. 5a). Only the trachyte from Reimerath (#19) lies in the field formed by the Quaternary East Eifel lavas. However, the linear arrays formed by the Tertiary Hocheifel and Quaternary West and East Eifel lavas converge towards the enriched Sr and Nd isotopic compositions.

In a $(^{206}\text{Pb}/^{204}\text{Pb})_i$ vs. $(^{208}\text{Pb}/^{204}\text{Pb})_i$ diagram (Fig. 5b), the Hocheifel lavas show a rather small range of values, from 19.40 to 19.74 and from 39.11 to 39.53 for $(^{206}\text{Pb}/^{204}\text{Pb})_i$ and $(^{208}\text{Pb}/^{204}\text{Pb})_i$ ratios, respectively. On the basis of the available Pb data, there is no distinction between the younger and older Hocheifel lavas. However, the Tertiary Hocheifel lavas have distinct Pb isotopic compositions from those of the Quaternary West and East Eifel lavas (Fig. 5b). At a given $(^{206}\text{Pb}/^{204}\text{Pb})_i$ the Hocheifel have lower $(^{208}\text{Pb}/^{204}\text{Pb})_i$ ratios, compared to the Quaternary Eifel lavas. In a $(^{206}\text{Pb}/^{204}\text{Pb})_i$ vs. $(^{207}\text{Pb}/^{204}\text{Pb})_i$ diagram (Fig. 5c), the data show considerable scatter, which makes the evaluation impractical.

The published Pb isotope data on the Quaternary Eifel lavas were obtained by conventional analytical methods and might be influenced by the effect of instrumental mass fractionation. Therefore, the comparisons should be taken with caution. Since there are only conventional Pb isotopes data available on the Quaternary Eifel lavas, this renders a comparison with our triple spike data difficult.

5. Discussion

5.1 Major and trace elements

5.1.1 Crustal contamination

Tertiary Hocheifel and Upper Rhine Graben lavas erupted through a continental lithosphere that, beneath the Rhenish Massif, is ~50-60 km thick (Babuska and Plomerova 1992; Goes, et al. 2000). Therefore, it is necessary to evaluate whether the Tertiary Hocheifel and Upper Rhine Graben lavas were contaminated by crustal material. While the lower crust beneath the Rhenish Massif is composed of mafic and felsic granulites (Rudnick and Goldstein 1990; Stosch and Lungmair 1984; Stosch and Lungmair 1986), the upper crust consists of Paleozoic sediments and volcanic rocks (Mengel, et al. 1991). Green-core clinopyroxenes from the Quaternary Eifel basanites and picrites show that these magmas have stagnated in the lower crust (Duda and Schmincke 1985; Sachs and Hansteen 2000). Thus, we have used the geochemical and isotopic characteristics of the lower crust to evaluate a possible crustal contamination of the Hocheifel and Upper Rhine Graben magmas.

Trace element patterns can be used to indicate whether or not magmas have been contaminated by crustal material. Positive Pb and negative Nb anomalies in the trace elements pattern are thought to be characteristic of the continental crust (Hofmann 1997). Thus, the presence of these anomalies would indicate the involvement of the crustal material. However, the trace element patterns of the Hocheifel lavas show no positive Pb and no negative Nb anomalies (Fig. 4). This implies that little, if any, crustal material was incorporated in the primitive Hocheifel magmas. In contrast, the differentiated lavas show distinct evidence for crustal contamination (see below).

Trace element ratios can also be used to characterize specific magmatic reservoirs. Ce/Pb and Nb/U remain constant and given Ce/Pb and Nb/U are therefore characteristic of specific magma reservoirs (Hofmann, et al. 1986). The Ce/Pb ratio of the average MORB and OIB is 25 ± 5 (Hofmann, et al. 1986) whereas the average continental crust shows Ce/Pb = 3.9 (Rudnick and Gao 2003). The average MORB and OIB have Nb/U = 47 ± 10 (Hofmann, et al. 1986) whereas the average continental crust exhibits the Nb/U ratio of 6.2 (Rudnick and Gao 2003). The majority of the Hocheifel and the Upper Rhine Graben basanites and basalts display Ce/Pb and Nb/U ratios which are significantly higher than those of the average continental crust. Instead, they lie within or above the range of the average MORB and OIB values (Fig. 6 a, b). For comparison, the Ce/Pb ratios of the crustal xenoliths from the Eifel area are shown in Fig. 6a. They have, in general, distinct Ce/Pb ratios from those of the Hocheifel lavas. However, two undifferentiated (#15 and # 18) and two differentiated (#17 and #19) samples have lower Ce/Pb ratios than those of the oceanic basalts and overlap with the crustal xenoliths values (Fig. 6a). Similarly, four undifferentiated (#15, # 18, #11 and #7) and all the differentiated Hocheifel samples have Nb/U ratios lower than those of oceanic basalts values. These features indicate a possible involvement of crustal material in some of the Hocheifel magmas. Especially the differentiated rocks appear to be significantly affected by crustal contamination.

Figure 6c shows that the Sr and Nd isotopic compositions of the Hocheifel lavas are (with the exception of three differentiated samples) distinct from those of the granulite xenoliths that represent the lower crust beneath the Eifel (Stosch and Lungmair 1984). The Hocheifel lavas overlap instead, the field of the mantle xenoliths recovered in the basalts from the West Eifel area studied by Stosch et al. (Stosch and Lungmair 1986).

The Pb isotopic compositions are sensitive indicator of the crustal contamination. Figure 6 (d, e) shows the Pb isotopic compositions of the Hocheifel lavas and granulite xenoliths. Although both groups are distinct in Pb isotope space, the differentiated sample (#13) tends towards crustal compositions. Additional Pb isotopes analyses would be necessary in order to estimate the amount of the crustal contamination of the Hocheifel magmas.

To summarize, on the basis of the trace element ratios and Sr, Nd and Pb isotopic compositions we cannot rule out some degree of crustal contamination of the Hocheifel magmas and especially differentiated samples. Nevertheless, in the least differentiated samples, this effect must be quite small.

5.1.2 Mantle source of the Hocheifel magmas

Although we cannot completely rule out a slight crustal contamination of the differentiated and two undifferentiated samples of the Hocheifel magmas, the majority of the basanitic and basaltic lavas have geochemical and isotopic characteristics distinct from those of the continental crust, which indicates that they were formed by melting of a mantle source. An estimation of depth and melting conditions can be made using the silica content and major elements oxides ratios. Kushiro (Kushiro 1996) showed that the silica under-saturated magmas are produced by melting of a garnet peridotite at high pressures. The basanitic and basaltic Hocheifel and Upper Rhine Graben lavas have low SiO₂ contents (41–47 %) suggesting that they originate from a garnet peridotite source. CaO/Al₂O₃, CaO/TiO₂ and Al₂O₃/TiO₂ ratios are strongly affected by melting (Herzberg 1992). Therefore, they can be used for evaluation of melting conditions. According to the experimental results of Kushiro (Kushiro 1996), melting of a garnet lherzolite at about 25-30 kbar and 1425-1500°C can produce magmas with low silica

content (~45%) and with the $\text{CaO}/\text{Al}_2\text{O}_3$, CaO/TiO_2 and $\text{Al}_2\text{O}_3/\text{TiO}_2$ ratios similar to those of Hocheifel and Upper Rhine Graben lavas (Fig. 7). Thus, the Hocheifel and Upper Rhine Graben basanitic and basaltic magmas appear to result from the melting of a garnet lherzolite, at high pressures (~25-30 kbar) and temperatures (~1425-1500°C). These pressures correspond to a depth of about 75 –90 km.

5.2. Isotopic compositions

In a $(^{87}\text{Sr}/^{86}\text{Sr})_i$ vs. $(^{143}\text{Nd}/^{144}\text{Nd})_i$ diagram, the Hocheifel lavas form an array from the depleted quadrant towards enriched compositions (Fig. 8a). The depleted end of the Hocheifel array tends towards low $^{87}\text{Sr}/^{86}\text{Sr}$ and high $^{143}\text{Nd}/^{144}\text{Nd}$ ratios, compositions which are similar to those of a HIMU reservoir (Fig. 8a). HIMU refers to a mantle component characterized by high time-integrated $^{238}\text{U}/^{204}\text{Pb}$ ratios (referred to as \square) (Zindler and Hart 1986). The enriched end of the Hocheifel array extends towards the bulk silicate earth (BSE) compositions and exhibits high $^{87}\text{Sr}/^{86}\text{Sr}$ and low $^{143}\text{Nd}/^{144}\text{Nd}$ compositions. The Hocheifel array can be interpreted in terms of binary mixing suggesting that the Hocheifel lavas result from mixing between two isotopically distinct end-members: a depleted and an enriched component. While the depleted component seems to originate from the mantle, the enriched end-member can reflect either the involvement of crustal material or an enriched mantle component. The available trace element and isotope data suggest that only the differentiated and two mafic Hocheifel lavas were probably affected by crustal contamination (Fig. 6). The majority of the undifferentiated lavas appears to be uncontaminated (Fig. 6). Therefore, it is likely that they were produced by mixing between two discrete mantle components.

5.2.1 Source(s) of the Hocheifel magmas – deep mantle involvement?

The Hocheifel magmas have elevated $^{206}\text{Pb}/^{204}\text{Pb}$ ratios (>19.4) and the depleted end of the Hocheifel array tends towards the Sr and Nd isotopic compositions similar to those of HIMU (Fig 8a). In addition, the trace element ratios, Rb/Nb, Ba/Th, Ba/Nb, Ba/La and K/Nd, which can also be used for discrimination between distinct mantle reservoirs (Weaver 1991) indicate that HIMU and enriched mantle 2 (EM 2) reservoirs were involved in the Hocheifel magmas (Fig. 9). However, on the basis of the Pb isotopic compositions, other mantle components can also be considered as being involved in the Hocheifel magmas. The Hocheifel magmas have significantly less radiogenic Pb isotopes than the HIMU reservoir (Fig. 8 b, c). They show instead, the Pb isotopic compositions similar to those of the so-called Focal Zone (Fig. 8 b, c). The Focal Zone (FOZO) compositions were first described by (Hart, et al. 1992) who suggested that it originates in the lower mantle and that it contributes to most Ocean Island Basalts (OIB). The FOZO Sr and Nd isotopic compositions are comparable to those of a depleted MORB mantle (DMM). In contrast, they are significantly more radiogenic $^{206}\text{Pb}/^{204}\text{Pb}$ ratios compared to DMM (Hofmann 2003). Although the exact values of the FOZO compositions are not yet well constrained, the approximate ranges of compositions are: $^{87}\text{Sr}/^{86}\text{Sr} \sim 0.7030 - 0.7040$, $^{143}\text{Nd}/^{144}\text{Nd} \sim 0.51300 - 0.51280$, $^{206}\text{Pb}/^{204}\text{Pb} \sim 18.50 - 19.50$, $^{207}\text{Pb}/^{204}\text{Pb} \sim 15.55 - 15.65$ and $^{208}\text{Pb}/^{204}\text{Pb} \sim 38.80-39.30$ (Hauri, et al. 1994). In addition, the high $^3\text{He}/^4\text{He}$ ratios ($> 8\text{Ra}$) of the FOZO indicates that it originates from the lower mantle (Hart, et al. 1992; Hauri, et al. 1994). In a Sr vs. Nd isotopes plot, the FOZO compositions partly overlap those of the HIMU, DM and EM 2. Since the depleted end of the Hocheifel trend extends towards the depleted HIMU and FOZO-like compositions (Fig. 8a) it seems unlikely that the DM represents the depleted end-member for the Hocheifel lavas. In ^{206}Pb - ^{208}Pb space, the Hocheifel trend extends between the

DM, EM 2 and/or FOZO Pb isotopic compositions (Fig. 8b). It does not tend towards the HIMU end-member suggesting that the HIMU-type material was not involved in the Hocheifel magmas. Consequently, the Sr, Nd and Pb isotopic compositions appear to indicate that the FOZO-like material corresponds to the depleted end-member of the Hocheifel mixing array. However, the slope of the Hocheifel array in the Pb isotope space (Fig. 8b) appears to be fully controlled by the Pb compositions of the least radiogenic sample and it is probable, that the slope will vary when we incorporate additional data. Thus, we cannot with certainty exclude the HIMU reservoir as being responsible for the Sr-Nd depleted signature of the Hocheifel lavas.

From the “depleted Sr-Nd end-member”, the Hocheifel array extends towards the enriched mantle compositions (Fig. 8a). Although the Sr and Nd isotopes point to enriched mantle 1 (EM 1), the trace element ratios (Fig. 6) and Pb isotopic compositions (Fig. 8 b, c) indicate the EM 2 reservoir to be involved in the Hocheifel magmas. The EM 2 reservoir was thought to be formed by recycled oceanic crust with addition of terrigenous sediments (Hart, et al. 1992; Hofmann and White 1982; Weaver 1991; White 1985; Zindler and Hart 1986). However, the most recent studies suggest that recycled sediment cannot be at the origin of the enriched EM 2 compositions (Workman, et al. 2004). Workman et al. (2004) suggest instead, that metasomatism of the subducted oceanic lithosphere followed by long time storage in the deep mantle are mechanisms responsible for the EM 2 signature.

To summarize, the Sr, Nd and Pb isotopic compositions of the Hocheifel lavas indicate that they result from mixing between, at least, two components: 1) a depleted component with FOZO- or HIMU- like Sr and Nd isotopic characteristics and 2) an enriched component with EM 2 geochemical and isotopic characteristics.

5.2.2 A mantle plume component in the Hocheifel magmas?

Large-scale seismological survey and geochemical investigations of the individual volcanic areas in Europe have contributed evidence about mantle upwellings beneath Europe.

For example, (Hoernle, et al. 1995) presented geochemical and isotopic data supported by evidence from seismological investigations and from regional geology, suggesting that there is a large-scale Low Velocity Anomaly in the upper mantle beneath Eastern Atlantic as well as Western and Central Europe. On the basis of isotopic compositions of Cenozoic volcanic rocks, Hoernle et al. (1995) were able to identify a common sub-lithospheric mantle source for the East Atlantic volcanic province, Western Mediterranean volcanic province and Central European Volcanic Province magmas. They have defined the isotope composition of this end-member, which corresponds to the seismic low velocity anomaly and was consequently called low velocity composition (LVC). Geochemical and isotopic data indicate that the LVC originates from the sub-lithospheric mantle. However, whether the LVC is sampled by a single upwelling or by numerous smaller localized upwellings remains a matter of debate.

Furthermore, on the basis of tomographic images, Goes et al. (Goes, et al. 1999) pointed out the existence of a low velocity structure in the lower mantle (600 to 2000 km depth) beneath Central Europe. They suggested that this anomaly represents a large scale lower mantle upwelling, which may feed smaller mantle plumes.

Finally, the most recent seismic tomography investigations revealed the presence of a low P-wave velocity anomaly below the Quaternary West and East Eifel volcanic areas (Ritter, et al. 2001). This anomaly extends to, at least, 400 km depth and is attributed to the excess temperature of about 150-200K. It has been suggested that this anomaly, also called the Eifel mantle plume, is at the origin of the Quaternary West and East volcanic activity (Ritter, et al.

2001). This hypothesis is supported by the geochemical and isotopic characteristics of the Quaternary Eifel lavas as well as by regional geology (Griesshaber 1992; Hoernle, et al. 1995; Meyer and Stets 1998; Wedepohl and Baumann 1999; White 1993). The time-life of this mantle plume is not yet constrained. Thus, the question whether the Tertiary Hocheifel lavas can represent a precursor activity of this plume remains unsolved.

The Tertiary Hocheifel lavas have primitive mantle-normalized trace element patterns similar to those of the Quaternary West and East Eifel lavas (Fig 4). They both display features typical of Ocean Island Basalts (OIB) which are traditionally associated with hot-spots. Their highly incompatible elements (Rb, Ba) are enriched compared to the less incompatible elements (Zr, Y) and they exhibit negative K and Pb anomalies (Fig. 4b). However, the Quaternary Eifel lavas have, with exception of Pb and Nb, higher trace element concentrations compared to the Tertiary lavas suggesting that the source of the Quaternary Eifel magmas was more enriched in trace elements compared to the source of the Tertiary magmas, or, alternatively, that the degree of melting was slightly lower.

The Tertiary Hocheifel and Quaternary West and East Eifel lavas have distinct Sr, Nd and Pb isotopic compositions (Fig. 5). The Hocheifel lavas have generally more depleted Sr and Nd isotope ratios. At a given $^{206}\text{Pb}/^{204}\text{Pb}$, they also have lower $^{208}\text{Pb}/^{204}\text{Pb}$ ratios than those of the Quaternary Eifel lavas. Thus the geochemical and isotopic characteristics indicate that the Tertiary and Quaternary Eifel magmas sampled isotopically different sources. However, in a Sr-Nd isotope plot (Fig. 5a), the Hocheifel, the West and East Eifel linear trends converge towards similar enriched Sr and Nd isotopic compositions (Fig. 5a). This feature suggests that the Tertiary Hocheifel and Quaternary West and East Eifel lavas were influenced by a similar enriched component (Fig. 5a) although this feature does not seem to be confirmed by the Pb

isotope data (Fig. 5 b, c). The Tertiary and Quaternary Eifel lavas show distinct Pb isotopic compositions. However, the number of data, especially for the Pb isotopic compositions (and the problems related to comparing Pb isotope data from different laboratories) render the identification of source differences of the Tertiary Hocheifel and Quaternary Eifel magmas rather difficult.

To summarize, the Hocheifel magmas bear particular geochemical and isotopic signatures: (1) Their Sr, Nd and Pb isotopic characteristics are similar to those of the FOZO composition which is thought to sample the lower mantle. (2) Their trace element concentrations display features typical for the Ocean Island Basalts (OIB) which are traditionally associated with hot-spots, and (3) their Sr and Nd isotopes indicate the involvement of an enriched component similar to the one of the plume related Quaternary Eifel lavas. Together, these geochemical and isotopic features tend to show that the Hocheifel magmas could be related to the activity of a mantle plume or could be the precursor of the activity of the Eifel mantle plume.

However, a recent study based on Ar-Ar dating of the same Tertiary Hocheifel and Rhine graben samples as the ones used in the present study tends to show that the Tertiary Hocheifel volcanism was controlled by the tectonic regime in Central Europe during the Tertiary and that the Hocheifel magmas were produced by decompression melting due to pre-rift tectonic activity in the Rhine Graben area (Fekiacova, et al. submit.). In addition, two features argue against a mantle plume origin for the Tertiary Hocheifel volcanism. (1) A hot-spot track would testify for the mantle plume origin of the both Quaternary and Tertiary Eifel magmas. However, none was identified in the Eifel area. (2) There is a time gap of almost 30 My between the Tertiary and the Quaternary volcanic activity in the Eifel area. Thus, if both Quaternary and

Tertiary Eifel magmas were related to the Eifel plume activity, one should search for the explanation of this huge time gap of the volcanic activity.

To summarize, the available geochemical and isotope data on the Hocheifel lavas indicate an involvement of a plume-type material. In contrast, the geochronology, tectonics and regional geology argue against the mantle plume origin of the Tertiary Hocheifel volcanism and point towards the extension-related magma generation mechanism. The two hypotheses are not necessarily incompatible and, for the time being, with available data we cannot rule out either of them.

5.3 Comparison with other CEVP occurrences

Individual CEVP areas have been subject of many geochemical studies that provided more or less complete data sets on the geochemical and isotopic compositions of their volcanic products. The data have been summarized in several compilations e.g. (Wedepohl and Baumann 1999; Wedepohl, et al. 1994; Wilson and Downes 1991; Wörner, et al. 1982). Compared to the relatively large number of data on the other CEVP occurrences, there was a considerable lack of data on the Tertiary Hocheifel volcanic area.

The volcanic activity in the CEVP produced mainly primitive mafic magmas, such as alkali olivine basalts, nepheline-basanites and olivine-nephelinites, and only minor occurrences of highly differentiated lavas (e.g. phonolites) (Wedepohl, et al. 1994). In a $^{87}\text{Sr}/^{86}\text{Sr}_i$ vs. $^{143}\text{Nd}/^{144}\text{Nd}_i$ diagram, the undifferentiated lavas from Hocheifel, Vogelsberg, Westerwald, Siebengebirge and Rhön form fields which converge at the depleted end (Fig. 10a). This feature indicates that the primitive Tertiary CEVP magmas shared a common isotopically depleted end-member. Its Sr and Nd isotopic compositions could be similar to the LVC described by

(Hoernle, et al. 1995). The $^{87}\text{Sr}/^{86}\text{Sr}$ ratios of the LVC range from 0.7030 to 0.7034 and the $^{143}\text{Nd}/^{144}\text{Nd}$ vary from 0.51282 to 0.51294 ($\epsilon_{\text{Nd}} \sim -3.5$ to 5.9). The LVC exhibits radiogenic Pb isotopic compositions, the $^{206}\text{Pb}/^{204}\text{Pb}$ ratios range from 19.9 to 20.1, $^{207}\text{Pb}/^{204}\text{Pb}$ ratios vary from 15.62 to 15.68 and $^{208}\text{Pb}/^{204}\text{Pb}$ ratios range between 39.6 and 39.90. The LVC was shown to be from the asthenospheric mantle (Hoernle, et al. 1995). Consequently, the depleted LVC material appears to represent a potential common source for the Tertiary Hocheifel and other CEVP magmas. However, the depleted end-member could also be FOZO-like, i.e. originating from much deeper than the LVC. Hoernle et al. (Hoernle, et al. 1995) suggested that the common LVC reservoir was sampled by small plumes which brought the asthenospheric material to the surface. In contrast, the Tertiary Hocheifel magmas appears to be produced by decompression melting controlled by pre-rift tectonic activity in Central Europe (Fekiacova, et al. submit.).

From the common depleted component, the fields formed by the individual primitive Tertiary CEVP lavas spread towards distinct enriched compositions (Fig. 10). The slopes of the trends formed by the individual CEVP lavas differ from each other. Each trend can be interpreted as resulting from a binary mixing line. Thus, it appears that the individual CEVP magmas shared the same depleted component but interacted with different types of enriched material. For example, the Rhön trend has the shallowest slope and extends towards the EM 2-type compositions. In contrast, the Vogelsberg lavas form trend with the steepest slope which extends towards the EM 1-type compositions.

Figure 10b shows the Pb isotopic compositions of the individual CEVP lavas. It is important to notice that the Pb data on the CEVP lavas were obtained by the conventional methods. In contrast to our Pb triple spike data, the conventional data can be biased by the instrumental mass fractionation. Therefore, care should be taken when considering these data.

In a $^{206}\text{Pb}/^{204}\text{Pb}$ vs. $^{208}\text{Pb}/^{204}\text{Pb}$ diagram, the Hocheifel, Westerwald and Siebengebirge lavas show more radiogenic Pb isotopic compositions than those of the Vogelsberg, Rhön and Hessian Depression lavas (Fig. 10b). Either this feature reflects Pb isotopes heterogeneities present in the common asthenospheric component, or it results from the involvement of distinct enriched end-members of the individual CEVP magmas. We can relate the differences in Pb isotopic composition to the localization of the CEVP volcanic occurrences: the lavas from the western part of the Rhenish Massif (Hocheifel, Westerwald, Siebengebirge) sampled more radiogenic Pb isotopic compositions than those of the eastern part (Vogelsberg, Rhön, Northern Hessian Depression). A similar separation has already been shown by Haase et al., 2004 (Haase 2004) and is now confirmed by our data. The volcanic occurrences from the central part of the Rhenish Massif (Hocheifel, Westerwald and Siebengebirge) have erupted in an area located between the Upper Rhine and Lower Rhine grabens (Fig 1). In contrast, the areas located in the eastern part of the Rhenish Massif (Vogelsberg, Rhön and Northern Hessian Depression) are close to the Leine Graben. Geochronological and tectonic evidences have shown that the Hocheifel volcanism represents a northwestern prolongation of the pre-rift volcanism in the Upper Rhine Graben (Fekiacova, et al. submit.). Similarly, it appears that the tectonic control also played an important role in the generation of the volcanic activity in the other Tertiary CEVP areas. However, more detailed geochronological and geochemical investigations investigation of the individual Tertiary CEVP volcanic products would be necessary in order to develop this hypothesis.

6 Conclusion

Based on our new geochemical and isotope data on the Tertiary Hocheifel and Upper Rhine Graben lavas we could evaluate the character of magmas, estimate the melting conditions and source components which were involved in their magmas, and we propose the following conclusions:

1/ The Tertiary Hocheifel and Upper Rhine Graben volcanic products are dominated by basanitic and basaltic compositions.

2/ The Hocheifel and Upper Rhine Graben magmas were produced by partial melting of a garnet peridotite at high pressures and temperatures which correspond to depths of about 75 to 90 km.

3/ The Hocheifel and the Upper Rhine Graben lavas erupted through relatively thick continental crust. However, the available geochemical and isotopic data indicate that these lavas were only slightly affected by crustal material.

4/ The source of the Hocheifel magmas appear to result from the mixing of two isotopically distinct mantle components: a depleted FOZO or HIMU - like component and an enriched component with EM 2 isotopic characteristics.

5/ The potential involvement of the FOZO-like compositions in the Hocheifel lavas indicate the possibility of the involvement of a deep mantle material.

6/ Although the available trace element and isotope data indicate that the Tertiary Hocheifel and the Quaternary Eifel lavas sample distinct sources, they both appear to be influenced by similar enriched component.

8/ The Hocheifel lavas most likely shared a common depleted LVC with other CEVP lavas.

9/ The Pb isotopic compositions of the individual CEVP volcanic occurrences suggest that the tectonic activity played an important role in a magma generation of the Tertiary CEVP magmas.

Finally, we cannot rule out the hypothesis that the Hocheifel volcanism was related to mantle dynamics and eventually to a mantle plume activity. Although the geochronological, tectonic and geological evidence favor the tectonic control at the origin of the Hocheifel volcanic activity (Fekiacova, et al. submit.), their geochemical and isotopic characteristics indicate deep mantle material involvement. We suggest that the Hocheifel magmas tapped sources which have been previously contaminated by plume-type material. Further geochemical investigations are necessary in order to confirm or reject this theory.

Acknowledgments

We thank Prof. Matthew Thirlwall (matthewt@gl.rhul.ac.uk) for providing the XRF data, Dr. Klaus Peter Jochum (kpj@mpch-mainz.de) and Brigitte Stoll (stoll@mpch-mainz.de) for helping with the LA-ICP MS analyses. This project was funded by the Deutsche Forschungsgemeinschaft (DFG, Bonn) via grant Me 1155/4-1 to D.F.M.

REFERENCES

- Abouchami W, Galer SJG, Koschinsky A (1999a) Pb and Nd isotopes in NE Atlantic Fe-Mn crusts: proxies for trace metal paleosources and paleocean circulation. *Geochem. Cosmo. Acta* 63:1489-1505
- Babuska V, Plomerova J (1992) The Lithosphere in central Europe-sismological and petrological aspects. *Tectonophysics* 207:141-163
- Bogaard PJF, Wörner G (2003) Petrogenesis of basanitic to tholeiitic volcanic rocks from the Miocene Vogelsberg, Central Germany. *J. Petrol.* 44(Number 3):569 - 602
- Cantarel P, Lippolt HJ (1977) Alter und Abfolge des Vulkanismus der Hocheifel. *Neues Jahrb. Geol. Paläontol. Monatsh.* 10:600-612
- Cebriá JM, Wilson M (1995) Cenozoic mafic magmatism in Western/Central Europe: A common European Asthenospheric Reservoir? *Terra Abstracts* 7:162
- Duda Q, Schmincke HU (1985) Polybaric differentiation of alkali basaltic magmas: evidence from green-core clinopyroxenes. *Contrib. Mineral. Petrol.* 91:340-353
- Duncan RA, Petersen, N., Hardgraves, R.B. (1972) Mantle plumes, movement of the European plate, and polar wandering. *Nature* 239(Sept.8):82-86
- Fekiacova Z, Mertz DF, Renne PR (submit.) Geodynamic setting of the Tertiary Hocheifel volcanism (Germany), Part I: $^{40}\text{Ar}/^{39}\text{Ar}$ dating. In: Ritter JRR, Christensen UR (eds) *Mantle plumes - A multidisciplinary approach*, vol. Springer Verlag,
- Galer SJG (1999) Optimal double and triple spiking for high precision lead isotopic measurements. *Chem. Geol.* 157:255-274
- Goes S, Govers R, Vacher P (2000) Shallow mantle temperatures under Europe from P and S wave tomography. *J. Geophys. Res.* 105:11153-11169
- Goes S, Spakman W, Bijwaard H (1999) A lower mantle source for central Europe volcanism. *Science* 286:1928-1930
- Griesshaber E, O'Nions, R.K., Oxburgh, E.R. (1992) Helium and carbon isotope systematics in crustal fluids from the Eifel, the Rhine Graben and Black Forest, FRG. *Chem. Geol.* 99:213-235
- Haase KM, Goldschmidt, B., Garbe-Schönberg, C.-D. (2004) Petrogenesis of Tertiary continental intraplate lavas from the Westerwald region, Germany. *J. Petrol.* 45(5):883-905
- Hart S, Hauri E, Oschmann LA, Whitehead JA (1992) Mantle plumes and entrainment: isotopic evidence. *Science* 256:517-520
- Hauri E, Whitehead JA, Hart S (1994) Fluid dynamic and geochemical aspects of entrainment in mantle plumes. *J. Geophys. Res.* 99(B12):24,275-224,300
- Herzberg C (1992) Depth and degree of melting of komatiites. *J. Geophys. Res.* 97:4521-4540
- Hoernle K, Zhang YS, Graham D (1995) Seismic and geochemical evidence for large-scale mantle upwelling beneath the eastern Atlantic and western and central Europe. *Nature*

- 374(2 March):34-39
- Hofmann AW (1997) Mantle geochemistry: the message from oceanic volcanism. In: *Nature*, vol 385. pp 219-229
- Hofmann AW (2003) Sampling mantle heterogeneity through oceanic basalts: isotopes and trace elements. In: *Treatise on Geochemistry*, vol 2. Elsevier, pp 61-101
- Hofmann AW, Jochum KP, Seufert M, White MW (1986) Nb and Pb in oceanic basalts: new constraints on mantle evolution. *Earth Planet. Sci. Letters* 79:33-45
- Hofmann AW, White WM (1982) Mantle plumes from ancient oceanic crust. *Earth Planet. Sci. Lett.* 57:421-436
- Huckenholz HG (1983) Tertiary volcanism of the Hocheifel area. In: Fuchs K, von Gehlen, K., Mälzer, H., Murawski, H., Semmel, A. (ed) *Plateau Uplift - Rhenish Shield - A case History*, vol. Springer Verlag, Berlin, pp 121-128
- Huckenholz HG, Büchel G (1988) Tertiären Vulkanismus der Hocheifel. *Fortschr. Miner.* 66:43-82
- Jung S (1995) Geochemistry and petrogenesis of rift-related Tertiary alkaline rocks from the Rhön area (Central Germany). *N. Jb. Mineral. Abh.* 169:193-226
- Jung S, Hoernes S (2000) The major- and trace-element and isotope (Sr, Nd, O) geochemistry of Cenozoic alkaline rift-type volcanic rocks from the Rhön area (central Germany): petrology, mantle source characteristics and implications for asthenosphere-lithosphere interactions. *J. Volcan. Geochem. Res.* 99:27-53
- Kushiro I (1996) Partial melting of a Fertile Mantle Peridotite at High Pressures: An Experimental Study Using Aggregates of Diamond. In: Union AG (ed) *Earth Processes: Reading the Isotopic Code*, vol 95. pp 109-122
- LeMaitre RW (1989) *A classification of Igneous Rocks and Glossary of Terms*, vol. Blackwell Scientific Publications, Oxford
- Lippolt H. J (1982) K/Ar Age Determinations and the Correlation of Tertiary Volcanic Activity in Central Europe. *Geol. Jb.* D52:113-135
- Lippolt H. J, Todt W (1978) Isotopische Alterbestimmungen an Vulkaniten des Westerwaldes. *Neues Jahrbuch für Geologie und Paleontologie Monatshefte*:332-352
- Lippolt HJ (1983) Distribution of volcanic activity in space and time. In: Fuchs K, von Gehlen, K., Mälzer, H., Murawski, H., Semmel, A. (ed) *Plateau uplift - Rhenish Shield - A case history*, vol. Springer Verlag, Berlin, pp 112-120
- Lippolt HJ, Fuhrmann U (1980) Vulkanismus der Nordeifel: Datierung von Gang- und Schlotbasalten. *Aufschluss* 31:540-547
- Lippolt HJ, Troesch M, Hess JC (1990) Excess argon and dating of Quaternary Eifel volcanism, IV. Common argon with high and lower-than-atmospheric $^{40}\text{Ar}/^{39}\text{Ar}$ ratios in phonolitic rocks, East Eifel, F.R.G. *Earth Planet. Sci. Letters* 101:19-33
- Lugmair GW, Galer SJG (1992) Age and isotopic relationship among the angrites Lewis Cliff

- 86010 and Angora dos Reis. *Geochemica Cosmochemica Acta* 56:1673-1694
- Mengel K, Sachs PM, Stosch HG, Wörner G, Loock G (1991) Crustal xenoliths from Cenozoic volcanic fields of Western Germany: Implications for structure and composition of the crust. *Tectonophysics* 195:271-289
- Mertes H, Schmincke H.U. (1985) Mafic potassic lavas of the Quaternary West Eifel field (Western Germany) I. Major and trace elements. *Contrib. Mineral. Petrol.* 89:330-345
- Mertes H, Schmincke H-U (1983) Age distribution of the volcanoes in the West-Eifel. *N. Jahrbuch. Geol. Paläontol. Abh.* 166(2):260-293
- Meyer W, Stets J (1998) Junge Tektonik im Rheinischen Schiefergebirge und ihre Quantifizierung. *Z. Dtsch. Geol. Ges.* 149:359-379
- Müller-Sohnius D, Horn P, Huckenholz HG (1989) Kalium-Argon-Datierungen an tertiären Vulkaniten der Hocheifel. *Chem.Erde* 49:119-136
- Raikes S, Bonjer, K.P. (1983) Large-scale mantle heterogeneity beneath the Rhenish Massif and its vicinity from teleseismic P-residuals measurements. In: Fuchs K, von Gehlen, K., Mälzer, H., Murawski, H., Semmel, A. (ed) *Plateau uplift - The Rhenish Shield - A case history*, vol. Springer Verlag, Berlin
- Ritter JRR, Jordan M, Christensen UR, Achauer U (2001) A mantle plume below the Eifel volcanic fields, Germany. *Earth and Planetary Science Letters* 186:7-14
- Rittmann U, Lippolt HJ (1998) Evidence for distortion of Tertiary K/Ar ages by excess argon - example given by three alkali olivine basalts from Northern Hesse, Germany. *Eur. J. Mineral* 10:95-110
- Rudnick RL, Gao S (2003) Composition of the continental crust. In: *Treatise on Geochemistry*, vol. Elsevier,
- Rudnick RL, Goldstein SL (1990) The Pb isotopic compositions of lower crustal xenoliths and the evolution of lower crustal Pb. *Earth Planet. Sci. Lett.* 98:192-207
- Sachs PM, Hansteen TH (2000) Pleistocene underplating and metasomatism of the lower continental crust: a xenolith study. *J. Petrol.* 41:331-356
- Stosch H-G, Lungmair GW (1984) Evolution of the lower continental crust: granulite facies xenoliths from the Eifel, West Germany. *Nature* 311:368-370
- Stosch H-G, Lungmair GW (1986) Trace element and Sr and Nd isotope geochemistry of peridotite xenoliths from the Eifel (West Germany) and their bearing on the evolution of the subcontinental lithosphere. *Earth and Planetary Science Letters* 80:281-298
- Thirlwall MF, Singer BS, Marriner GF (2000) ^{39}Ar - ^{40}Ar ages and geochemistry of the basaltic shield stage of Tenerife, Canary Islands, Spain. *J. Volcanol. Geotherm. Res.* 103:247-297
- Weaver BL (1991) Trace element evidence for the origin of ocean-island basalts. *Geology* 19:123-126
- Wedepohl KH, Baumann A (1999) Central European Cenozoic plume volcanism with OIB

- characteristics and indications of lower mantle source. *Contrib. Mineral. Petrol.* 136:225-239
- Wedepohl KH, Gohn E, Hartmann G (1994) Cenozoic alkali basaltic magmas of western Germany and their products of differentiation. *Contrib. Mineral. Petrol.* 115:253-278
- White MW (1985) Source of oceanic basalts: radiogenic isotopic evidence. *Geology* 25:611-614
- White RS (1993) Melt production rates in mantle plumes. *Philos. Trans. R. Soc. Lond. A* 342:137-153
- Wilson M, Downes H (1991) Tertiary-Quaternary extension related alkaline magmatism in Western and Central Europe. *J. petrol.* 32:811-849
- Wilson M, Downes H (1992) Mafic alkaline magmatism in the European Cenozoic rift system
In: Ziegler, P.A., *Geodynamics of Rifting, Volume I. Case History Studies on Rifts: Europe and Asia. Tectonophysics* 208:173-182
- Workman RK, Hart S, Jackson M, Regelous M, Farley KA, Bluzstajn J, Kurz M, Staudigel H (2004) Recycled metasomatized lithosphere as the origin of the Enriched Mantle II (EM2) end-member: Evidence from the Samoan Volcanic Chain. *Geochem. Geophys. Geosyst.* 5(4)
- Wörner G, Schmincke HU, Schreyer W (1982) Crustal xenoliths from the Quaternary Wehr volcano (East Eifel). *N. Jb. Mineral. Abh.* 144:29-55
- Wörner G, Zindler A, Staudigel H, Schmincke HU (1986) Sr, Nd, and Pb isotope geochemistry of Tertiary and Quaternary alkaline volcanics from West Germany. *EPSL* 79:107-119
- Ziegler PA (1992) European Cenozoic rift system. *Tectonophysics* 208:91-111
- Zindler A, Hart S (1986) Chemical geodynamics. *Ann. Rev. Earth Planet Sci.* 14:493-571

FIGURE CAPTIONS:

Figure 1: Map of the Central Europe showing different volcanic fields of the Central European Volcanic Province (CEVP) and major tectonic features (Upper Rhine, Lower Rhine and Leine grabens).

Figure 2: (a) Total-alkali-silica (TAS) diagram (LeBas, et al. 1986; LeMaitre 1989). Used abbreviations: T - trachyte, L - latite, S - shoshonite and H - hawaiite. (b-i) Major element oxides variations of the Hocheifel and Upper Rhine Graben lavas.

Figure 3: Chondrite-normalized Rare Earth Element (REE) patterns of the Hocheifel lavas (blue symbols and lines) and Upper Rhine Graben volcanic rocks (green symbols and lines). (a) Undifferentiated samples, (b) differentiated samples. Numbers correspond to sample numbers. The normalization data on the C1 chondrite are from Evensen et al., 1987).

Figure 4: Primitive-normalized trace elements patterns of the (a) undifferentiated Hocheifel (blue symbols and lines) and Upper Rhine graben lavas (orange symbols and lines) and (b) differentiated Hocheifel lavas (numbers correspond to sample numbers). The normalization data from McDonough and Sun, 1995). For comparison, the PM-normalized trace element patterns of the average OIB (c) and of the Quaternary West and East Eifel lavas (d). St. Helena and Gough were taken as two examples of the OIB, data are from McDonough and Sun, 1985 and from GEOROC. Data for the Quaternary Eifel lavas from (Schmincke 1983).

Figure 5: Sr, Nd (a) and Pb (b, c) isotopic compositions of the Hocheifel lavas. Age data are from (Fekiacova, et al. submit.). Solid lines represent linear trends formed by individual groups of lavas. Data for the West and East Eifel lavas are from (Wedepohl, et al. 1994; Wörner, et al. 1986). 2σ error is of symbol size.

Figure 6: Evaluation of the crustal contamination of the Hocheifel lavas. (a) Ce/Pb and (b) Nb/U ratios vs. SiO₂ content (wt. %) of the Hocheifel and Upper Rhine Graben lavas compared to the average values of the oceanic basalts and continental crust. Ce/Pb ratios of the crustal xenoliths from the Eifel area are also shown, for comparison. The dashed lines with green fields show the average Ce/Pb and Nb/U ratios of the oceanic basalts. The dashed-dotted lines represent the average Ce/Pb and Nb/U ratios of the continental crust. Data for the oceanic basalts and continental crust are from (Hofmann, et al. 1986; Rudnick and Gao 2003), data for the crustal xenoliths from (Loock, et al. 1990; Rudnick and Goldstein 1990; Stosch and Lungmair 1986). (c) Sr and Nd isotopic compositions of the Hocheifel lavas and of the xenoliths from the lower crust and mantle below the Eifel. The data for the lower crustal granulites and mantle peridotites are from (Stosch and Lungmair 1984; Stosch and Lungmair 1986). (d) Pb isotopic compositions of the Hocheifel lavas and crustal xenoliths from the Eifel (Rudnick and Goldstein 1990).

Figure 7: Experimental results of Kushiro (Kushiro 1996) on the melting of a garnet peridotite at high pressures and temperatures. Green field envelopes pressure of 25 kbar and temperatures of 1425-1500°C. Orange field corresponds to the pressure of 25 kbar and temperatures of 1460-1500°C. Filled blue circles-Hocheifel basalt s and basanites, filled red diamonds-differentiated Hocheifel lavas, open green squares-Upper Rhine Graben volcanic rocks.

Figure 8: (a) Sr and Nd isotopic compositions of the Hocheifel lavas and of different mantle reservoirs. Blue circles - Hocheifel lavas. Dotted lines indicate the Bulk Silicate Earth compositions. (b, c) Pb isotopic compositions of the Hocheifel lavas (blue circles), Quaternary Eifel lavas (red diamonds-West Eifel, green squares-East Eifel) and different mantle reservoirs. Solid lines represent linear arrays of individual magma groups. Blue rectangle corresponds to FOZO compositions (data from (Hauri, et al. 1994)), yellow rectangle represent the LVC (data from (Hoernle, et al. 1995)). Data for the other mantle reservoirs from GEOROC and PeTB database.

Figure 9: Ratios of the trace elements with similar degrees of incompatibility: (a) Ba/Th vs. Rb/Nb, (b) Ba/La vs. Ba/Nb and (c) Rb/Nb vs. K/Nb. The fields of HIMU -yellow, Enriched mantle 1 (EM-1) - blue and Enriched Mantle 2 (EM-2) - violet are shown for comparison. Data for the HIMU, EM-1 and EM-2 are from Weaver (Weaver 1984).

Figure 10: (a) Sr and Nd isotopic compositions of the primitive Tertiary lavas from different volcanic fields of the Central European Volcanic Province (CEVP). Solid lines represent linear trends formed by different CEVP volcanic fields. Squared-field corresponds to the LVC (Data from (Hoernle, et al. 1995)). Dashed lines indicate the BSE compositions (Data from (Carter, et al. 1978)). Different mantle reservoirs are indicated for comparison. (c) Pb isotopic compositions of different Tertiary and Quaternary lavas from the CEVP. Data for the lavas of CEVP are from (Bogaard and Wörner 2003; Haase 2004; Wedepohl, et al. 1994; Wörner, et al. 1986). Data for the mantle reservoirs are from GEOROC and PETB databases.

Appendix

Figures and tables

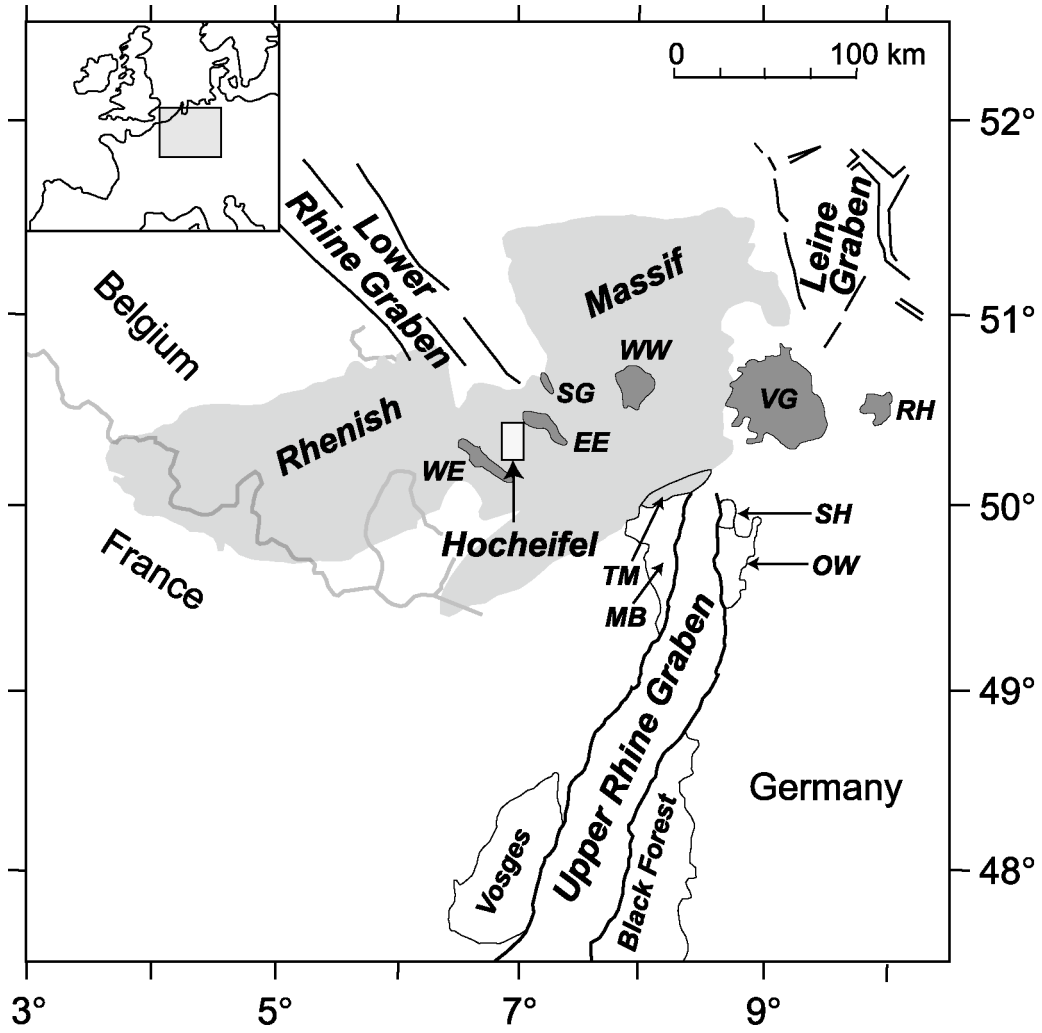


Figure 1

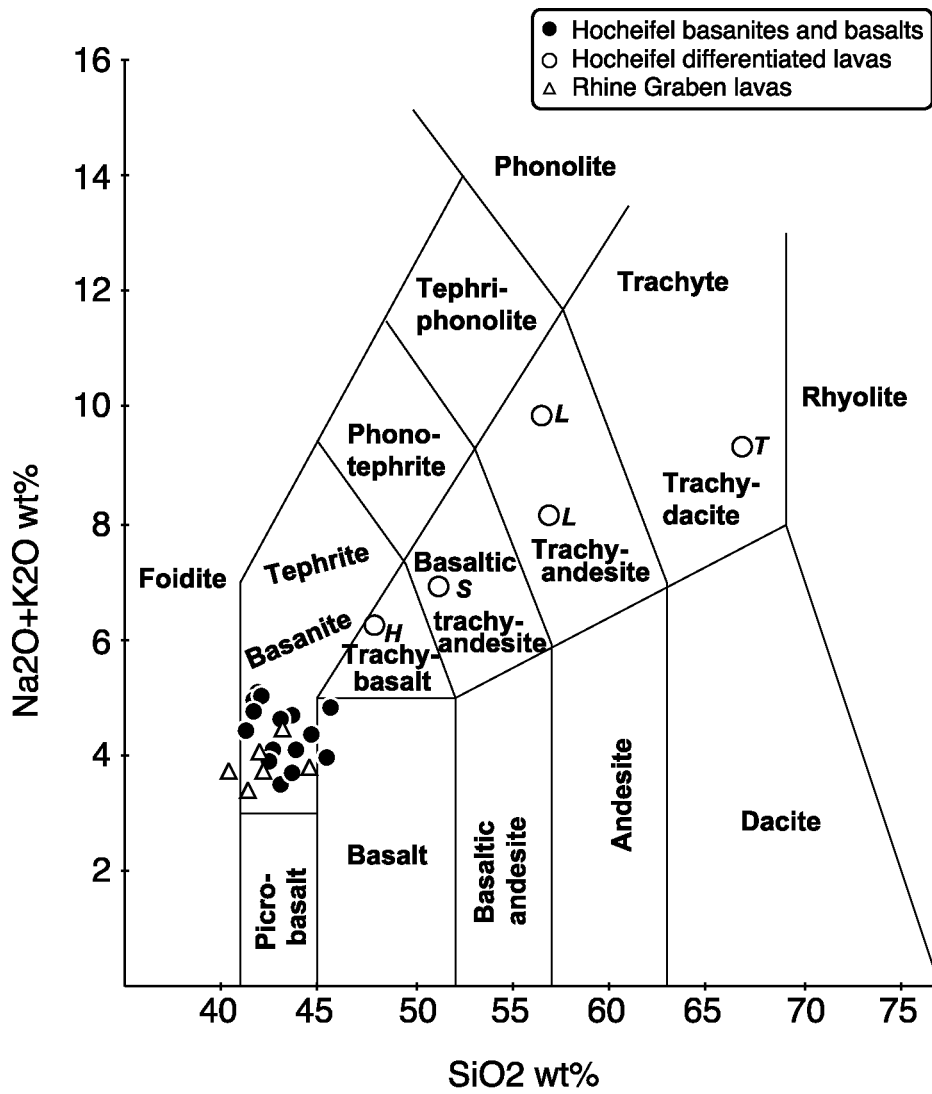


Figure 2a

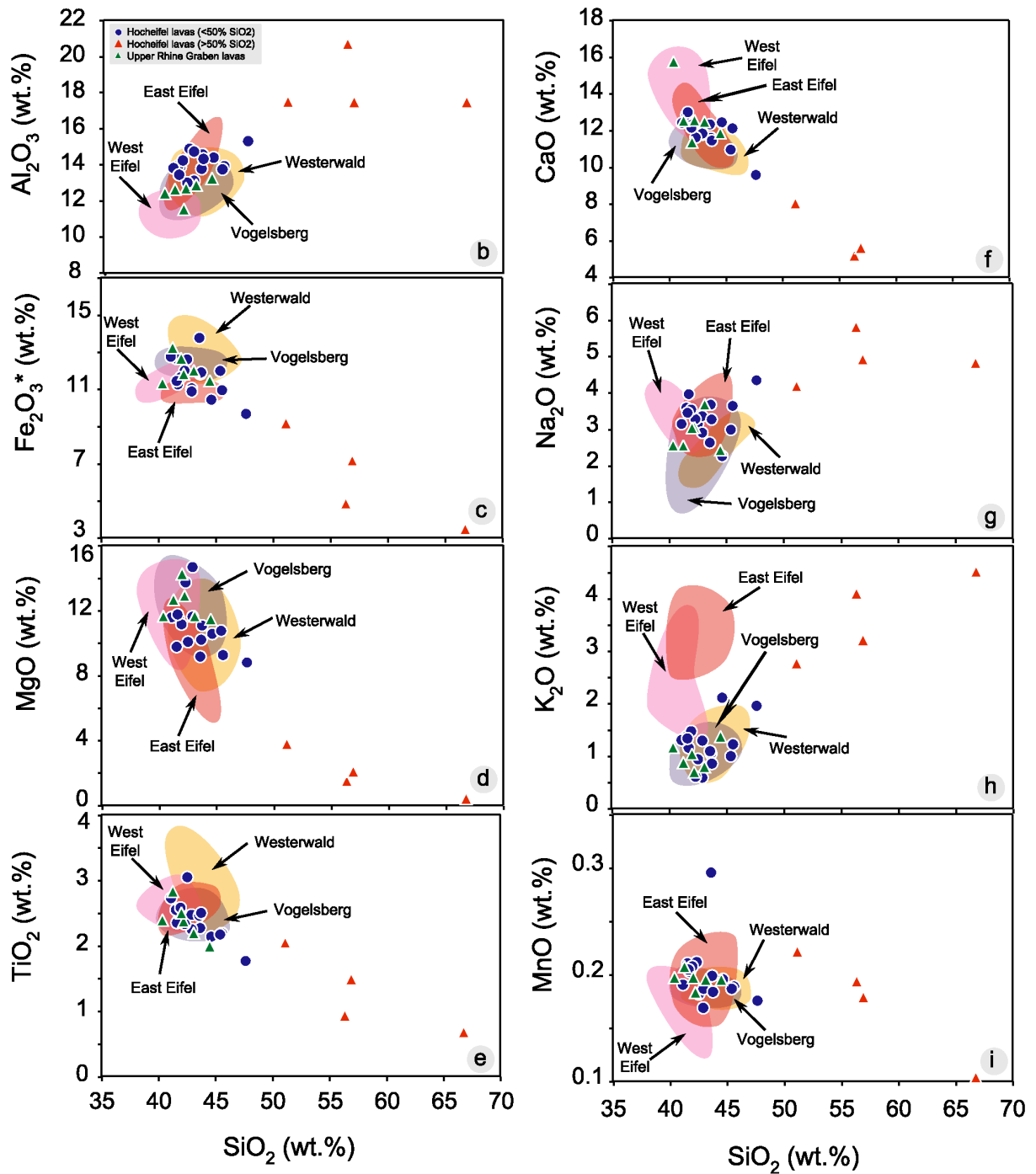


Figure 2

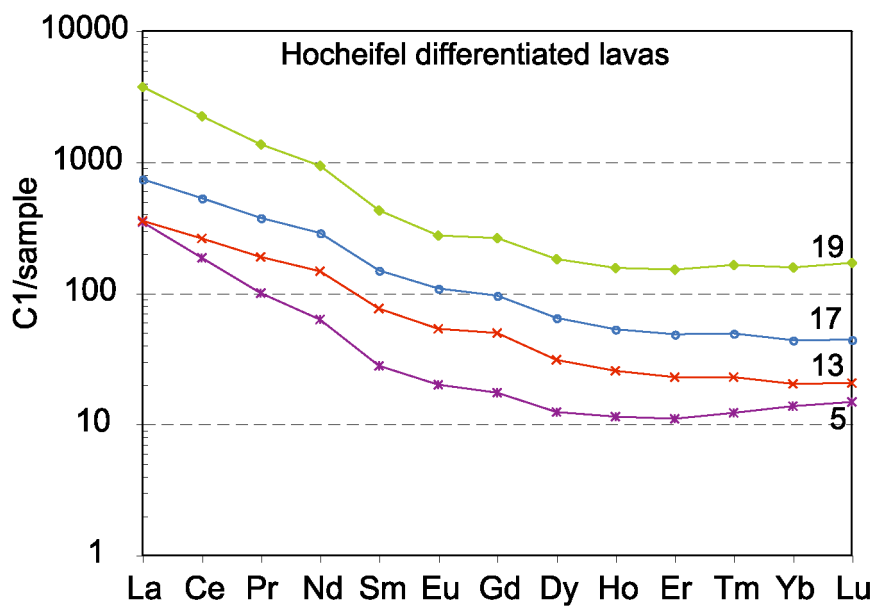
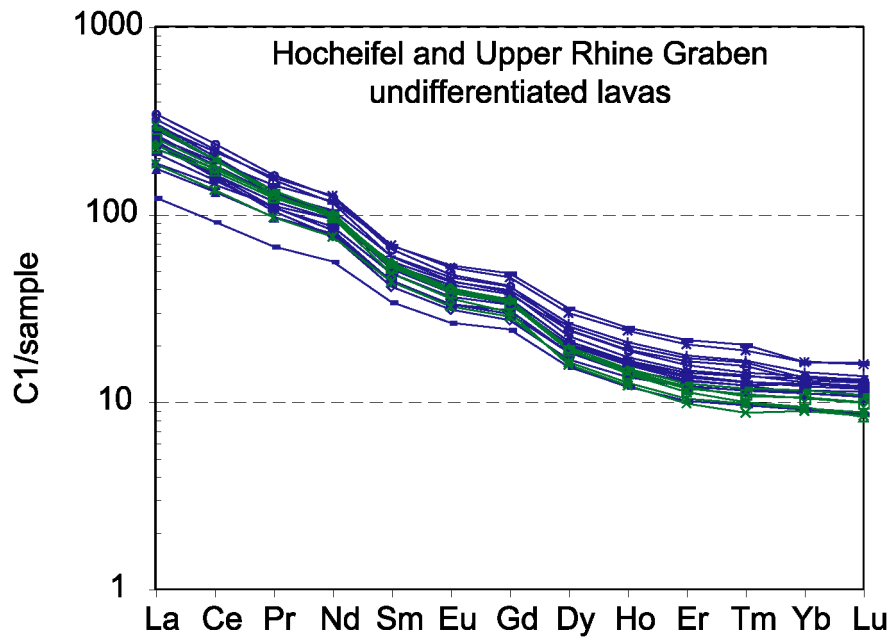


Figure 3

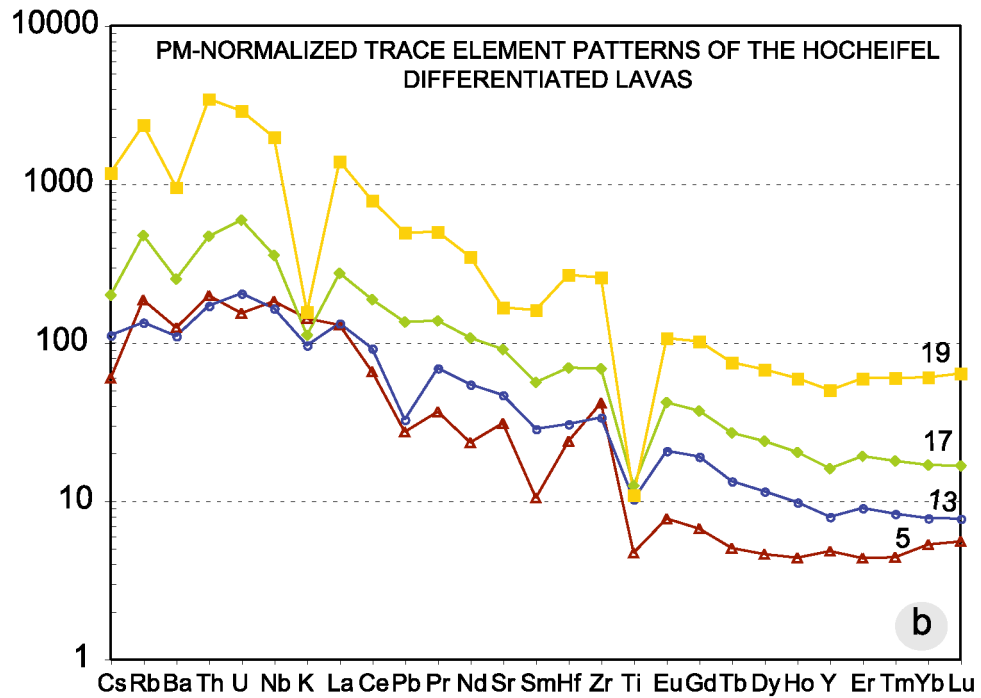
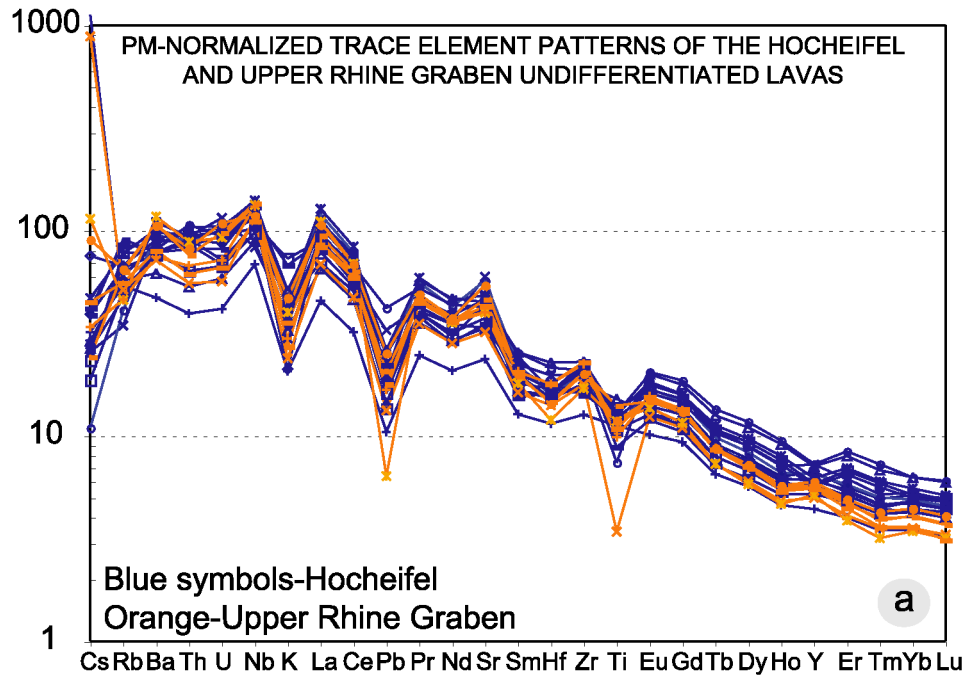


Figure 4

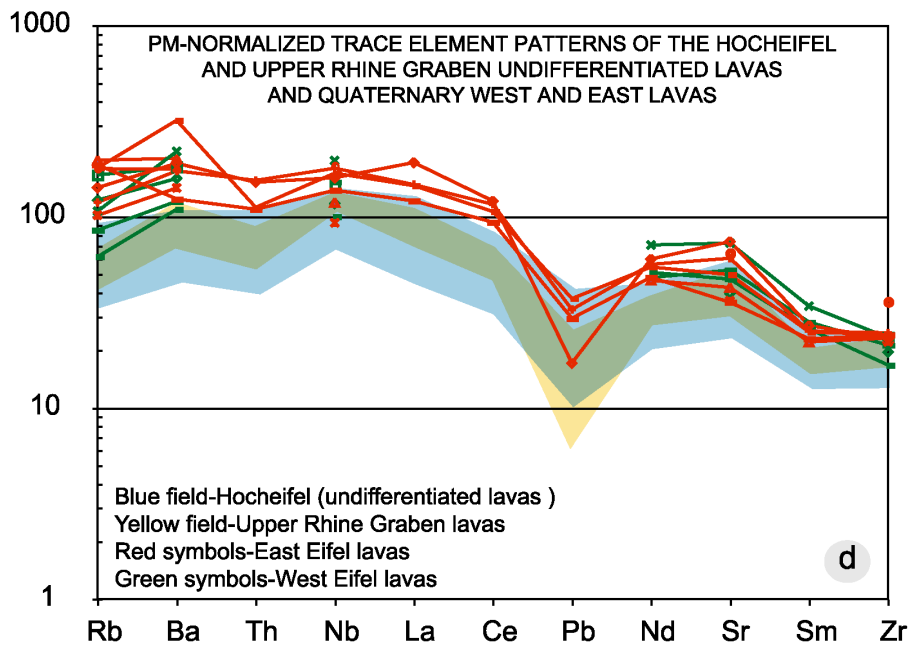
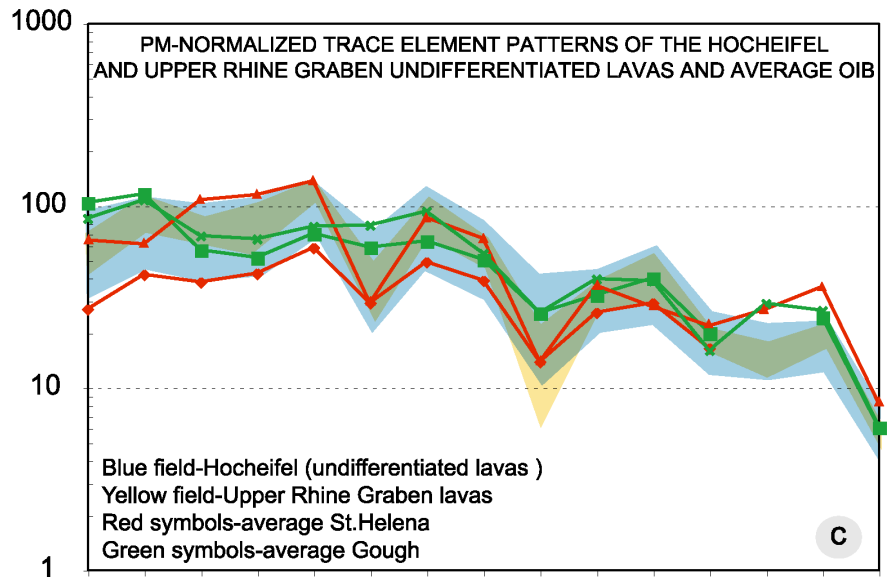


Figure 4

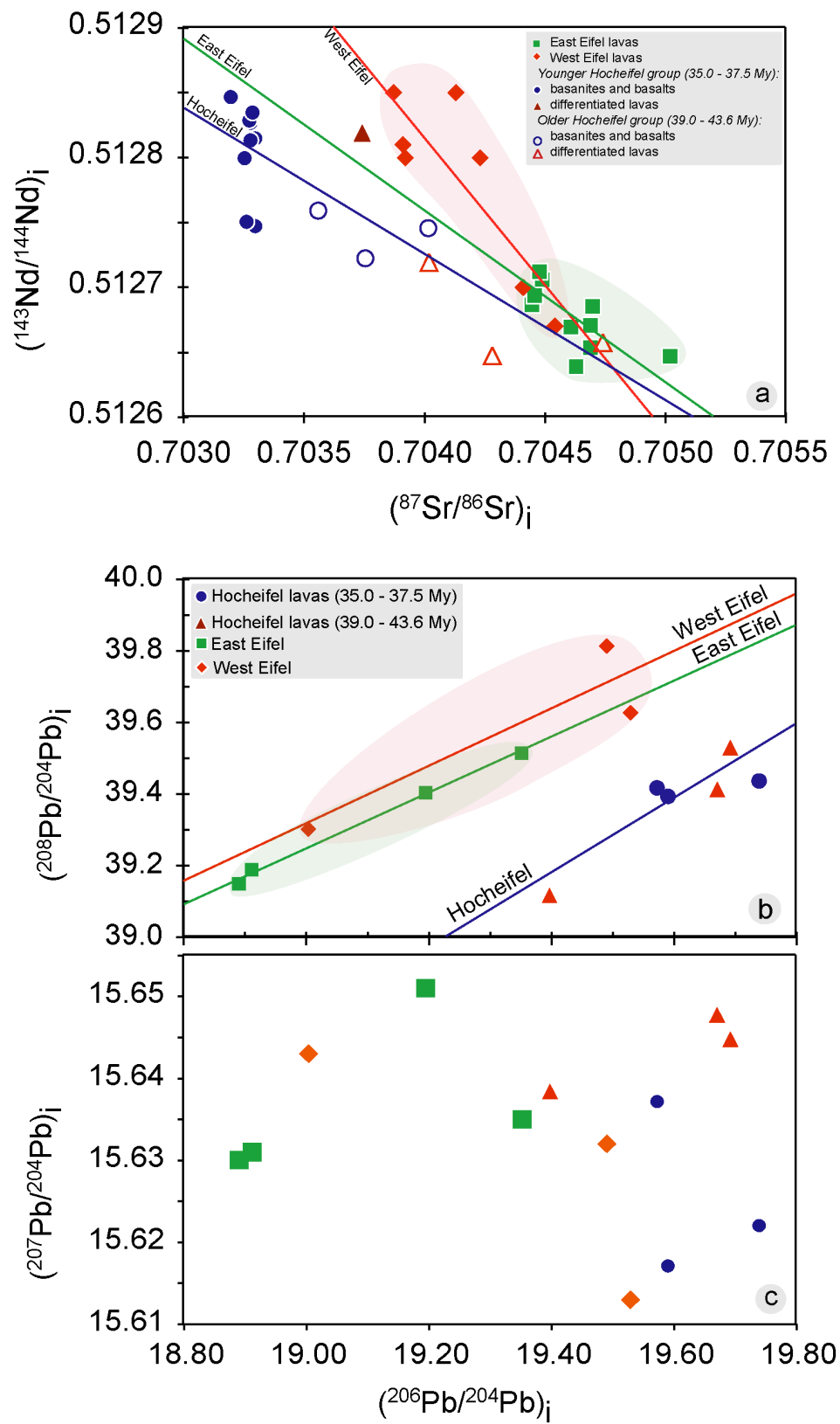


Figure 5

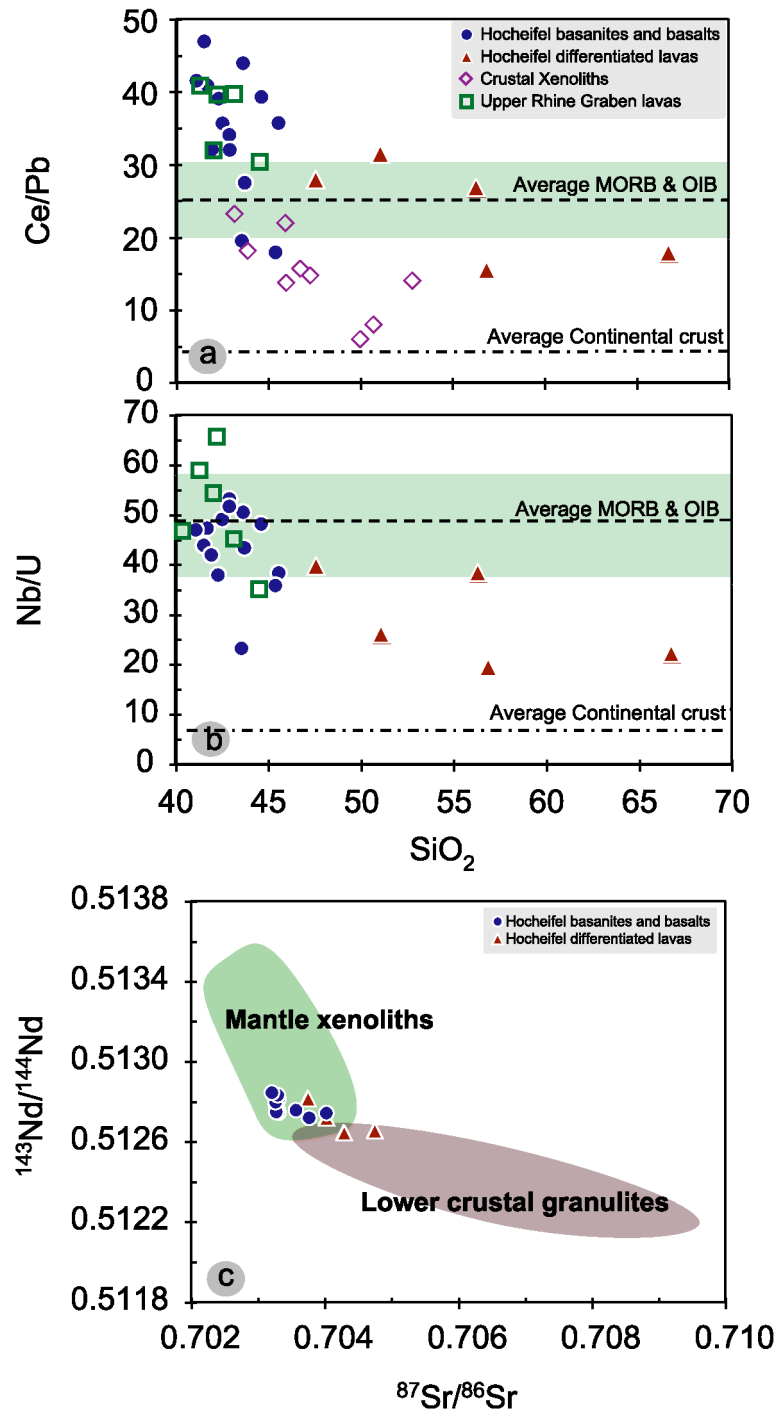


Figure 6

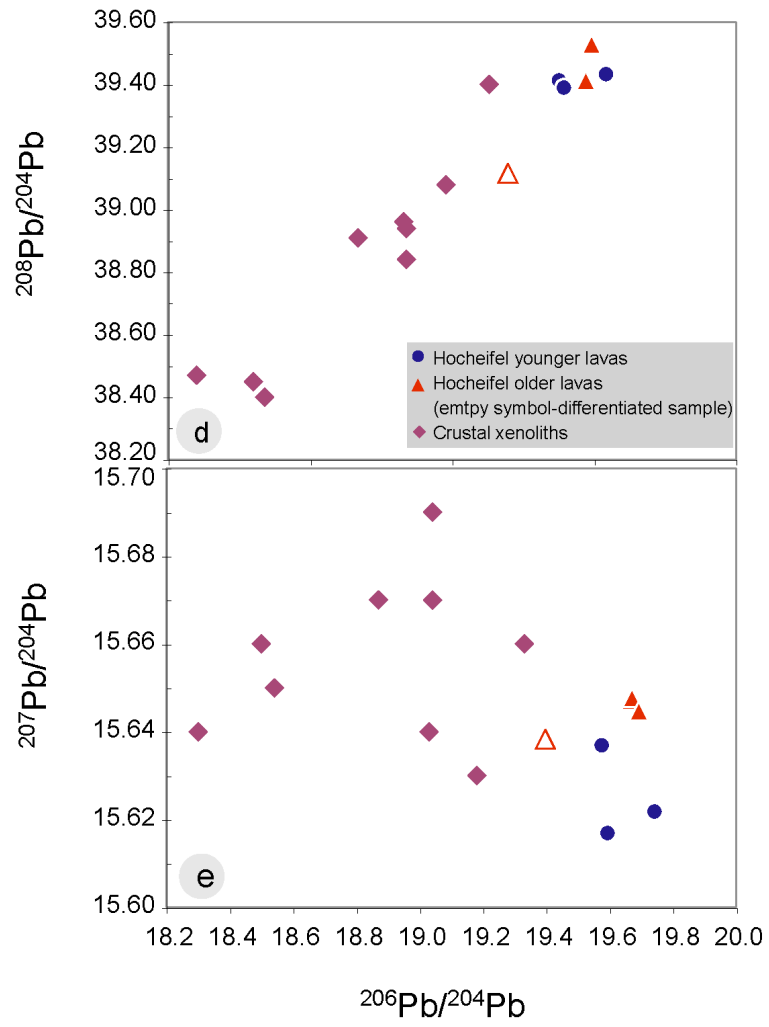


Figure 6

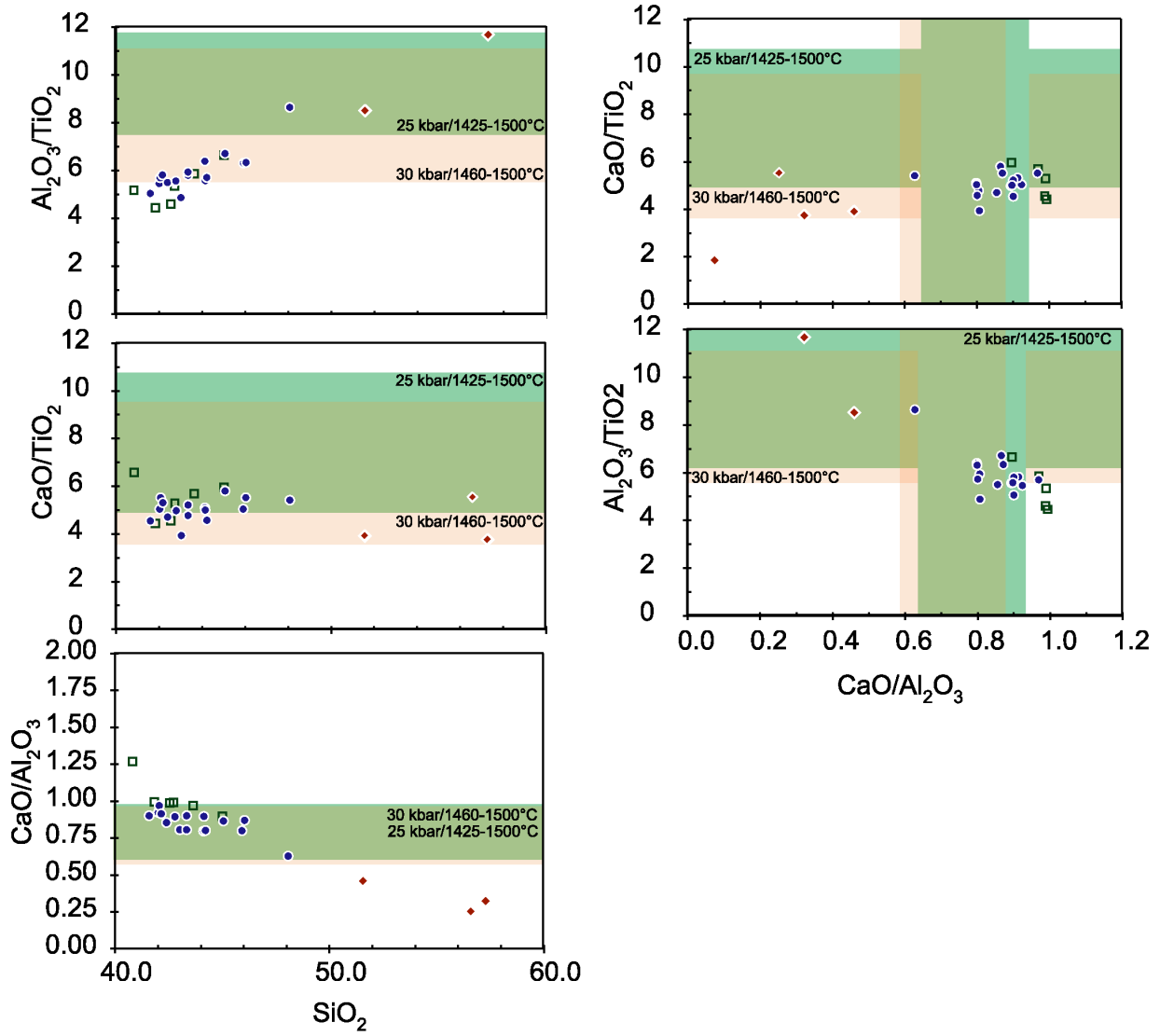


Figure 7

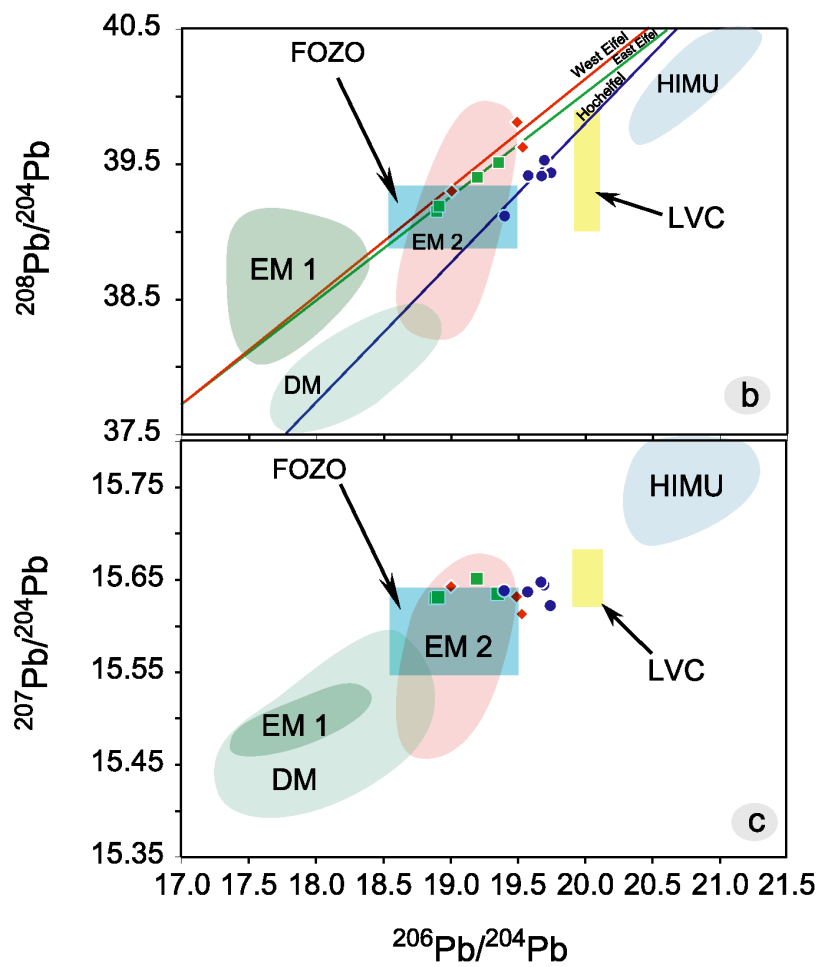
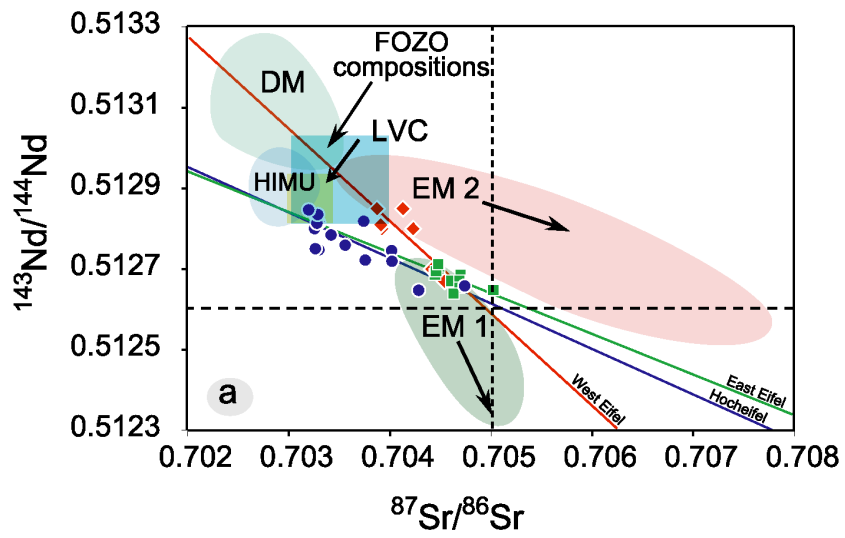


Figure 8

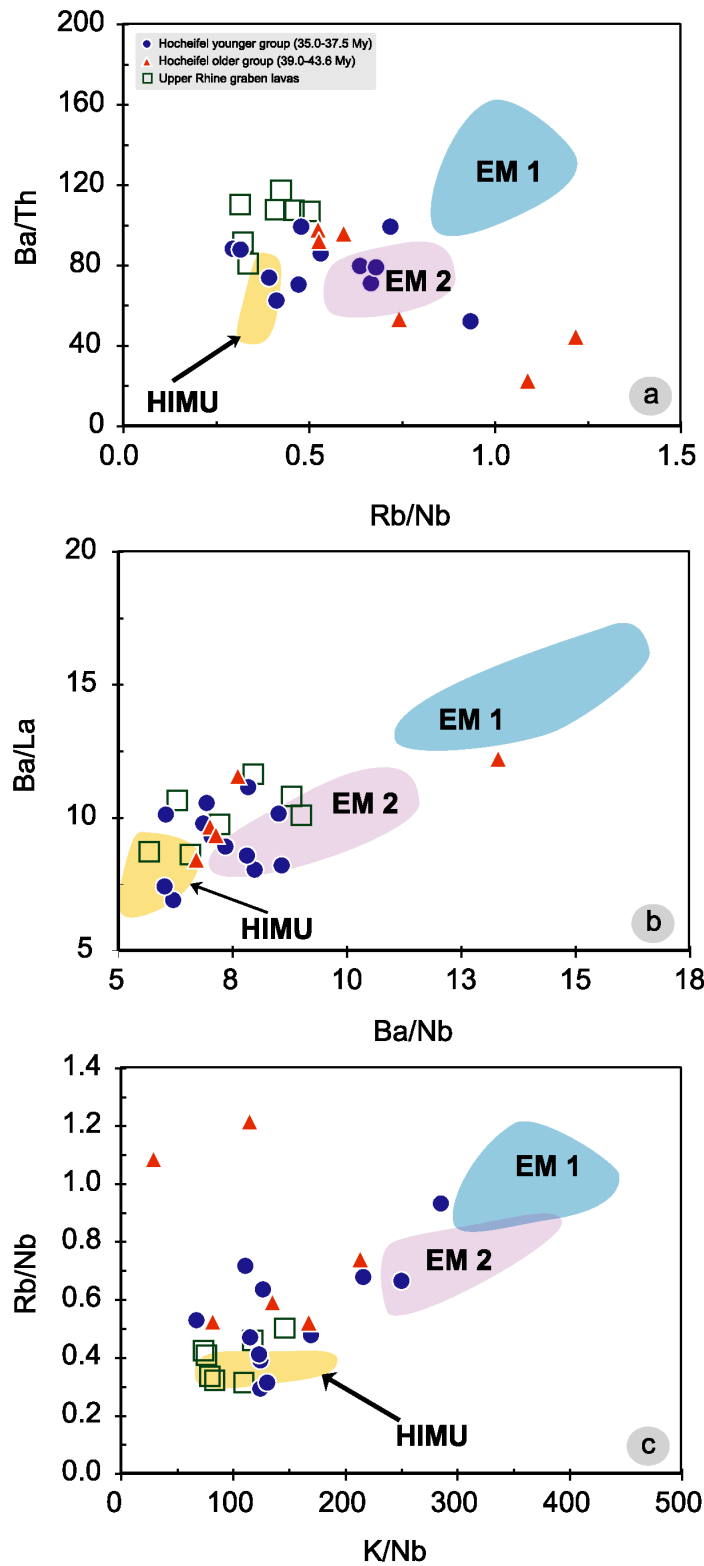


Figure 9

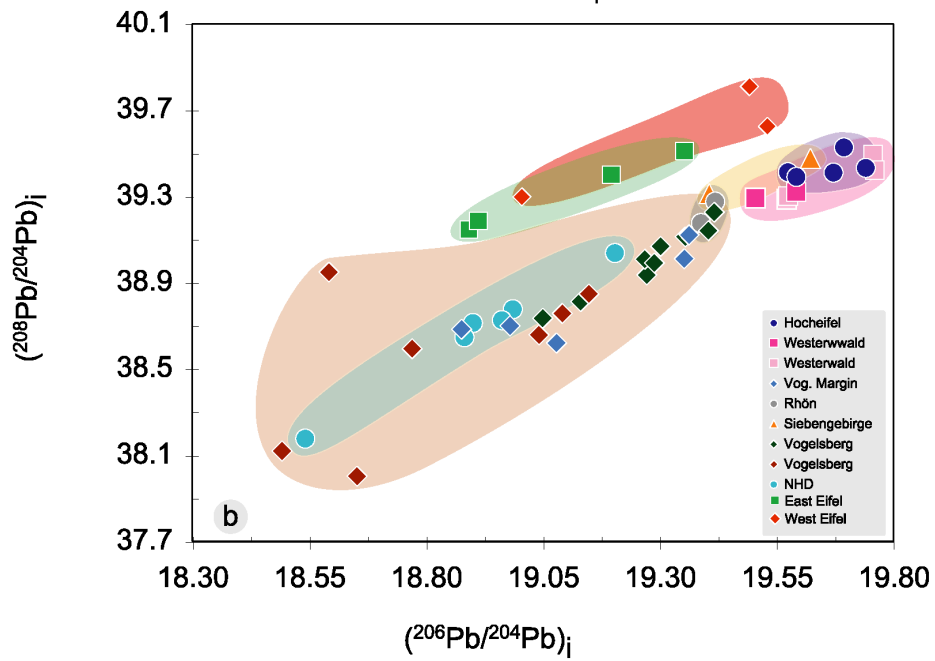
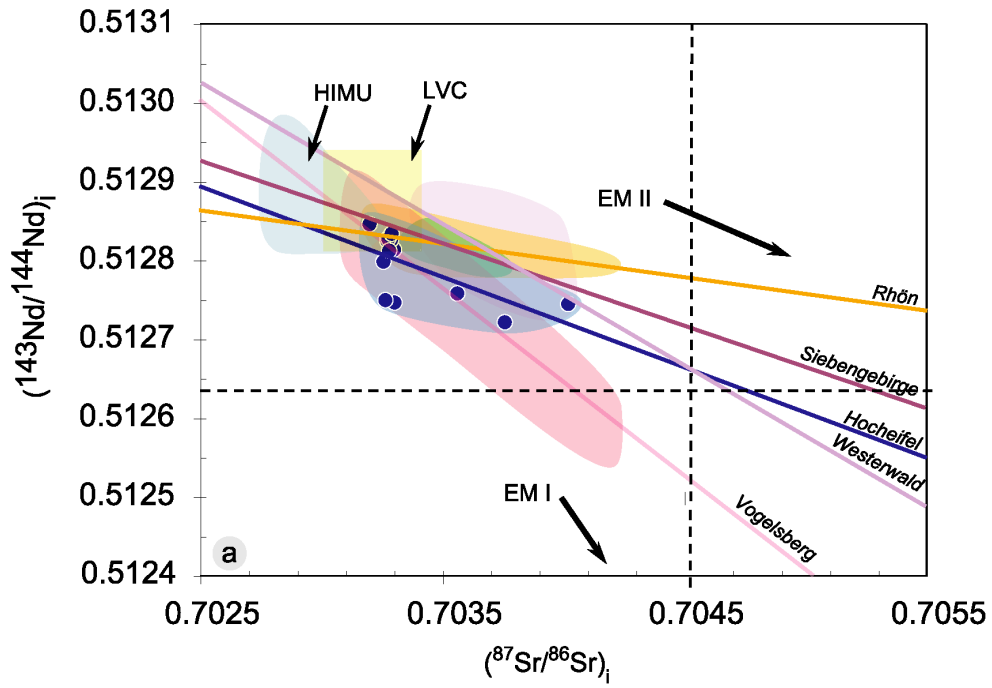


Figure 10

Table 1: Major elements oxides and trace element compositions of the Hocheifel and Upper Rhine Graben lavas

Sample	1	2	3	4	5	6	7	8	9	10	11	12	13	14	15	16	17	18	19	20	
Hochelief samples																					
SiO ₂	41.68	44.59	42.48	43.61	56.31	41.48	45.53	42.87	47.60	41.06	42.27	41.90	51.09	41.90	43.53	41.57	56.87	45.36	66.74	43.69	
Al ₂ O ₃	13.89	14.41	14.89	14.58	20.71	13.95	13.93	13.11	15.31	15.31	13.02	13.82	14.74	14.24	13.78	13.45	17.49	13.75	17.49	14.34	
FeO	8.127	7.522	9.092	8.523	2.635	7.897	7.869	7.846	6.103	6.103	8.645	9.200	5.375	8.393	9.919	8.249	3.887	8.652	1.570	8.588	
Fe ₂ O ₃	2.278	2.090	2.526	2.368	1.952	2.194	2.192	2.180	2.907	2.907	2.402	2.556	3.217	2.332	2.756	2.292	2.880	2.404	1.745	2.386	
MgO	11.55	10.59	10.10	10.22	1.56	9.78	14.69	11.65	8.82	11.18	13.75	11.60	3.82	11.18	9.18	11.77	2.12	10.77	0.45	11.10	
CaO	12.68	12.47	12.01	11.63	5.21	12.88	12.13	11.86	9.60	11.64	11.64	12.44	8.05	12.17	12.36	13.02	5.62	10.98	0.28	11.48	
Na ₂ O	3.980	2.270	3.160	3.690	3.600	3.290	3.290	3.370	4.360	3.290	3.290	3.290	4.200	3.550	3.460	3.460	3.280	3.000	4.840	3.864	
K ₂ O	1.163	2.121	1.053	1.053	1.379	1.228	1.053	1.303	1.965	1.311	0.614	1.311	2.776	1.480	1.099	1.342	3.216	3.008	4.518	0.864	
TiO ₂	2.385	2.147	3.052	2.280	0.941	2.553	2.197	2.259	2.482	1.772	2.337	2.736	2.056	2.587	2.468	2.359	1.497	2.179	0.688	2.507	
MnO	0.203	0.196	0.182	0.199	0.194	0.211	0.189	0.169	0.176	0.212	0.212	0.191	0.222	0.208	0.296	0.206	0.179	0.187	0.104	0.184	
P ₂ O ₅	0.821	0.482	0.507	0.661	0.188	0.722	0.375	0.551	0.471	0.639	0.639	0.603	0.651	0.618	0.559	0.986	0.573	0.553	0.199	0.485	
Total	98.74	98.89	98.95	98.81	99.62	98.58	98.94	98.96	99.03	99.08	98.82	98.68	98.97	98.66	98.59	98.70	99.27	98.84	99.62	98.90	
Mg#*	67	67	61	63	39	63	63	72	64	64	69	64	45	65	57	67	64	64	20	65	
TAS	basalt	basalt	basalt	basalt	basalt	basalt	basalt	basalt	basalt	basalt	basalt	basalt	shoshonite	basalt	basalt	basalt	latite	basalt	trachyte	basalt	
Location	Bas.Neu.Berg	Staufskopf	Reifferscheid	basalt	basalt	Nürburg	Role Heck	Hohe Acht	basalt	basalt	Kopp	Kastelberg	shoshonite	Basarberg	basalt	basalt	latite	Scharfer Kopf	Reimerath	Hillsheid	
										hawaii					Nollenbach	Steineberg	Bocksberg				
										Steinmelskopf						ger Ley					

Sample	1	2	3	4	5	6	7	8	9	10	11	12	13	14	15	16	17	18	19	20
Rb	39.570	46.908	34.571	20.711	111.446	36.139	24.675	32.302	54.455	51.448	40.306	30.731	80.208	40.662	28.571	n.d.	284.11	28.016	1415.2	46.331
Ba	504.68	516.82	408.67	603.47	817.52	572.12	624.77	311.63	516.25	532.63	646.19	503.80	724.41	594.87	726.61	n.d.	1664.2	531.68	6264.0	670.18
Pb	2.8239	2.4251	2.1706	2.7190	4.0944	2.9801	3.6650	1.5769	2.7930	3.3284	2.7468	2.0408	4.8926	3.9542	4.9168	n.d.	20.233	6.2960	73.923	3.7369
Th	7.1456	7.2614	4.2513	6.8351	15.6662	7.7280	7.1087	3.1387	6.4719	6.7241	7.5038	5.0691	13.5298	8.2190	7.4348	n.d.	37.134	8.5048	273.92	7.2634
U	1.7702	1.4608	1.1885	1.3916	3.1127	2.0996	2.0361	0.8442	1.6514	1.9060	1.9975	1.3653	4.1529	2.1377	2.4321	n.d.	12.034	1.8956	58.711	2.0238
Nb	84.013	70.449	58.408	70.435	119.350	92.413	78.299	45.027	85.557	75.658	75.993	64.304	108.181	89.839	54.627	n.d.	233.50	88.108	1301.4	88.050
Ta	4.3227	3.5696	3.3305	3.5532	4.4701	5.1458	4.1022	2.5608	4.3053	3.8088	4.4096	4.5038	7.3249	6.0008	3.7173	n.d.	17.096	4.5134	83.283	5.9303
Sr	820.87	867.95	667.67	1187.87	615.28	965.01	1138.01	470.13	745.71	697.49	834.60	668.46	929.77	892.66	945.85	n.d.	1707.9	845.73	3315.1	916.02
Hf	4.3327	4.5194	4.3379	4.3796	6.7295	4.6939	4.4826	3.2529	4.8009	4.5909	4.2716	5.0095	8.6469	6.4456	4.8181	n.d.	19.642	6.0998	75.336	5.5947
Zr	210.57	233.81	187.30	224.41	435.37	229.07	208.88	133.42	212.69	240.55	188.91	172.05	353.11	241.75	168.51	n.d.	719.89	219.83	2689.6	208.81
Cs	0.820	0.490	0.608	0.540	1.248	0.587	0.230	0.674	0.814	0.879	1.587	0.394	2.328	0.560	23.643	n.d.	4.1677	0.5541	24.715	0.9838
Y	28.822	25.004	23.862	26.600	20.749	31.192	28.088	18.991	25.971	22.416	23.384	25.162	34.143	30.671	24.489	n.d.	69.052	31.310	215.29	26.716
La	67.976	57.916	42.225	73.467	83.535	82.818	77.643	29.493	50.992	57.338	63.597	45.175	85.838	71.461	59.369	n.d.	177.737	61.904	900.34	57.872
Ce	115.68	95.521	77.539	119.65	109.68	140.15	131.07	53.804	89.544	92.811	107.50	84.947	153.81	127.10	96.192	n.d.	312.96	113.14	1313.9	103.04
Pr	12.371	10.111	8.999	12.386	9.310	15.032	14.193	6.270	10.076	9.638	11.843	10.284	17.486	14.560	10.894	n.d.	34.776	13.288	126.87	11.932
Nd	46.914	38.153	36.549	45.554	29.172	57.289	53.345	26.011	39.798	35.657	46.206	43.817	67.981	58.271	43.755	n.d.	133.79	54.317	433.87	48.746
Sm	0.0389	0.0650	0.0654	0.07544	0.0318	0.09206	0.0394	0.01836	0.03390	0.02563	0.03300	0.02595	0.015798	0.03955	0.01848	n.d.	22.704	10.328	64.825	0.0922
Eu	2.3182	1.9698	1.9715	2.2690	1.9118	2.8274	2.6199	1.8383	2.1517	1.8383	2.3464	2.5886	3.1835	3.0758	2.5012	n.d.	6.4408	3.1617	16.375	2.7374
Gd	6.9916	5.8042	6.0834	6.6313	3.4287	8.2043	7.5733	4.7976	6.5074	5.3754	6.7527	7.7792	9.7849	9.1264	7.4262	n.d.	14.971	9.5637	52.123	8.1122
Tb	0.9030	0.7846	0.7668	0.8675	0.4985	1.0644	0.9769	0.6465	0.8564	0.7084	0.8763	1.0659	1.3179	1.2451	1.0231	n.d.	2.8563	1.3410	7.3782	1.1170
Dy	5.2376	4.5847	4.5799	4.9670	3.0957	5.9927	5.6072	3.8260	5.0803	4.1951	4.9827	6.2899	7.7453	7.4091	6.0340	n.d.	16.099	7.8806	45.380	6.5501
Ho	0.9459	0.8391	0.8123	0.9080	0.6507	1.0682	0.9667	0.6862	0.9265	0.7733	0.8958	1.1345	1.4563	1.3629	1.0825	n.d.	3.0147	1.4158	8.8557	1.1876
Er	2.4680	2.2357	2.1063	2.3361	1.9066	2.7157	2.5387	1.7524	2.3920	2.0834	2.2578	2.9523	3.9402	3.4903	2.8403	n.d.	8.3865	3.6872	26.091	3.0520
Tm	0.3359	0.3023	0.2828	0.3129	0.3005	0.3418	0.3526	0.2362	0.3160	0.2850	0.3011	0.3997	0.5639	0.4626	0.3835	n.d.	1.2121	0.4962	4.0555	0.4099
Yb	2.2665	2.1161	1.8837	2.1224	2.3405	2.3289	2.1576	1.5445	1.8798	1.9446	1.8798	2.2745	3.4418	2.7684	2.2078	n.d.	7.4222	2.7709	26.594	2.4451
Lu	0.3276	0.3066	0.2721	0.3027	0.3749	0.3309	0.3077	0.2183	0.2978	0.2878	0.2703	0.3357	0.5233	0.4021	0.3207	n.d.	1.1213	0.4091	4.3078	0.3473

Mg#=100(Mg²⁺+W_{HfO})/(Mg²⁺+W_{HfO}+Fe²⁺+W_{FeO}) W - Molecular weight
n.d.-not determined

Table 1-cont

Major elements oxides

Sample	Upper Rhine Graben samples						
	21	22	23	24	25	26	
SiO2	41.27	42.02	42.22	40.37	44.50	43.12	
Al2O3	12.60	11.50	12.66	12.39	13.22	12.86	
FeO	9.523	9.099	8.509	8.131	8.242	8.638	
Fe2O3	2.646	2.528	2.364	2.259	2.290	2.400	
MgO	12.64	14.23	12.90	11.62	11.46	11.64	
CaO	12.52	11.36	12.53	15.74	11.84	12.47	
Na2O	2.540	3.030	3.040	2.550	2.420	3.680	
K2O	0.867	1.031	0.691	1.159	1.364	0.791	
TiO2	2.829	2.501	2.371	2.392	1.989	2.195	
MnO	0.207	0.197	0.183	0.197	0.195	0.195	
P2O5	0.709	0.609	0.600	1.101	0.774	0.821	
Total	98.35	98.10	98.07	97.90	98.29	98.81	
Mg#*	65	69	68	67	67	66	
TAS	basanite	basanite	basanite	foiidit	basanite	basanite	
Location	Rabenkopf	Am Hörkopf	Forst	Steiteritz	Steinbuckel	Forstberg	

Trace element compositions

Sample	21	22	23	24	25	26
	Rb	27.771	33.464	30.930	27.658	39.021
Ba	489.47	526.40	474.41	772.59	698.26	710.74
Pb	2.5214	3.1050	1.9965	0.9583	3.7895	2.6744
Th	5.3584	4.9024	4.4064	7.0063	6.5309	6.0489
U	1.4624	1.3423	1.1482	1.8775	2.2099	1.9786
Nb	86.282	72.955	75.494	87.895	77.632	89.483
Ta	4.6301	4.1309	4.0928	4.1422	4.0965	4.6303
Sr	797.57	853.54	637.00	792.65	1075.9	922.24
Hf	5.0845	5.1069	3.9878	3.3915	4.0683	4.1582
Zr	235.83	239.90	187.31	179.89	211.13	213.77
Cs	0.7117	0.9461	18.514	2.4024	1.9011	0.5089
Y	24.738	23.874	21.440	22.193	25.799	24.565
La	56.136	53.995	44.598	71.530	69.201	61.077
Ce	103.18	99.477	79.227	115.67	115.24	106.39
Pr	11.746	11.368	8.950	11.949	12.450	11.563
Nd	46.154	45.489	35.273	44.560	47.119	45.097
Sm	8.3779	8.3243	6.6178	7.3522	8.1394	7.9234
Eu	2.4080	2.3794	1.9102	2.1098	2.3184	2.2717
Gd	6.8217	6.9367	5.6166	5.9393	6.7466	6.6619
Tb	0.8602	0.8531	0.7210	0.7243	0.8643	0.8449
Dy	4.7282	4.7987	4.0619	3.9277	4.8938	4.7170
Ho	0.8395	0.8034	0.7192	0.6972	0.8569	0.8171
Er	2.0852	1.9460	1.8006	1.6957	2.1615	2.0320
Tm	0.2641	0.2454	0.2414	0.2162	0.2902	0.2714
Yb	1.7985	1.5900	1.5668	1.5167	1.9565	1.7785
Lu	0.2527	0.2104	0.2233	0.2136	0.2757	0.2496

Table 2: Sr, Nd and Pb isotopic compositions of the Hocheifel lavas

Sample	$(^{86}\text{Sr}/^{87}\text{Sr})_m$	$(^{86}\text{Sr}/^{87}\text{Sr})_i$	$(^{143}\text{Nd}/^{144}\text{Nd})_m$	$(^{143}\text{Nd}/^{144}\text{Nd})_i$	$(^{206}\text{Pb}/^{204}\text{Pb})_m$	$(^{206}\text{Pb}/^{204}\text{Pb})_i$	$(^{207}\text{Pb}/^{204}\text{Pb})_m$	$(^{207}\text{Pb}/^{204}\text{Pb})_i$	$(^{208}\text{Pb}/^{204}\text{Pb})_m$	$(^{208}\text{Pb}/^{204}\text{Pb})_i$
1	0.703350	0.70328	0.512878	0.512827						
	0.000015		0.000006							
2	0.703380	0.70330	0.512803	0.512747						
	0.000011		0.000028							
3	0.703640	0.70356	0.512821	0.512759	19.9434	19.6918	15.6567	15.6448	39.8194	39.5303
	0.000011		0.000009		0.0009		0.0010		0.0030	
4	0.703300	0.70327	0.512880	0.512829						
	0.000015		0.000006							
5	0.704020	0.70374	0.512865	0.512819						
	0.000012		0.000006							
6	0.703350	0.70330	0.512867	0.512815						
	0.000013		0.000008							
7	0.703450		0.512837		19.8083	19.5724	15.6483	15.6372	39.6810	39.4170
	0.000014		0.000006		0.0008		0.0008		0.0027	
8	0.703360	0.70326	0.512813	0.512751						
	0.000010		0.000007							
9	0.703360	0.70325	0.512856	0.512800	19.9893	19.7390	15.6338	15.6221	39.7509	39.4363
	0.000010		0.000007		0.0008		0.0008		0.0023	
10	0.703390	0.70328	0.512870	0.512813						
	0.000016		0.000006							
11	0.703360	0.70329	0.512888	0.512835						
	0.000009		0.000007							
12	0.703700	0.70320	0.512909	0.512847	19.8842	19.5903	15.6310	15.6171	39.7434	39.3936
	0.000011		0.000015		0.0010		0.0011		0.0035	
13	0.704160	0.70402	0.512778	0.512719	19.7977	19.3971	15.6573 ±8	15.6384	39.5353	39.1170
	0.000013		0.000012		0.0008		0.0008		0.0025	
14	0.703390									
	0.000014									
15	0.703810	0.70375	0.512790	0.512722	19.9057	19.6704	15.6588	15.6477	39.6523	39.4132
	0.000013		0.000016		0.0006		0.0006		0.0021	
16	0.703360	0.70336								
	0.000014									
17	0.704540	0.70428	0.512705	0.512647						
	0.000010		0.000025							
18	0.703430	0.70338								
	0.000014									
19	0.705440	0.70474	0.512709	0.512658						
	0.000010		0.000009							
20	0.704110	0.70402	0.512816	0.512746						
	0.000010		0.000009							

*m - measured ratio

**i - initial ratio

second line below the measured ratios-2 σ

Chapter 4

Fekiacova, Z. and Abouchami, W.:
The Ko'olau Scientific Drilling Project: Lead isotope
evolution of Ko'olau Volcano.

This manuscript will be submitted to the Earth and Planetary Science Letters

**The Ko'olau Scientific Drilling Project: Lead isotope evolution of
Ko'olau Volcano.**

Z. Fekiacova and W. Abouchami

Abstract

The Ko'olau Scientific Drilling Project (KSDP) has been initiated in order to evaluate the long-term evolution of Ko'olau volcano and obtain information about the Hawaiian mantle plume. High precision Pb triple spike data, as well as Sr and Nd isotope data on KSDP lavas and Honolulu Volcanic Series (HVS) reveal compositional source variations during Ko'olau growth. At least, three Pb end-members are present in Ko'olau lavas and the contribution of each individual component is recorded in the Pb, Sr, and Nd isotopes stratigraphy. Lead, Sr and Nd isotopic compositions indicates that one radiogenic and two unradiogenic components are present in Ko'olau lavas. The radiogenic component is shared by lavas from three stages of Ko'olau growth. It has "high- μ " signature and shows affinities with the least radiogenic Kea-lo8 lavas present in Mauna Kea. The contribution of this component has decreased during the shield building-stage. The first unradiogenic component was predominantly sampled by the subaerial stage lavas, but it is also present in variable and smaller proportions in the main shield-stage (KSDP) lavas. This component has EM1-type isotopic characteristics and corresponds to the "Ko'olau" end-member of the Hawaiian mantle plume. The second unradiogenic end-member, so far only sampled by Honolulu lavas, has Pb, Sr and Nd isotopic characteristics similar to those of a depleted mantle. However, they differ from those of the recent Pacific lithosphere providing evidence that the HVS are not derived from MORB-related source. We suggest, instead, that the HVS result from melting of plume material and that the Pb, Sr and Nd isotopic variations recorded in Ko'olau lavas can be related to melting of different part of the mantle plume. Thus the evolution of a single Hawaiian volcano records the geochemical and isotopic changes within the Hawaiian mantle plume.

1. Introduction

Hawaiian volcanoes, which sample the Hawaiian mantle plume, form one of the most studied volcanic chains of the world. Currently, the hot-spot is centered between Mauna Kea, Kilauea and Loihi volcanoes. Various mantle components, such as a depleted upper mantle and recycled slab material are generally accepted to be present in the source of the Hawaiian mantle plume [1-7]. Most of the existing data on Hawaiian volcanoes have been obtained on near-surface samples (<http://georoc.mpch-mainz.gwdg.de/georoc/>). However, recent drill cores and underwater samples from submarine landslides have allowed access to the shield's interior. For example, the Hawaiian Scientific Drilling Project (HSDP), which provides a section through Mauna Kea shield [8], was initiated with the ultimate objective of sampling the lavas from all stages of volcano growth in order to evaluate temporal changes in source(s) composition. Similarly, the aim of the Ko'olau Scientific Drilling Project (KSDP) is to study the geochemical and temporal evolution of Ko'olau volcano [9], which represents an extreme "endmember" of the Hawaiian mantle plume in isotope space and thus may provide information about the evolution of the Hawaiian mantle plume.

Ko'olau is an extinct volcano located on the eastern part of the Oahu Island, in the Hawaiian archipelago (Fig. 1). Three main volcanic suites have erupted on Oahu: the volumetrically largest Waianae volcanics, the Ko'olau lavas and the post-erosional Honolulu Volcanics [10]. During its growth, Ko'olau went through the different evolutionary stages of a typical shield volcano. The shield building stage, from 1.8-2.6 Ma [11], produced mainly

tholeiitic lavas and is subdivided into an old main shield stage and a younger subaerial stage, referred to as Makapu'u subaerial stage. There is no evidence for a post-shield stage volcanic activity on Ko'olau [12]. After ~1 Ma of erosion and, at least, 1 km of subsidence of Ko'olau shield [12], a rejuvenated stage, or post-erosional stage of volcanism produced alkaline lavas referred to as Honolulu Volcanic Series (HVS).

The "Ko'olau component" described in the literature represents the geochemically and isotopically enriched end-member of the Hawaiian mantle plume [2, 10]. Ko'olau lavas are characterized by the highest SiO₂ content, the highest ⁸⁷Sr/⁸⁶Sr and ¹⁸⁷Os/¹⁸⁸Os ratios and the lowest ϵ_{Nd} , ϵ_{Hf} and ²⁰⁶Pb/²⁰⁴Pb values among Hawaiian shield lavas [3, 13-15]. These features have been interpreted as reflecting contribution from an old recycled oceanic crust [13, 15]. However, the definition of the "Ko'olau component" is essentially based on the characteristics of Makapu'u subaerial lavas which are not representative of the main shield-building stage. Samples from the lava flows discovered in the highway trans-Ko'olau tunnel [16] and on the submarine flanks of Ko'olau volcano [17], for example, have geochemical and isotopic compositions resembling those of recent Kilauea and Mauna Loa [17, 18]. Geochemical and petrological studies of Nuuanu submarine landslide blocks which originate from Ko'olau volcano [18] also indicate that Ko'olau underwent a multistage isotopic evolution starting from Kilauea-like to Mauna Loa-like and ending as the "Ko'olau"-type [18].

The KSDP have allowed to sample deeper stratigraphic levels than those exposed subaerially [9] and thus, to evaluate the geochemical and temporal changes within Ko'olau source during the main building stage. The KSDP drill site is located on the western side of lower Kalihi valley, at an elevation of 47m [9]. The drill core is composed of two parts, the rotary section, from 0 to 300 meters below sea level (mbsl), and the cored section, from 300 to

632 mbsl. Hundred and four petrological units have been described in the cored section [9]. The existence of geochemical variations within Ko'olau lavas, and specifically differences between KSDP and subaerial Makapu'u lavas, suggest indeed that Ko'olau source composition varied during its growth [9]. Unraveling the evolution of a single Hawaiian volcano can thus reveal crucial information about the Hawaiian mantle plume chemical structure. Here we report Pb isotopic compositions on samples from KSDP lavas and Honolulu Volcanic Series (hereafter referred to as "HVS") obtained with the aims of (1) resolving compositional isotopic changes during Ko'olau volcano's growth, (2) evaluating the relationships between shield-building stage and post-erosional stage lavas and (3) assessing the origin of Honolulu volcanic sources - it is still unclear whether or not they sample the old underlying Hawaiian lithosphere [10, 19, 20].

2. Samples and methods

Lead isotopic compositions of 29 KSDP and 5 HVS samples have been determined using the Pb triple spike technique to correct for instrumental mass fractionation [21]. Prior to dissolution, chips of KSDP lavas and powders of HVS were rinsed and sonicated for 15 minutes with ultrapure Milli-Q water in order to eliminate dust and impurities. Following on, samples were leached in hot 6N HCl for 1 hour and the leachates discarded. For the altered samples from the deeper levels of the KSDP core (below 500 m), the leaching time was increased to 3 hours and both leachate and residue were analyzed. After leaching, the samples were rinsed several times with Milli-Q water in order to ensure complete removal of the leached fraction. Samples were dissolved in a mixture of concentrated HF and HNO₃ and Pb was separated by anion exchange resin (AG1-X8, 100-200 mesh), following the procedure described by Lugmair and

Galer [22]. A Pb blank was measured with each batch of samples (N=9) and ranged from 12 to 80 pg and is negligible compared to the amount of sample Pb (120-180 ng).

After Pb elution, an aliquot of the sample was spiked with an optimal amount of triple spike. Spiked and unspiked aliquots were analyzed separately on a Finnigan MAT 261 in static multicollection mode using Re-filaments and a silica-gel activator [23]. All results are referenced to the values of NIST-SRM-981 Pb standard, with $^{206}\text{Pb}/^{204}\text{Pb}$, $^{207}\text{Pb}/^{204}\text{Pb}$ and $^{208}\text{Pb}/^{204}\text{Pb}$ of 16.9401 ± 23 , 15.4968 ± 29 and 36.7234 ± 44 ($2\sigma_{\text{ext}}$, N=73), respectively.

We also report Sr isotope data on 12 KSDP lavas and 5 Honolulu Volcanics. Sr was separated using a cationic exchange resin and Sr isotope ratios are reported relative to a value of NIST-SRM 987 of 0.710250. Lead and Sr isotopic compositions of KSDP lavas and Honolulu Volcanics are reported in Table 1 together with the average values of NIST-SRM 981 and NIST-SRM-987 (N=8) standard replicates measured during this study. Our dataset includes also Pb isotopic compositions of one replicate analysis and two leachates. The Pb isotopic compositions of the HCl 6N leachates are shifted towards higher Pb isotopes ratios relative to the residues. The differences are significant and outside the analytical errors (see Table 1).

3. Results

3.1 *Pb and Sr isotope stratigraphy*

Variations of $^{206}\text{Pb}/^{204}\text{Pb}$ ratios of KSDP lavas with depth are shown in Fig. 2b. Despite a small total range (0.15 variability), $^{206}\text{Pb}/^{204}\text{Pb}$ ratios fluctuations can be resolved outside analytical error. These variations form a general “bell” trend with an increase of $^{206}\text{Pb}/^{204}\text{Pb}$ from the top of the section to ~450 mbsl, followed by a decrease to ~600 mbsl (Fig. 2b). The altered

samples recovered in the deepest part of the core, under ~575 mbsl, do not follow this general trend and are scattered. Superimposed on the “bell” trend, $^{206}\text{Pb}/^{204}\text{Pb}$ ratios oscillate on smaller length-scale, with cycles recurrence at about 25 m depth intervals.

The $^{208}\text{Pb}^*/^{206}\text{Pb}^*$ ratio represents the time integrated $^{238}\text{U}/^{232}\text{Th}$ ratio since the formation of the Earth and is defined as $[(^{208}\text{Pb}/^{204}\text{Pb})_{\text{sample}} - 29.475] / [(^{206}\text{Pb}/^{204}\text{Pb})_{\text{sample}} - 9.307]$ [24]. Significant differences can be distinguished between KSDP lavas, Makapu’u subaerial lavas and Honolulu Volcanics based on their $^{208}\text{Pb}^*/^{206}\text{Pb}^*$ ratios (Fig. 2c). Honolulu Volcanics exhibit low and uniform $^{208}\text{Pb}^*/^{206}\text{Pb}^*$ ratio (0.941 to 0.946), KSDP lavas show intermediate values varying from 0.945 to 0.969 and Makapu’u subaerial lavas have the highest values ranging from 0.968 to 0.987. Note that the KSDP lavas seem to exhibit more variability in the lower part of the core, below 575 mbsl, i.e. in the part where the samples are altered. Thus, there has been an increase in $^{208}\text{Pb}^*/^{206}\text{Pb}^*$ from the main-shield building stage to the subaerial stage, followed by a reversal and drop in $^{208}\text{Pb}^*/^{206}\text{Pb}^*$ ratios during the post-erosional stage.

Similarly, KSDP, Makapu’u subaerial lavas and Honolulu Volcanics exhibit distinct Sr isotopic compositions (Fig. 2d), with a pattern of variation that is very similar to that of $^{208}\text{Pb}^*/^{206}\text{Pb}^*$ ratios. That is, $^{87}\text{Sr}/^{86}\text{Sr}$ ratios increase going from KSDP lavas (0.70361 to 0.70386) to Makapu’u subaerial lavas (0.7040 to 0.70435) and drop in the Honolulu Volcanics (0.70331 to 0.70336) which display a restricted and uniform range of $^{87}\text{Sr}/^{86}\text{Sr}$ ratios (Fig. 2d). Hf and Nd isotope data on KSDP (Salters, pers. comm.) and those published on HVS [15] and Makapu’u subaerial lavas [13] exhibit similar patterns to those described here for Sr and Pb isotopes. Our new Sr isotope data on the HVS are consistent with those reported earlier on the same samples by Stille et al. [10]. Altogether, the correlated variations in Sr, Nd, Hf and Pb

isotope ratios demonstrate that there has been significant compositional shift in Ko'olau sources during its evolution.

3.2 Isotopic covariations

Lead isotope ratios of KSDP lavas and Honolulu Volcanics display a relatively small total range. For KSDP, they vary from 18.00 to 18.15, 15.44 to 15.46 and 37.82 to 37.87, for $^{206}\text{Pb}/^{204}\text{Pb}$, $^{207}\text{Pb}/^{204}\text{Pb}$ and $^{208}\text{Pb}/^{204}\text{Pb}$, respectively. Pb isotopic compositions of Honolulu Volcanics range from 18.05 to 18.23, 15.45 to 15.47 and 37.74 to 37.88, for $^{206}\text{Pb}/^{204}\text{Pb}$, $^{207}\text{Pb}/^{204}\text{Pb}$ and $^{208}\text{Pb}/^{204}\text{Pb}$, respectively. In $^{208}\text{Pb}/^{204}\text{Pb}$ vs. $^{206}\text{Pb}/^{204}\text{Pb}$ plot (Fig. 3a), the KSDP lavas and Honolulu Volcanics form two distinct, well-defined linear arrays ($R^2_{\text{KSDP}} = 0.69$, $N=29$ and $R^2_{\text{HVS}} = 0.98$, $N= 5$), despite the range in Pb isotope ratios. At a given $^{206}\text{Pb}/^{204}\text{Pb}$ ratio, Honolulu Volcanics have lower $^{208}\text{Pb}/^{204}\text{Pb}$ ratio than KSDP lavas (Fig. 3a). In $^{207}\text{Pb}/^{204}\text{Pb}$ vs. $^{206}\text{Pb}/^{204}\text{Pb}$ space (Fig. 3b), KSDP and Honolulu Volcanics trends cannot be unambiguously resolved. Pb isotope data on Makapu'u stage subaerial lavas [25] are also plotted and lie at the unradiogenic extension of the KSDP trend in Fig. 3a. The linear arrays found in ^{208}Pb - ^{206}Pb space indicate, if interpreted as binary mixing lines, the presence of three distinct Pb components. This result is entirely consistent with the inference from Sr and Pb isotope stratigraphy of temporal changes in sources composition during Ko'olau evolution.

4. Discussion

4.1 *Pb isotopes – implications on source(s) and evolution of Ko’olau volcano*

Isotopic heterogeneities between Hawaiian volcanoes have been explained as resulting from mixing of several isotopically distinct components. Based on the Pb, O and Os isotopic compositions of Hawaiian lavas, two [3, 13, 26], three [7, 27] and four [5, 28] components mixing models have been proposed to describe the sources of Hawaiian magmas. One of these components is the so-called “Ko’olau component” which, when used in this paper, refers to the one of the end-members of the Hawaiian mantle plume described previously in the literature [2, 10]. Our data show that this component is represented essentially by the Makapu’u subaerial lavas although it did contribute to the shield building stage of Ko’olau.

Case studies of several Hawaiian shield volcanoes reveal differences at the scale of a single volcano. For example, three different Pb isotope arrays were described in the HSDP record of Mauna Kea [28, 29]. Similarly, several studies on Ko’olau lavas have revealed an intrinsic heterogeneity within the source of Ko’olau [17, 30]. For example, it has been shown that the Nuuanu submarine landslide blocks, which result from the collapse of the eastern part of Ko’olau volcano [18], have geochemical and isotopic characteristics that are different from those of Makapu’u subaerial lavas. Although the Nuuanu blocks originate from Ko’olau volcano, their trace element and isotopic compositions resemble those of modern Mauna Loa

lavas [17]. Furthermore, Pb isotopic compositions of lavas from different stages of Ko'olau volcanism encompass the whole range found in Hawaiian lavas, evolving from Kilauea-like, through Mauna Loa-like and "Ko'olau"-like compositions. The KSDP lavas represent deeper stratigraphic levels of Ko'olau volcano and were erupted during the main shield building stage. Major and trace elements compositions of KSDP lavas [30, 31] indicate that they are chemically distinct from Makapu'u subaerial stage lavas, but show close resemblance with recent Mauna Loa lavas. In addition, the trace elements compositions of KSDP lavas are intermediate between those of Makapu'u stage and recent Mauna Loa lavas [31].

With the objective of decoding the changes in the Ko'olau source, we have compared the Pb isotopic compositions of the lavas from different evolutionary stages of Ko'olau. In $^{208}\text{Pb}/^{204}\text{Pb}$ vs. $^{206}\text{Pb}/^{204}\text{Pb}$ isotope space (Fig. 3a), the KSDP lavas and Honolulu Volcanics form two linear arrays that converge at the radiogenic end. The KSDP and Honolulu Pb isotope arrays are well-resolved, given the analytical precision on $^{208}\text{Pb}/^{204}\text{Pb}$ and $^{206}\text{Pb}/^{204}\text{Pb}$ ratios. This relationship can be interpreted in terms of binary mixing, which in turn imply the presence of, at least, three isotopically distinct components in the Ko'olau source. While the radiogenic end-member is common to HVS, KSDP and Makapu'u, the low $^{206}\text{Pb}/^{204}\text{Pb}$ (unradiogenic) end-members can be distinguished on the basis of their $^{208}\text{Pb}/^{204}\text{Pb}$ ratios, the KSDP end member having a higher ratio than that of the HVS end member (Fig. 5a).

The radiogenic end-member is defined by the intersection of the KSDP and Honolulu trends in a $^{208}\text{Pb}/^{204}\text{Pb}$ vs. $^{206}\text{Pb}/^{204}\text{Pb}$ plot (Fig 5a). This end-member is characterized by relatively high $^{208}\text{Pb}/^{204}\text{Pb}$ (~ 37.9) and $^{206}\text{Pb}/^{204}\text{Pb}$ (~ 18.2) ratios and a higher " μ " compared to the unradiogenic components. This radiogenic end-member is common to the main shield-stage lavas (KSDP), the Makapu'u subaerial lavas, and the post-erosional Honolulu Volcanics. It has

been previously suggested that the so called “Kea component” of the Hawaiian mantle plume [2], contributed to the mixing that produced Ko’olau shield lavas [17]. The “Kea-component” is characterized by the highest $^{206}\text{Pb}/^{204}\text{Pb}$ and $^{143}\text{Nd}/^{144}\text{Nd}$ together with the lowest $^{87}\text{Sr}/^{86}\text{Sr}$ and $^{187}\text{Os}/^{188}\text{Os}$ ratios of Hawaiian shield lavas [1-3, 7] and is therefore thought to reflect an enrichment of the recycled lithospheric mantle [2] or entrained upper mantle during plume ascent [4, 7]. However, in $^{208}\text{Pb}/^{204}\text{Pb}$ vs. $^{206}\text{Pb}/^{204}\text{Pb}$ diagram (Fig. 6), the KSDP trend extends towards the most depleted end of the “Kea-lo8” field [29] and not towards the “Kea” component. “Kea-lo8” trend is one of the three linear arrays described in Mauna Kea HSDP lavas and is defined by the late shield building lavas of Mauna Kea volcano. It has been suggested that the “Kea-lo8” lavas sample peripheral part of the Hawaiian mantle plume [29] as the volcano moves away from the plume center. The extension of the KSDP trend towards the most depleted “Kea-lo8” compositions suggests the presence of a component similar to that present in Mauna Kea in the Ko’olau lavas.

The lower extension of the KSDP trend is represented by the enriched compositions, low $^{206}\text{Pb}/^{204}\text{Pb}$ and high $^{208}\text{Pb}/^{204}\text{Pb}$, low ϵ_{Nd} and high $^{87}\text{Sr}/^{86}\text{Sr}$ (Fig. 5). Consequently, the KSDP lavas result from mixing between a depleted “Kea-lo8”-type material and an enriched, unradiogenic component. The unradiogenic component present in KSDP lavas exhibits EM1-type Pb isotopic characteristics, which are similar to those of the Makapu’u subaerial stage lavas [25]. In addition, this component shows the highest $^{87}\text{Sr}/^{86}\text{Sr}$ ratios and the lowest ϵ_{Nd} [25] among Ko’olau lavas (Fig. 5 b, c). Therefore, we conclude that the enriched component of KSDP lavas corresponds to the “Ko’olau end-member” of Hawaiian shields previously described in the literature [2, 15]. The enriched isotopic characteristics of “Ko’olau component” have been interpreted as reflecting contribution from recycled oceanic crust and/or sediment [5, 13].

Although the “Ko’olau component” of the Hawaiian mantle plume appears to be predominantly sampled during Makapu’u subaerial stage, nevertheless its contribution has been waxing and waning and it has been a long-lasting and recurrent feature in the main shield building stage of Ko’olau. The relative contribution of this “Ko’olau component” varied during the main shield-stage of Ko’olau growth as shown by Pb and Sr isotope stratigraphy (Fig. 2a, b) and also Nd and Hf isotopic variations [32] of KSDP lavas.

The second unradiogenic end-member, identified here for the first time, lies at the low $^{208}\text{Pb}/^{204}\text{Pb}$ -low $^{206}\text{Pb}/^{204}\text{Pb}$ end of the HVS trend (Fig. 5a). In addition to its unradiogenic Pb isotopic characteristics, this component has the lowest $^{87}\text{Sr}/^{86}\text{Sr}$ and the highest $^{143}\text{Nd}/^{144}\text{Nd}$ ratios among Ko’olau volcano lavas (Fig. 5 b, c). Such isotopic features are similar to those of a depleted mantle and will be discussed later. The “HVS” Pb isotope array indicates that the post-erosional Honolulu Volcanics generate from mixing between a depleted mantle-type material and a “Kea-lo8”-type material. The nature of the depleted material involved in the Honolulu Volcanics will be discussed in section 4.3, which is focused on the source of the post-erosional lavas.

In order to examine the relationships between different stages of Ko’olau volcano, we have also compared Pb isotopic compositions of Ko’olau lavas with those reported on Nuuanu landslide blocks [17] (Fig. 6 a). The Nuuanu landslide blocks, recovered on the submarine slopes north of Oahu, originated from the collapse of Ko’olau volcano [18]. However, the major element chemistry and petrology of the Nuuanu blocks are distinct from those of Ko’olau lavas, and broadly similar to those of modern Mauna Loa lavas [18]. In $^{208}\text{Pb}/^{204}\text{Pb}$ vs. $^{206}\text{Pb}/^{204}\text{Pb}$ diagram (Fig. 6 a), the field of KSDP lavas overlaps that of Nuuanu-2 landslide blocks suggesting that there are similarities between KSDP lavas and recent Mauna Loa lavas. A

comparable observation was made by Haskins and Garcia [30] based on the major and trace element systematics. In order to evaluate whether a relationship between the sources of KSDP and Mauna Loa lavas exists, we have compared their Pb isotopic compositions with those of other Hawaiian shield volcanoes (Fig. 6 b).

Hawaiian shield volcanoes form two geographically distinct chains that have been described as Loa trend and Kea trend [16]. In addition to their distinct geographic positions, both trends are characterized by systematic differences in isotopic compositions. Different models have been proposed to explain the geographical and isotopic structure of the Hawaiian volcanic chains. An early model proposes that the Hawaiian plume is concentrically zoned and that the Loa trend volcanoes sample more central part of the plume whereas the Kea trend volcanoes preferentially sample the periphery of the plume [4, 7, 33]. An alternative model suggests that there is a large-scale lateral asymmetry in the Hawaiian mantle plume and that this asymmetry is reflected by differences in Pb isotopic compositions of the volcanoes of both trends [25], Loa trend having higher $^{208}\text{Pb}/^{204}\text{Pb}$ than Kea trend, at a given $^{206}\text{Pb}/^{204}\text{Pb}$. In $^{208}\text{Pb}/^{204}\text{Pb}$ vs. $^{206}\text{Pb}/^{204}\text{Pb}$ diagram, the KSDP lavas fall on the Loa trend, whereas the Honolulu Volcanics lie along the Kea trend (Fig. 6 b). The Pb isotopic compositions of KSDP lavas overlap those of recent Mauna Loa lavas. However, KSDP and Mauna Loa Pb isotope arrays exhibit significantly different slopes (0.3048 and 0.7477, respectively) in $^{208}\text{Pb}/^{204}\text{Pb}$ vs. $^{206}\text{Pb}/^{204}\text{Pb}$ diagram (Fig. 6 b) indicating that they do not share similar source components. While the KSDP trend extends towards the lowest end of the “Kea-lo8” lavas, the Mauna Loa trend shows affinities with Kilauea lavas (Fig. 6b). Thus, the similarity between the sources involved in KSDP and Mauna Loa lavas do not appear to be sustained by the Pb isotope data.

We propose instead that the lavas from the different evolutionary stages of Ko'olau volcano result from mixing of various proportions of the three following components: (1) a radiogenic end-member similar to the depleted "Kea-lo8" component of Mauna Kea, (2) the "Ko'olau component" of the Hawaiian mantle plume and (3) a depleted-mantle-like component. The "Kea-lo8"-type end-member is present in variable proportions in the lavas of the three stages of Ko'olau. It largely contributes to the main-shield stage (KSDP) while the "Ko'olau component" of the Hawaiian mantle plume is predominantly sampled during the Makapu'u subaerial stage, but remains a recurrent feature during shield-building stage. Finally, the depleted-mantle-like component produced the post-erosional Honolulu Volcanics by mixing with the radiogenic "Kea-lo8"-type end-member of Ko'olau lavas.

4.2 Pb isotope stratigraphy

Lead isotope stratigraphy records fluctuations in magma source compositions. Recurrence of cycles indicates variations in the input of different components in the Ko'olau lavas source. The radiogenic spike that we observe in the $^{206}\text{Pb}/^{204}\text{Pb}$ ratios stratigraphy at ~450 mbsl (Fig. 2a) is also observed in the ϵ_{Nd} and ϵ_{Hf} variations with depth [32]. This spike reflects a maximum contribution of a radiogenic component in the KSDP source. The comparison of the Pb isotope stratigraphy of Mauna Kea and Ko'olau shields (HSDP and KSDP cores, respectively) reveals differences in the fluctuation rate of Pb isotope ratios between these two volcanoes (Fig. 4). The overall variation of $^{206}\text{Pb}/^{204}\text{Pb}$ ratios in KSDP lavas is ± 0.15 over 300 m core length, while it is ± 0.25 over $\pm 3000\text{m}$ within the Mauna Kea shield. The high sampling density over the KSDP core (one sample every 2 to 5 m) allows us to identify rapid changes in

Pb isotopic compositions in Ko'olau lavas. These changes can be resolved at intervals of about 25m, which cannot be seen in the HSDP core. This feature can reflect either a purely sampling effect or alternatively, the rate of fluctuations is lower in magmas producing Kea lavas. Although, the high frequency variations have not been observed in the HSDP core, rapid changes similar to those observed in Ko'olau were described in Kilauea lavas [34]. Thus these rapid variations appear to be a relatively common feature in the Hawaiian mantle.

Lead isotope stratigraphy shows that individual source components of Ko'olau were dominant during different time spans of Ko'olau growth. The samples from the bottom and from the top of the KSDP core have the lowest $^{206}\text{Pb}/^{204}\text{Pb}$ but the highest $^{208}\text{Pb}^*/^{204}\text{Pb}^*$ ratios. Thus, at the beginning and at the end of the main shield building stage of Ko'olau, the low $^{206}\text{Pb}/^{204}\text{Pb}$ - high $^{208}\text{Pb}/^{204}\text{Pb}$ component which corresponds to the "Ko'olau end-member" of the Hawaiian plume played a dominant role in the source. In the middle of the KSDP core, the $^{206}\text{Pb}/^{204}\text{Pb}$ peak correlated with the lowest $^{208}\text{Pb}^*/^{206}\text{Pb}^*$ ratios indicates a strengthening of the radiogenic, component in Ko'olau lavas. The high frequency variations observed in the $^{208}\text{Pb}^*/^{204}\text{Pb}^*$ stratigraphy (Fig. 2b) suggest that the proportion of the "Ko'olau component" and "Kea-lo8"-type component changed rapidly with time. Our data reveal that the so-called "Ko'olau component" represents a recent ephemeral feature of Hawaiian plume, which has been described in the literature.

4.3 Source(s) of post-erosional Honolulu Volcanics

The source(s) of post-erosional Honolulu Volcanics are still a matter of debate. Based on petrological studies and trace element analyses, Clague and Frey [19] suggested that Honolulu

Volcanics originate from a garnet-lherzolite enriched mantle source. Low Sr and high Nd isotopic ratios indicate a long-term history of incompatible element depletion of the source [19] which was subsequently affected by a recent metasomatic event [14]. In contrast to the heterogeneity of Ko'olau tholeiites, Honolulu Volcanics show a remarkable homogeneity of Sr, Nd, Pb and Hf isotopic ratios [6, 7, 12, 24] and, at the same time, a variable enrichment in highly incompatible elements. These features have been explained in terms of variable degrees of melting of a compositionally homogeneous source [14]. Roden et al. [14] also pointed out the similarity of Sr and Nd isotopic compositions of Honolulu Volcanics with those of Mid-Ocean Ridge Basalts (MORBs). As an alternative model to the metasomatic event proposed previously [14, 19], they suggested that Honolulu Volcanics result from the mixing of high proportion (97%) of a relatively enriched mantle with few percents (~2.5%) of a very low degree (~0.26%) melt of MORB source.

The most recent Os and Pb isotopes data [3, 20] support the hypothesis that Honolulu post-erosional lavas assimilated a depleted mantle component which is related to the source of Pacific MORBs. Samples thought to be representative of the oceanic crust near Hawaii include basalts from ODP 843 Site [35] and gabbroic xenoliths recovered from Hualalai lavas [3], which represent fragments of the pre-Hawaiian Pacific middle to lower crust [3]. Figure 9 shows a comparison of our Pb triple spike data on Honolulu Volcanics with those of ODP 843 basalts [35] and Hualalai gabbroic xenoliths [3]. Any similarities could testify for the involvement of the Pacific lithosphere in the post-erosional Honolulu Volcanics source. However, the available data, which were obtained by conventional methods, show reasonable scatter (see Fig. 7) which makes a direct comparison with our Pb triple spike data difficult and thus evaluation of this hypothesis impractical.

To overcome this problem, we have chosen to evaluate a possible involvement of Pacific MORB-related source in Honolulu Volcanics by comparing our data with the Pb triple spike data obtained on East Pacific Rise MORBs (EPR MORBs) [36]. The latter are thought to represent the Pb isotopic compositions of recent Hawaiian lithosphere and indicate a significant heterogeneity in the Pacific MORB source, since individual segments form linear arrays in Pb isotope space [36]. In Pb isotope space (Fig. 8 a, b), KSDP lavas, Honolulu Volcanics and EPR MORBs when taken as a whole form three distinct groups. At a given $^{206}\text{Pb}/^{204}\text{Pb}$ ratio, KSDP lavas have higher $^{208}\text{Pb}/^{204}\text{Pb}$ ratio than EPR MORBs and Honolulu Volcanics exhibit intermediate values between those of KSDP and EPR MORBs (Fig. 8a). As previously mentioned, KSDP and Honolulu Volcanics trends cannot be unambiguously resolved in a $^{207}\text{Pb}/^{204}\text{Pb} - ^{206}\text{Pb}/^{204}\text{Pb}$ plot (Fig. 8b). However, the two datasets can be clearly distinguished from EPR MORBs since EPR MORBs have, at a given $^{206}\text{Pb}/^{204}\text{Pb}$ ratio, higher $^{207}\text{Pb}/^{204}\text{Pb}$ ratio than both KSDP and Honolulu Volcanics. In addition to the Pb isotopic differences, Sr and Nd isotopes data confirm the distinct characteristics of Honolulu Volcanics and recent MORBs. At a given $^{206}\text{Pb}/^{204}\text{Pb}$ ratio, Honolulu Volcanics have higher $^{87}\text{Sr}/^{86}\text{Sr}$ and lower $^{143}\text{Nd}/^{144}\text{Nd}$ ratios than EPR MORBs (Fig. 5 b, c). On the basis of this comparison, it appears that post-erosional Honolulu Volcanics have distinct Pb, Sr and Nd isotopic characteristics compared to those of the recent Pacific lithosphere, suggesting that Honolulu Volcanics are not derived from the melting of a MORB-related lithospheric source. Instead, we propose that Honolulu Volcanics sample a depleted component which may be inherent to the Hawaiian mantle plume, and concur with the conclusion of Frey et al [37]. If this component represents material entrained by the Hawaiian mantle plume on its ascent, then it may be derived from the second melting zone of the dynamical model of Ribe and Christensen [38]. Based on this model, Hawaiian shield stage

lavas result from melting in a primary melting zone, located in the hottest, central part of the plume, while the secondary melting zone, which is located between 300 and 500 km downstream of the plume center, produces the post-erosional lavas. Our results show that post-erosional lavas do not sample a MORB-related lithosphere but result from melting of a depleted material with MORB affinities present in the Hawaiian mantle plume. Frey et al. [37] suggested, based on the Pb, Hf and Nd isotopes, that the depleted component sampled by the Hawaiian rejuvenated lavas is formed by low degrees of melting of a depleted recycled peridotite intrinsic to the plume. This component has been available for 80 Ma but is sampled only under specific conditions [37].

Comparison of HVS with post-erosional lavas from other Hawaiian volcanoes, in particular East Molokai (Xu et al. *subm.*) and West Maui (<http://georoc.mpch-mainz.gwdg.de/georoc/>), shows that the homogeneity of Sr and Nd isotopes is a general feature of post-erosional lavas independent of whether they belong to Kea or Loa trend. Similar observation has already been made by (Xu et al., *subm.*). Despite this homogeneity, Pb isotope systematics still indicate the existence of a $^{208}\text{Pb}/^{204}\text{Pb}$ difference between Loa and Kea as has been observed for the main shield lavas [25]. That is, HVS have a higher $^{208}\text{Pb}/^{204}\text{Pb}$ at a given $^{206}\text{Pb}/^{204}\text{Pb}$ ratio compared to East Molokai and West Maui (Kea trend). This observation suggests that the Loa-Kea compositional boundary, defined on the basis of the Pb isotopic compositions of main shield lavas, survives in the late stage evolution of Hawaiian volcanoes. This observation bears important implications on models of the Hawaiian mantle plume, and in particular makes the concentrically-zoned plume model untenable [3, 39].

5. Conclusions

Our Pb isotope data on KSDP lavas and Honolulu Volcanics show that Ko'olau Volcano experienced compositional source variations at different evolutionary stages. We have shown that at least three isotopically distinct components are present in the source of Ko'olau lavas. Lead, Sr, Nd and Hf isotope stratigraphy record variations of the contribution of each individual component. Based on our Pb triple spike data, we have been able to identify a common radiogenic and two distinct unradiogenic components in Ko'olau source. The common radiogenic component has a higher " μ ", compared to two unradiogenic end-members, and shows affinities with the most depleted component (Kea-lo8) present in Mauna Kea lavas. This component is present in variable proportions in the Makapu'u subaerial, main-shield stage and post-erosional lavas. Its proportion is greater during the main shield-building stage (KSDP) than in the Makapu'u stage lavas, indicating that its contribution decreased with time. The first unradiogenic component has EM-1 type isotopic characteristics: low $^{206}\text{Pb}/^{204}\text{Pb}$, high $^{208}\text{Pb}/^{204}\text{Pb}$, high $^{87}\text{Sr}/^{86}\text{Sr}$ and low $^{143}\text{Nd}/^{144}\text{Nd}$. This EM-1 type unradiogenic component corresponds to the "Ko'olau" end-member of the Hawaiian mantle plume. Although, the EM-1-type component is predominantly sampled by Makapu'u subaerial lavas, it is also present in variable and smaller proportions in the main-shield stage (KSDP) lavas. The second unradiogenic component is characterized by low $^{206}\text{Pb}/^{204}\text{Pb}$ and $^{208}\text{Pb}/^{204}\text{Pb}$, low $^{87}\text{Sr}/^{86}\text{Sr}$ and high $^{143}\text{Nd}/^{144}\text{Nd}$ ratios and testifies for the involvement of a depleted mantle-type source in the post-erosional lavas. The distinct Pb, Sr and Nd isotopic characteristics of the Honolulu Volcanics compared with those of the recent Pacific lithosphere represented by compositions of EPR MORBs provide evidence

that the Honolulu post-erosional lavas are not derived from a MORB-related source. We propose instead, that post-erosional Honolulu Volcanics result from melting of plume material.

The isotopic study (Pb, Sr, Nd and Hf) of lavas from different stages of Ko'olau eruptive history demonstrates that the isotopic variations can be related to melting of different parts of the mantle plume and indicate source heterogeneity. Thus, the life of a single volcano gives indication about geochemical and isotopic changes in the Hawaiian mantle plume composition. It would be therefore interesting to make combined isotopic study of shield, post-shield and post-erosional lavas from other Hawaiian volcanoes, in order to draw a detailed picture of the Hawaiian mantle plume evolution.

References

- 1 M. Tatsumoto, Isotopic composition of lead in oceanic basalt and its implication to mantle evolution, *Earth Planet. Sci. Lett.* 38, 63-87, 1978.
- 2 P. Stille, D.M. Unruh and M. Tatsumoto, Pb, Sr, Nd and Hf isotopic constraints on the origin of Hawaiian basalts and evidence for a unique mantle source, *Geochim. Cosmochim. Acta* 50, 2303-2319, 1986b.
- 3 J.C. Lassiter and E.H. Hauri, Osmium-isotope variations in Hawaiian lavas: evidence for recycled oceanic lithosphere in the Hawaiian plume, *Earth Planet. Sci. Lett.* 164, 483-496, 1998.
- 4 J.C. Lassiter, D.J. DePaolo and M. Tatsumoto, Isotopic evolution of Mauna Kea volcano: Results from the initial phase of the Hawaiian Scientific Drilling Project, *J. Geophys. Res.* B101(11769-11780), 1996.
- 5 J.M. Eiler, K.A. Farley, J.W. Valley, A.W. Hofmann and E.M. Stolper, Oxygen isotopes constraints on the sources of Hawaiian volcanism, *Earth Planet. Sci. Lett.* 144, 453-468, 1996.
- 6 A.W. Hofmann and W.M. White, Mantle plumes from ancient oceanic crust, *Earth Planet. Sci. Lett.* 57, 421-436, 1982.
- 7 E. Hauri, Major-element variability in the Hawaiian mantle plume, *Nature* 382, 415-419, 1996.
- 8 E.M. Stolper, D.J. DePaolo and D.M. Thomas, Introduction to special section: Hawaii Scientific Drilling Project, *J. Geophys. Res.* 101(No. B5), 11593-11598, 1996.
- 9 E.H. Haskins, Core drilling of Ko'olau volcano reveals a rapid change in shield-stage geochemistry: implications for compositional variability of the Hawaiian source, Master of Science, University of Hawaii, 2002.
- 10 P. Stille, D.M. Unruh and M. Tatsumoto, Pb, Sr, Nd and Hf isotopic evidence of multiple sources for Oahu, Hawaii basalts, *Nature* 304, 25-29, 1983.
- 11 R.R. Doell and G.B. Dalrymple, Potassium-argon ages and paelomagnetism of the Waianae and Koolau Volcanic Series, Oahu, Hawaii, *GSA bull.* 84, 1217-1242, 1973.
- 12 D.A. Clague and G.B. Dalrymple, The Hawaiian-Emperor volcanic chain. Part I, Geologic evolution, in: *Volcanism in Hawaii*, P.H. Stauffer, ed., U.S. Geological Survey Professional Paper, pp. 5-73, 1987.
- 13 J. Blichert-Toft, F.A. Frey and F. Albarede, Hf isotope evidence for pelagic sediments in the source of Hawaiian basalts, *Science* 285, 879-882, 1999.
- 14 M.F. Roden, F.A. Frey and D.A. Clague, Geochemistry of tholeiitic and alkalic lavas from the Koolau range, Oahu, Hawaii: implications for Hawaiian volcanism, *Earth Planet. Sci. Lett.* 69, 141-158, 1984.

- 15 P. Stille, Unruh, D. M., Tatsumoto, M., Pb, Sr, Nd and Hf isotopic evidence of multiple sources for Oahu, Hawaii basalts, *Nature* 304, 25-29, 1986a.
- 16 M.C. Jackson, F.A. Frey, M.O. Garcia and R.A. Wilmoth, Geology and geochemistry of basaltic lava flows and dikes from the Trans-Koolau Tunnel, Oahu, Hawaii, *Bull. Volcan.* 60(5), 381-401, 1999.
- 17 R. Tanaka, E. Nakamura and E. Takahashi, Geochemical evolution of Koolau volcano, Hawaii, in: *Hawaiian Volcanoes: Deep Underwater Perspectives*, A.G. Union, ed., Geophysical Monograph 128, pp. 311-332, 2002.
- 18 K. Shinozaki, R. Zhong-Yuan and E. Takahashi, Geochemical and petrological characteristics of Nuuanu and Wailau landslide blocks, in: *Hawaiian Volcanoes: Deep Underwater Perspectives*, A.G. Union, ed., Geophysical Monograph 128, pp. 27-310, 2002.
- 19 D.A. Clague and F.A. Frey, Petrology and Trace Element Geochemistry of the Honolulu Volcanics, Oahu: Implications for the Oceanic Mantle below Hawaii, *J. Petrol.* 23, 447-504, 1982.
- 20 J.C. Lassiter, Hauri, E. H., Reiners, P. W., Garcia, M. O., Generation of Hawaiian post-erosional lavas by melting of a mixed lherzolite/pyroxenite source, *Earth Planet. Sci. Lett.* 178, 269-284, 2000.
- 21 S.J.G. Galer, Optimal double and triple spiking for high precision lead isotopic measurements, *Chem. Geol.* 157, 255-274, 1999.
- 22 G.W. Lugmair and S.J.G. Galer, Age and isotopic relationship among the angrites Lewis Cliff 86010 and Angora dos Reis, *Geochim. Cosmochim. Acta* 56, 1673-1694, 1992.
- 23 H. Gerstenberger and G. Haase, A highly effective emitter substance for mass spectrometric Pb isotope ratio determinations, *Chem. Geol.* 136(3-4), 309-312, 1997.
- 24 S.J.G. Galer and K. O'Nions, Residence time of thorium, uranium and lead in the mantle with implications for mantle convection, *Nature* 316, 778-782, 1985.
- 25 W. Abouchami, A.W. Hofmann, S.J.G. Galer, F.A. Frey, J. Eisele and M. Feigenson, Long-lived heterogeneities and lateral dichotomy of the Hawaiian Plume, *Nature*, submitted.
- 26 V.C. Bennett, T.M. Esat and M.D. Norman, Two mantle-plume components in Hawaiian picrites inferred from correlated Os-Pb isotopes, *Nature* 381, 221-224, 1996.
- 27 C.Y. Chen and F.A. Frey, Origin of Hawaiian tholeiite and alkali basalt, *Nature* 302, 785-789, 1983.
- 28 W. Abouchami, S.J.G. Galer and A.W. Hofmann, High precision lead isotope systematics of lavas from the Hawaiian Scientific Drilling Project, *Chem. Geol.* 169, 187-209, 2000.
- 29 J. Eisele, W. Abouchami, S.J.G. Galer and A.W. Hofmann, The 320 kyr Pb isotope evolution of Mauna Kea lavas recorded in the HSDP-2 drill core, *Geochem. Geophys. Geosyst.* 4(N. 5), 2003.
- 30 E.H. Haskins and M.O. Garcia, Scientific drilling reveals geochemical heterogeneity within the Ko'olau shield, Hawaii, *Contrib. Mineral. Petrol.* 147, 162-188, 2004.

- 31 S. Huang and F.A. Frey, Temporal geochemical variation within the Ko'olau shield: A trace element perspective, *Contrib. Mineral. Petrol.*, submit.
- 32 V. Salters, Pers. com.
- 33 M.D. Kurz, Kenna, T. C., Lassiter, J. C., DePaolo, D. J., Helium isotopic evolution of Mauna Kea Volcano: first results from the 1-km drill core, *J. Geophys. Res.* 101, 11781-11791, 1996.
- 34 A.J. Pietruszka and M.O. Garcia, A rapid fluctuation in the mantle source and melting history of Kilauea Volcano inferred from the geochemistry of its historical summit lavas (1790-1982), *J. Petrol.* 40(8), 1321-1342, 1993.
- 35 A.J. King, D.G. Waggoner and M.O. Garcia, Geochemistry and petrology of basalts from Leg 136, Central Pacific Ocean, in: *Proceedings of the Ocean Drilling Program, Scientific Results, e. al., ed. 136, pp. 107-118, 1993.*
- 36 S.J.G. Galer, W. Abouchami and J.D. Macdougall, East Pacific Rise MORB Through the Pb Isotope Looking-Glass, in: *AGU Fall Meeting, AGU, San Francisco, 1999.*
- 37 F.A. Frey, S. Huang, J. Blichert-Toft and M. Boyet, Origin of depleted components in lavas related to the Hawaiian hotspot: evidence from Hf isotope data, *Geochem. Geophys. Geosys.*, submit.
- 38 N.M. Ribe and U.R. Christensen, The dynamical origin of Hawaiian volcanism, *Earth Planet. Sci. Lett.* 171, 517-531, 1999.
- 39 DePaolo, D. J., Bryce, J. G., Dodson, A., Shuster, D. L. & Mack Kennedy, B. Isotopic evolution of Mauna Loa and the chemical structure of the Hawaiian plume. *Geochem. Geophys. Geosyst.* **2**, 2000GC000139 (2001).

FIGURE CAPTIONS

Figure 1. Map of the island of O‘ahu showing the location of Ko‘olau volcano [9]. The KSDP drill site is located in the Western part of the lower Kalihi valley (red dot). WAFB – Wheeler Air Force Base. From Haskins and Garcia [30].

Figure 2: Depth variations of Pb and Sr isotopic compositions in KSDP lavas, Makapu‘u subaerial lavas [25] and Honolulu Volcanics. (a) Lost on ignition (LOI) and K_2O/P_2O_5 ratio variations with depth showing that samples below ~575 mbsl were affected by alteration (after Haskins [9]). (b) $^{206}Pb/^{204}Pb$ ratios of KSDP lavas increase with depth until ~450 mbsl and then decrease until ~600 mbsl. The dashed line shows the general “bell trend” of the $^{206}Pb/^{204}Pb$ variations (see text for explanation). The dotted line at ~575 mbsl marks the limit between unaltered and altered samples. Samples recovered below this level do not follow the general bell trend and are scattered. (c) $^{208}Pb^*/^{206}Pb^*$ represents the time integrated $^{232}Th/^{238}U$ ratio since the formation of the Earth and is determined as $[(^{208}Pb/^{204}Pb)_{sample}-29.475]/[(^{206}Pb/^{204}Pb)_{sample}-9.307]$ [24]. Based on their $^{208}Pb^*/^{206}Pb^*$ ratios, KSDP lavas, Makapu‘u subaerial lavas and Honolulu Volcanics can clearly be distinguished. (d) Similar differences are also observed in the variation of $^{87}Sr/^{86}Sr$ ratios with depth.

Figure 3: Pb isotopic compositions of Ko‘olau Scientific Drilling Project (KSDP) lavas and Honolulu Volcanics (HVS) obtained using the Pb triple spike technique [21]. (a) In $^{208}Pb/^{204}Pb$ vs. $^{206}Pb/^{204}Pb$ diagram, KSDP lavas and Honolulu Volcanics form two well-defined linear arrays which converge at the radiogenic end. (b) In $^{207}Pb/^{204}Pb$ vs. $^{206}Pb/^{204}Pb$ plot, the two arrays cannot be unambiguously resolved. The error bar (2σ) is similar to the symbol size.

Figure 4: Comparison of $^{206}\text{Pb}/^{204}\text{Pb}$ variations with depth between Ko’olau shield lavas (KSDP drill core) and Mauna Kea shield lavas (Hawaiian Scientific Drilling Project: HSDP-2 and HSDP-1). Pb triple spike data for the HSDP-2 core from [29] and HSDP-1 [28].

Figure 5: (a) Sources of Ko’olau lavas. Solid lines represent the linear trends formed by KSDP lavas (KSDP trend) and Honolulu Volcanics (HVS trend). In $^{208}\text{Pb}/^{206}\text{Pb}$ vs. $^{206}\text{Pb}/^{204}\text{Pb}$ diagram, three isotopically distinct components can be identified: (A) radiogenic ”Kea-lo8”-type end-member defined by the intersection of the KSDP and HVS trends, (B) EM-1 type end-member located at the low $^{206}\text{Pb}/^{204}\text{Pb}$ - high $^{208}\text{Pb}/^{204}\text{Pb}$ end of the KSDP trend and (C) Depleted Mantle-type end-member located at the low $^{206}\text{Pb}/^{204}\text{Pb}$ – low $^{208}\text{Pb}/^{204}\text{Pb}$ end of the HVS trend (DM-type). (b, c) Sr and Nd isotopic compositions of the individual end-members: EM-1 type end-member has the highest $^{87}\text{Sr}/^{86}\text{Sr}$ and lowest ϵ_{Nd} values whereas the DM-type end-member exhibits the lowest $^{87}\text{Sr}/^{86}\text{Sr}$ and highest ϵ_{Nd} values. For comparison, data on the East Pacific Rise MORBs (EPR MORBs) are also shown (b, c). Data for KSDP lavas and Honolulu Volcanics are from this work, data for the Makapu’u subaerial lavas are from Abouchami et al. [25]. Data for EPR MORBs are from Galer et al. [36]. Data on different stages of Ko’olau from [17]. ϵ_{Nd} data on the KSDP lavas are from Salters [32], the error (2σ) is ~ 0.2 . The error bar (2σ) on the Pb triple spike data is similar to the symbol size. Data from [17], re-normalized to our NIST SRM 981

Figure 6: (a) Comparison of Pb isotopic compositions of lavas from different stages of Ko’olau growth: KSDP lavas and Honolulu Volcanics (this work), Makapu’u stage lavas [25] and

Nuuuanu landslide blocks [17]. The KSDP lavas overlap with the Nuuanu-2 landslide blocks. For comparison, the data of Tanaka et al. [17] were re-normalized to our NIST SRM 981 values. The dashed line represents the compositional Pb isotopic division between Loa trend and Kea trend volcanoes [25]. Pb isotopic compositions of the lavas from the subaerial Makapu'u, Lower Makapu'u and Upper main-shield stage, as well as those from Oahu North a and Oahu North b are shown for comparison. (b) Comparison of Pb isotopic compositions of Ko'olau lavas with other Hawaiian shield volcanoes [25]. KSDP and Makapu'u subaerial lavas belong to the Loa trend volcanoes, whereas the Honolulu Volcanics plot along the Kea trend. The linear trends formed by KSDP and Mauna Loa lavas are shown as solid lines. Note that the Pb isotopic compositions of KSDP lavas display a range similar to that of Mauna Loa lavas, but KSDP and Mauna Loa Pb arrays have distinct slopes. The KSDP linear trend extends from the Makapu'u subaerial lavas towards the most depleted "Kea-lo8" lavas [29]. The Pb triple spike data on Kilauea lavas are shown for comparison [25].

Figure 7: Comparison of Pb isotopic compositions of Honolulu Volcanics with Ocean Drilling Project basalts from ODP Leg 136 site 843 (19°21'N 159°06'W) [35] and crustal xenoliths recovered in Hualalai lavas [3]. The initial Pb isotopic compositions of ODP 843 basalts are rough estimates [35]. In contrast to the well-defined Pb isotope array defined by Honolulu Volcanics (triple spike data) shown as a solid line, Pb isotope data on ODP 843 basalts and gabbroic xenoliths show a large scatter which renders the comparison difficult.

Figure 8: Comparison of Pb triple spike data on KSDP lavas and Honolulu Volcanics with those of East Pacific Rise Mid-Ocean Ridge Basalts (EPR MORBs) [36]. In $^{208}\text{Pb}/^{204}\text{Pb}$ vs.

$^{206}\text{Pb}/^{204}\text{Pb}$ diagram (a), KSDP and Honolulu Volcanics (HVS) trends are shown as solid lines. EPR MORBs data represent several independent segments of the East Pacific Rise [36], and are shown here as a field. In $^{207}\text{Pb}/^{204}\text{Pb}$ vs. $^{206}\text{Pb}/^{204}\text{Pb}$ diagram (b), KSDP and Honolulu Volcanics fields cannot be unambiguously distinguished, but both datasets have at a given $^{206}\text{Pb}/^{204}\text{Pb}$ lower $^{207}\text{Pb}/^{204}\text{Pb}$ ratio than EPR MORBs.

Appendix

Figures and tables

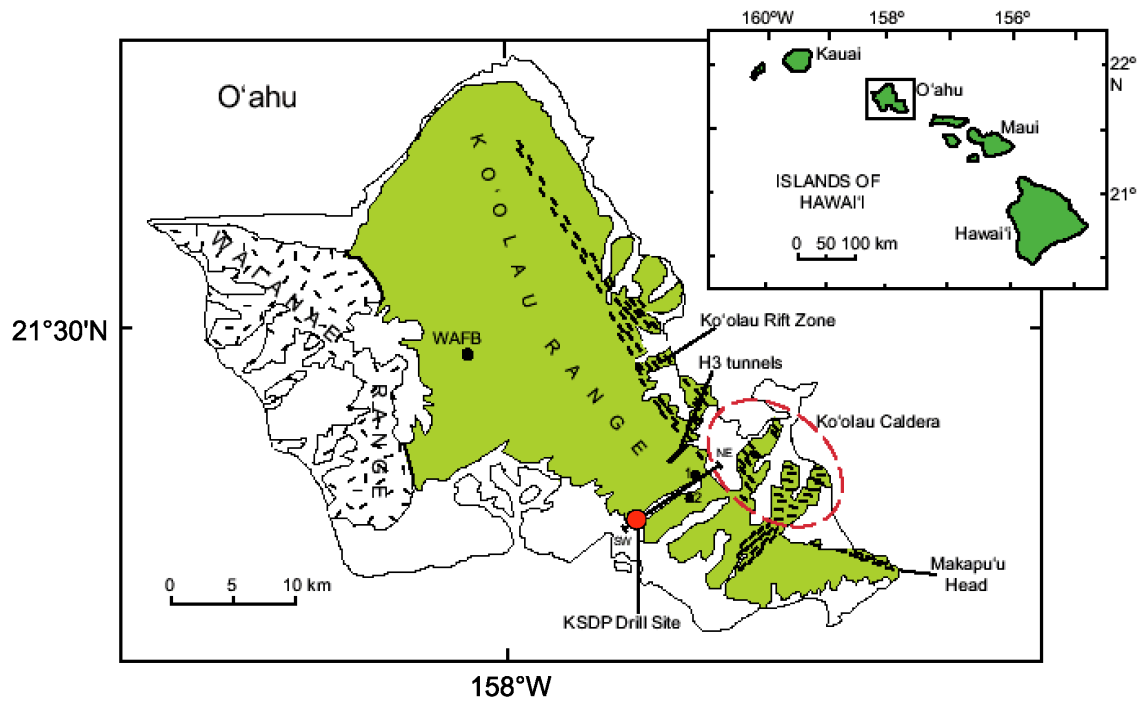


Figure 1

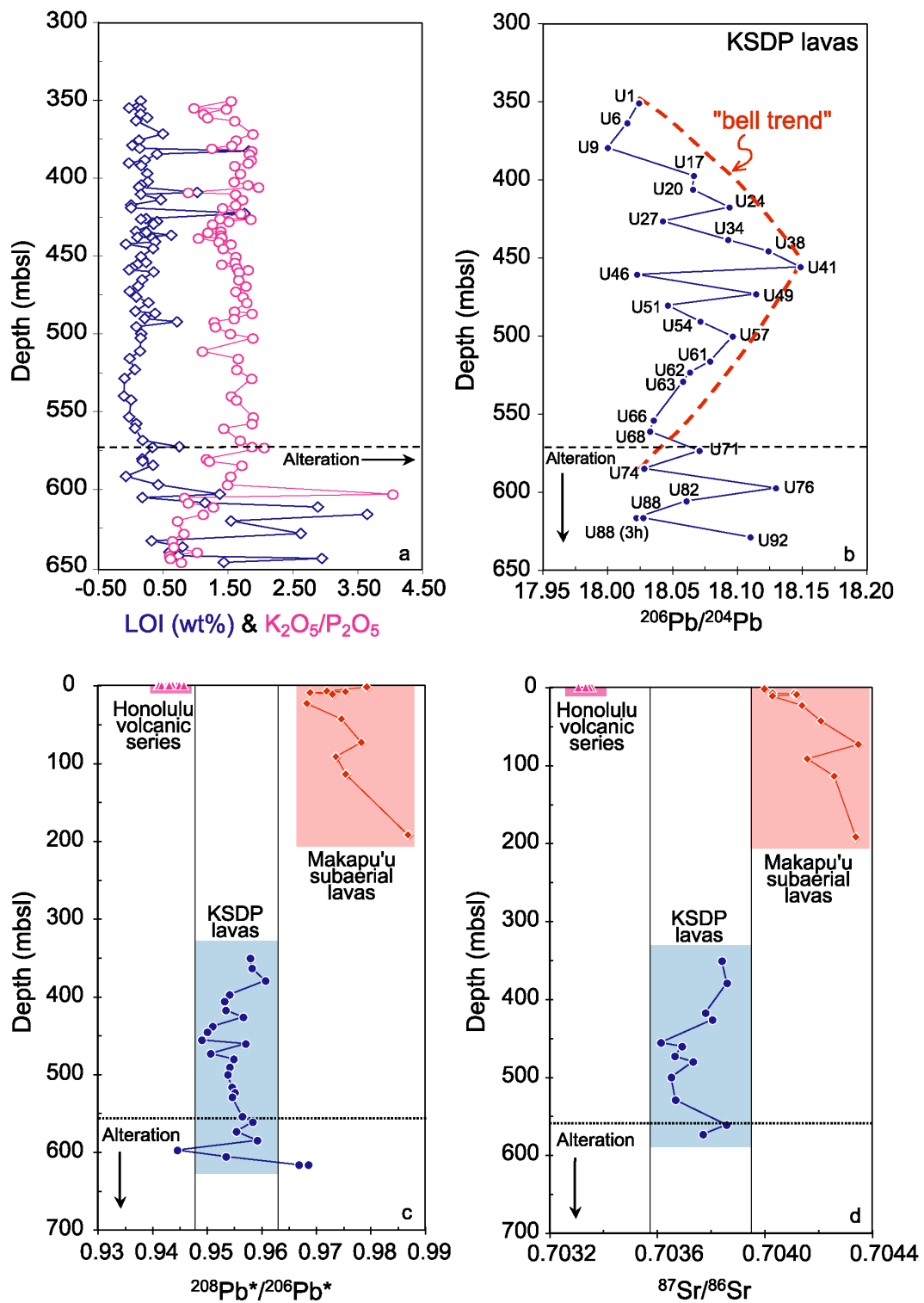


Figure 2

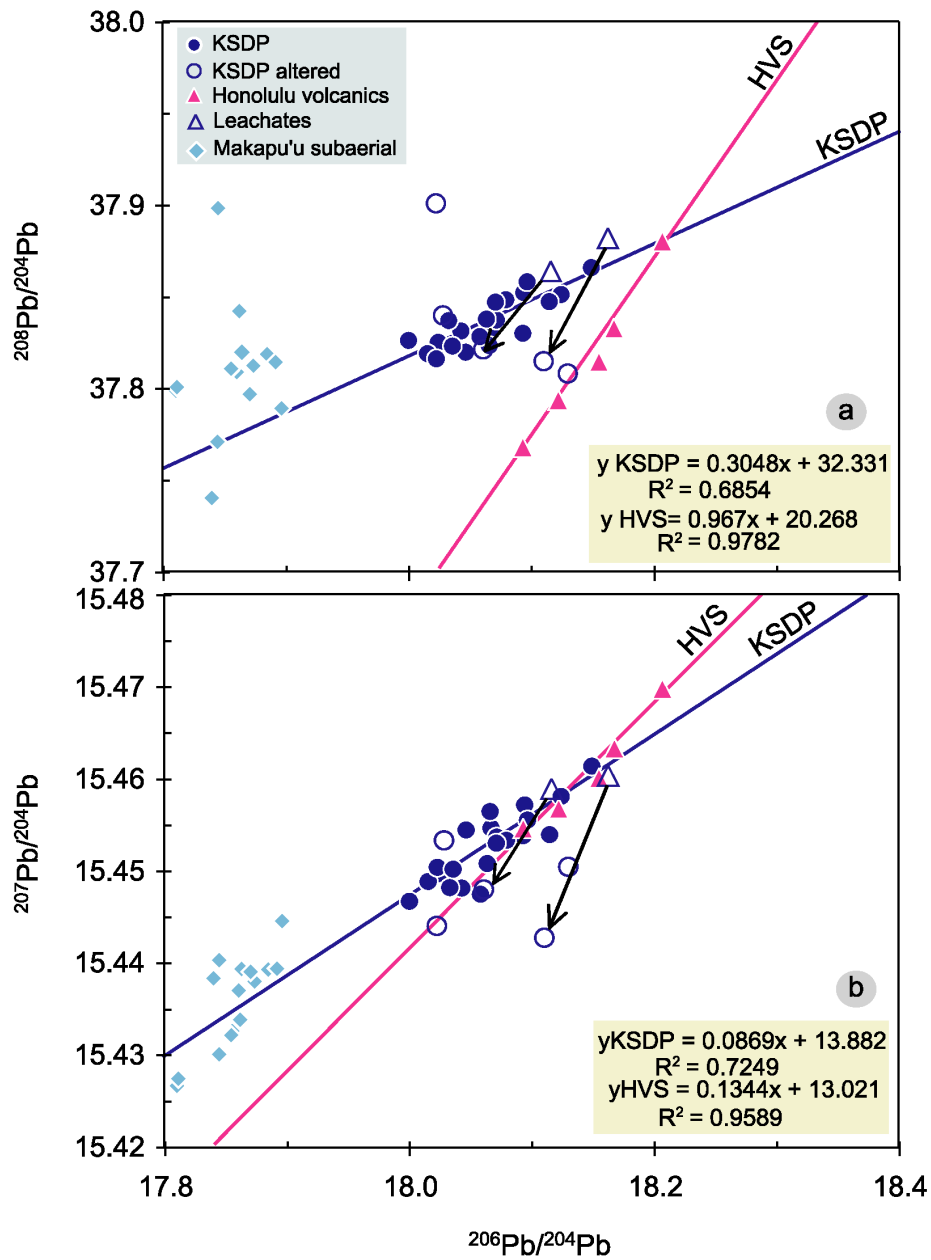


Figure 3

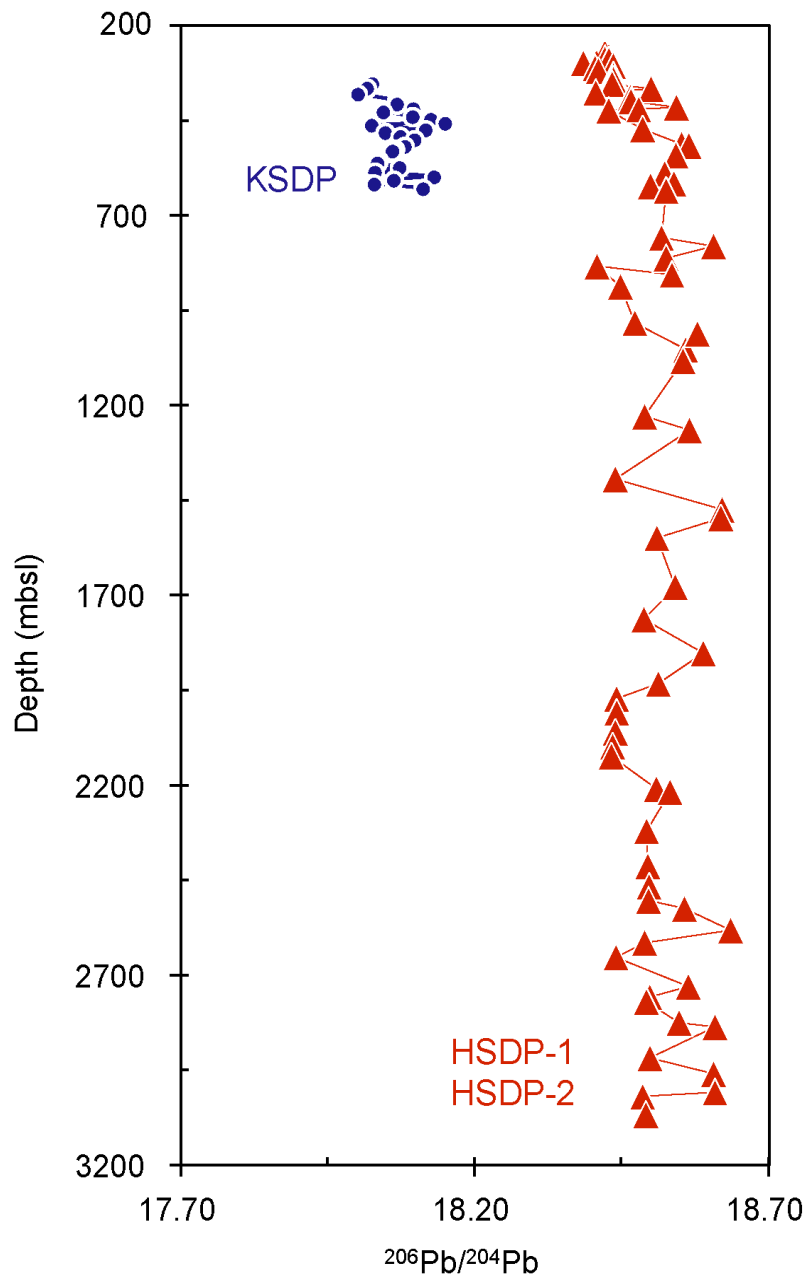


Figure 4

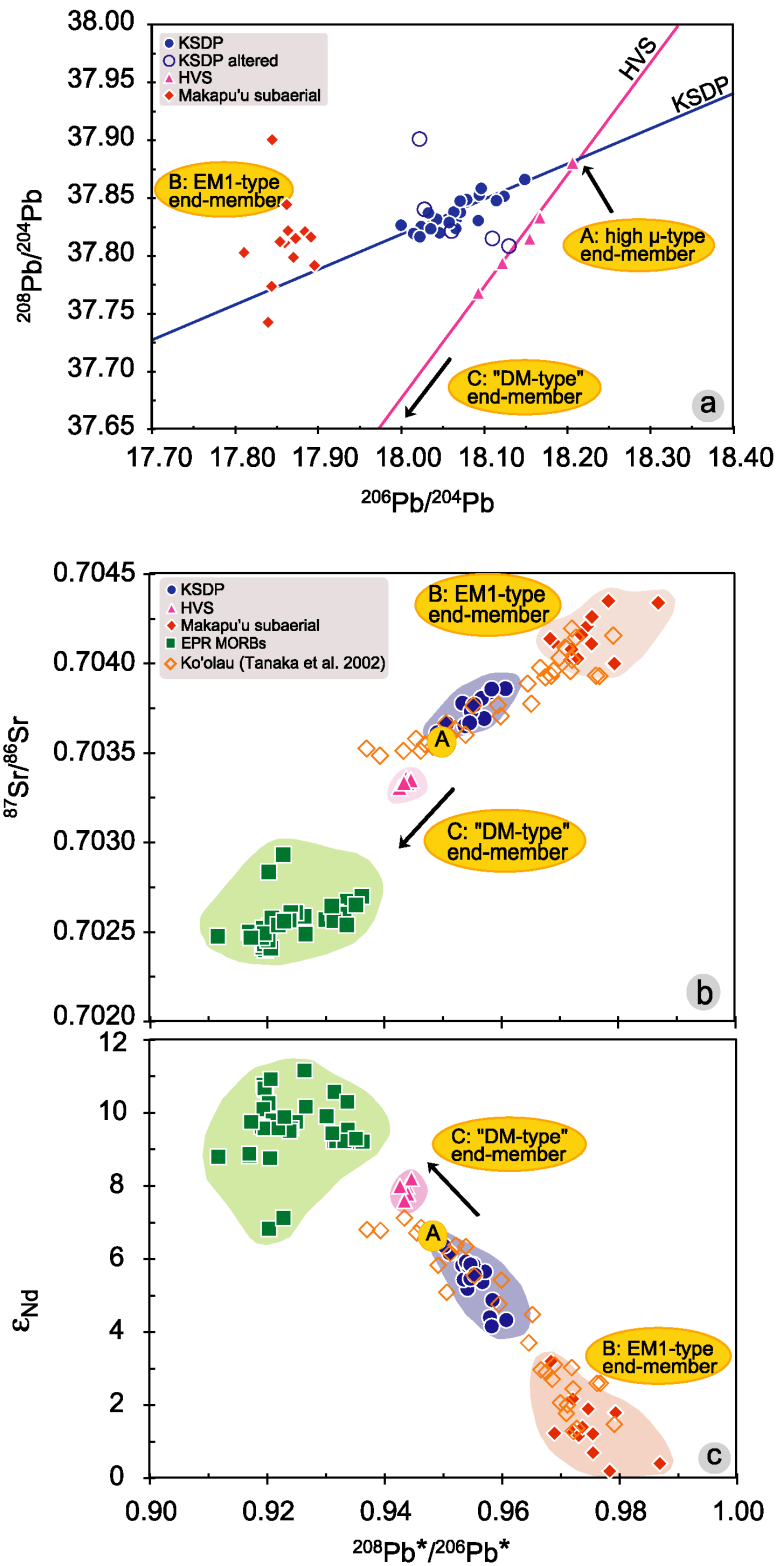


Figure 5

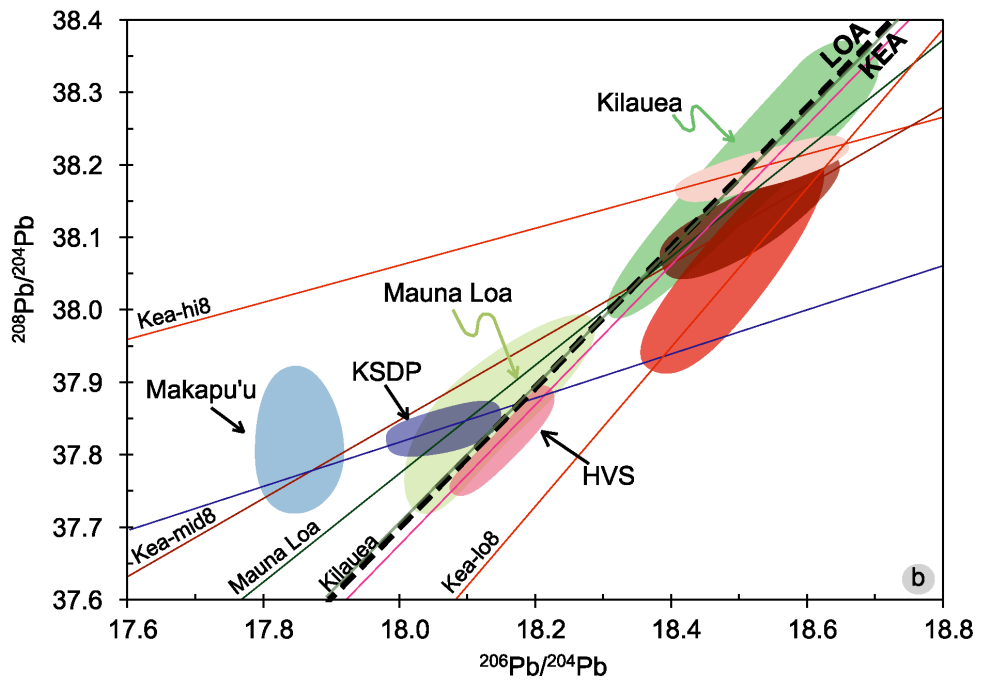
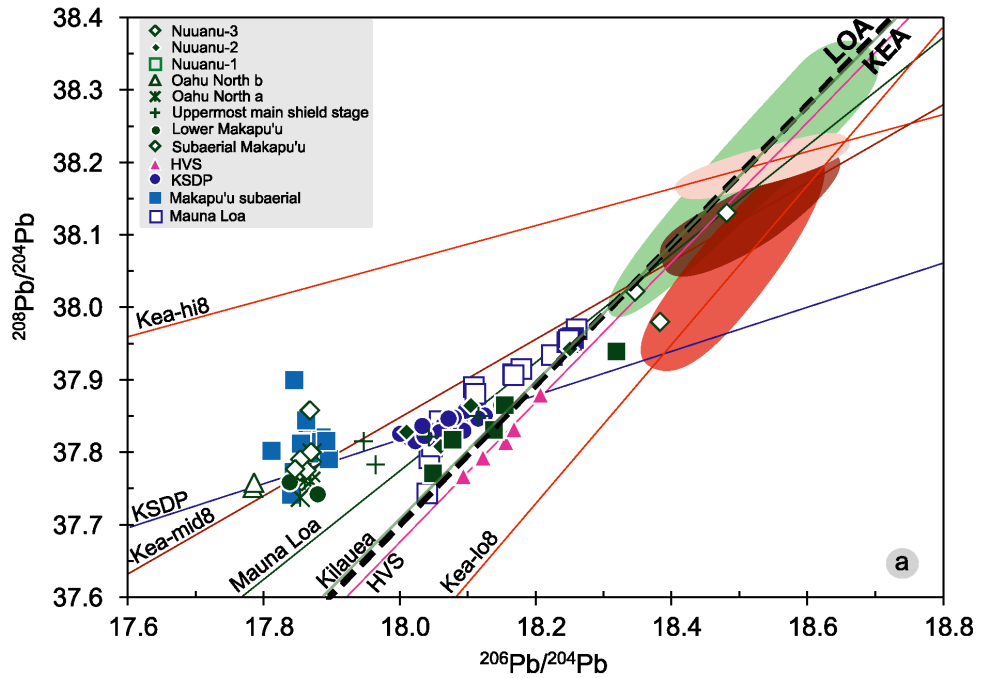


Figure 6

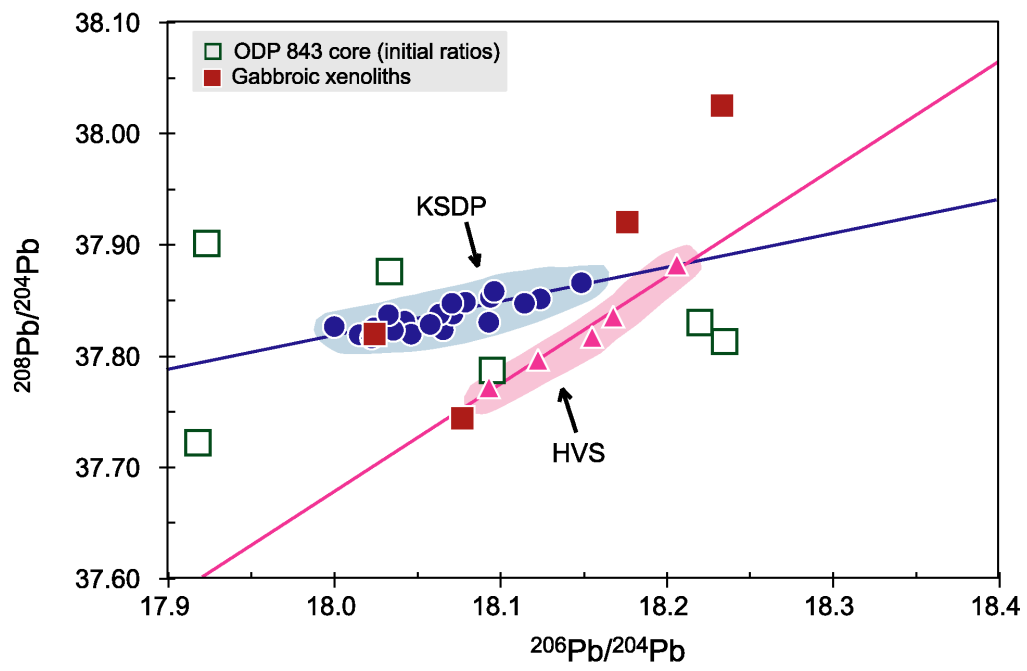


Figure 7

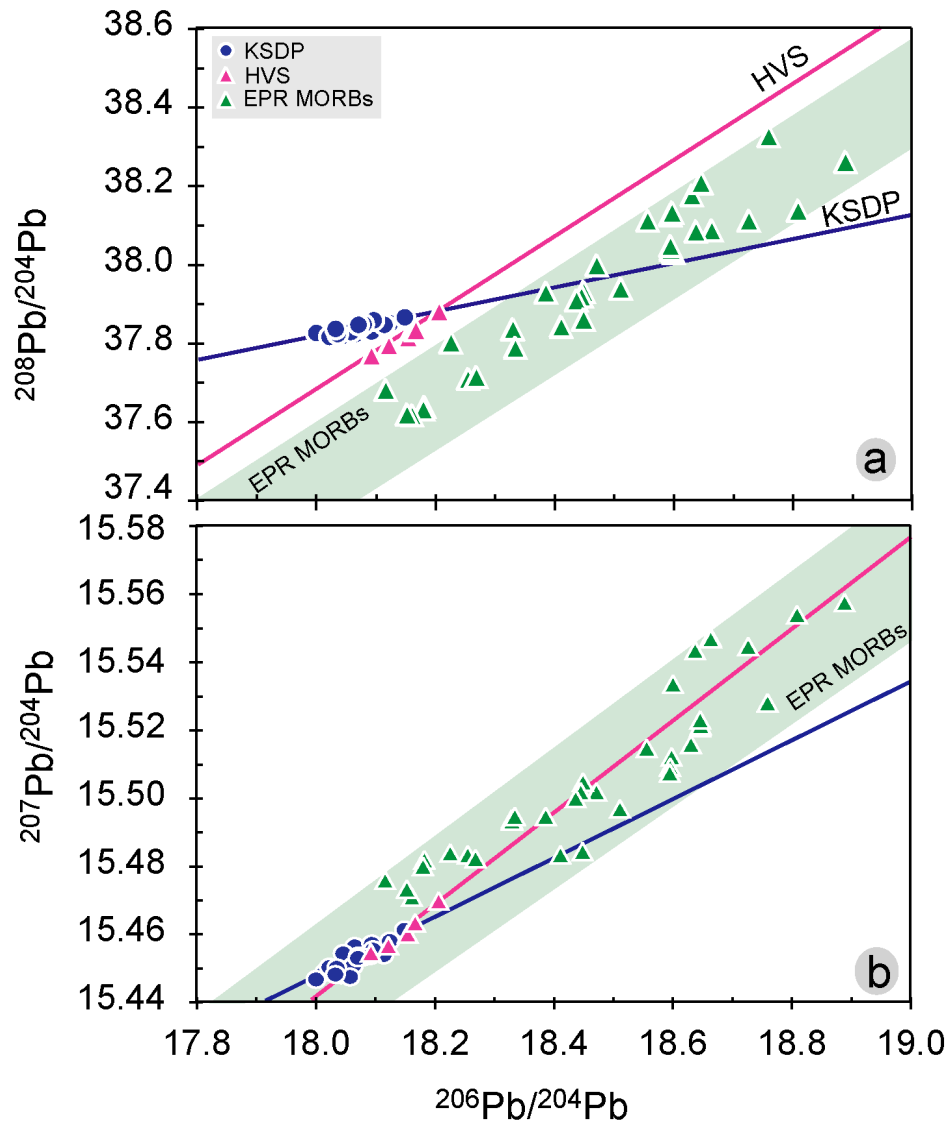


Figure 8

Table 1. Pb and Sr isotope compositions of KSDP and Honolulu volcanics samples

	depth (mbsl)	age model (ka)	²⁰⁶ Pb		²⁰⁷ Pb		²⁰⁸ Pb		²⁰⁸ Pb*		⁸⁷ Sr	
			²⁰⁶ Pb/ ²⁰⁴ Pb	2σ	²⁰⁷ Pb/ ²⁰⁴ Pb	2σ	²⁰⁸ Pb/ ²⁰⁴ Pb	2σ	²⁰⁸ Pb*/ ²⁰⁶ Pb*	⁸⁷ Sr/ ⁸⁶ Sr	2σ	
KSDP												
KSDP U1	350.7		18.0239	9	15.4498	9	37.8254	26	0.9580	0.70384		
KSDP U6	363.5		18.0147	10	15.4489	12	37.8193	37	0.9583			
KSDP U9	379.3		17.9997	10	15.4467	10	37.8264	28	0.9607	0.70386		
KSDP U17	397.3		18.0661	8	15.4547	8	37.8325	23	0.9541			
KSDP U20	406.1		18.0655	9	15.4565	9	37.8238	25	0.9532			
KSDP U24	417.5		18.0936	8	15.4572	8	37.8527	25	0.9535	0.70378		
KSDP U27	426.4		18.0423	11	15.4482	11	37.8316	30	0.9567	0.70381		
KSDP U34	438.3		18.0926	7	15.4539	7	37.8305	23	0.9510			
KSDP U38	445.5		18.1237	8	15.4581	8	37.8516	24	0.9501			
KSDP U41	455.7		18.1485	8	15.4614	8	37.8661	25	0.9491	0.70361		
KSDP U46	460.5		18.0223	7	15.4505	8	37.8165	24	0.9571	0.70369		
KSDP U49	473.0		18.1142	9	15.4540	8	37.8477	25	0.9507	0.70367		
KSDP U51	480.3		18.0460	8	15.4545	8	37.8200	24	0.9549	0.70373		
KSDP U54	490.6		18.0711	7	15.4537	8	37.8377	24	0.9542			
KSDP U57	500.2		18.0961	7	15.4556	8	37.8584	25	0.9538	0.70365		
KSDP U61	516.2		18.0788	8	15.4534	8	37.8486	24	0.9546			
KSDP U62	523.3		18.0631	6	15.4508	7	37.8380	22	0.9551			
KSDP U63	529.1		18.0577	8	15.4475	8	37.8287	22	0.9546	0.70367		
KSDP U66	553.9	2.9 ± 0.22 Ma	18.0352	6	15.4502	7	37.8234	21	0.9565			
KSDP U68	561.1		18.0324	9	15.4483	10	37.8372	28	0.9584	0.70386		
KSDP U71	573.4		18.0705	6	15.4531	8	37.8475	24	0.9554	0.70377		
KSDP U74	584.8		18.0278	8	15.4533	8	37.8402	25	0.9592			
KSDP U76 (3H)	597.3		18.1293	10	15.4505	11	37.8084	35	0.9446			
KSDP U82 (3H)	605.6		18.0604	12	15.4480	11	37.8216	31	0.9535			
L-KSDP U82 6N HCl leachate	605.6		18.1163	9	15.4588	12	37.8637	34	0.9523			
KSDP U88	616.4		18.0271	13	15.4482	13	37.9215	41	0.9686			
KSDP U88 (3H) duplicate	616.4		18.0218	13	15.4440	12	37.9012	32	0.9669			
KSDP U92 (3H)			18.1098	16	15.4428	14	37.8152	36	0.9474			
L-KSDP U92 6N HCl leachate	628.7		18.1629	9	15.4603	9	37.8816	27	0.9493			
Honolulu volcanics												
OA3			18.1670	10	15.4634	11	37.8332	32	0.9434	0.70333		
OA4		0.41	18.2061	10	15.4698	12	37.8807	35	0.9446	0.70335		
OA5		0.58	18.1545	11	15.4601	11	37.8149	32	0.9426	0.70331		
OA6		0.10	18.0925	12	15.4547	12	37.7682	34	0.9440	0.70334		
OA10		0.06	18.1216	7	15.4568	8	37.7941	25	0.9438	0.70336		
NIST SRM 981 (n=73)			16.9401	22	15.4968	29	36.7234	69	0.9496			
NIST SRM 987 (n=8)										0.71018		10

Chapter 5

Conclusions

Conclusions

Two distinct occurrences of the intra-plate volcanic activity were in the focus of our investigations during the three years of my Ph. D. Using geochronological, geochemical and geophysical tools we were able to assess the timing of volcanic activity, estimate the conditions and depth of magma-generation, as well as identify possible sources involved in the magmas. Here, I will present you the conclusions that come out of the combined geochronological, geochemical and isotopic studies. In the first part, I will present the conclusions on the geotectonic setting of the Hocheifel volcanism and on its relationship to the other volcanic areas of the Central European Volcanic Province. In the second part, I will present the conclusions on the evolution of the Ko'olau volcano, Hawaii and on the implications that these conclusion bring on the Hawaiian mantle plume. Finally, in a third part, I will give some perspectives of research that I would be interested to pursue on these two topics.

1. The Tertiary Eifel volcanism and the Central European Volcanic Province

In Europe, the Central European Volcanic Province (CEVP) and Cenozoic Rift System (CRS) represent a major volcanic and tectonic features. Studies on individual volcanic areas of the CEVP bring important conclusions on the volcanic and tectonic history of Europe.

The Tertiary Hocheifel volcanism that we have studied during this Ph.D. belongs to the CEVP. K-Ar dating provided poorly reliable dates for the volcanic activity in the Hocheifel area. Using the $^{40}\text{Ar}/^{39}\text{Ar}$ dating technique, we were able to further constrain the age of the Hocheifel volcanic activity. We found that the Hocheifel volcanism occurred in two main steps.

The oldest volcanoes erupted between 43.6.0 and 39.0 Ma. A younger phase of volcanism developed from 37.5 to 35.0 Ma. In addition, we found that the samples from the northern Upper Rhine Graben (URG) yield an age range from 59 to 47 Ma. No clear relationships between age and chemical composition could be established. However, basanites appear to erupt mostly during the younger phase of volcanic activity, whereas the more evolved lavas occurred between 37 Ma and 40 Ma.

The volcanic activity in the northern Upper Rhine Graben area started about 15 m.y. earlier than the initial phase of rifting in the Rhine Graben, i.e. during the pre-rift period. In contrast, only sporadic volcanism accompanied the major subsidence and rifting in the Rhine Graben. The Hocheifel volcanism closely follows in time the pre-rifting volcanism of the northern Upper Rhine Graben. In addition, our data show that the Hocheifel activity propagates with time towards the north. Simultaneously with the Hocheifel volcanic activity, the tectonic situation in the Hocheifel area was controlled by stress conditions identical to those in the Upper Rhine Graben. Thus, we suggest that the Hocheifel volcanic activity represents the northwestern propagation of the pre-rifting volcanism of the northern Upper Rhine Graben. Consequently, it is likely that the Hocheifel magmas were generated by decompression related to Middle-Late Eocene extension processes.

The geochemical and isotope data of the Tertiary Hocheifel and Upper Rhine Graben lavas indicate that these magmas were produced by partial melting of a garnet peridotite at depths of about 75 to 90 km. Although the Hocheifel and the Upper Rhine Graben lavas erupted through a relatively thick (50-60 km) continental crust, our geochemical and isotopes data show that these lavas were either not affected or only slightly affected by crustal contamination. Nd, Sr and Pb isotopic compositions of the Hocheifel lavas indicate that they result from the mixing between a depleted FOZO or HIMU-like component and an enriched EM 2-like end-member.

The potential involvement of FOZO-like material, which is thought to originate from the lower mantle, indicates a possible involvement of deep mantle material in the Hocheifel lavas. Although the Sr and Nd isotopic compositions show that the Tertiary Hocheifel and Quaternary Eifel lavas are influenced by similar enriched component, the trace elements and Pb isotopes show that their sources are likely to be different. In particular, contrary to the Quaternary Eifel lavas, the Hocheifel lavas appear to share a common depleted Low Velocity Component defined by Hoernle et al. (1995) with other Tertiary CEVP lavas.

Consequently, we cannot rule out the hypothesis that the Hocheifel volcanism was related to mantle dynamics and eventually to the activity of a mantle plume. Although the geochronological, tectonic and geological evidences favor a tectonic control of the Hocheifel volcanic activity, the geochemical and isotopic characteristics of the Hocheifel lavas tend to show deep mantle material involvement. We suggest that the extension-related Eocene volcanism tapped mantle source which was previously contaminated by plume-type material. Further studies are needed to reconcile these views. In particular, further geochemical investigations, especially using Pb isotopes, are necessary to distinguish between these two theories.

2. The Ko'olau volcanism

In contrast to the controversial opinions about the origin of the Tertiary Hocheifel volcanism, it is generally accepted that the Hawaiian volcanoes are related to the Hawaiian mantle plume.

Our new Pb isotope data on lavas from different stages of the Ko'olau volcano indicate that Ko'olau experienced compositional source variations during its growth. At least three isotopically distinct components are present in the source of Ko'olau lavas and the contribution

of each individual component is recorded in the Pb, Sr, Nd and Hf isotope stratigraphy. One common radiogenic and two distinct unradiogenic components are responsible for the isotopic signature of Ko'olau lavas. The common radiogenic component has by comparison to two unradiogenic components high " μ " and shows affinities with the depleted "Kea-108" end-member present in Mauna Kea lavas. Although this component is present at all stages of Ko'olau growth, its contribution is decreasing with time. The first unradiogenic component has EM-1-type isotopic characteristics and corresponds to the "Ko'olau" end-member of the Hawaiian mantle plume. Although the EM-1-type component is predominantly sampled by Makapu'u subaerial lavas, it is also present in variable and smaller proportions in the main-shield stage (KSDP) lavas. The second unradiogenic component has only been identified so far in the post-erosional lavas. The Sr, Nd and Pb isotopic compositions of this second component testify for the involvement of a depleted mantle-type source. However, the isotopic characteristics of the post-erosional lavas are distinct compared to those of the East Pacific Rise Mid Ocean Ridge Basalts (EPR MORB), which are thought to represent the recent Pacific lithosphere (Galer 1999). This feature provides evidence that the Honolulu post-erosional lavas are not derived from a MORB-related source. We propose instead, that post-erosional Honolulu Volcanics result from the melting of plume material. The isotopic study (Pb, Sr, Nd and Hf) of lavas from different stages of Ko'olau eruptive history demonstrates that the isotopic variations can be related to the melting of different parts of the mantle plume. Thus, the life of a single volcano records geochemical and isotopic changes in the Hawaiian mantle plume composition.

3. Perspectives

Thanks to the new geochronological, geochemical and isotope data presented in this study, we were able to decipher major characteristics of the Hocheifel volcanic activity, as well

as the evolution of the Ko'olau volcano. New questions were raised by these studies and opened new perspectives which we intend to follow in the near future. Additional isotope data on the Hocheifel lavas would help to clearly identify the sources of the Hocheifel magmas. This would help clarifying the relationships between the Hocheifel volcanism, the tectonic activity and the potential involvement of a mantle plume. In addition, detailed investigations, similar to those that we have done on the Hocheifel samples, could be performed on samples from the whole Upper Rhine Graben. This would allow us to establish a large-scale relationship between the volcanism in the Rhenish Massif and Rhine Graben extension.

Similarly, additional isotope data of shield, post-shield and post-erosional lavas from other Hawaiian volcanoes could be obtained. A combined isotopic study would be helpful to draw a detailed picture of the Hawaiian mantle plume evolution.

References

- Galer, S. J. G. (1999). Optimal double and triple spiking for high precision lead isotopic measurements. *Chem. Geol.* **157**: 255-274.
- Hoernle, K., Y. S. Zhang and D. Graham (1995). Seismic and geochemical evidence for large-scale mantle upwelling beneath the eastern Atlantic and western and central Europe. *Nature* **374**(2 March): 34-39.

Appendix

Curriculum vitae

Curriculum Vitae
Zuzana Fekiacova

Surname: Fekiacova

Given name: Zuzana

1. EDUCATION

January 2002: Diploma in Geology, University of Johannes Gutenberg Mainz, Germany

2000 – 2001: Maîtrise in Earth Sciences (equivalent of Honours program), at the Ecole Normale Supérieure de Lyon, France
Scholarship of the French government

1999 – 2000: Licence in Earth Sciences (equivalent of BSc degree), at the Ecole Normale Supérieure de Lyon, France
Scholarship of the Region Rhone - Alpes (TEMPRA)

1999: Competitive selection to enter the Ecole Normale Supérieure de Lyon, France
(Selection via evaluation of the study results)

1996 – 1999: University studies, Department of Earth Sciences, Faculty of Natural Sciences, University of Komensky in Bratislava, Slovakia
Scholarship of merit (1999)

1991 – 1996: Lycée bilingue, Bilingual French- Slovak section
Baccalaureat in French and Slovak language, june 1996

2. LABORATORY AND WORK EXPERIENCE

November 2003: $^{40}\text{Ar}/^{39}\text{Ar}$ dating of the Tertiary Upper Rhine Graben volcanic rocks. Berkeley Geochronology Center, California, USA.

August 2002: $^{40}\text{Ar}/^{39}\text{Ar}$ dating of the Tertiary Hocheifel volcanic rocks. Berkeley Geochronology Center, California, USA.

June - August 2000: Summer studentship: Evaluation of the stability of a hydraulic gallery in the Alps. Exploration and statistical valorisation of structural data. (Centre for Study of Tunnels in Bron, France)

April - May 2000: Personal project: Characteristics of the fusion and recrystallisation of the volcanic glass by Raman spectroscopy. Study of the evolution of the properties of volcanic glass with temperature.

Summer 1999: Fieldwork: Paleoreconstruction of the stratovolcano of Banska Stiavnica, Slovakia. In cooperation with Geological Survey of the Slovak Republic.

3. TECHNICAL AND ANALYTICAL SKILLS

- Clean-lab work (Pb, Sr, REE separations by ion exchange chromatography)
- $^{40}\text{Ar}/^{39}\text{Ar}$ dating technique (Berkeley Geochronology Center, California)
- Sr and Nd isotopic compositions analyses by TIMS MAT 261 Finnigan
- Pb isotopic compositions analyses by triple spike technique, by TIMS
- Nd isotopic compositions analyses by MC ICP MS Nu plasma
- Trace element analyses by laser ablation and in solution ICP MS Element 2

4. RESEARCH INTERESTS

* Geotectonic setting of the Hocheifel volcanism, Western Germany: geochemical characterisation of volcanic rocks from the Hocheifel volcanic area. Main focus on Sr, Nd and Pb isotopes analyses and dating by $^{40}\text{Ar}/^{39}\text{Ar}$ method. Determination of the origin of the Hocheifel magmas and of the geodynamic setting of the Tertiary Hocheifel volcanism.

* Isotopic evolution of Ko'olau volcano, Oahu, Hawaii: study of the Pb isotopic compositions of Ko'olau lavas using the triple spike technique (samples of Ko'olau lavas obtained during the Ko'olau Scientific Drilling Project). Comparison of the different evolutionary stages of Ko'olau. Study of the origin(s) of magmas and evolution of the Hawaiian plume.

5. INTERNATIONAL MEETINGS AND WORKSHOPS

- **Goldschmidt 2004 Conference**, Copenhagen, Denmark:
Z. Fekiacova and W. Abouchami*, The “Ko'olau component”: An Ephemeral feature of the Hawaiian mantle plume. (Poster presentation).
- **AGU 2003 Fall Meeting, San Francisco, CA, USA:**
Z. Fekiacova and W. Abouchami*, Pb isotopic evolution of Ko'olau, Oahu. (Poster presentation)
- **Hawaii Scientific Drilling Project Workshop**, E.O. Lawrence Berkeley National Laboratory December 7, 2003, Berkeley, CA, USA:
Z. Fekiacova and W. Abouchami*, Pb isotopic compositions of KSDP lavas, Ko'olau volcano, Oahu, Hawaii. (Oral presentation)
- **2003 Iceland Penrose Conference**, Hveragerdi, Iceland:
Z. Fekiacova, D. Mertz and P. Renne*, Tertiary Eifel volcanism - intraplate mantle plume or extension-related activity? (Poster presentation)
- **EGS - AGU - EUG Joint Assembly 2003**, Nice, France:
Z. Fekiacova, D. Mertz and P. Renne*, Geodynamic setting of the Hocheifel volcanism, Western Germany (Poster presentation)

* presenting author

6. LANGUAGES

Slovak: mother tongue

French: bilingual

English: fluent

German: basic knowledge

Russian: basic knowledge, read

7. COMPUTER SKILLS

Languages: Latex, Matlab, C (notions), HTML

Softwares: Microsoft office, Adobe Illustrator, MassSpec RB PPC, Stereonet

Exploitation system: Unix, Windows